Investigating the Formation of Organic Nitrogen Species during the Atmospheric Oxidation of Volatile Organic Compounds

Naomi J. Farren

Doctor of Philosophy

University of York

Chemistry

July 2017

Abstract

Particulate matter less than 2.5 μm in diameter, termed $PM_{2.5}$, lies within the respirable size range for humans and is therefore considered an important air quality standard. Within the respirable and often toxic chemical constituents in $PM_{2.5}$ exist a range of organic nitrogen (ON) compounds. Atmospheric ON is difficult to characterize due to its various complexities; it spans a wide range of volatilities and polarities and originates from both biogenic and anthropogenic sources. This thesis details the use of two-dimensional gas chromatography (GC×GC) coupled to nitrogen chemiluminescence detection (NCD) for the analysis of ON compounds in atmospheric aerosol.

The development of a highly sensitive analytical technique, relying on GC×GC-NCD, allowed for time-resolved measurements of carcinogenic nitrosamines in urban ambient $PM_{2.5}$ to be made. The total nitrosamine concentrations in London exceeded the public health recommendations, prompting an estimation of the lifetime cancer risk from exposure to nitrosamines *via* inhalation to be made.

The GC×GC-NCD technique was also used to investigate the formation of carcinogenic nitrosamines and nitramines formed during the atmospheric degradation of amines relevant to CO_2 capture. Implementation of amine-based CO_2 capture technology results in small but significant amounts of amines being emitted to the atmosphere. The atmospheric photo-oxidation pathways of various amines were investigated during a series of chamber experiments at the European Photoreactor. Complementary techniques such as ion chromatography (IC) were also used, to monitor the formation of aminium nitrate salts for example.

Later work in this thesis includes the use of IC to characterise water-soluble ions in aerosol on the East coast of Peninsular Malaysia, and to study the influence of highly industrialised regions on aerosol composition at rural coastal locations. Additionally, GC×GC coupled to time-of-flight mass spectrometry (TOF-MS) was used as part of a collaborative project focusing on the composition of gas and particle phase cooking emissions.

Contents

List of Figures

List of Tables

List of Schemes

Acknowledgements

I would like to thank my supervisor, Dr Jacqui Hamilton, for all her support throughout my PhD. It has been a pleasure to work with you; I am very grateful for everything you have taught me and all the exciting projects and trips you have allowed me to be part of. I would also like to thank my second supervisor, Professor Ally Lewis, for his advice on the nitrosamines publication and for allowing me to work in a fantastic lab with lots of different instruments. I am also grateful to NERC for funding my PhD.

A big thank you to the whole Atmospheric Chemistry group at York, you are all great to work with. Special thanks to Martyn, Richard and Rachel for their GC expertise! Also thanks to David for his advice on using R, and to Mustafa and Noelia for helping me get started with my research. Many thanks go to Will Unsworth for synthesising some weird and wonderful compounds, and to Will Dixon and Kelly for helping me with the experiments at EUPHORE. I am also grateful to those in Brendan Keely's group for teaching me how to use their sample extraction instrument.

I would like to thank Professor Claus Nielsen and his team for their advice and support at EUPHORE, as well as the interesting weekends exploring Valencia. Many thanks also go to Felix and his colleagues at PSI; it was great to get involved with your cooking emissions project.

Thanks to my Bristol mates, Jo, Rach, Robyn, Colette and Meg, for keeping in touch and travelling up north to visit me. Also thanks to my friends back home, as well as Abby, Jess, Emma and Hannah for never being more than a phone call away. Special thanks to Shani for the lunch time chats – work wouldn't be the same without you!

Thank you also to Jackie and John, for supporting Jamie and I over the last couple of years. We can always count on you for a good laugh and endless cups of Yorkshire tea.

Mum and Dad, thanks for being fun and relaxed parents and always being there for me. Thanks also to my sister Emma for lots of enjoyable weekends in Shrewsbury, and thanks to my brother and sister-in-law, Ben and Heidi, for an amazing trip to New Zealand earlier this year.

Finally, I would like to thank Jamie for all his love and support over the last few years. I was lucky to meet you during the first few weeks of my PhD and I can't wait to see what our next adventure will be!

Declaration

I declare that the research described in this thesis is original work, which I undertook at the University of York during 2013 – 2017. Except where stated, all of the work contained within this thesis represents the original contribution of the author. Collaborative publications are listed at the beginning of the chapter to which they relate.

1 Organic Nitrogen in the Atmosphere

1.1 Reactive nitrogen in the environment

Nitrogen, existing in its inert state as N_2, is the most abundant element in the Earth's atmosphere. However, for nitrogen to be chemically useful for organisms, it must be converted into a variety of forms, collectively known as 'reactive nitrogen'. This process is referred to as nitrogen fixation, and compounds generated include nitrous oxide (N_2O), ammonia (NH_3), nitric oxide (NO), nitrogen dioxide (NO_2), nitric acid (HNO_3), the nitrate radical (NO_3), nitrous acid (HONO) and an array of organic nitrogen compounds (collectively termed ON). Nitrogen fixation can occur naturally by two processes, biological nitrogen fixation (BNF) and lightning fixation of nitrogen. BNF, discovered by Beijerinck in 1901, can occur in both marine and terrestrial ecosystems and is carried out by a specialized group of prokaryotes.[1] The microorganisms rely on the enzyme nitrogenase to convert atmospheric N_2 to ammonia (NH_3). Nitrogen is also fixed naturally as NO_x ($NO + NO_2$) by lightning. A review of the global nitrogen cycle by Fowler *et al.* predicts that in 2010, the total global natural sources of reactive nitrogen were 203 Tg N yr^{-1}, of which 58 Tg N yr^{-1} was attributed to pre-industrial terrestrial BNF, 140 Tg N yr^{-1} to marine BNF, and 5 Tg N yr^{-1} to lightning fixation.[2] Pre-industrial terrestrial BNF was estimated by combining information on N fluxes with ^{15}N relative abundance data for terrestrial ecosystems, as described by Vitousek *et al.*[3] Pre-industrial terrestrial BNF is the rate of BNF before the global nitrogen cycle was altered by human activity and is estimated to be around 1750 (prior to substantial fossil fuel nitrogen fixation). Although this is a reasonable estimate, it is worth noting that some nitrogen fixation would have been altered by human land use by 1750. A further 210 Tg N yr^{-1} was formed *via* anthropogenic nitrogen fixation. In fact, an exceedance in the amount of reactive nitrogen produced by anthropogenic activities compared to natural processes has been observed throughout the last few decades and can be attributed to three main causes. The first Haber-Bosch process was developed in the early 1900s and relies on a high temperature and high pressure reaction between N_2 and H_2 in the presence of an iron catalyst to produce ammonia (NH_3).[4] It is estimated that the Haber-Bosch process was responsible for producing 120 Tg N of NH_3 annually in the first decade of the 21st century. Approximately 80% of the NH_3 is used as agricultural fertilizer and 20% is used as feedstock for industrial processes.[5] The second cause of increasing reactive nitrogen is the widespread cultivation of legumes, rice, and other crops that can convert N_2 to organic N through BNF. In 2008, Herridge *et al.* estimated that nitrogen-fixing agricultural crops and grazed savannahs were responsible for the fixation of 50 – 70 Tg N yr^{-1}.[6] Combustion is the third anthropogenic source of reactive nitrogen.

Combustion within internal combustion engines and industrial power plants oxidises atmospheric N_2 to NO_x. Additional NO_x can also be emitted from reactive nitrogen compounds present in the fuel, but this contribution is not representative of new reactive nitrogen fixation. van Vuuren *et al.* predicted that global NO_x production and emissions for the year 2000 were 40 Tg N yr^{-1}, of which 30 Tg N yr^{-1} is new reactive nitrogen, and the rest is from reactive nitrogen already present in fuel and biomass.[7]

A summary of the key processes in the atmospheric cycle of nitrogen compounds is shown in Figure 1.1. ON compounds, which undergo a more complex series of reactions in the atmosphere, are not included at this stage and will be discussed in considerably more detail later in this chapter.

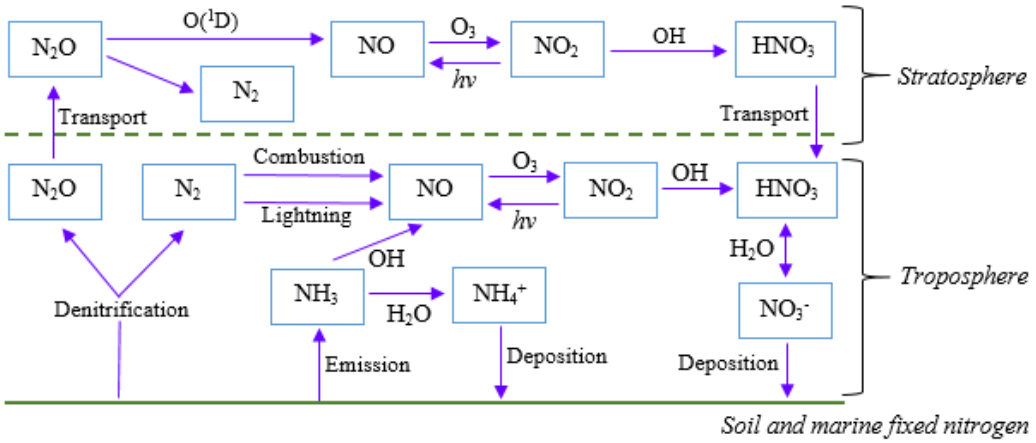

Figure 1.1. Key processes in the atmospheric cycle of nitrogen compounds. Adapted from Seinfeld and Pandis.[8]

The next section of this chapter will provide an overview of the sources and atmospheric behaviour of the key species in the atmospheric nitrogen cycle (Figure 1.1).

Nitrous oxide, N_2O: N_2O is emitted to the atmosphere as a result of bacterial action in soils and water. Whilst the concentration of N_2O in the atmosphere is considerably lower than CO_2 or H_2O, it is a potent greenhouse gas, due to its long residence time in the atmosphere and large energy absorption capacity per molecule (per unit mass the global warming potential of N_2O is 300 times that of CO_2).[8] The major sink of N_2O (~90%) is photodissociation in the stratosphere, as shown in Figure 1.1.

Ammonia, NH_3: The largest source of NH_3 in the atmosphere is agriculture, which includes emissions from animal husbandry and NH_3-based fertilizers.[9] NH_3 has a much shorter residence time than N_2O as it is readily absorbed by surfaces such as water and soil *i.e.* it is removed from the atmosphere by both wet and dry deposition. NH_3 acts as a base upon dissolution in water, which leads to the formation of ammonium (NH_4^+). NH_4^+ can exist as

various salts in atmospheric aerosol, such as ammonium sulphate ($[NH_4]_2SO_4$) and ammonium nitrate (NH_4NO_3).

Reactive odd nitrogen (NO_y): Reactive odd nitrogen, NO_y, can be defined as the sum of the two oxides of nitrogen (NO_x) and all compounds that are products of the atmospheric oxidation of NO_x.[10] These species include HNO_3, NO_3, HONO, N_2O_5, HO_2NO_2, peroxyacetyl nitrates ($RC(O)OONO_2$) and organic nitrates ($RONO_2$). N_2O and NH_3 are not considered to be NO_y species as they cannot be formed from NO or NO_2.

NO_x: NO_x is a collective term for two oxides of nitrogen, NO and NO_2. NO is the major oxide of nitrogen formed during high temperature combustion, either from the reaction of N_2 and O_2 in air, or the interaction of nitrogen in fuel with O_2. As shown in Equations 1.1 - 1.3, NO can undergo rapid oxidation to form NO_2 in the atmosphere. This occurs by reaction with O_3, or radicals formed during the photo-oxidation of volatile organic compounds (VOCs), such as hydroperoxy (HO_2) or alkyperoxy (RO_2).

$$NO + O_3 \rightarrow NO_2 + O_2 \quad (1.1)$$

$$NO + RO_2 \rightarrow NO_2 + RO \quad (1.2)$$

$$NO + HO_2 \rightarrow NO_2 + OH \quad (1.3)$$

NO_2 undergoes photo-dissociation at wavelengths less than 420 nm to give NO and an oxygen atom (Equation 1.4), the latter of which can react with molecular oxygen to form ozone (Equation 1.5).

$$NO_2 + h\nu \rightarrow NO + O \quad (1.4)$$

$$O + O_2 + M \rightarrow O_3 + M \quad (1.5)$$

Nitric acid, HNO_3: The atmospheric oxidation of NO_2 leads to the formation of HNO_3, which can rapidly undergo dissolution due to its high water solubility. As shown in Equation 1.6, HNO_3 dissociates readily to nitrate, further increasing its solubility. Gaseous NH_3 can neutralize condensed acidic nitrate through the formation of particulate ammonium nitrate (NH_4NO_3).

$$NO_{2(g)} + OH_{(g)} \rightarrow HNO_{3(g)} \leftrightarrow HNO_{3(aq)} \leftrightarrow NO^-_{3(aq)} + H^+_{(aq)} \quad (1.6)$$

Nitrate radical, NO_3: The NO_3 radical is formed from the reaction between NO_2 and O_3 (Equation 1.7). It is rapidly photolyzed in the daytime to form either NO or NO_2, for which the relative and absolute yields depend on the wavelength of light (Equations 1.8 and 1.9).[11] Significant concentrations of the NO_3 radical can build up at night-time when photolysis does not occur, making it one of the most important night-time oxidising species in the

troposphere. During the night, NO_3 can react with NO_2 to produce dinitrogen pentoxide, N_2O_5 (Equation 1.10).

$$NO_2 + O_3 \rightarrow NO_3 + O_2 \quad (1.7)$$

$$NO_3 + hv \rightarrow NO + O_2 \quad (1.8)$$

$$NO_3 + hv \rightarrow NO_2 + O \quad (1.9)$$

$$NO_3 + NO_2 + M \rightarrow N_2O_5 + M \quad (1.10)$$

Nitrous acid, HONO: Significant accumulation of HONO can occur overnight, and undergo photodissociation upon sunrise, injecting large amounts of OH radicals into the troposphere (Equation 1.11).[12] Oxidation by OH can also contribute to HONO losses (Equation 1.12).

$$HONO + hv \rightarrow OH + NO \quad (1.11)$$

$$HONO + OH \rightarrow H_2O + NO_2 \quad (1.12)$$

Whilst there are still some uncertainties surrounding the sources and transformations of HONO in the atmosphere, it is generally agreed that there are three main types of HONO formation. HONO can form homogeneously through reaction of NO with OH, heterogeneously through several pathways, or can be emitted directly. HONO is formed heterogeneously on surfaces through the reaction of NO_2 with H_2O.[13] Direct HONO emissions from vehicle exhausts,[14] aircraft[15] and biomass burning[16] have been reported. Due to the high levels of particulate nitrite (NO_2^-) observed in the troposphere in recent years, it has also been proposed that NO_2^- in aerosol serves as a reservoir for HONO.[17-18] The gas-to-particle partitioning of HONO, and the subsequent reversible reaction between HONO and NO_2^- is shown in Equation 1.13; production of particulate NO_2^- is likely to occur on aqueous surfaces such as wet aerosols, fog drops and surface water.[19]

$$HONO_{(g)} \leftrightarrow HNO_{2(aq)} \leftrightarrow NO_{2(aq)}^- + H_{(aq)}^+ \quad (1.13)$$

HONO is a source of OH to the atmosphere, but can also react with amines to form nitrosamines, which are a highly carcinogenic class of ON compounds. The role of HONO in nitrosamine formation will be discussed later in this chapter.

Organic nitrogen, ON: The chemistry of ON compounds is complex and will be discussed in more detail in the next section of this chapter. ON compounds contain at least one carbon atom and one nitrogen atom and include species such as amines, amides, amino acids, nitrophenols, nitriles, organic nitrates, nitrosamines, nitramines and nitrated polycyclic aromatic hydrocarbons (nitro-PAHs). This emerging class of pollutants originate from

various primary and secondary sources, exist in both the gas and particle phase, and span a wide range of polarities and volatilities.

To convert reactive nitrogen back to inert gaseous N_2, a process known as denitrification occurs, which is primarily carried out by bacteria in soils and water bodies. In some cases, a portion of the reactive nitrogen is converted back to the intermediate product, N_2O, which contributes to the greenhouse effect and stratospheric ozone depletion. Due to the increased anthropogenic production of reactive nitrogen in recent decades, there is now an excess of reactive nitrogen in the environment *i.e.* there is a lack of sufficient removal by denitrification processes. Excessive global quantities of reactive nitrogen have impacted a variety of environmental systems, including the atmosphere, agroecosystems, forests, grasslands, groundwater supplies, wetlands and rivers, and marine coastal regions. The relationships between these systems and the effects incurred when reactive nitrogen moves from one system to another can be referred to as the nitrogen cascade, and has been described by Galloway *et al.* in extensive detail.[20] For example, the main reactive nitrogen species emitted to the atmosphere are NO_x and NH_3. These species cannot form N_2 by denitrification, and undergo rapid internal cycling in the atmosphere before returning to the Earth's surface within hours or days. There is a cascade of effects which occur as a result of increased NO_x and NH_3 emissions; for example, VOC oxidation in the presence of NO_x can lead to the formation of fine particulate matter (PM) and O_3, both of which can have negative effects on human health.[8] Furthermore, elevated O_3 concentrations can contribute to the greenhouse effect, whilst fine PM can decrease atmospheric visibility and alter radiative forcing. Ozone deposition can also have a negative impact on agricultural crops, forests and other types of sensitive vegetation. NH_3 can be rapidly converted to ammonium aerosol, which can contribute to the direct and indirect effects of aerosol on radiative forcing.[21] NH_3 can also be deposited, along with NH_4^+, NO_y and ON, leading to ecosystem acidification, fertilization and eutrophication.[20] Various policies have been introduced in Europe for the abatement of excessive reactive nitrogen in the environment, such as the Convention on Long-Rang Transboundary Air Pollution (CLRTAP), the Sofia Protocol and the Gothenburg Protocol.[22] However, it will become increasingly important in the future to consider the impact of emerging pollutants such as ON compounds, and a better understanding of the behaviour of ON in the atmosphere is required if we are to produce effective mitigation strategies. The next section of this chapter will review previous studies of ON in the atmosphere and provide an overview of the main primary and secondary sources of ON, as well as the atmospheric transport and degradation pathways.

1.2 Atmospheric organic nitrogen compounds

ON is ubiquitous in the atmosphere; there are thousands of different species, spanning a wide range of polarities and volatilities. Classes of ON compounds include amines, amides, amino acids, urea, nitrophenols, nitro-PAHs, nitrosamines, nitramines, organic nitrates, nitriles, and a range of N-heterocyclic alkaloids. The general structures of the key ON functional groups are shown in Table 1.1. The complexity of ON in the atmosphere can be attributed to the fact that the many classes of compounds all have different sources, atmospheric processes and sinks. Although there has been extensive study of the sources, formation and composition of oxygenated organics in recent years, ON has been less well-characterized and a full description of its chemical composition is not available. ON compounds are challenging to measure using a single instrumental technique, especially as they are often present in trace level quantities within a complex atmospheric mixture. There is often a compromise between the number of functional groups identified and the percentage of the total ON analysed. It is important that better measurement techniques are developed for characterising ON species, as many classes of compounds are toxic and carcinogenic, posing a risk to human health. Several ON compounds are included in the US EPA's list of hazardous air pollutants, which are species known to cause cancer and other serious health effects. Several nitrosamines, amides and nitrosamines are listed, as well as other species such as quinoline, oxadiazon, *p*-nitrophenol, 2-nitropropane and ethyl carbamate.[23] It is important that we gain a molecular level understanding of how ON compounds behave in the atmosphere by studying different atmospherically relevant processes, such as photochemical degradation, brown carbon formation, and long-range transport. This will help us to understand how the composition of ON can vary in the atmosphere, and the impacts this can have on particle properties such as hygroscopicity, toxicity and bio-availability. In turn, a better understanding of ON in the atmosphere will allow for the impacts on both air quality and climate to be predicted more accurately.

Table 1.1. General structures of key ON functional groups. R, R' and R'' refer to H or an organic group *e.g.* alkyl, aryl etc.

Class of ON compound	General structure	Class of ON compound	General structure
Amine	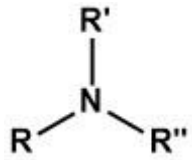	Nitrosamine	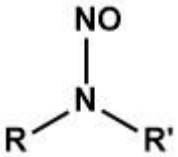
Amide	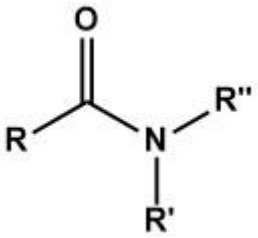	Nitramine	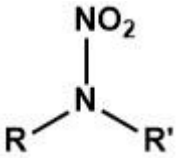
Imine	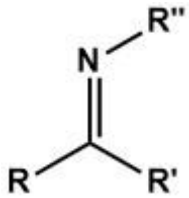	Nitro	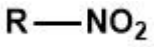
Nitrile	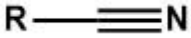	Organic nitrate	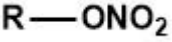

1.2.1 Atmospheric ON cycle

1.2.1.1 Sources of atmospheric ON

An overview of the main primary and secondary sources of ON (described by Cape *et al.*) is illustrated in Figure 1.2.[24] ON can be emitted from a wide range of primary sources, which are both biogenic and anthropogenic in origin, and include emissions associated with agriculture, biomass burning, combustion and vehicle exhaust, atmospheric dust, and marine biota. Table 1.2 provides a summary of the primary ON sources and the compounds that have been reported in the literature from each specific source. There are a variety of secondary processes responsible for both the formation of new ON compounds and the transformation of existing ON compounds. These processes include photochemical ON formation, gas-to-particle conversion, and reactions in solution. ON can be removed from the atmosphere to the surface by deposition of the gas, or by wet or dry deposition of particles.

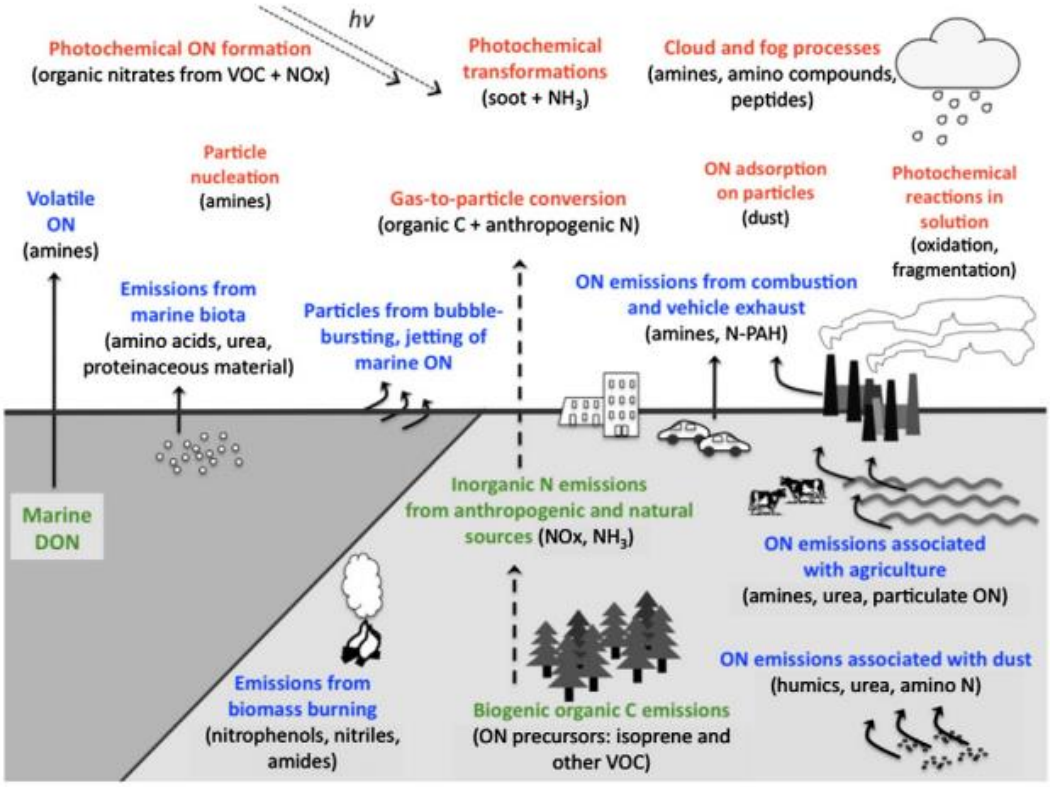

Figure 1.2. Illustration to show the ON precursors (green), primary sources (blue) and secondary processes (red) in the atmosphere. Image taken from Cape *et al.*[24]

In addition to the primary sources of ON compounds listed in Table 1.2, photochemical ON formation can also occur in the atmosphere. An example of this is the formation of organic nitrates ($RONO_2$) in polluted atmospheres. In the troposphere, OH radicals produced from the photolysis of O_3 or HONO can react with gas-phase organics to form alkyl radicals (Equation 1.14). The formation of alkylperoxy radicals (RO_2) occurs quickly as a result of the reaction of between alkyl radicals and O_2 (Equation 1.15). Whilst RO_2 radicals may react with each other, at higher NO_x levels there is an increased likelihood for RO_2 to react with either NO or NO_2 and form organic nitrates (Equations 1.16 to 1.18).[25]

$$RH + OH \rightarrow R + H_2O \quad (1.14)$$

$$R + O_2 + M \rightarrow RO_2 + M \quad (1.15)$$

$$RO_2 + NO + M \rightarrow ROONO + M \rightarrow RONO_2 \quad (1.16)$$

$$RO + NO_2 \rightarrow RONO_2 \quad (1.17)$$

$$RO_2 + NO_2 \rightarrow RO_2NO_2 \quad (1.18)$$

Table 1.2. Primary sources of ON compounds in the atmosphere and examples of previous studies.

Source	ON compounds	Example studies
Agriculture	Amines Urea	Ge *et al.* 2011[26] Cornell *et al.* 1998[27] Mace *et al.* 2003[28]
Biomass burning	Amines, Amides N-heterocyclic alkaloids Nitriles Nitrophenols Urea	Paglione *et al.* 2014[29] Simoneit *et al.* 2003[30] Laskin *et al.* 2009[31] Iinuma *et al.* 2007[32] Mace *et al.* 2003[28]
Carbon capture and storage	Amines Amides	Nielsen *et al.* 2012[33] Sexton *et al.* 2011[34] Zhu *et al.* 2013[35]
Combustion and vehicle exhaust	Amines Nitro-PAHs Nitrophenols Nitrosamines	Ge *et al.* 2011[26] Hu *et al.* 2013[36] Nojima *et al.* 1983[37] Goff *et al.* 1980[38]
Cooking	Amines Amides Nitro-PAHs N-heterocyclic alkaloids	Rogge *et al.* 1991[39] Wu *et al.* 1998[40] Abdullahi *et al.* 2013[41] Ge *et al.* 2011[26]
Dust	Amino N Humics, Urea	Timperley *et al.* 1985[42] Mace *et al.* 2003[28]
Marine sources	Amines Amino acids Urea	Muller *et al.* 2009[43] Kuznetsova *et al.* 2005[44] Matsumoto *et al.* 2005[45]
Tobacco smoking	Amides, Amines N-heterocyclic compounds Nitriles, Nitroalkanes Nitroarenes, Nitrophenols N-nitrosamines Tobacco-specific nitrosamines	Schmeltz *et al.* 1977[46] Hecht *et al.* 1988[47]

1.2.1.2 Fate of atmospheric ON

Whilst many ON species in the atmosphere will undergo secondary transformations and form particles, a fraction of the gaseous ON species will be removed to the surface by gas deposition, or will be rapidly destroyed by the OH radical.[26] The lifetimes of amines with respect to hydroxyl radical attack are typically on the order of hours for example. Schade and Crutzen studied the photochemical decomposition of methylamine and proposed the formation of various degradation products, including HCN, N_2O, CO, CO_2 and NH_3.[48]

There are several different routes for the formation of ON in the particle phase; these processes can be exemplified by considering the atmospheric behaviour of amines, as these compounds have been relatively well-characterised compared to other groups of ON compounds. An extensive review by Ge *et al.* reveals that amines can be emitted from a wide variety of sources, including cooking, tobacco smoke, animal husbandry, combustion and vehicle exhausts, sewage wastewater, pesticides, oceans, carbon capture and storage (CCS), vegetation and biomass burning.[26] One of the key atmospheric transformation processes to consider is atmospheric oxidation. The most dominant oxidation pathway for amines, and indeed many other tropospheric trace gases, is reaction with OH radicals.[49] For example, Nielsen *et al.* studied the atmospheric photo-oxidation of methylamine and found that the major products resulting from OH oxidation were methanimine and formamide.[50] N-nitromethylamine was a minor product and the yield depended on the local NO_x mixing ratios. It is also likely that O_3, Cl atoms and NO_3 radicals are relevant atmospheric amine oxidants.[33] Although there has been extensive study of amine gas-phase oxidation pathways involving OH and O_3, the resulting secondary aerosol formation has received less attention. The formation of secondary organic aerosol (SOA) is a result of the gas-to-particle partitioning of less volatile compounds formed upon oxidation. The extent of partitioning depends on the volatility of the compound, the gas phase concentration, and the amount of absorptive mass present.[51-52] The formation of PM can have adverse effects on human health, contributing to both lung and heart disease as well as premature mortality and morbidity, particularly among more sensitive population groups, such as asthmatics, children and the elderly.[53] The formation of fine particulates is of particular concern, as the deposition of particles upon inhalation is largely dependent on size. Smaller particles tend to reach lower parts of the respiratory tract, such as the alveolar region where gas exchange occurs, whereas larger particles are normally trapped in the upper respiratory tract and removed more rapidly.[54]

As many ON compounds are basic, they can also form particulate salts by reacting with gaseous atmospheric acids such as HNO_3 and H_2SO_4. For example, Equations 1.19 and 1.20 show the reactions between gaseous amines and HNO_3 and H_2SO_4 respectively.[55]

$$NR_{3(g)} + HNO_{3(g)} \leftrightarrow HNR_3NO_{3(s)} \quad (1.19)$$

$$2NR_{3(g)} + H_2SO_{4(g)} \leftrightarrow (HNR_3)_2SO_{4(s)} \quad (1.20)$$

Unlike the atmospheric reactions between gaseous ammonia and nitric or sulphuric acid, the reactions shown above have not been extensively studied. However, it is reported that the equilibrium of these reactions depends on temperature, relative humidity and particle acidity.[55] Another important process for amine particle formation, and indeed many other ON species, is reactive uptake into liquid aerosol. The two steps in the process are the equilibrium partitioning of the amine according to Henry's Law (Equation 1.21), and then dissolution of the aqueous amine in the aqueous phase to form an aminium ion (Equation 1.22).[56]

$$NR_{3(g)} \overset{k_H}{\leftrightarrow} NR_{3(aq)} \quad (1.21)$$

$$NR_{3(aq)} + H^+_{(aq)} \leftrightarrow HNR^+_{3(aq)} \quad (1.22)$$

Hygroscopic particles containing ON can be activated into cloud condensation nuclei (CCN) once they reach a critical size in diameter, enhancing the formation of cloud droplets, haze and fog.[56] ON compounds can be removed from the atmosphere by dry and wet deposition; as particulate amines are highly soluble in water, it is thought that these species are removed quickly by wet scavenging.[57]

Another important atmospheric transformation process to consider is particle nucleation, which leads to the formation of atmospheric nanoparticles (clusters and particles with a diameter less than 20 nm).[56] Murphy *et al.* studied secondary aerosol formation from atmospheric reactions of aliphatic amines and found that amines directly participated in particle nucleation events.[55] During the photo-oxidation experiments, trimethylammonium nitrate salt began to nucleate soon after the injection of trimethylamine into the photo-oxidation chamber. The concentration of nucleated salt particles peaked shortly after amine injection, and then decreased as the gas-particle equilibrium was established.

Whilst the sources of amines in the atmosphere have been extensively studied, a better understanding of their atmospheric degradation pathways is essential. Furthermore, there are several related species which require further attention, such as amides, imines, nitrosamines and nitramines. Many atmospheric ON species are of concern from a human health perspective; in particular, nitrosamines and nitramines are suspected to be highly toxic and carcinogenic and a more detailed discussion of these compounds is provided in the next section of this chapter.

1.2.2 Nitrosamines and nitramines

Non-specific nitrosamines (N-nitrosamines) are of interest due to their occurrence in the environment and their potentially detrimental effects on human health. Tobacco-specific nitrosamines (TSNAs), which are potent carcinogens formed specifically from the oxidation of the amine nicotine (the most abundant organic compound emitted during cigarette smoking).[58] Although less information is available in the literature, nitramines are also suspected to be damaging to human health.

1.2.2.1 N-nitrosamines and nitramines

N-nitrosamines ($R^1N(-R^2-)-N=O$) and nitramines ($R^1N(-R^2-)-NO_2$) can either be emitted to the atmosphere directly or formed *via* amine oxidation. N-nitrosamines have been classified by the International Agency for Research on Cancer (IARC) as extremely potent human carcinogens,[59] and have been highlighted as environmental contaminants of increasing health concern. Their carcinogenicity is determined by reviewing all relevant epidemiological studies and cancer bioassays in experimental animals. Table 1.3 shows the different IARC carcinogen classifications and examples of nitrosamines which belong to each category.[59] Nitramines are not included in Table 1.3, as their carcinogenicity has not been classified by the IARC.

Table 1.3. List of carcinogenic nitrosamines and their respective IARC classifications.[59]

IARC classification	Example nitrosamines
Group 1	N-nitrosonornicotine (NNN)*, 4-(N-nitrosomethylamino)-1-(3-pyridyl)-1-butanone (NNK)*
Group 2A	N-nitrosodiethylamine, N-nitrosodimethylamine
Group 2B	N-nitrosodi-n-butylamine, N-nitrosodiethanolamine, N-nitrosodi-n-propylamine, N-nitrosomethylethylamine, N-nitrosomethylvinylamine, N-nitrosomorpholine, N-nitrosopiperidine, N-nitrosopyrrolidine, N-nitrososarcosine.
Group 3	N-nitrosodiphenylamine, N-nitrosoproline, N'-nitrosoanabasine (NAB)*, N'-nitrosoanatabine (NAT)*
Group 1 – known carcinogen. Group 2A – probable carcinogen. Group 2B – possible carcinogen. Group 3 – not classifiable as to its carcinogenicity to humans. *Tobacco-specific nitrosamines.	

N-nitrosamines can be either emitted to the atmosphere directly *e.g.* from tobacco smoke, cooking or vehicle exhaust; alternatively they are formed *via* the photo-oxidation of gaseous

amines by various nitrogen oxides. These environmental contaminants have been found in food products,[60] cosmetic products,[61] house dust,[62] and water,[63] as well as in PM samples.[64-65] Nitrosation reactions can lead to the formation of N-nitrosamines during the production and storage of nitrite preserved meat products.[66] N-nitrosamine formation in meat products can depend on a number of factors, including residual and added nitrite concentration, cooking method and cooking time and temperature.[60]

N-nitrosodimethylamine (NDMA), which is a group 2A carcinogen, is amongst the most widely detected nitrosamine in drinking water.[67] It primarily forms during the chlorination of drinking water supplies, alongside other N-nitrosamines. The Californian Department of Public Health have recommended that NDMA levels in drinking water do not exceed 3 ng L^{-1}, to prevent possible detrimental health impacts.[68] N-nitrosamines directly emitted to the atmosphere include NDMA from leather tanneries and rubber and tyre industries.[69,70] The presence of NDMA and N-nitrosopyrrolidine have been reported in cooking emissions during the frying of bacon,[71] and Goff *et al.* have found NDMA and N-nitrosomorpholine in vehicle exhaust.[38] Schmeltz and Hoffman have reviewed the chemical components of tobacco smoke and report the presence of 8 different N-nitrosamines.[46] Whilst some N-nitrosamines may be produced directly, the majority of N-nitrosamines are formed by the atmospheric oxidation of amines. During the daytime, amine oxidation is dominated by reaction with the OH radical, which is produced photolytically. Reaction of amines with OH leads to hydrogen abstraction at either the -CH or the -NH group. If hydrogen abstraction occurs at the -NH group, nitrosamine and nitramine formation occurs due to the subsequent reaction with NO or NO_2 respectively. There have been various mechanistic studies of gas-phase amine + OH reactions,[33, 56, 72] and Scheme 1.1 shows the major routes in the atmospheric photo-oxidation of dimethylamine.[33, 50]

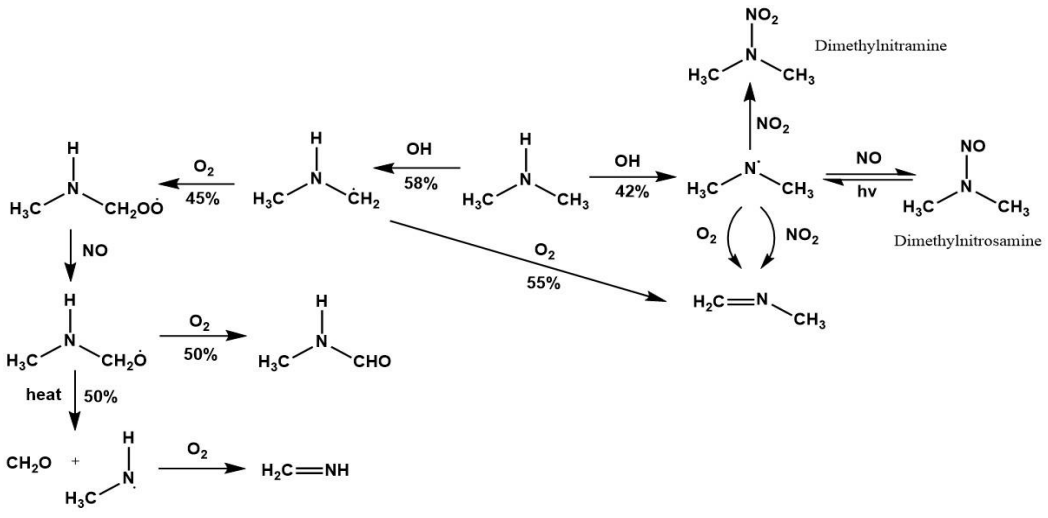

Scheme 1.1. Major routes in atmospheric photo-oxidation of dimethylamine.[33, 50]

Once formed, N-nitrosamines and nitramines continuously undergo photolysis and formation in the atmosphere, and therefore it is the overall amount of the N-nitrosamine or nitramine in the atmosphere that is of interest.[73] The Norwegian Institute of Public Health (NIPH) recommend that total nitrosamine and nitramine levels do not exceed 0.3 ng m^{-3} in the atmosphere.[74] Some nitrosamines and nitramines are more stable than others, which drastically affects the likelihood of formation and the potential cancer risk from exposure *via* inhalation. For example, primary nitrosamines undergo rapid decay to form a carbocation and N_2 gas,[75] whilst primary nitramines are not photolabile and may accumulate to significant levels in the atmosphere. Nitrosamine formation from secondary amines is more likely than from tertiary amines, as secondary amines can form nitrosamines directly, whereas dealkylation must occur before a tertiary amine can be nitrosated. In general, the same principle applies to nitramines *i.e.* the tertiary amine must be dealkylated to a secondary amine precursor. Overall, nitramines are more stable in the atmosphere than their nitrosamine counterparts. Recent studies, although limited, have suggested that whilst nitrosamines are photolyzed rapidly in the gas phase, significant concentrations of nitrosamines may persist in aerosol/fogs due to light shielding by nitrite or nitrate.[76] In terms of night-time nitrosamine and nitramine formation, it is likely that species such as HONO and the NO_3 radical (which are photolyzed during the day) play more of an important role. For example, Pitts *et al.* reported that gaseous diethylnitrosamine formation occurs in the dark when *ca*. 0.5 ppm of DEA is added to a 50 m^3 outdoor atmospheric simulation chamber at 20-50% relative humidity.[72] Ambient levels of NO and NO_2 were added to the chamber, which led to HONO formation. It was found that the nitrosamine yield was approximately 3%, and depended on the amount of HONO initially present. There are a limited number of studies which report the presence of N-nitrosamines in ambient air. For example, Özel *et al.* collected $PM_{2.5}$ samples at an urban background site in Birmingham and detected N-nitrosodiethylamine, N-nitrosopiperidine and N-nitrosodibutylamine at average concentrations of 0.3, 12.1 and 1.4 ng m^{-3} respectively.[77] In Tarragona, PM_{10} samples were collected at urban and harbour-side locations. N-nitrosomorpholine, N-nitrosopyrrolidine and N-nitrosopiperidine were detected, and reported maximum concentrations were 0.2, 1.8 and 0.3 ng m^{-3}.[65] Furthermore, N-nitrosamines were detected in the Zonguldak province of Turkey, and were attributed to the coal mining and iron-steel industries in the area.[64]

1.2.2.2 Tobacco-specific nitrosamines (TSNAs)

TSNAs form specifically from nicotine oxidation, which is the most abundant organic compound emitted during smoking.[58] Scheme 1.2 shows the structures and formation pathways of the main TSNAs.[73] TSNAs are some of the most commonly occurring carcinogens in tobacco smoke and can induce lung, oral, oesophageal and pancreatic

cancer.[78] As shown previously in Table 1.3, NNN and NNK are group 1 carcinogens (known carcinogens) whilst NAB and NAT are group 3 carcinogens (not classifiable as to its carcinogenicity to humans).[59] The carcinogenicity of NNAL has not yet been assessed by the IARC but it is likely that this compound also has harmful effects on human health.

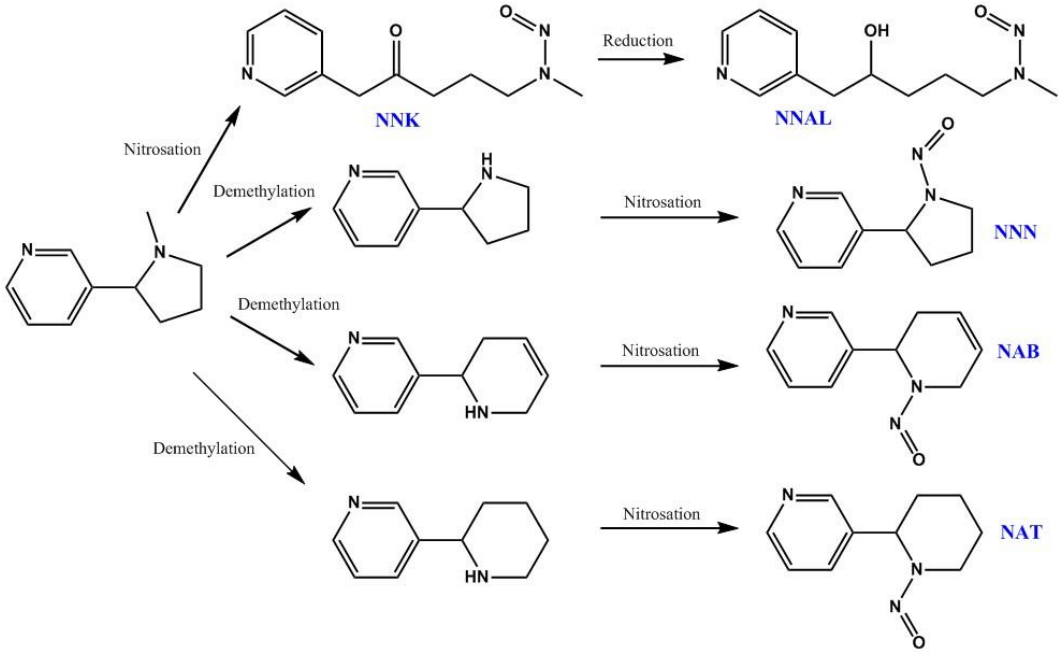

Scheme 1.2. Structures and formation pathways of the main TSNAs.[73]

TSNAs can be released directly from tobacco smoke, or can form during atmospheric oxidation of nicotine emitted during smoking. In addition, Sleiman *et al.* have reported that TSNAs can form *via* surface-mediated reactions of nicotine with HONO.[79] Residual nicotine from tobacco smoke sorbed to indoor surfaces can react with ambient HONO (which is less vulnerable to photolysis in indoor environments) to form TSNAs. The study raised concerns about exposure to tobacco smoke residue, that has recently been referred to as 'third-hand smoke'.[80] To address these concerns, Ramirez *et al.* carried out a number of studies which investigated the presence of both N-nitrosamines and TSNAs in house dust.[62, 73] House dust is often contaminated with residual smoke gases and particles, which can revolatilise to gas phase species or breathable particles, posing a risk to human health from exposure *via* inhalation. Furthermore, non-dietary ingestion of settled house dust, and dermal absorption from the dust attached to fabrics and surfaces are also concernable routes of exposure. This is particularly concerning for young children and toddlers, as they spend relatively more time indoors, have hand-to-mouth behaviours, and are more vulnerable to chemical exposure due to their immature metabolism.[81] The study by Ramírez *et al.* found that for children aged 1 to 6 years old, the cancer risks from exposure to the observed levels of TSNAs exceeded the upper-bound risk recommended by the US EPA in 77% of smokers' and 64% of

non-smokers' homes.[73] Furthermore, the presence of N-nitrosamines in house dust in non-smokers' homes, and its lack of correlation with nicotine, indicated that the main source of these compounds was likely to be outdoor ambient air pollution.

As a result, it is essential to gain a better understanding of the formation of N-nitrosamines and TSNAs in ambient air. To our knowledge, there are only limited studies of N-nitrosamines in ambient air and no studies of TSNAs in ambient air. Accurate time-resolved measurements of these compounds in the atmosphere are essential, in order to assess the cancer risk from exposure to these carcinogens. The next section of this chapter will focus on another potential source of nitrosamines and nitramines in the atmosphere, amine-based post-combustion carbon capture.

1.2.3 Carbon capture and storage (CCS)

CCS is the fasting growing industrial use of amines, and incorporates a range of technologies designed to reduce the amount of CO_2 emitted to the atmosphere. Amines are used as solvents to absorb or 'capture' the CO_2. In 2015, the amount of CO_2 emitted to the atmosphere was estimated to be 36 billion tonnes, and so reductions in the amounts of this greenhouse gas are essential.[82]

1.2.3.1 Commercialisation of CCS

Large scale CCS facilities can be defined as those which are capable of capturing at least 800,000 tonnes of CO_2 per annum from coal-based power plants, or at least 400,000 tonnes of CO_2 per annum from other emissions-intensive industrial facilities.[83] Currently, the only operational large-scale post-combustion CO_2 capture plant is the Boundary Dam facility in Canada, which began operating in 2014 and captured 800,000 tonnes of CO_2 in 2016, with the carbon capture process in operation 85% of the time throughout the year.[84] There are 4 other post-combustion capture facilities anticipated to start operating in the 2020's, all of which will rely on the use of amine solvents to absorb CO_2. These facilities are located in the Netherlands, South Korea and China (Shanwei City and Dongying City).

Aside from large-scale projects there are also numerous other pilot and demonstration projects across the globe, which rely on a range of capture technologies and provide essential information for the design and development of large scale CCS facilities. For example, the largest hydrogen production unit in France, located at Port Jérôme in Normandy, relies on a cryogenic process to capture CO_2 released during hydrogen production; the system has an annual capture capacity of 100,000 tonnes of CO_2 at the site.[85] There are also a wide range of test centres and other initiatives which are mainly located in North America and Europe. Technology Centre Mongstad (TCM) in Norway is located next to the Mongstad oil refinery

on the West coast of Norway and has been operating since summer 2012.[86] Two main types of post-combustion CO_2 capture are being tested, amine-based chemical absorption and chilled ammonia absorption. The main aims of TCM are to test different CO_2 capture technologies owned by vendors, reduce environmental and financial risks, and encourage the international development of CO_2 capture technologies.

1.2.3.2 Amine-based CCS technology

CCS technologies that rely on amine solvents for CO_2 absorption may have potentially detrimental effects on the environment and human health as there is potential for small amounts of amines to escape into the atmosphere.[33] Figure 1.3 shows a schematic for a typical post-combustion CO_2 set up.[87] The first stage of the process is CO_2 absorption. Flue gas containing CO_2 (from a coal power plant for example) enters the bottom of an absorption tower, which is comprised of an 8 – 12 m absorption column. An aqueous amine solution is added to the top of the column, and a chemical absorption process occurs when the flue gas and the liquid amine interact, leading to the formation of carbamate salts. The metallic structured packing of the absorption column provides a large surface area for the gas and liquid to meet, which drastically improves the efficiency of the capture process.[88] The flue gas left over after CO_2 has been removed is cleaned in a water wash at the top of the absorption tower. This removes the residual amines from the flue gas before it is released to the atmosphere. The next stage of the process is to separate the CO_2 rich amine solvent so that the CO_2 is ready to be compressed and transported to storage, and the liquid amine solution can be pumped back to the absorber for reuse. This process occurs in the regenerator, where steam is used to reverse the chemical reaction between the amine and CO_2. As this reverse reaction is endothermic, the heat from the steam provides the energy of dissociation to release the CO_2 from the aqueous amine solution.[89]

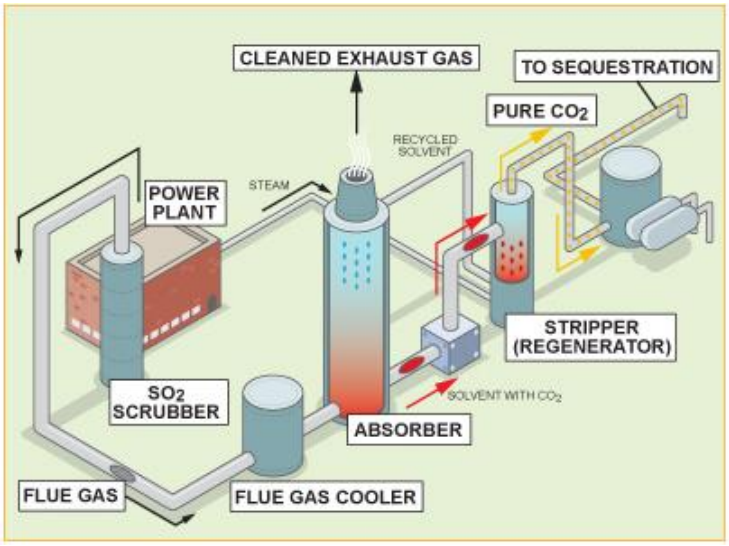

Figure 1.3. Schematic of a typical post-combustion CO_2 capture plant.[87]

1.2.3.3 Nitrosamine and nitramine formation

In 2009, amine emissions were estimated for a proposed full scale CO_2 capture plant at the 420 MW gas power plant in Kårstø, Norway.[89] Without CCS, this power plant has the potential to emit 1.2 million tonnes of CO_2 per year if operated continuously. The implementation of CCS could potentially emit 40 to 160 tonnes per year of amine emissions, creating atmospheric amine concentrations of 1 – 4 ppm in the region. Once the amines are in the atmosphere, they may react with oxidants and NO_x to form carcinogens such as nitramines and nitrosamines. For example, Scheme 1.3 shows the atmospheric photo-oxidation of morpholine to form both N-nitrosomorpholine and N-nitromorpholine. N-nitrosomorpholine has been classified by the IARC as a group 2b carcinogen *i.e.* it is a possible human carcinogen.[59] Whilst there is no toxicity data available for N-nitromorpholine, it is also assumed to be carcinogenic.

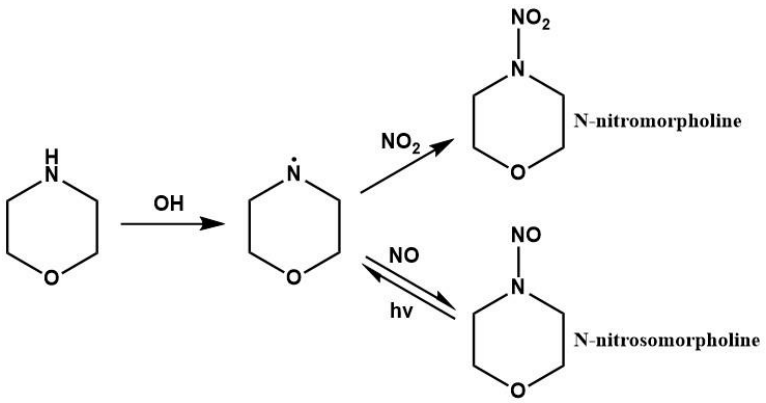

Scheme 1.3. Atmospheric photo-oxidation of morpholine to form N-nitromorpholine and N-nitrosomorpholine.

A better understanding of the implications of amine emissions from CO_2 capture plants can only be achieved by investigating the subsequent atmospheric behaviour of the amines once they are emitted. Characterising the degradation pathways of individual amines under atmospherically relevant conditions using an outdoor atmospheric simulation chamber can provide valuable information. In this type of experiment, a suite of analytical instruments can be used to measure organic and inorganic compounds in both the gas and particle phase. The information obtained can be fed into theoretical models and used to predict steady-state concentrations of carcinogenic compounds such as nitrosamines and nitramines in the atmosphere. As nitrosamines and nitramines are constantly undergoing photolysis and formation in the atmosphere, the steady-state predictions are a useful way to determine whether emissions from CO_2 capture plants fall within recommended guidelines.[74] In turn, these results will allow for more accurate environmental impact assessments to be carried out, and for more informed decisions to be made regarding the implementation of CCS.

1.3 Measurement techniques for atmospheric ON

1.3.1 'Bottom-up' vs 'top-down' approach

Over the last century, dissolved ON in precipitation has been studied extensively due to its important role in atmospheric nitrogen deposition.[90] The methods developed for measuring ON in rainwater and fog were applied to early studies of ON in atmospheric aerosol, and therefore the results obtained were representative of the water-soluble organic nitrogen (WSON) fraction of aerosol. In order to determine total WSON in rain and aerosol samples, Equation 1.23 can be used, in which ON is expressed as total nitrogen (TN) minus inorganic nitrogen (IN).[91] This is referred to as the 'top-down' approach. IN is mainly comprised of NH_4^+, NO_3^- and NO_2^- and can be measured by ion chromatography or colourimetry.

$$ON = TN - IN \tag{1.23}$$

After the inorganic components have been measured, strong oxidation can be applied to convert all nitrogen-containing compounds to their inorganic form, enabling an estimation of TN to be made. There are various different oxidising techniques that can be used, such as wet chemical oxidation using strong chemical oxidants,[24] photochemical oxidation,[92] and high temperature oxidation with or without a catalyst.[93-94] The main problem with this method is the propagation of errors associated with three individual analyses. This is particularly problematic when analysing samples of low ON concentration and high IN concentration; in some cases the coefficient of variation may be of the same order of magnitude as the concentration.[90] Most analyses that use the 'top-down' approach have been carried out on aqueous aerosol filter paper extracts or filtered rain samples, meaning that

measurements are often only representative of WSON content. This means that there are likely to be a range of non-water-soluble or partially soluble ON species which are unaccounted for. Zhang *et al.* estimated WSON in $PM_{2.5}$ from northern California and reported an average concentration of 3.6 µgN m^{-3}.[57] Other examples include the investigation of seasonal variations of WSON in a deciduous forest in Japan,[95] as well as measurements of WSON during the fog season in the Po Valley, Italy.[96] Duan *et al.* calculated total ON (rather than WSON) using PM samples collected in Beijing, China.[97] Approximately 30% of TN was found to exist as ON, with an average concentration of 3.2 µgN m^{-3}. Further studies have highlighted the significance of a non-water soluble (NWSON) fraction. For example, Russell *et al.* measured the NWSON fraction of atmospheric nitrogen at the mid-Atlantic US coast, and found it to be three times larger than the water-soluble fraction.[98] In another study, total ON was determined in remote marine aerosols and the proportion of ON in TN was high compared with other studies – on average, ON contributed 70% to TN, suggesting the possible presence of NWSON components.[99]

It is clear that to characterize the ON fraction of aerosol in greater detail a 'bottom-up' approach is required, which involves measuring ON compounds individually using a separation technique such as gas chromatography (GC) or liquid chromatography (LC). For the best results, a technique that can measure as many different classes of ON compounds as possible is needed, thus characterizing as much of the total ON fraction as possible. As there are thousands of ON compounds in the atmosphere that span a wide range of volatilities and polarities, there is not currently an instrumental technique capable of measuring every single ON compound present in ambient air. However, one particularly powerful technique is comprehensive two-dimensional gas chromatography (GC×GC), which will be discussed in more detail later in section 1.3.2. There have been a limited number of studies of ON compounds in aerosol using GC×GC. For example, Ochiai *et al.* used a combination of quadrupole mass spectrometry (QMS) and nitrogen phosphorus detection (NPD) coupled to GC×GC to predict the identity of 15 nitrogen-containing compounds in nanoparticles (29 - 58 nm particle diameter) in a roadside atmosphere.[100] Furthermore, Özel *et al.* have performed two GC×GC studies of ON compounds in urban aerosol samples.[77, 101] The measurements made at an urban background site in Birmingham led to the detection of 57 ON compounds using GC×GC-NCD, including nitriles, nitrophenols, alkyl nitro compounds, amides, nitrosamines and nitro-PAHs.

A typical method used to collect atmospheric aerosol for quantitative analysis is sampling onto quartz microfibre filters. To prepare the aerosol filter samples for analysis by GC, the target compounds need to be extracted from the solid matrix. Pressurized liquid extraction (PLE) is a relatively new technique which relies on using high temperature solvents

(maintained in the liquid state by applying pressure to the extraction cell) to extract analytes from an aerosol filter sample.[102] At temperatures of around 100 – 200 °C, and high pressures of approximately 100 bar, the solvent is considered to exist in its subcritical state, exhibiting advantageous mass transfer properties. For example, the high temperature means that the solvent is less viscous, with an improved ability to disrupt solute-matrix interactions and solubilise the target compounds.[103] Furthermore, the elevated pressure favours infiltration of the solvent into the matrix, which also aids with the extraction process. There has been a growing interest in PLE in the last decade and a variety of commercial systems are now available. The technique is generally favoured over more traditional extraction methods, such as Soxhlet extraction, sonication, and solid-liquid extraction. These older techniques tend to be more time-consuming, requiring large amounts of samples and organic solvents (which are expensive and have a negative impact on the environment), and additional concentration and clean-up steps are often needed prior to sample analysis.[104] PLE is a highly efficient and reliable extraction technique that can easily be automated, and offers improved extraction yield alongside reduced solvent consumption. The numerous advantages of PLE means that it is suitable for compounds that are sensitive, thermolabile or present in low concentrations. The degradation of thermolabile compounds can be avoided by carefully optimizing extraction parameters. PLE has been adopted by the US EPA and many laboratories as a sample preparation technique.[105-106] It has been applied to several solid matrices for the extraction of environmental contaminants, such as soils,[107] house dust,[62, 73] and sewage sludge.[108] Moreover, it has proven to be a suitable technique for complex atmospheric PM samples, demonstrated by the extraction of contaminants such as N-nitrosamines,[65] PAHs,[109] phthalates and organophosphate esters.[110]

1.3.2 Comprehensive two-dimensional gas chromatography

Comprehensive two-dimensional gas chromatography (GC×GC) was first introduced by Phillips in the 1990s,[111-112] and was later applied to the analysis of atmospheric samples in 2000.[113] GC×GC is an orthogonal hyphenated chromatographic technique that has revolutionised the analysis of complex organic mixtures. Figure 1.4 shows a schematic for a typical GC×GC setup; the modulator is positioned between two columns, which usually have distinctly different separation mechanisms. For example, the first GC column may be a long (~30 m) non-polar column that separates compounds according to their volatility, whilst the second GC column is often a mid-polarity column of much shorter length (~ 0.5 – 3 m), which separates compounds according to their polarity under essentially isothermal conditions.

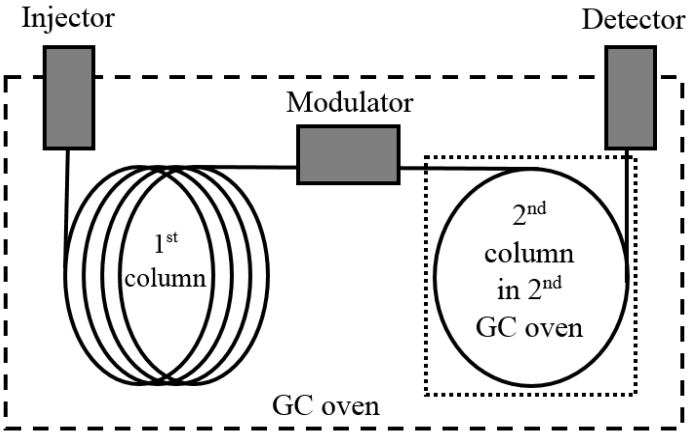

Figure 1.4. Schematic of a typical GC×GC system.

The modulator is used to transfer small fractions of eluent from the first column to the second column. The modulation cycle, which is the time between two successive injections of analyte into the second column, typically lasts around 5 s. As the second column is very short, separation in the second dimension can be completed within an individual modulation cycle. Ideally the modulator should be able to concentrate a small fraction of eluent and release it onto the second column in a narrow band to ensure that maximum resolution on the second column is achieved.[114]

The most commonly used modulators in atmospheric chemistry are cryogenic and valve modulators. Valve modulators operate by means of a switching valve, which diverts eluent from the primary column to the secondary column. The first valve modulator was introduced by Bruckner *et al.* in 1998,[115] but there has since been extensive work to improve the sensitivity and reliability of valve modulators.[116-119] The GC×GC systems described throughout this thesis rely on cryogenic modulation. Whilst these modulators are highly reliable and can operate across a large temperature range, they are expensive to buy and operate (due to the large quantities of cryogen consumed). The first cryogenic modulator was the longitudinal modulated cryogenic system developed by Marriott and Kinghorn in 1997.[120-124] Modulation was achieved through the use of a mechanical cryogenic trap, which moved along the column to focus and release analytes onto the second column; unfortunately the use of moving parts on a fragile GC column led to various operational problems over time. As a result, Beens *et al.* developed a cryogenic modulator that does not rely on moving parts, instead focusing analytes using liquid CO_2.[125] In this system, an alternating cycle of two CO_2 jets is used to trap and release analytes. The design was further modified and in 2000, Ledford and Billesbach reported an improved CO_2 jet-cooled modulator.[126] An illustration of the sequence of events responsible for trapping, releasing and re-focusing, and re-injecting the analytes into the second column is shown in Figure 1.5.[127] The cold jets flow

continuously, and solenoid valves are used to pulse hot jets of gas when required. This dual-stage quad-jet cryogenic modulator drastically minimizes the breakthrough of analytes. However, the main drawback of the modulators developed by both Beens *et al.* and Ledford and Billesbach is the use of liquid CO_2. The temperature of liquid CO_2 is approximately -70 °C, which is not sufficient to focus highly volatile compounds such as benzene and butadiene. Pursch *et al.* resolved this problem by developing a modulator that utilizes liquid N_2 for cryo-focusing instead of liquid CO_2.[128] Lower temperatures can be reached using liquid N_2, improving the efficiency of the modulator and allowing highly volatile analytes to be captured. Liquid N_2 can also be used to pre-cool gaseous N_2 for modulation, and such systems have been commercialised by ZOEX Corporation and LECO Corporation. The LECO modulators relying on cooled N_2 gas are installed in the GC×GC systems discussed throughout this thesis.

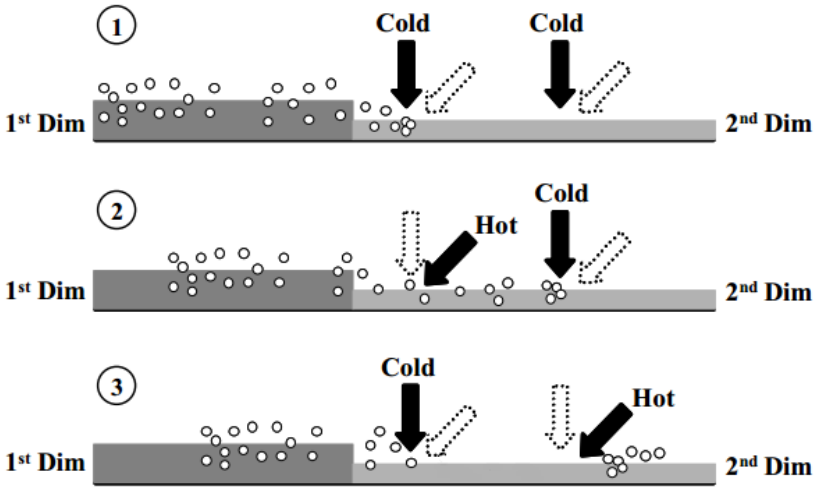

Figure 1.5. Sequence of events responsible for (1) trapping, (2) releasing and re-focusing, and (3) re-injecting into the second column using a dual-stage quad-jet cryo-modulator. Diagram adapted from Focant *et al.*[127]

As GC×GC is an orthogonal technique, *i.e.* it relies on two different independent separation mechanisms, the peak capacity is considerably greater than one dimensional or heart-cut GC systems.[129] This means that much greater resolution can be obtained when analysing complex organic mixtures. In addition, the modulation process leads to the production of very narrow peaks in the second dimensions (peak width ~ 10 – 100 ms), which due to mass conservation means that sensitivity is drastically improved compared to one dimensional GC.[130] Whilst analysis and interpretation of complex mixtures can be challenging, compound identification is made easier by the fact that GC×GC produces ordered chromatograms in which compounds of similar functionality are grouped into bands.

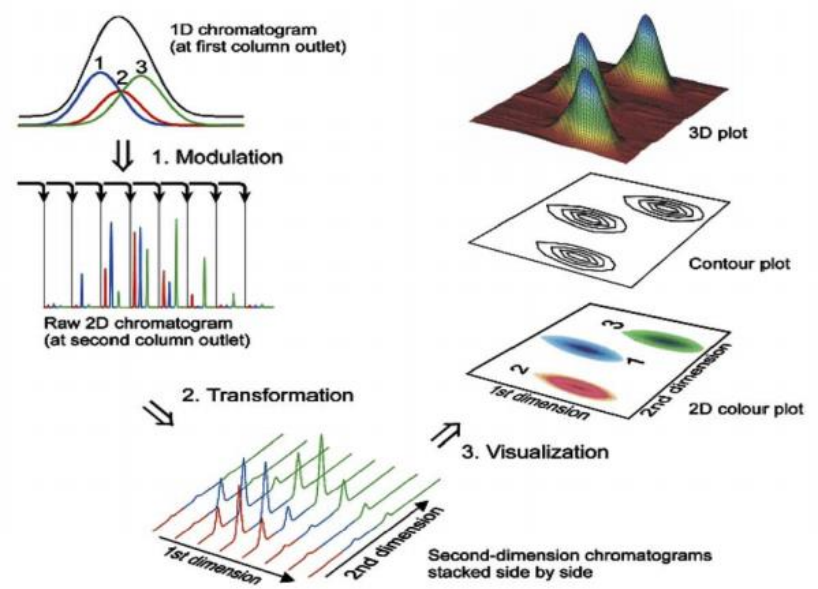

Figure 1.6. Data generation and visualization in GC×GC.[131]

As shown in Figure 1.6, there are several stages in the GC×GC data generation and visualization process.[131] The diagram in stage 1 shows the co-elution of three analytes in the first dimension, which undergo modulation and are transferred as narrow bundles of eluent to the second column. This produces a series of short second-dimension chromatograms in which the three analytes have been resolved. As shown in stage 2, the data is then transformed into a 2D representation, in which the second-dimension chromatograms are stacked side by side, and the two axes represent first and second retention time. Further data treatment is carried out (represented by stage 3) using specialised GC×GC software, in order to visualize the data as either a 2D colour plot or 3D contour plot.

All GC detectors must be reliable and stable, offer high sensitivity and a linear response over a wide range of analyte concentrations, and have a low background signal. In GC×GC a detector with a high acquisition rate is also particularly important; narrow peak widths of tens to hundreds of ms can be achieved, and therefore the detector must have a sufficient acquisition rate (tens to hundreds of Hz) to fully characterize the eluting peaks. Various detectors can be used with GC×GC, including the flame ionization detector (FID), and different types of mass spectrometers and element-specific detectors. During FID detection, organic compounds eluting from the GC column are combusted in a hydrogen flame, resulting in the formation of ions which are monitored using a detector electrode.[132] There is a potential difference between the jet and the electrode, so when ions form a signal is recorded due to the increase in current. The FID is a stable and robust detector offering high sensitivity, yet the lack of structural information obtained means that more powerful detectors can sometimes be required to analyse complex mixtures.

GC×GC coupled to mass spectrometry creates an extremely powerful technique, as mass spectral information is obtained for each individual peak separated by the GC×GC system. A review by Tranchida *et al.* assessed the number and type of GC×GC-MS applications between 2008 and 2014 and revealed that 17% of the published work since 2008 relied on the use of quadrupole mass spectrometry (QMS).[133] It was extensively reported in these works that whilst QMS instruments can be used for qualitative purposes, they are too slow for GC×GC quantification. The most popular system, used in roughly 78% of the published work between 2008 and 2014, was GC×GC coupled to low mass resolution time-of-flight mass spectrometry (TOF-MS).[133]

There are also a range of more selective detectors that can be used with GC×GC for atmospheric analysis. Nitrogen-specific detectors are ideal for the analysis of ON compounds in complex atmospheric mixtures and are therefore discussed in more detail in the next section of this chapter.

1.3.3 Nitrogen-specific detectors

The most common nitrogen-specific detectors are the nitrogen chemiluminescence detector (NCD)[134] and the nitrogen-phosphorus detector (NPD).[135] The NPD relies on an electrically heated novel alkali metal salt and a conventional flame ionization detector jet and block assembly; ionization of the compounds occurs in a low-temperature plasma rather than a flame.[135] The detector response is approximately 100,000 times more sensitive to nitrogen- and phosphorus-containing compounds than normal hydrocarbons, and therefore generates a linear response selective to organic compounds containing nitrogen or phosphorus.[136]

The NCD was used for all applications in this thesis and Figure 1.7 shows a schematic diagram of the NCD, including the dual plasma burner and dual plasma controller.[137] The detector can be coupled to either a GC or GC×GC system, and effluent from the GC column undergoes a two-stage combustion process at 900 °C in the dual plasma burner. During the first stage, analytes are combusted in an oxygen rich flame (plasma), which converts ON compounds to nitric oxide (NO) and potentially other nitrogen oxide species. The second combustion stage relies on a catalyst to ensure any other nitrogen oxide species are converted to NO. The two-stage combustion technique, which is summarised in Equation 1.24 also converts hydrocarbons to CO_2 and H_2O, which do not chemiluminesce with ozone.[137] As shown in Figure 1.7, hydrogen and oxygen are supplied to the dual plasma burner, preventing the formation of background NO in the detector flame. Operational parameters such as burner pressure, burner temperature, and hydrogen and oxidant flow rate are controlled by the dual plasma controller.

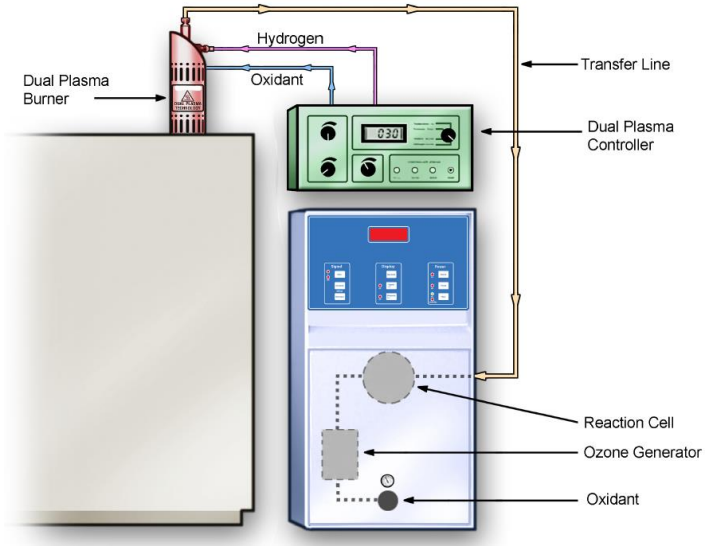

Figure 1.7. Schematic diagram of the NCD with dual plasma burner and dual plasma controller.[137]

$$R - N \xrightarrow{H_2, O_2, \Delta} NO + CO_2 + H_2O \quad (1.24)$$

$$NO + O_3 \rightarrow NO_2^* + O_2 \rightarrow NO_2 + O_2 + hv \quad (1.25)$$

The next stage of the detection process occurs in the reaction cell and is summarised in Equation 1.25. Ozone, produced by corona discharge from a source of oxygen, reacts with NO to produce electronically excited nitrogen dioxide (NO_2*). As NO_2* relaxes back to the ground state, light is emitted in the red and infrared region of the spectrum; this light is optically filtered using a red cut-off filter, and is detected by a photomultiplier tube. The number of photons detected is proportional to the amount of nitrogen in the sample. Although a small background signal is inevitable, due to ozone-wall interactions and low level nitrogen contamination from carrier and detector gases, the combination of an efficient dual-stage combustion process and red cut-off filter eliminates interference from other species that have chemiluminescence reactions with O_3, such as SO_2 and alkenes.[137] This means that the NCD is highly specific to ON compounds, ammonia, hydrazine, hydrogen cyanide and NO_x, and there are no interferences from non-nitrogen-containing species in the sample matrix, allowing complex air samples to be analysed.[138] The NCD offers excellent repeatability and a linear response over at least four orders of magnitude;[139] O_3 is in excess during detection, so the reaction with NO is pseudo first order and the detector response is linear to the nitrogen concentration in the original sample.[140] As all the ON compounds are converted into NO during combustion, the NCD should exhibit an equimolar response to ON compounds, regardless of the molecular structure of the analyte or its chemical environment. This allows for ease of calibration and accurate quantitation of various ON compounds, without requiring analytical standards for every single analyte.[140] This is highly

advantageous when compared to the NPD response, which can vary by up to 30-fold depending on how the nitrogen is bound in the compound, making quantitation of unknowns highly unreliable.[139] In addition, the NCD is not subject to solvent quenching (unlike the NPD)[139] and offers picogram detection limits for a wide range of different ON compounds, such as nitrosamines, nitroalkanes, nitriles, amides and nitrophenols. It is possible to reach such low detection levels because the chemiluminescence process occurs in a dark environment without interference from other light sources, allowing the full sensitivity of the detection system to be utilised.[140]

GC-NCD has been used for a variety of applications, including petroleum analysis, the food/flavour industry, and environmental analysis. For example, in 1995 Tomkins *et al.* developed a method relying on GC-NCD to determine ppt levels of N-nitrosodimethylamine (NDMA) in groundwater.[141] GC-NCD has also been used to detect trace levels of 2-ethylhexyl nitrate in diesel fuel, which is used to enhance the cetane number of the fuel.[142] Although NPD can also be used in various applications, such as the determination of N-nitrosamines in tap and swimming pool water,[143] NCD is generally viewed as a better alternative for the detection of trace level ON compounds. For example, Grebel *et al.* carried out a comparative study of NPD and NCD for the detection of volatile nitrosamines in water matrices and reported that NCD showed greater sensitivity to the compounds than NPD.[63] Whilst both NCD and NPD compared favourably with chemical ionization mass spectrometry results for NDMA analysis in a variety of water samples, the instrument detection level for NDMA was lower for NCD (2.6 μg L^{-1}) than NPD (4.0 μg L^{-1}). Furthermore, Ramírez *et al.* compared GC×GC-NCD and gas chromatography-ion trap-tandem mass spectrometry (GC-IT-MS) for determining nicotine and carcinogenic ON compounds in thirdhand tobacco smoke and found that whilst the GC-IT-MS method performed well, the optimized GC×GC-NCD method gave lower limits of detection (4 – 22 ng g^{-1}) and better repeatability and reproducibility at low concentration levels (%RSD < 8%).[144]

1.3.4 Complementary techniques

The GC×GC-NCD system is a highly sensitive and specific technique suitable for the determination of trace level ON compounds in complex atmospheric matrices, but peak identification is based solely on direct comparison of retention times on both GC columns to those of individual standards. Compound identification is made easier by the fact that GC×GC produces ordered chromatograms in which compounds of similar functionality are grouped into bands, but the nitrogen-specific detector does not provide mass spectral information. As a result, it can be beneficial to use GC×GC-TOF-MS as a complementary

technique. Whilst it is considerably more difficult to detect and quantify trace level ON compounds using GC×GC-TOF-MS due to the presence of hundreds of more abundant hydrocarbons in atmospheric mixtures, mass spectral information is obtained for the fraction of ON compounds that can be resolved. This provides a useful insight into the types of ON compounds that are likely to be present in the atmospheric sample. It is then possible to purchase a range of carefully selected analytical standards, and inject them into the GC×GC-NCD system to determine which ON compounds are present. The use of GC×GC-NCD and GC×GC-TOF-MS as complementary techniques means that a greater number of ON compounds can be characterised. Furthermore, the GC×GC-TOF-MS also provides additional information about the non-nitrogen-containing fraction of the aerosol, meaning that various groups of compounds such as alkanes, alkenes, aromatics, ketones and esters can be detected.

Ion chromatography (IC) is also a useful complementary analytical technique, as it can be used to investigate the inorganic nitrogen fraction of atmospheric aerosol, through the accurate quantification of NO_3^-, NO_2^- and NH_4^+. In addition, IC can also be used to measure other water-soluble ions in atmospheric aerosol, such as SO_4^{2-}, Cl^-, Na^+, Ca^{2+} and K^+, as well as various organic acids and protonated amines. IC is a form of liquid chromatography that relies on ion exchange to separate and quantify various anions and cations in an ionic solution. Ions in the sample solution are carried through the system by an ionic solution, known as the eluent or mobile phase. The separation column is packed with an ion exchange resin, which is coated with either positive or negative charged active sites, to analyse anions or cations respectively. Ions migrate through the IC column at different rates, depending on the strength of the interactions between the sample ions and the active sites; the extent of the interaction is a factor of both ionic charge and ionic ratio. Anions and cations are quantified by measuring the change in conductivity as the species passes through the detector.

1.4 Thesis outline

The majority of the work in this thesis has been carried out to improve our understanding of ON compounds in the atmosphere, with a specific focus on nitrosamine and nitramine formation. Additional work has involved characterising organic compounds (including nitrogen-containing species) emitted to the atmosphere during cooking, and measuring water-soluble ions present in atmospheric PM.

Chapter 2 presents time-resolved measurements of nicotine, and 8 non-specific and 4 tobacco-specific nitrosamines in ambient PM from central London over two 5-week periods in winter and summer. A description of the highly sensitive analytical method, capable of separating over 700 ON compounds, is provided. The total nitrosamine

concentrations are compared to the current public recommended levels, and the lifetime cancer risk from exposure *via* inhalation is estimated. Correlations between nitrosamines and other atmospheric pollutants are examined, to determine whether any observed correlations can be used to predict nitrosamine levels in other cities and the resulting exposure to human health.

Chapter 3 describes the method development and optimisation work carried out in preparation for a series of photo-oxidation experiments at the European Photoreactor, as part of the Atmospheric Chemistry of Amines project. This project was set up to improve our understanding of the atmospheric degradation of amines emitted to the atmosphere from CO_2 capture plants. A full description of the GC×GC-NCD technique set up to measure nitrosamine and nitramine formation in the atmospheric simulation chamber is provided. Two of the target analytes required derivatization to make them suitable for GC analysis, and a discussion of this process is provided in this chapter. IC was used to measure aminium nitrate salts formed during the photo-oxidation experiments; optimization of gradient elution methods required to make these measurements are discussed.

Chapter 4 details the results of a series of amine photo-oxidation experiments carried out as part of the Atmospheric Chemistry of Amines project; *tert*-butylamine, aminomethyl propanol, morpholine, piperidine and piperazine are investigated. The GC×GC-NCD measurements of potentially carcinogenic nitrosamines and nitramines are analysed and contribute towards a better understanding of the photochemical degradation of amines in the atmosphere. Furthermore, a discussion of the formation of both aminium nitrate salts and additional ON compounds, identified by IC and GC×GC-TOF-MS respectively, is provided.

Chapter 5 investigates the chemical composition of gas phase and particulate emissions from a broad variety of cooking styles and techniques. A combination of GC×GC-TOF-MS and proton transfer reaction time-of-flight mass spectrometry (PTR-TOF-MS) are used to characterize gaseous emissions from heated vegetable oils and cooked vegetables and meats. These techniques are also used to characterise terpene emissions from cooking with herbs and pepper, and to predict their SOA production potential. The composition of particulate emissions produced from heating olive oil, frying beef, and charbroiling chicken, beef and beef burgers is investigated using GC×GC-TOF-MS. The implications for indoor air quality are discussed, and potentially suitable markers for identifying gas and particle phase cooking emissions in ambient air are identified.

Chapter 6 focuses on the chemical composition of water-soluble ions in atmospheric PM at a rural site on the East coast of Peninsular Malaysia. Using ion chromatography, time-resolved measurements of major atmospheric ions in aerosol are made over a 3-week

period during the winter monsoon season. Backward air mass trajectories are used to determine the influence of air mass origin on aerosol composition, and to study the influence of industrialization in rapidly developing Southeast Asian counties such as China. Correlation analyses amongst ionic species and assessment of ratios between different ions provides information regarding common ion sources and formation pathways, and helps to determine the extent of atmospheric mixing with anthropogenic pollutants.

Chapter 7 provides a summary of the main findings from this thesis and discusses potential ideas for future work.

2 Estimated Exposure Risks from Carcinogenic Nitrosamines in Urban Airborne Particulate Matter

The majority of the work presented in this chapter has been published as a scientific paper with the same title: Naomi J. Farren, Noelia Ramírez, James D. Lee, Emanuela Finessi, Alastair C. Lewis and Jacqueline F. Hamilton. *Environmental Science & Technology*, **2015**, *49* (16), 9648-9656.

2.1 Introduction

Nitrosamines are a particular class of ON compounds which have been classified by the IARC as extremely potent human carcinogens,[59] and have been highlighted in recent studies as environmental contaminants of increasing health concern.[62, 64-65, 73] In a previous study, Ramírez *et al.* measured nitrosamines in house dust (which is often contaminated with residual smoke gases and particles, known as third hand smoke) collected from homes occupied by both smokers and non-smokers, and reported an increased human cancer risk from exposure to nitrosamines. Interestingly, the presence of N-nitrosamines in non-smokers' homes, and its lack of correlation with nicotine, indicated that the main source of these compounds was likely to be outdoor ambient air pollution.[73] It was therefore decided to investigate the presence of nitrosamines in outdoor ambient air. Although there are a few studies that have provided one-off identification of N-nitrosamines in ambient air,[64-65, 77] to our knowledge, there are no other time-resolved measurements of both N-nitrosamines and TSNAs in ambient air. Time-resolved sampling is essential to capture variability in concentration, enabling reasonable estimates of exposure to be calculated.

This work formed part of the UK Natural Environment Research Council (NERC) funded Clean Air for London (ClearfLo) project, which was set up to provide long-term integrated measurements of the meteorology, composition and particulate loading of London's urban atmosphere at both street level and elevated sites.[145] The samples were collected at an urban background site considered to be representative of background air quality in central London, over two 5 week intensive observation periods (IOPs) in winter and summer 2012. As shown in Figure 2.1, the site is located in North Kensington, 7 km to the west of central London. The site is in the grounds of a school and there are no major influences of local roads or point sources; further information about the site location and the experimental campaigns can be found in Bohnenstengel *et al.* and Bigi *et al.*[146-147]

This chapter will begin by discussing the method validation of a technique based on PLE-GC×GC-NCD, which has been used to make time-resolved measurements of N-nitrosamines and TSNAs in ambient air PM samples collected at the North Kensington urban background site. For the first time, a comparison of ambient nitrosamine levels with recommended guidelines will be provided, and an exposure assessment will be carried out to determine the human cancer risk through inhalation of these species.

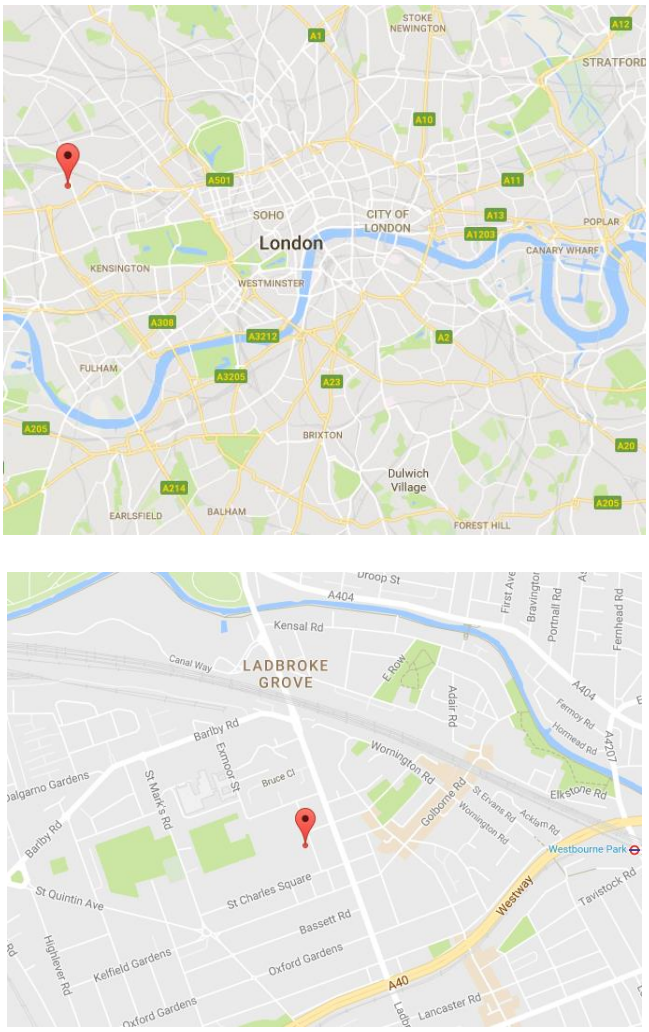

Figure 2.1. Maps to show the location of the North Kensington urban background site (51°31'15.8''N, 0°12'48.6''W).

2.2 Experimental

2.2.1 Standards and solutions

A mixed standard solution of 9 N-nitrosamines (EPA 8270/Appendix IX Nitrosamines Mix) containing N-nitrosodimethylamine (NDMA), N-nitrosomethylethylamine (NMEA), N-nitrosodiethylamine (NDEA), N-nitrosodi-n-propylamine (NDPA), N-nitrosomorpholine (NMor), N-nitrosopyrrolidine (NPyr), N-nitrosopiperidine (NPip),

N-nitrosodi-n-butylamine (NDBA) and N-nitrosodiphenylamine (NDPhA) was used (2,000 mg L^{-1} in methanol). Individual standards of nicotine, N'-nitrosonornicotine (NNN), N'-nitrosoanatabine (NAT), N'-nitrosoanabasine (NAB), 4-(methylnitrosoamino)-1-(3-pyridyl)-1-butanone (NNK) and 4-(methylnitrosoamino)-1-(3-pyridyl)-1-butanol (NNAL) were also used. All standards were purchased from Sigma Aldrich Ltd (Dorset, UK) and had a minimal purity of 97% except for NNAL, which was ≥92%. Standard solutions were prepared in ethyl acetate (GC grade, 99.9% purity) from VWR International Ltd (Leicestershire, UK). The chemical structures of the target compounds and their respective carcinogen classifications set out by the IARC are shown in Figure 2.2.[59]

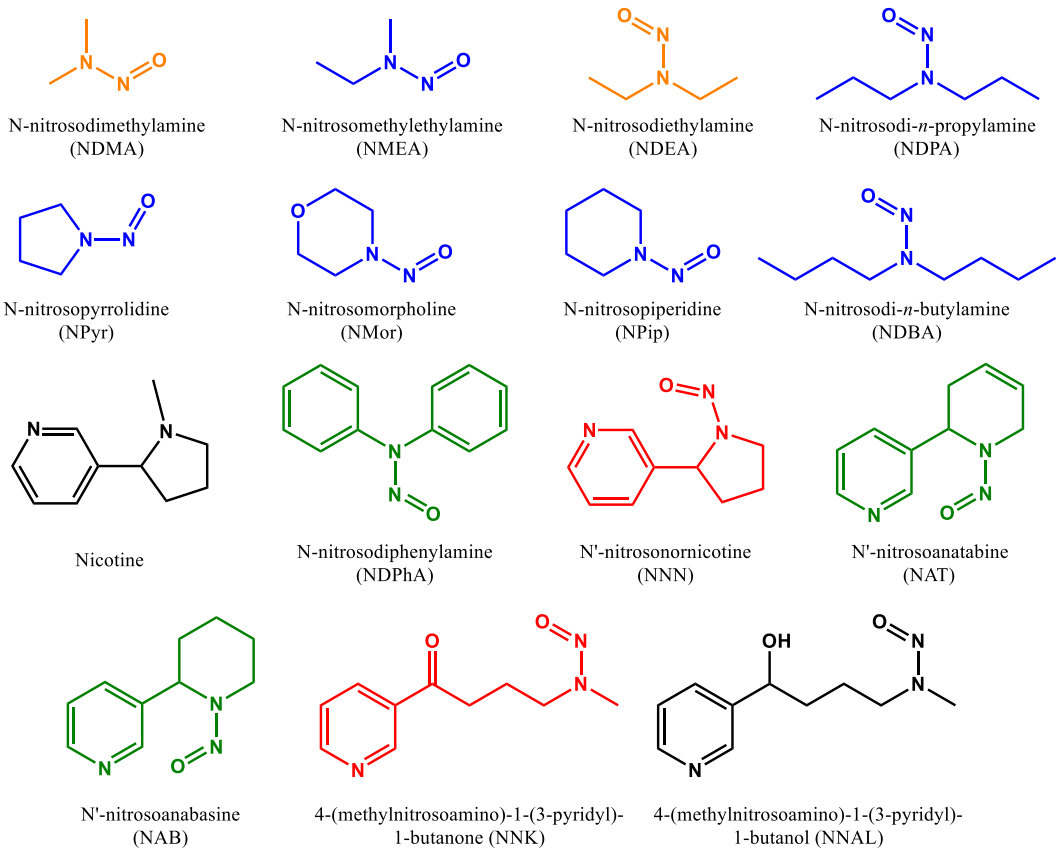

Figure 2.2. Chemical structures of the target N-nitrosamines, TSNAs and nicotine and their respective IARC classifications: group 1 (red), known carcinogen to humans; group 2A (orange), probable carcinogen to humans; group 2B (blue), possible carcinogen to humans; group 3 (green), not classifiable as to its carcinogenicity to humans.[59] The carcinogenicity of nicotine and NNAL (black) have not been assessed by the IARC.

2.2.2 Sample Collection and Preparation

As part of the UK NERC funded ClearfLo project, 77 $PM_{2.5}$ filter samples were collected at the North Kensington site (51°31'15.8''N, 0°12'48.6''W) using a High Volume Air Sampler (Ecotech HiVol 3000, Victoria, Australia) operating at 1.13 m^3 min^{-1}. 52 samples were collected during winter 2012 between 10-01-2012 and 08-02-2012 throughout both the daytime (09:00-17:00) and the nighttime (17:00-09:00). The remaining 25 samples collected in summer 2012 (July 22-August 16, 2012) were changed at midday and represent 24 h sampling intervals. The $PM_{2.5}$ quartz fibre filters (20.3 cm × 25.4 cm) supplied by Whatman (Maidstone, U.K.) were prebaked at 550 °C for a minimum of 12 h prior to sample collection. After collection, the filters were wrapped in aluminium foil and stored at -18 °C until analysis.

2.2.3 Additional Measurements

HONO measurements were obtained using a highly sensitive long-path absorption photometer (LOPAP) instrument from the University of Wuppertal, Germany.[148] The instrument was successfully validated against the spectroscopic DOAS technique under urban conditions and in a smog chamber.[149] During the campaign the detection limit was 1 pptV for a time resolution of 5 min, and a precision of 1% and an accuracy of 10% were obtained. The $PM_{2.5}$ filter samples were analysed for OC and EC using a Sunset thermal-optical carbon analyser (Sunset Laboratory Inc., Portland, U.S.), following the EUSAAR2 thermal protocol.[150] Hourly $PM_{2.5}$ data, which was measured at the North Kensington site using a TEOM-FDMS, was supplied by UK-AIR.[151]

2.2.4 Pressurized Liquid Extraction (PLE)

A quarter of each $PM_{2.5}$ sample was extracted using an accelerated solvent extraction system (ASE 350, Dionex, CA, U.S.). The base of each 5 mL stainless steel extraction cell was lined with two glass microfiber filter papers (Fisher Scientific, Loughborough, U.K.) and then packed with the sample. Extractions were carried out in ethyl acetate (GC grade, 99.9% purity) at 80 °C and 1500 psi for three consecutive 5 min cycles. A 50% flush volume and 60 s purge time were used. Extracts obtained were stood in an ice bath whilst evaporated under nitrogen to a final volume of 1 mL, and stored at -18 °C prior to analysis by GC×GC-NCD. Recovery and optimization tests were performed using 9 cm^2 portions of the collected $PM_{2.5}$ samples, which were heated (300 °C, 1 hour) to remove semi-volatile compounds and then spiked with a mixed nitrosamine standard (100 µL, 50 ppm, 5 µg of each target analyte). The remaining dead volume in the extraction cell was filled with blank prebaked filter paper, and the recovery test samples were extracted under the same

conditions as previously described for the $PM_{2.5}$ samples. Procedural blanks were carried out and no detectable amounts of target compounds were found.

2.2.5 Chromatographic Analysis

Chromatographic analysis was carried out on a GC×GC-NCD system comprised of an Agilent 7890 gas chromatograph and an Agilent 255 NCD system (Palo Alto, U.S.). The first column was a non-polar Ultra Inert DB5 (30 m × 0.32 mm i.d. × 0.25 µm film thickness) from Agilent Technologies Ltd. (Stockport, UK) and the second column a mid-polarity BPX50 (2 m × 0.10 mm i.d. × 0.10 µm film thickness) from SGE Analytical Science (Milton Keynes, UK). The initial temperature of the first dimension column was 40 °C for 2 min, followed by a heating rate of 7 °C min^{-1} to 100 °C for 8 min, and then further heating at 7 °C min^{-1} until 270 °C was reached and held isothermally for a further 5 min. A temperature offset of 30 °C was applied to the second dimension column throughout the GC temperature program. A liquid nitrogen two stage cold jet modulation system was used, with a modulation period of 5 s and a +15 °C offset from the primary GC oven temperature. Data was collected at 200 Hz over the entire course of the analysis, using hydrogen as a carrier gas at 1.4 mL min^{-1}. Injections of 1 µL were performed in splitless mode at an injection temperature of 200 °C using an automated liquid injector (Gerstel, Mülheim an der Ruhr, Germany). Pyrolysis of the analytes in the NCD was carried out at 900 °C under a hydrogen flow rate of 4 mL min^{-1} and an oxygen flow rate of 10 mL min^{-1}.

2.2.6 Cancer Risk Assessment

The cumulative lifetime cancer risk associated with exposure to the target nitrosamine species was determined according to the Superfund Program's approach for the determination of inhalation risk; the concentration of the target chemical in air (µg m^{-3}) is used as the exposure metric, rather than the intake of a contaminant in air based on inhalation rate and body weight (mg kg^{-1} day^{-1}).[152] Initially, the time-weighted averaged exposure concentration is calculated for each individual contaminant according to Equation 2.1.[152]

$$EC_i = \frac{(CA_i \cdot ET \cdot EF \cdot ED)}{AT} \tag{2.1}$$

EC_i is the exposure concentration specific for each carcinogen (µg m^{-3}), CA_i is the target contaminant concentration in air (µg m^{-3}), ET is the exposure time (hours day^{-1}), EF is the exposure frequency (days $year^{-1}$), ED is the exposure duration (years), and AT is the averaging time (lifetime in years × 365 days $year^{-1}$ × 24 hours day^{-1}). The cumulative lifetime cancer risk is then calculated using Equation 2.2.[152]

$$\text{Risk}_{inhalation} = \sum_{i=1}^{n} \text{IUR}_i \cdot \text{EC}_i \tag{2.2}$$

IUR_i is the inhalation unit risk specific for each carcinogen (μg m^{-3}) and can be defined as 'the upper-bound excess lifetime cancer risk estimated to result from continuous exposure to an agent at a concentration of 1 μg m^{-3} in air'.[152] IUR values were taken from the databases provided by the Integration Risk Information System (IRIS)[23] and the Office of Environmental Health Hazard Assessment (OEHHA),[153] giving priority to IRIS values. As toxicological values have only been officially established for NDMA, NDEA, NDPA, NPyr, NMor, NPip, NDBA, NDPhA and NNN, the cumulative cancer risk presented is a sum of the risks from these 9 compounds only.

Chemicals sometimes cause cancer by a mutagenic mode of action and therefore pose a higher risk of cancer to humans when exposure occurs during early life. In these cases, Age-Dependent Adjustment Factors (ADAFs) can be applied to assess the additional risk.[154] Equation 2.2 is altered to include the ADAFs, as shown in Equation 2.3.[152]

$$\text{Risk}_{\text{inh}} = \sum_{i=1}^{n}[(\text{IUR}_i \cdot \text{EC}_{<2} \cdot \text{ADAF}_{<2}) + (\text{IUR}_i \cdot \text{EC}_{2-16} \cdot \text{ADAF}_{2-16}) + (\text{IUR}_i \cdot \text{EC}_{16-70})] \quad (2.3)$$

$EC_{<2}$ and $ADAF_{<2}$ represent the exposure concentration and ADAF for children under 2 years of age respectively, and EC_{2-16} and $ADAF_{2-16}$ are the exposure concentration and ADAF for children aged between 2 and 16 years of age. Values for all parameters and chosen age intervals are recommended by the US EPA and are shown in Table 2.1. Nitrosamine concentrations below the limits of detection (LODs) and limits of quantification (LOQs) were replaced with a value equal to half the LOD or half the LOQ respectively for all risk assessment calculations, as recommended by the US EPA.[155]

Table 2.1. Values for all of the parameters used for the cancer risk assessment. The chosen age intervals are recommended by the U.S. EPA.[152]

Age group / years	EF[a] / days $year^{-1}$	ED[b] / years	AT[c] / hours	ADAF[d]
0 to < 2	365	2	613200	10
2 to < 16	365	14	613200	3
16 to 70	365	54	613200	1
[a]Exposure frequency. [b]Exposure duration. [c]Averaging time. [d]Age-dependent adjustment factor.				

2.3 Results and discussion

2.3.1 PLE conditions

Ethyl acetate was initially chosen as the extraction solvent because it proved to be suitable in previous studies that relied on PLE for the determination of nitrosamines in both house dust and atmospheric PM.[62, 65] Furthermore, ethyl acetate is a suitable solvent for liquid injection to the GC×GC-NCD, which means that the sample extracts obtained by PLE do not need to be reconstituted in a different solvent. Not only does this save time and resources, it also means that evaporation of the sample extracts to complete dryness can be avoided; this prevents excessive compound loss of species with low vapour pressures.[110] The extraction solvent was tested at three temperatures (70, 80 and 100 °C) under the chosen PLE conditions. Recovery levels were low at 70 °C, ranging from 1% for nicotine to 20% for NNN, but were considerably higher at both 80 and 100 °C, averaging 66% and 62% respectively. An additional set of recovery tests were performed at 80 °C under the same PLE conditions, but the extracts were stood in an ice bath during evaporation under nitrogen to a final volume of 1 mL. Furthermore, the extraction vials were stored at -18 °C before and after the extraction. Recovery levels at 80 °C improved dramatically to an average of 91% under the newly modified extraction procedure; individual recovery levels and the associated errors are provided in Table 2.2.

Table 2.2. Recovery levels and %RSD[a] of the target compounds under the final PLE conditions.[b]

N-nitrosamine	% recovery	%RSD	TSNA	% recovery	%RSD
NDMA	91.3	3.2	NNN	91.0	5.8
NMEA	92.3	3.9	NAT	96.6	6.1
NDEA	92.7	4.2	NAB	94.5	5.9
NDPA	95.6	4.2	NNK	95.0	5.9
NPyr	90.6	8.3	NNAL	82.0	8.0
NMor	99.6	1.6			
NPip	95.4	4.5	**Other**	**% recovery**	**%RSD**
NDBA	98.8	3.9	Nicotine	53.0	16.3
NDPhA	104.0	6.9			

[a]% Relative standard deviation. [b]PLE conditions: ethyl acetate, 80 °C, 1500 psi, three 5 min cycles, 50% flush volume, 60 s purge time.

2.3.2 Method Validation

The main instrumental parameters of the GC×GC-NCD system were evaluated and are shown in Table 2.3. Instrumental LODs and LOQs were calculated according to the EPA protocol 40 CFR 136; multiplying the standard deviation (derived from the peak areas of 10 standards injected at 0.01 ppm) by the Student *t*-value (N = 10, 95% confidence interval) gave the LOD, and multiplying the standard deviation by 10 gave the LOQ.[155] The LODs and LOQs obtained ranged from 2.0 to 10.5 pg and from 7.2 to 37.2 pg respectively, with the exception of NNAL, which exhibited significantly higher detection limits. It is clear that combining the GC×GC with the element specific NCD is a successful way of measuring trace level nitrogen-containing compounds. Good correlation coefficient values (R^2) between 0.9697 and 0.9999 were obtained for the stated linear ranges.

Instrument repeatability was monitored over the course of the sample analysis period using a mixed nitrosamine standard (100 pg, N = 19). The precision (%RSD) remained below 13% for all compounds except nicotine and NNAL; this can possibly be attributed to the lack of equimolar response for these species or degradation during pyrolysis. Total errors were estimated by combining errors associated with the instrument and the recovery process, and remained below 14% for all compounds except nicotine and NNAL (individual %RSD values for each compound are provided later in Table 2.4).

Table 2.3. Instrumental parameters for the GC×GC-NCD system.

Compound	1st RT[a] / s	2nd RT / s	LOD[b] / pg	LOQ[c] / pg	Linear range / pg	R^2
NDMA	480	1.89	2.3	8.1	5 - 1000	0.9999
NMEA	550	1.90	2.6	9.3	5 - 500	0.9999
NDEA	660	2.02	2.0	7.2	5 - 1000	0.9998
NDPA	970	2.77	3.0	10.7	5 - 250	0.9999
NPyr	960	3.73	2.6	9.3	5 - 500	0.9998
NMor	975	3.77	2.4	8.6	5 - 500	0.9998
NPip	1090	4.00	3.9	13.8	5 - 250	0.9996
NDBA	1485	2.32	4.4	15.4	5 - 250	0.9999
Nicotine	1645	2.44	10.5	37.2	10 - 5000	0.9932
NDPhA	2010	2.61	6.0	21.4	5 - 1000	0.9997
NNN	2140	3.11	2.9	10.3	5 - 250	0.9976
NAT	2200	3.03	4.9	17.5	5 - 500	0.9998
NAB	2210	3.06	3.3	11.8	5 - 250	0.9994
NNK	2315	3.03	4.9	17.5	5 - 1000	0.9909
NNAL	2395	3.19	36.1	128.0	50 - 1000	0.9697

[a]Retention time. [b]Limit of detection. [c]Limit of quantification.

2.3.3 Analysis of Ambient Particulate Matter in London

The $PM_{2.5}$ samples were collected during the two 5 week IOPs in the winter and summer of 2012, at the Sion Manning School in North Kensington, London (classified as an urban background site). The PLE-GC×GC-NCD method was applied to measure ambient N-nitrosamine, nicotine and TSNA concentrations in the collected $PM_{2.5}$ samples. To ensure accurate quantification of all target compounds, external calibration curves were obtained for each compound. GC×GC-NCD chromatograms are shown in Figure 2.3 for typical

samples collected in winter and summer 2012. The chromatograms show the complexity of ON in London, and more than 700 ON compounds were observed in both samples.

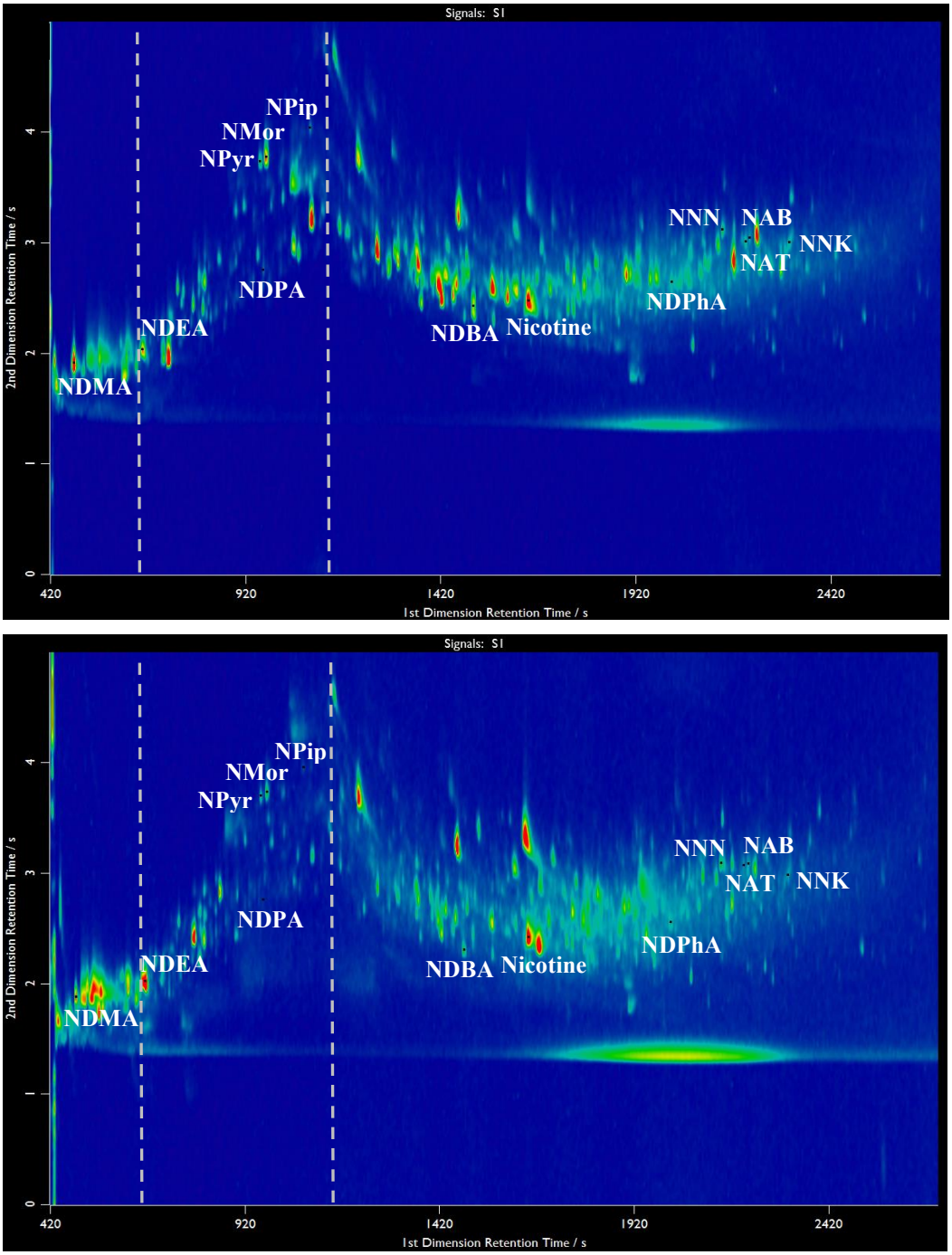

Figure 2.3 Typical GC×GC-NCD chromatograms of ambient $PM_{2.5}$ samples collected during the winter (upper panel, 06-02-2012 17:17 to 07-02-2012 08:37) and the summer (lower panel, 10-08-2012 12:56 to 11-08-2012 11:55).

Peak identification was based on direct comparison of retention times on both GC×GC columns to those of individual standards. The method successfully separated and identified the majority of the target compounds; an isothermal period (highlighted within the grey dashed lines on each chromatogram) was introduced to the method to separate NPyr and NMor, which caused some loss of the typical structured chromatograms associated with GC×GC. Although it was possible to detect NMEA, coelution with other ON compounds meant that it was not possible to accurately determine the concentration. It was also difficult to confirm the concentration of NNAL because the levels were close to the LOD and precision was low (RSD = 45%).

Nicotine was the most abundant target compound and was found in all $PM_{2.5}$ samples in both winter and summer, with average concentrations of 21.1 ng m^{-3} and 6.8 ng m^{-3}, respectively. Nicotine reached a maximum concentration of 118.1 ng m^{-3} in winter and 30.6 ng m^{-3} in summer. Although nicotine itself is not classified as carcinogenic,[59] it can undergo a series of atmospheric oxidation reactions to form TSNAs, which are carcinogenic.[79] Elevated exposure of the public to nicotine in ambient PM is primarily of concern due to the potential for co-inhalation of its more harmful degradation products.

The median, mean and maximum nitrosamine concentrations in $PM_{2.5}$ in winter and summer respectively are shown in Table 2.4 (the frequency of occurrence of each compound is also included). Of the 8 N-nitrosamines measured during the winter, NDMA and NDPhA had the highest concentrations of 1.36 and 1.22 ng m^{-3}, respectively. The overall average concentrations were slightly lower for NDEA and NMor, but maximum concentrations reached 3.51 and 2.27 ng m^{-3}, respectively. In summer, the highest average concentration was seen for NDEA at 2.08 ng m^{-3}, followed by NDPhA at 0.60 ng m^{-3} and NDMA at 0.49 ng m^{-3}. NNK was the most abundant TSNA measured in both winter (0.58 ng m^{-3}) and summer (0.30 ng m^{-3}). The concentrations of the other three TSNAs averaged 0.22 and 0.16 ng m^{-3} in winter and summer, respectively, but the frequency of occurrence of TSNAs was higher in the summer (56 – 100%) compared to winter (39 – 79%).

Table 2.4. Median, mean and maximum nitrosamine concentrations in $PM_{2.5}$ in winter and summer, expressed in ng m^{-3}.

Compound	Winter				Summer				%RSD[b]	IUR / ng m^{-3}
	Median / ng m^{-3}	Mean / ng m^{-3}	Max. / ng m^{-3}	%Qt[a]	Median / ng m^{-3}	Mean / ng m^{-3}	Max. / ng m^{-3}	%Qt		
NDMA	0.45	1.36	6.37	83	0.24	0.49	3.54	92	8.6	1.4×10^{-2}
NDEA	0.62	0.89	3.51	96	1.13	2.08	12.33	100	8.7	4.3×10^{-2}
NDPA	0.05	0.07	0.25	42	0.04	0.05	0.18	72	8.3	2.0×10^{-3}
NPyr	0.01	0.08	0.48	39	0.02	0.04	0.24	36	8.3	6.1×10^{-4}
NMor	0.10	0.32	2.27	56	0.13	0.23	1.35	96	11.1	1.9×10^{-3}
NPip	0.03	0.04	0.28	15	0.03	0.05	0.36	40	8.6	2.7×10^{-3}
NDBA	0.15	0.18	0.72	60	0.22	0.33	1.26	100	8.5	1.6×10^{-3}
NDPhA	0.95	1.22	4.08	94	0.34	0.60	2.58	88	9.1	2.6×10^{-6}
NNN	0.12	0.21	0.75	54	0.14	0.20	0.58	96	7.8	4.0×10^{-4}
NAT	0.18	0.31	1.94	58	0.14	0.16	0.91	68	6.8	no data
NAB	0.03	0.14	1.21	39	0.06	0.11	0.86	56	7.5	no data
NNK	0.41	0.57	2.35	79	0.25	0.29	0.98	100	13.8	no data

[a]Percentage of samples in which the target species were above the LOQ. [b]Total error associated with each compound.

2.3.4 Nitrosamine Exposure

As shown previously in Figure 2.2, the target compounds can be classified according to their carcinogenicity.[59] Box-plot representations of measured nitrosamine concentrations (according to these classifications) are shown in Figure 2.4 for winter and summer (upper and lower panel respectively), alongside total nitrosamine concentrations. In 2011, the Norwegian Institute of Public Health (NIPH) recommended that the total amount of nitrosamines in ambient air should not exceed 0.3 ng m^{-3},[74] represented in Figure 2.4 as a black line.

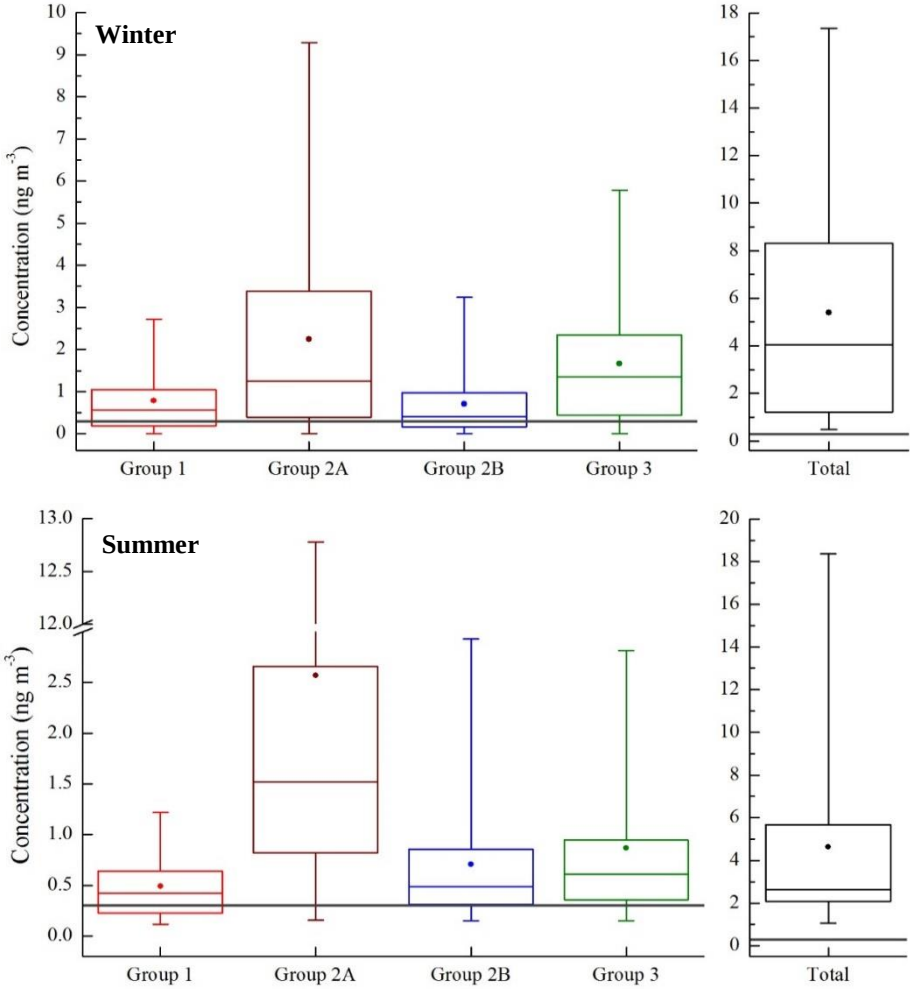

Figure 2.4 Ambient particle-borne nitrosamine concentrations categorised according to their IARC classifications in winter (upper panel) and summer (lower panel). Separate box plots are given for total nitrosamine concentrations. Each box plot represents the 25th and 75th percentiles of the observed concentrations, and the bottom and top lines indicate minimum and maximum concentrations. The circle is mean concentration, and the horizontal line inside the box represents the median concentrations. The horizontal black line at 0.3 ng m^{-3} represents the NIPH recommended level.[74]

In both seasons, the lowest recorded total nitrosamine concentration exceeded 0.3 ng m^{-3}, with average total nitrosamine concentrations of 5.40 and 4.63 ng m^{-3} for winter and summer, respectively. Furthermore, in both winter and summer, average nitrosamine concentrations of compounds in each IARC group also exceeded 0.3 ng m^{-3}. Of the four different classifications, group 2A carcinogens were observed at the highest levels, with average concentrations of 2.24 and 2.57 ng m^{-3}, and maximum concentrations of 9.29 and 12.78 ng m^{-3} in winter and summer, respectively. This direct comparison of measured ambient atmospheric nitrosamine concentrations with recommended air quality guidelines indicates that the ambient concentrations, at least in London, are currently at levels that are likely to pose a significant long-term cancer risk. We find no obvious reason why London would be an abnormal or unrepresentative urban environment for ON in general or nitrosamines specifically.

2.3.5 Risk assessment

The nitrosamine concentrations observed in London demonstrate a *prima facie* case that a cancer risk assessment of exposure *via* inhalation is necessary. The World Health Organization (WHO) states that inhalation is the only concernable route of exposure when considering the direct effects of atmospheric PM on human health.[156] Toxicological data is only available for nine of the target nitrosamines; therefore, the carcinogenic risk assessed here only accounts for these compounds.

The original approach used to estimate exposure to inhaled contaminants in air was outlined in the US EPA's Risk Assessment Guidance for Superfund (RAGS) Part A.[157] Using a function of the concentration of the chemical in air, inhalation rate, body weight, and exposure scenario, this approach allows for the estimation of the daily intake of a contaminant in air (mg kg^{-1} day^{-1}). However, this approach was developed before the release of the US EPA's Inhalation Dosimetry Methodology (IDM), which provides details of the interpretation of occupational exposures of human to airborne chemicals.[158] Under this methodology, human equivalent concentrations (HECs) can be extrapolated from experimental exposures, which in turn can be used to develop the IUR values required for cancer risk assessments. In response to the IDM, the Superfund Program released an updated approach for estimating cancer risk *via* inhalation. The new approach relies on the concentration of the chemical in air as the exposure metric (μg m^{-3}), rather than the intake of a contaminant in air (mg kg^{-1} day^{-1}).[152] The new approach is considered more accurate as it accounts for the fact that the amount of chemical reaching the target site is not a simple function of inhalation rate and body weight. In fact, important considerations of the anatomy and physiology of the respiratory system and the characteristics of the inhaled agent are

required, to account for the fact that the amount of pollutant entering the body through the upper respiratory tract and lung is less than the amount measured at the boundary of the body. An estimation of exposure time (ET) is also required to assess lifetime cancer risks using this approach. In this analysis, we assume that an individual is only exposed to the observed values when outside and that indoor exposure is zero, due to lack of available data. The ET was increased from 1 to 8 h in 1 h increments to represent a range of different individual scenarios, and the corresponding exposure concentrations were estimated using Equation 2.1. Values for all parameters at the chosen age intervals are provided in Table 2.1. The cumulative lifetime cancer risk was then calculated using Equation 2.2, and ADAF's were applied if necessary using Equation 2.3. In this study, NDMA and NDEA were determined to operate by a mutagenic mode of action and therefore ADAFs were applied to these compounds.[159-161] Figure 2.5 shows estimated cumulative cancer risks as a function of ET (0-8 h), expressed as the number of excess cancer cases per million population exposed. The proportion of the total lifetime cancer risk resulting from early life exposure (< 2 years and 2-16 years) is also shown. The corresponding data for both winter and summer is provided in Tables A1 and A2 respectively (Appendix A).

This initial assessment shows that the US EPA guideline of negligible risk (1 excess cancer case per 1 million population exposed) is exceeded after less than 1 h of exposure to ambient air in both winter and summer.[162] Additionally in the summer, the minimal cancer risk (defined by the US EPA as 10 excess cancer cases per 1 million population exposed)[162] is exceeded after less than 1 h of exposure to outdoor ambient air. The risk is slightly lower in winter, with the "minimal cancer risk" level reached after 3 h. In the summer, NDEA contributed to 92.1% of the total cancer risk and NDMA contributed 7.1% to the total cancer risk; as shown in Table 2.4, these compounds had the highest maximum concentrations (3.5 and 12.3 ng m^{-3} respectively) and the largest IUR values. In winter, the average concentration of NDEA (1.4 ng m^{-3}) was higher than the average concentration of NDMA (0.9 ng m^{-3}) and these two carcinogens contributed to 32.8% and 65.8% of the total cancer risk respectively. In both seasons, relatively high concentrations of NDPhA were also observed compared to the remaining nitrosamines (1.2 ng m^{-3} in winter and 0.6 ng m^{-3} in summer), but NDPhA contributed to less than 0.01% of the total cancer risk; this is because it has the lowest IUR value (2.6×10^{-6} μg m^{-3}). As ADAFs have been applied to compounds acting by a mutagenic mode of action, a significant fraction of the estimated lifetime cancer risk is a result of exposure occurring during early life. In this study, 17% of the cancer risk is estimated to be due to exposure in the first 2 years of life, and 36% due to exposure between the ages of 2 and 16. The remaining 47% of the cancer risk is due to adult exposure after the age of 16.

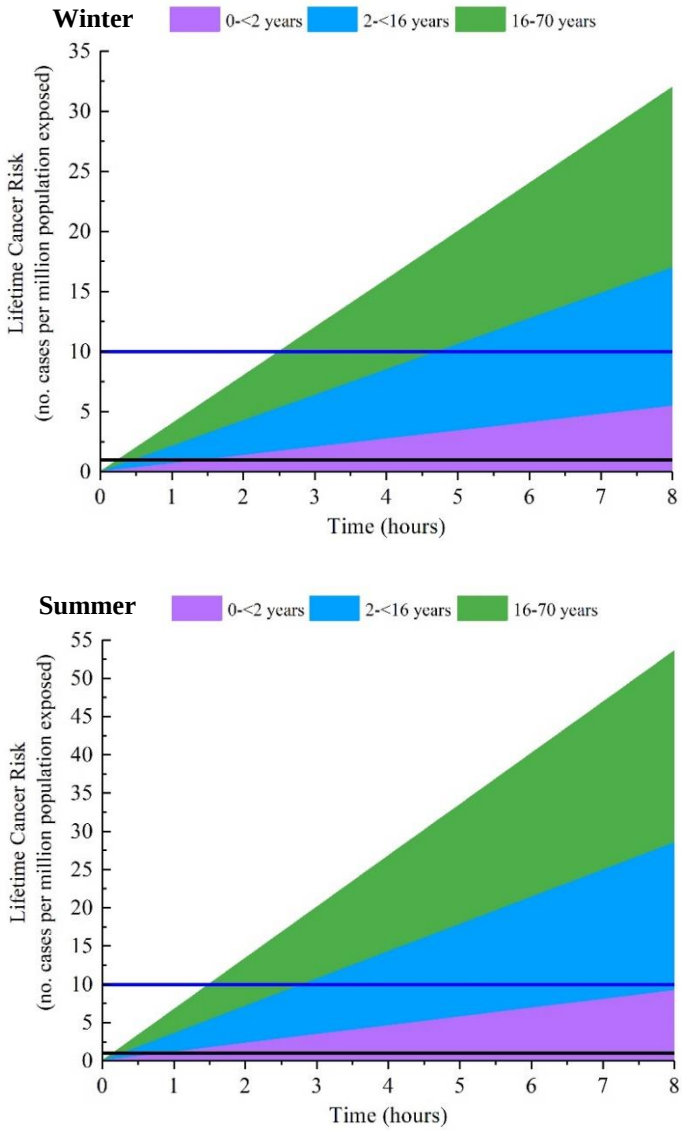

Figure 2.5. Estimated lifetime cancer risk as a function of ED for the inhalation of NMDA, NDEA, NDPA, NPyr, NMor, NPip, NDBA, NDPhA and NNN, expressed as the number of excess cancer cases per million population exposed in both winter (upper panel) and summer (lower panel). The age groups (0 - <2, 2 - <16 and 16 - 70 years) show the proportion of the total lifetime cancer risk resulting from early life exposure compared to adult exposure. The horizontal black and blue lines indicate the US EPA guidelines of 1 and 10 excess cancer cases per 1 million population exposed, respectively.[159]

The relevance of the presented risk estimates can be assessed by comparing the values to estimates of other carcinogens in urban air. For example, benzo(a)pyrene (BaP) is a commonly occurring PAH in ambient air and is used as a single indicator carcinogen to represent the carcinogenic potential of the complex mixture of PAHs.[163] Currently, the EU guideline for BaP is 1 ng m^{-3}, which corresponds to a lifetime cancer risk of 100 excess

cancer cases per 1 million population exposed.[164] However, it has been suggested by the UK expert panel on air quality since 1999 that 0.25 ng m^{-3} would be a more suitable level (*i.e.*, 25 cancer cases per 1 million people).[165] The estimates of cancer risks in this study from nitrosamine exposure are approximately 96 and 161 excess cancer cases per 1 million people in winter and summer respectively (assuming 24 h exposure per day for average adult lifetime in the same way as for BaP). These values are in fact higher than the recent recommendation by the UK expert panel on air quality, and therefore they can be considered relevant and of concern.

Inevitably, there are limitations and uncertainties associated with the presented cancer risk evaluation. Currently, the US EPA recommends that a simple additive approach is applied when calculating cumulative cancer risks less than 10^{-1}. However, this assumes independence of action by the compounds involved (*i.e.*, that there are no synergistic or antagonistic chemical interactions and that all chemicals produce the same effect, *i.e.* cancer).[157] Also, the assessment presented only accounts for carcinogenic effects, but realistically, some compounds may also pose chronic and acute non-carcinogenic effects. Nitrosamine concentrations below the LODs and LOQs were replaced with a value equal to half the LOD or LOQ, which can possibly overestimate the calculated risk.[155] To quantify the potential overestimation, we have also calculated the risks when the concentrations below the LODs and LOQs are replaced with zero values (Tables A1 and A2, Appendix A). This analysis shows that the potential for overestimation is low; on average the risk is only 0.14% lower when the zero values are applied, with a maximum reduction of 0.29%. A key limitation is the lack of data available for indoor air; this means that we assume indoor exposure is zero and only estimate the outdoor air contribution to total exposure. As people spend a considerable amount of time indoors on a daily basis, it is likely that the exposure risks are significantly higher, indicating that the risk presented is almost certainly an underestimate of true exposure. Currently, there is no appropriate toxicological data available for some nitrosamines (NAT, NAB, and NNK), and so these are not included in the exposure assessment. Furthermore, it is likely that the nitrosamines of higher volatility also exist in the gas phase, which would add an additional cancer risk.[166] Overall, the calculated risks are likely to be underestimates, indicating that ambient nitrosamine concentrations have the potential to adversely affect human health in urban areas to a greater extent than presented here. Despite these limitations, this study presents the first estimation of the cancer risk associated with inhalation of nitrosamines in ambient outdoor air.

2.3.6 Nitrosamine concentration correlations

Time series of N-nitrosamines, TSNAs and nicotine for both winter and summer are provided in Figure 2.6. Additional time series for HONO, OC and $PM_{2.5}$ are shown in Figure 2.7. HONO and $PM_{2.5}$ measurements have been time-averaged to the filter paper sampling times. Strong positive correlation between nicotine and total TSNA concentration was seen in both winter ($R = 0.73$, $p < 0.001$) and summer ($R = 0.82$, $p < 0.001$). This trend may be attributed to both the co-emission of nicotine and TSNAs during smoking, and the formation of TSNAs in urban air (nicotine is the sole precursor for TSNAs that are not emitted directly).[79] As expected, the correlation between nicotine and total N-nitrosamine concentration is weaker in both winter ($R = 0.48$, $p < 0.001$) and summer ($R = 0.47$, $p < 0.02$), as N-nitrosamines are either emitted directly or formed from the oxidation of a range of secondary amines.[26] Interestingly, a degree of positive correlation between total N-nitrosamine concentration and total TSNA concentration is seen; $R = 0.68$ ($p < 0.001$) in winter and $R = 0.66$ ($p < 0.001$) in summer. The positive relationship between N-nitrosamine and TSNA concentration indicates that the pollutants are probably influenced by common atmospheric factors, such as boundary layer height/ dilution, deposition rate, atmospheric chemistry, and meteorological conditions. A moderate to strong correlation was also observed between total nitrosamine (non-specific and tobacco-specific) concentration and particle mass, both $PM_{2.5}$ ($R = 0.84$, $p < 0.001$ in winter and $R = 0.67$, $p < 0.001$ in summer) and the OC mass ($R = 0.80$, $p < 0.001$ in winter and $R = 0.78$, $p < 0.001$ in summer). This suggests that gas-particle partitioning and the amount of available absorbing mass limits the particle phase concentration of nitrosamines.[51] Scatter plots of these correlations can be found in Figures A1 and A2 (Appendix A).

The time series show that the temporal variation of HONO is similar to the nitrosamine observations. Correlations between HONO and N-nitrosamine concentrations were observed in winter ($R = 0.62$, $p < 0.001$) and summer ($R = 0.74$, $p < 0.001$). Stronger positive correlation was found between HONO and TSNA concentrations; $R = 0.88$ ($p < 0.001$) in winter and $R = 0.79$ ($p < 0.001$) in summer; it is possible that this correlation arises from the fact that HONO is thought to be a key atmospheric oxidant for nitrosamine formation.[79] The observed correlations may be useful in predicting nitrosamine levels and the resulting exposure to human health. The relatively strong correlation to $PM_{2.5}$ in winter, a pollutant which is continually monitored at various urban sites in London and indeed very many other cities around the world, could allow for nitrosamine levels to be estimated at other urban locations over different periods of time. Where direct measurements of nitrosamines are not available, a value of 1.88 ± 2.60 ng m^{-3} (total nitrosamine) per 10 µg m^{-3} $PM_{2.5}$ is recommended for estimates of exposure. For example, the average $PM_{2.5}$ concentration in

Beijing in Jan/ Feb 2016 was 58.6 µg m^{-3}.[167] At these ambient particulate concentrations, the total nitrosamine level in $PM_{2.5}$ is predicted to be 11.0 ± 2.60 ng m^{-3}, posing a potential cancer risk to human health.

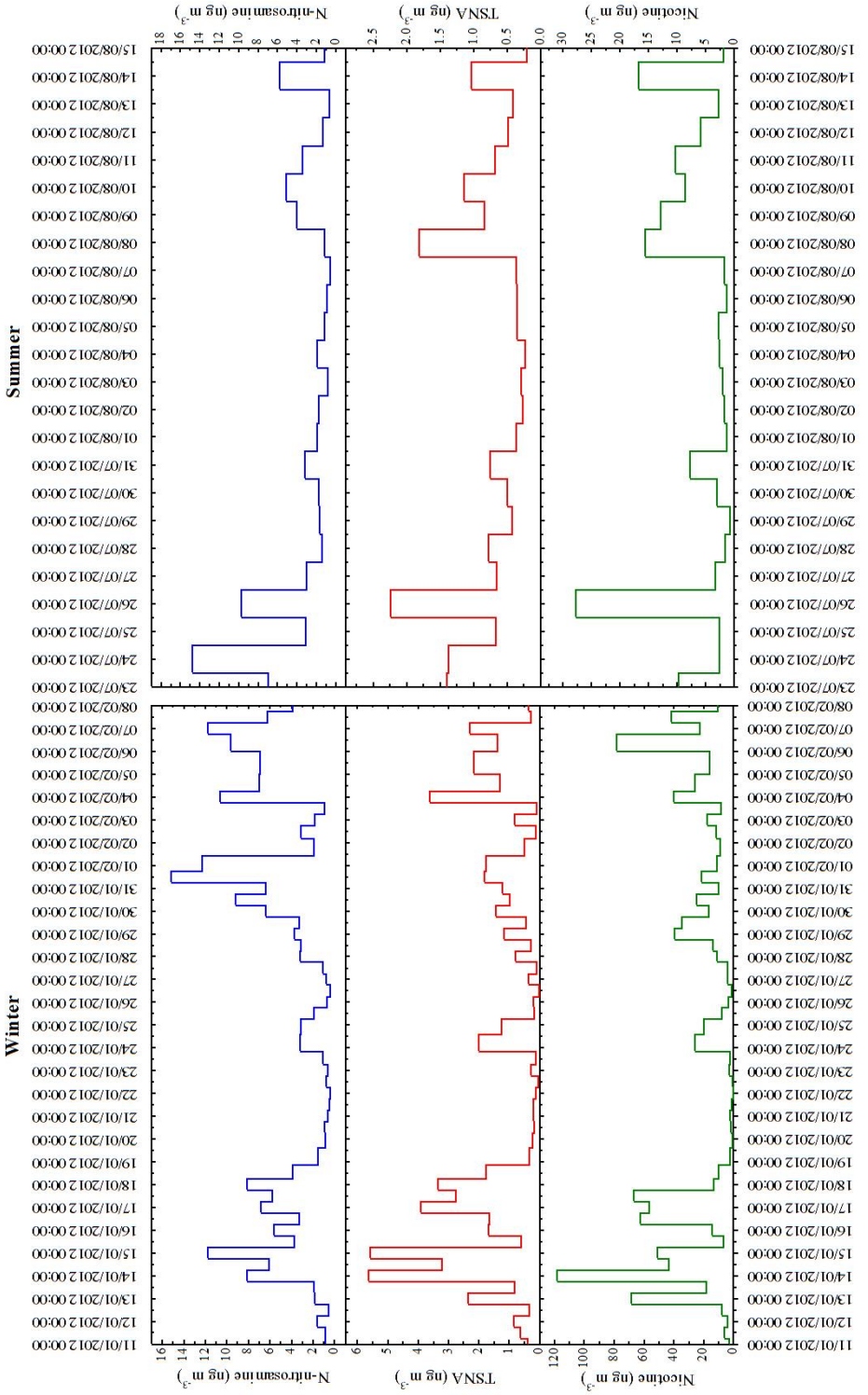

Figure 2.6. Time series of N-nitrosamines, TSNAs and nicotine measured during the 2012 ClearfLo campaign in winter and summer.

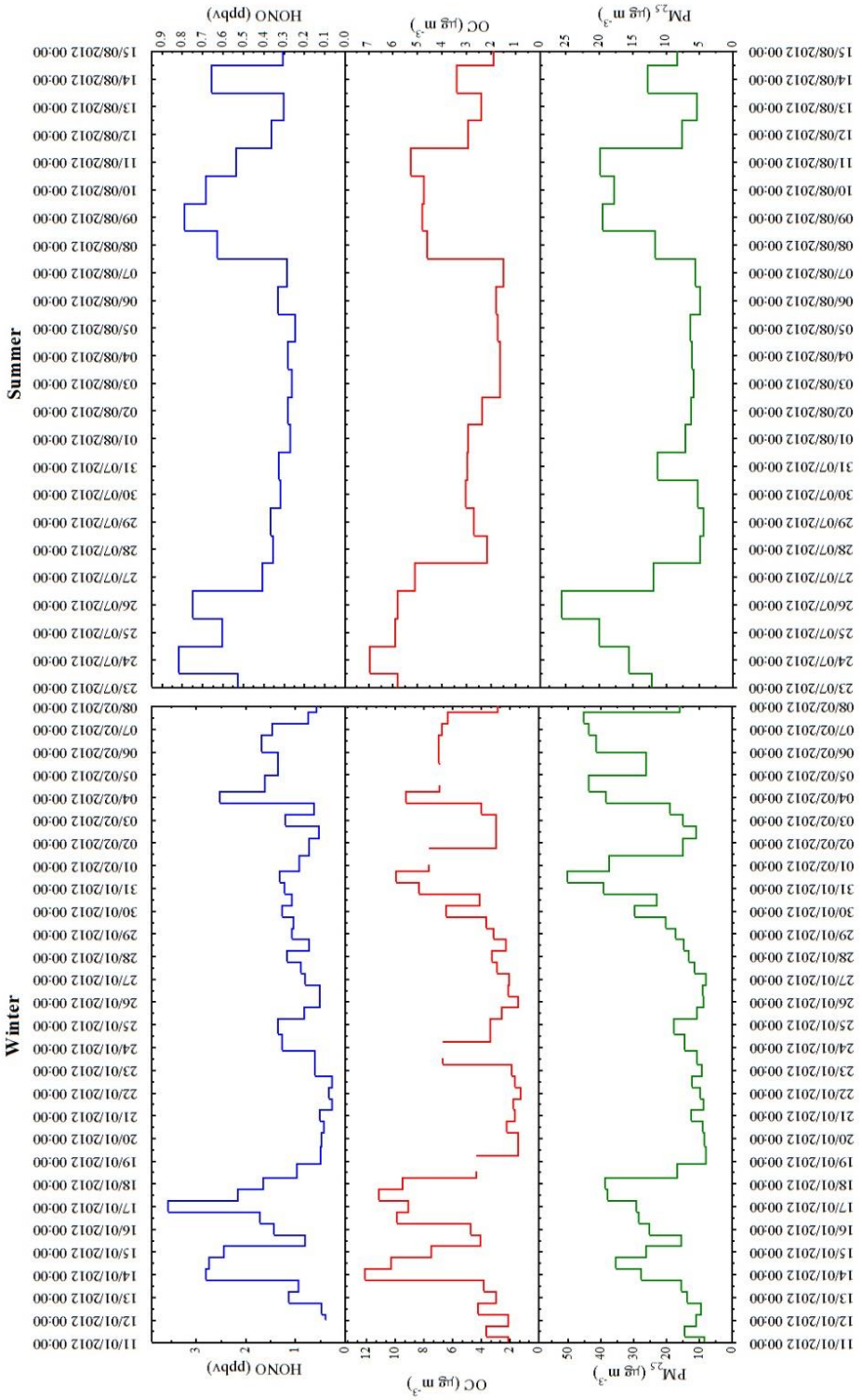

Figure 2.7. Time series of HONO, OC and $PM_{2.5}$ measured during the 2012 ClearfLo campaign in winter and summer.

2.4 Conclusions

Nitrosamines are a class of ON compounds known to be highly carcinogenic and include species formed from nicotine degradation, yet previous studies have not provided detailed time-resolved estimates of their abundance in ambient air. In this study, a highly sensitive and specific analytical method, relying on PLE-GC×GC-NCD, was developed in order to investigate nitrosamines in ambient PM from central London. The $PM_{2.5}$ filter samples were collected at an urban background site in North Kensington, London, as part of the ClearfLo project; this project was set up to investigate boundary layer pollution across London. The PLE method enabled the target compounds to be extracted from the filter samples with high efficiency and reproducibility; an average recovery level of 91% was obtained, and RSD was less than 8% for all species except nicotine (RSD = 16.3%). The GC×GC-NCD technique proved to be capable of separating over 700 ON compounds, and limits of detection for the target compounds ranged from 2.0 to 36.1 pg. It was therefore possible to determine the daily variability in nicotine, and 8 non-specific and 4 tobacco-specific nitrosamines in London over two 5-week periods in winter and summer. The average total nitrosamine concentration was 5.2 ng m^{-3}, substantially exceeding a current public recommendation of 0.3 ng m^{-3} on a daily basis. In fact, in both winter and summer, average nitrosamine concentrations of compounds in each individual IARC group classification also exceeded 0.3 ng m^{-3}; this indicated that the ambient concentrations, at least in London, are currently at levels that are likely to pose a significant long-term cancer risk. A cancer risk assessment was carried out using the Superfund Program's updated approach for the determination of inhalation risk, in which the concentration of each target chemical in air is used as the exposure metric.[152] The results revealed that the lifetime cancer risk from nitrosamines in urban PM exceeded the US EPA guideline of 10 excess cancer cases per 1 million population exposed after 1-3 h of exposure to observed concentrations per day over the duration of an adult lifetime. Strong positive correlations were observed between the concentrations of nicotine and TSNAs, most likely due to both the co-emission of nicotine and TSNAs during smoking, and the formation of TSNAs in urban air (nicotine is the sole precursor for TSNAs that are not emitted directly). There was also a positive relationship between N-nitrosamines and TSNAs, which showed that these kinds of pollutants are likely to be influenced by common atmospheric factors such as boundary layer height/ dilution, atmospheric chemistry and meteorological conditions. A clear relationship between ambient nitrosamines and total $PM_{2.5}$ was observed with 1.9 ng m^{-3} ± 2.6 ng m^{-3} (total nitrosamine) per 10 µg m^{-3} $PM_{2.5}$. These observed correlations may help to predict nitrosamine levels and the resulting exposure to human health at various urban sites in London and other cities around the world.

3 Atmospheric Chemistry of Amines project: method validation for the identification and quantification of amine degradation products

3.1 Introduction

Carbon capture and storage (CCS) is a potential technique for the mitigation of climate change. It is now recognised that progress on CO_2 technologies is essential in order to limit the release of greenhouse gas emissions and stall global temperature rises to between 1.5 °C and 2 °C. Negative emissions technologies will be required if net-zero emissions are to be achieved between 2050 and 2100.[168] One of the more established technologies is a post-combustion technique that relies on amine absorbents; a liquid mixture of water and amines is used to absorb CO_2 directly from the flue gas.[33] Technology Centre Mongstad (TCM) in Norway is home to the world's largest facility for testing and improving CO_2 capture technologies. At TCM, companies from across the globe can use the facilities to test their various CO_2 capture techniques. It is hoped that this facility will aid the international development of carbon abatement technology, whilst simultaneously reducing the technical, environmental and financial risks associated with such projects.[88] However, techniques relying on amine absorbents are of environmental concern because large scale deployment could lead to small but potentially significant amounts of amines being emitted to the atmosphere during operation.[33] Regardless of which parent amine is used in the absorber, simple amines will always form as process degradation products and be present in the flue gas.[169] It is essential that the atmospheric fate of these simple amines is investigated, in order to assess the environmental impact of amine-based CO_2 capture. Therefore, the Atmospheric Chemistry of Amines (ACA) project was set up to investigate the atmospheric degradation of amines emitted to the atmosphere from CO_2 capture plants.[50] The main objectives of the project were to identify gas phase degradation products emitted to the atmosphere, to verify and update existing photo-oxidation mechanisms for amines to account for all of the products formed, to investigate the conditions required for aerosol formation, and to characterise the composition of the aerosol formed.

In 2015, the University of York began to participate in the ACA project, which is led by the University of Oslo. The main aim was to test the suitability of a new technique, relying on GC×GC-NCD, for the determination of nitrosamines and nitramines. These compounds can form during the atmospheric photo-oxidation of amines and present a potential risk to human health from exposure *via* inhalation. Several nitrosamines have been classified as highly carcinogenic by the IARC, and many other nitrosamines and nitramines are also suspected carcinogens, although their level of carcinogenicity has not yet been determined.[58] The University of York was involved in campaigns carried out at the European Photoreactor (Valencia, Spain) in 2015 and 2016. This is an outdoor atmospheric simulation chamber used to study the photochemical degradation of atmospheric pollutants.[170-171] Offline sampling was carried out using both Thermosorb-N air sampling cartridges and quartz microfibre filters, which were shipped back to the University of York and analysed in the laboratory. Thermosorb-N air sampling cartridges have been designed for the collection of N-nitrosamines in ambient air (Cambridge Scientific Instruments Ltd., U.K.) and a recommended method for sampling and analysis, using a gas chromatograph – thermal energy analyser (GC-TEA), has been developed previously.[172] The cartridges contain a solid adsorbent to collect N-nitrosamines and an amine trap and nitrosation inhibitor to prevent artificial analyte formation. The use of quartz fibre filters (Whatman, U.K.) for the collection of aerosol samples is a well-established sampling technique.[173-175] The filters contain pores of 0.22 µm diameter, which means that all particles larger than 0.22 µm are collected, and gases and smaller particles pass through the filter. The compounds of interest can then be extracted from the collected samples, and analysed using a range of analytical techniques.

In this study, we describe the method optimization and validation for the determination of amine degradation products. GC×GC-NCD was selected to measure nitrosamines and nitramines, as it is a highly sensitive and selective technique capable of separating and detecting several hundred trace level ON compounds.[77, 176] Furthermore, an IC method has been developed for the detection of amine salts present in the aerosol. To our knowledge, this is the first time that methods relying on GC×GC-NCD and IC have been applied to the measurement of amine degradation products relevant to CO_2 capture.

3.2 Experimental

3.2.1 Two-dimensional gas chromatography – nitrogen chemiluminescence detection (GC×GC-NCD)

3.2.1.1 Standards and solutions

N-nitrosomorpholine and N-nitrosopiperidine were commercially available as 5000 µg mL^{-1} solutions in methanol (Sigma-Aldrich Ltd., Dorset, U.K.). Solid standards of N-nitrosopiperazine and 1,4-dinitrosopiperazine were purchased from Santa Cruz Biotechnology (CA, U.S.). The remaining standards were synthesised at the Norwegian University of Life Sciences in Oslo, Norway. Compounds synthesised included N-nitromorpholine, N-nitropiperidine, N-nitropiperazine, *tert*-butyl(nitro)amine (*t*BA-NO_2). 4,4-dimethyl-3-nitro-1,3-oxazolidin-2-one was also shipped to the University of York as a precursor compound to 2-methyl-2-(nitroamino)propan-1-ol (AMP-NO_2). N-nitrosopiperazine and N-nitropiperazine were derivatized prior to analysis. The chemical structures of the target nitrosamines and nitramines are shown in Figure 3.1.

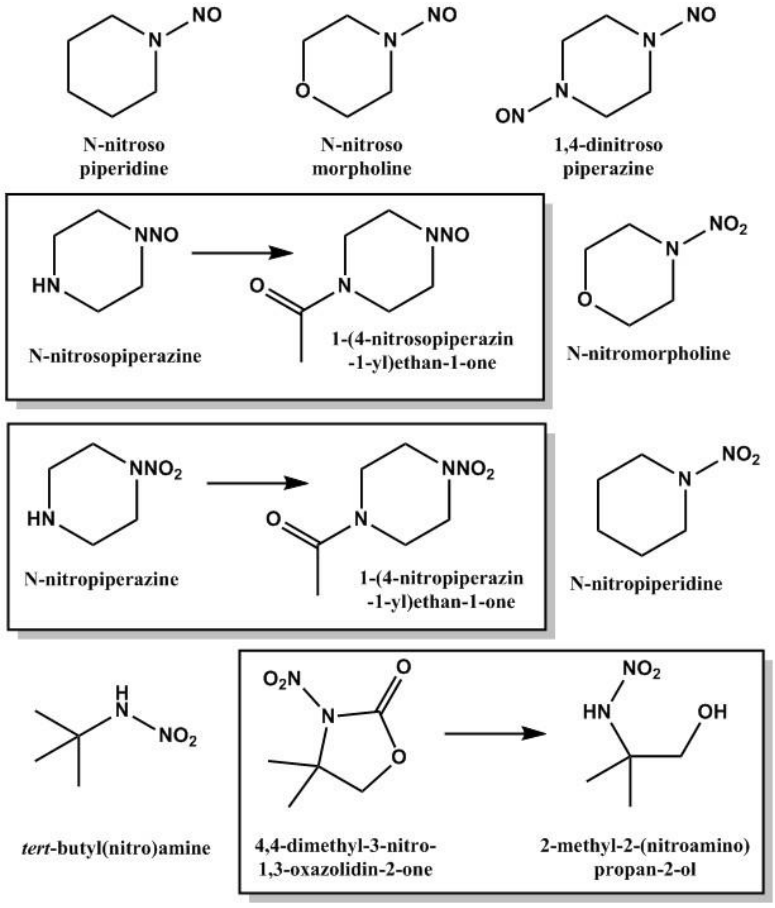

Figure 3.1. Chemical structures of the target nitrosamines and nitramines.

3.2.1.2 Preparation of 2-methyl-2-(nitroamino)propan-2-ol (AMP-NO_2)

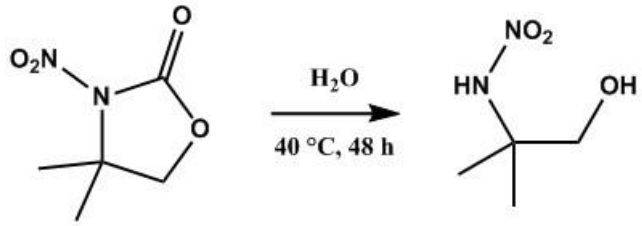

4,4-dimethyl-3-nitro-1,3-oxazolidin-2-one (50 mg, 0.31 mmol) was dissolved in deionised water (1.4 mL) and stirred at 40 °C for 48 hours. The aqueous phase was then extracted with EtOAc (20 mL) and the organic portion was dried ($MgSO_4$), filtered and concentrated under vacuum to produce 2-methyl-2-(nitroamino)propan-2-ol as a white solid (38 mg, 0.28 mmol, 93%); ^{1}H NMR ($CDCl_3$, 400 MHz): δ 8.49 (broad s, 1H, OH), 3.66 (s, 2H, CH_2), 1.38 (s, 6H, CH_3); $^{13}C\{^1H\}$ NMR ($CDCl_3$, 100 MHz): δ 67.24 (CH_2), 59.91 (C), 21.90 (CH_3).

3.2.1.3 Method validation

Stock solutions for analysis by GC×GC were prepared in EtOAc (HPLC grade, >99.5% purity, Fisher Scientific Ltd., Leicestershire, U.K.) at concentrations of 5000 ppm. Stepwise dilutions were carried out to obtain analytical standards at concentrations ranging from 0.005 ppm to 5 ppm, allowing for the external calibration of each target compound.

To develop a method suitable for gas phase sampling of the target compounds, Thermosorb-N air sampling cartridges from Ellutia (Cambridgeshire, U.K.) were tested. A 10 cm length of ¼" stainless steel tubing was packed with glass wool and attached to the cartridge inlet using a series of adaptors. The cartridge outlet was connected to ¼" PFA tubing, followed by a mass flow controller (Alicat whisper series, 0-2 SLPM, PCT Ltd., U.K.) and a corrosion resistant vacuum pump (KNF Neuberger, Oxfordshire, U.K.). All tubing was purchased from Swagelok, Teesside, U.K. A 3D printed holder, made out of polylactic acid (PLA) was used to hold the cartridges firmly in place, as shown in Figure 3.2.

Figure 3.2. Set up used for testing the Thermosorb-N air sampling cartridges.

Recovery tests were carried out by spiking the glass wool located at the inlet with either *t*BA-NO_2 or AMP-NO_2 (20 µL of 500 ppm solution, 10 µg). The cartridges were vapour spiked by sampling at the recommended flow rate (1 L min^{-1}) for 60 min. The cartridges were eluted against the direction of air flow using 3 mL of DCM/ MeOH (75:25), evaporated to near dryness under a gentle stream of nitrogen, and made up to a final volume of 1 mL in EtOAc. Several blank cartridges that had not been vapour spiked were also eluted using the same method to check that none of the target analytes were present.

The aerosol sampling method was tested using quartz fibre filters supplied by Whatman, Maidstone, U.K. Each filter was pre-baked at 550 °C for 6 hours before use, and wrapped in aluminium foil and stored at -18 °C until required. To perform the recovery tests, 47 mm diameter quartz fibre filters were spiked with the target analytes (1.0 – 10 µg) and extracted using an accelerated solvent extraction system (ASE 350, Dionex, CA, United States). The base of each 5 mL stainless steel extraction cell was lined with two glass microfibre filter papers (Fisher Scientific Ltd., Loughborough, U.K.) and then packed with the spiked filter paper. Extractions were carried out in EtOAc (GC grade, 99.9% purity) at 80 °C and 1500 psi for three consecutive 5 min cycles. A 50% flush volume and 60 s purge time were used. The extracts were evaporated under nitrogen to 1 mL and stored at -18 °C prior to analysis. Procedural blanks were carried out to check for the presence of target analytes in detectable amounts. Extracts containing N-nitrosopiperazine and N-nitropiperazine were derivatized before analysis; both compounds were stirred in 1 mL EtOAc at RT for 30 mins with 1.7 equiv. of acetyl chloride and 2.2 equiv. of triethylamine.

3.2.1.4 Chromatographic analysis

Chromatographic analysis was carried out on a GC×GC-NCD system comprised of an Agilent 7890 gas chromatograph and an Agilent 255 NCD system (Palo Alto, CA, United States). The first column was a non-polar Ultra Inert DB5 (30 m × 0.32 mm i.d. × 0.25 µm film thickness) and the second column a mid-polarity DB-17 (3 m × 0.10 m i.d. × 0.10 µm film thickness). Both columns were purchased from Agilent Technologies Ltd., Stockport, U.K. The initial temperature of the first dimension column was 40 °C for 2 min, followed by a heating rate of 7 °C min^{-1} to 100 °C for 8 min and then further heating at 7 °C min^{-1} until 270 °C was reached and held isothermally for a further 5 min. A temperature offset of 30 °C was applied to the second dimension column throughout the GC temperature program. A liquid nitrogen two-stage cold jet modulation system was used, with a modulation period of 5 s and a +15 °C offset from the secondary GC oven temperature. Data was collected at 200 Hz over the entire course of the analysis, and hydrogen was used as a carrier gas at 1.4 mL min^{-1}. Injections of 1 µL were performed in splitless mode at an injection temperature of 200 °C using an automated liquid injector (Gerstel, Mülheim an der Ruhr, Germany).

Pyrolysis of the analytes in the dual plasma burner was carried out at 900 °C under a hydrogen flow rate of 4 mL min^{-1} and an oxygen flow rate of 10 mL min^{-1}.

3.2.2 Ion chromatography

3.2.2.1 Eluents and analytical standards

Ultrapure milli-Q water from an ELGA LabWater purification system (18 MΩ cm^{-1}) was used to prepare all of the required eluents and analytical standards. A solution of 8 mM Na_2CO_3 /1 mM $NaHCO_3$ (Sigma-Aldrich Ltd., Dorset, U.K.) was used as the eluent for anion-exchange chromatography. Methanesulfonic acid, also available from Sigma-Aldrich Ltd., was used to prepare the eluent for cation-exchange chromatography at concentrations ranging from 20 to 100 mM. Table 3.1 provides a summary of the compounds used to prepare the analytical standards for both anion and cation chromatography. All of the compounds were purchased from either Sigma-Aldrich Ltd. (Dorset, U.K.) or Fisher Scientific Ltd. (Loughborough, U.K.).

Table 3.1. Compounds used to prepare stock solutions for both anion- and cation-exchange chromatography and their respective ion concentrations.

Stock solutions for anion-exchange chromatography		
Compound	**Target anion**	**[anion] / ppm**
Sodium chloride, NaCl	Cl^-	540.7
Sodium nitrite, $NaNO_2$	NO_2^-	514.0
Sodium nitrate, $NaNO_3$	NO_3^-	493.9
Sodium dihydrogen phosphate, H_2NaPO_4	PO_4^{3-}	502.6
Sodium sulfate, Na_2SO_4	SO_4^{2-}	467.7
Stock solutions for cation-exchange chromatography		
Compound	**Target cation**	**[cation] / ppm**
tert-Butylamine, $C_4H_{11}N$	$[C_4H_{12}N]^+$	10,000
Aminomethyl propanol, $C_4H_{11}NO$	$[C_4H_{12}NO]^+$	10,000
Morpholine, C_4H_9NO	$[C_4H_{10}NO]^+$	10,000
Piperidine, $C_5H_{11}N$	$[C_5H_{12}N]^+$	10,000
Piperazine, $C_4H_{10}N_2$	$[C_4H_{11}N_2]^+$	10,000

3.2.2.2 Method validation

The stock solutions for anion-exchange chromatography were diluted with milli-Q water to prepare a mixed analytical standard containing all of the target anions at 50 ppm. Further stepwise dilutions of the mixed standard were carried out to obtain standards at 25, 10, 5, 2.5, 1, 0.5, 0.25, 0.1, 0.05 and 0.01 ppm; these solutions were used to obtain an external calibration curve for each target ion. For cation-exchange chromatography the same dilution procedure was carried out, except that the amine-based stock solutions were individually diluted to 500 ppm prior to combination with each other.

Recovery tests were performed by spiking sections of 47 mm diameter quartz fibre filters (Whatman, Maidstone, U.K.) with the target analytes (7.5 – 15 µg). Prior to spiking, the filters were pre-baked at 550 °C for 6 hours and then wrapped in aluminium foil and stored at -18 °C until required. To replicate the real samples collected at the chamber, recovery tests were carried out on two different filter sizes (a whole 47 mm diameter filter and one quarter of a 47 mm diameter filter). The spiked filters were dissolved in 2 or 3 mL of milli-Q water respectively and sonicated at room temperature for 30 mins. The extract was filtered using a Millex-GP 33 mm diameter hydrophilic syringe filter with a pore size of 0.22 µm (Millipore UK Limited, Watford, U.K.). Procedural blanks were also carried out using 47 mm diameter quartz fibre filters and blank subtractions were applied to any target ions found in detectable amounts.

3.2.2.3 Chromatographic analysis

Chromatographic analysis was carried out using an ICS-110 integrated IC system equipped with an AS-DV autosampler (Dionex Corporation, CA, United States). The column configuration used for anion exchange consisted of an IonPac AG14A guard column (4 × 50 mm) and an IonPac AS14A analytical column (4 × 250 mm). Cation exchange chromatography was performed using an IonPac CG12A guard column (4 × 50 mm) and an IonPac CS12A analytical column (4 × 250 mm). AERS 500 and CSRS 300 self-regenerating suppressors (4 mm) were used for anion and cation exchange respectively. All columns and suppressors were supplied from Dionex Corporation. The system used a DS6 heated conductivity cell for ion detection. All anion-exchange experiments were carried out in isocratic mode but some cation-exchange experiments relied on gradient elution. Gradient elution was achieved using a Dionex reagent free controller (RFC-30) in combination with a Dionex EGC 111 MSA eluent generator cartridge and a continuously regenerated trap column. A summary of the separation methods for anion and cation chromatography is provided in Table 3.2, and additional details of the gradient elution system can be found in Table 3.3. All data obtained was analysed using the Chromeleon v7.1 software package.

Table 3.2. Method parameters used for both anion exchange and cation exchange chromatography.

method parameter	anion exchange	cation exchange	
run time	18 min	15 min	24-27 min
flow type	isocratic	isocratic	gradient
flow rate	1 mL/min	1 mL/min	1 mL/min
injection volume	100 µL	100 µL	100 µL
data collection rate	5 Hz	5 Hz	5 Hz
column temperature	30 °C	30 °C	30 °C
suppressor current	45 mA	59 mA	59 – 293 mA

Table 3.3. Gradient methods employed for the analysis of $[C_5H_{12}N]^+$ and $[C_4H_{12}N_2]^{2+}$.

Gradient method for protonated piperidine, $[C_5H_{12}N]^+$		
Rate / mM min^{-1}	**Target concentration / mM**	**Duration / min**
Initial	20	10
4.00	60	10
Final	20	4
Gradient method for protonated piperazine, $[C_4H_{12}N_2]^{2+}$		
Rate / mM min^{-1}	**Target concentration / mM**	**Duration / min**
Initial	20	4
4.21	100	19
Final	20	2

3.3 Results and discussion

3.3.1 Method validation for the GC×GC-NCD system

3.3.1.1 Thermosorb-N air sampling cartridges

For the ACA 2015 campaign, there were two target compounds for gas phase sampling using Thermosorb-N cartridges; *t*BA-NO_2 and AMP-NO_2. It was not possible to perform recovery tests using AMP-NO_2 before the campaign, because the compound was not commercially available and synthesis at the Norwegian Institute of Life Sciences had not yet been achieved. However, recovery tests using *t*BA-NO_2 were carried out in triplicate. *t*BA-NO_2 was easily observed in the GC×GC-NCD chromatogram, and is shown as peak A in Figure 3.3. Recovery of the target analyte from the Thermosorb-N cartridge was calculated by comparing the peak area obtained from the spiked cartridge with the peak area obtained by direct injection of the standard to the GC×GC-NCD. The cartridge sampling system was set up as described in section 3.2.1.3 and the glass wool was spiked with 20 µL of 500 ppm solution (10 µg). After 60 min of sampling for each recovery test (n = 3), the cartridge was eluted using 3 mL of DCM/ MeOH (75:25) and an average recovery level of 61.5% was achieved (%RSD < 12%).

After the campaign, AMP-NO_2 was synthesised and tested using the same method but unfortunately the recovery of this compound from the cartridge was poor (*ca.* 4%). The next step would normally be to optimise the extraction method to improve the recovery of the compound, by altering the composition or volume of the solvent mixture for example. However, it was becoming increasingly evident that some of the material present in the Thermosorb-N cartridges was contaminating the eluted extracts and damaging the ultra inert GC column installed in the GC×GC-NCD. For example, peaks B, C and D shown on the chromatogram (Figure 3.3) are unidentified contaminants from the Thermosorb-N cartridge; the broad peak shapes and the observed carryover of these compounds indicated that they may have contributed to the column damage.

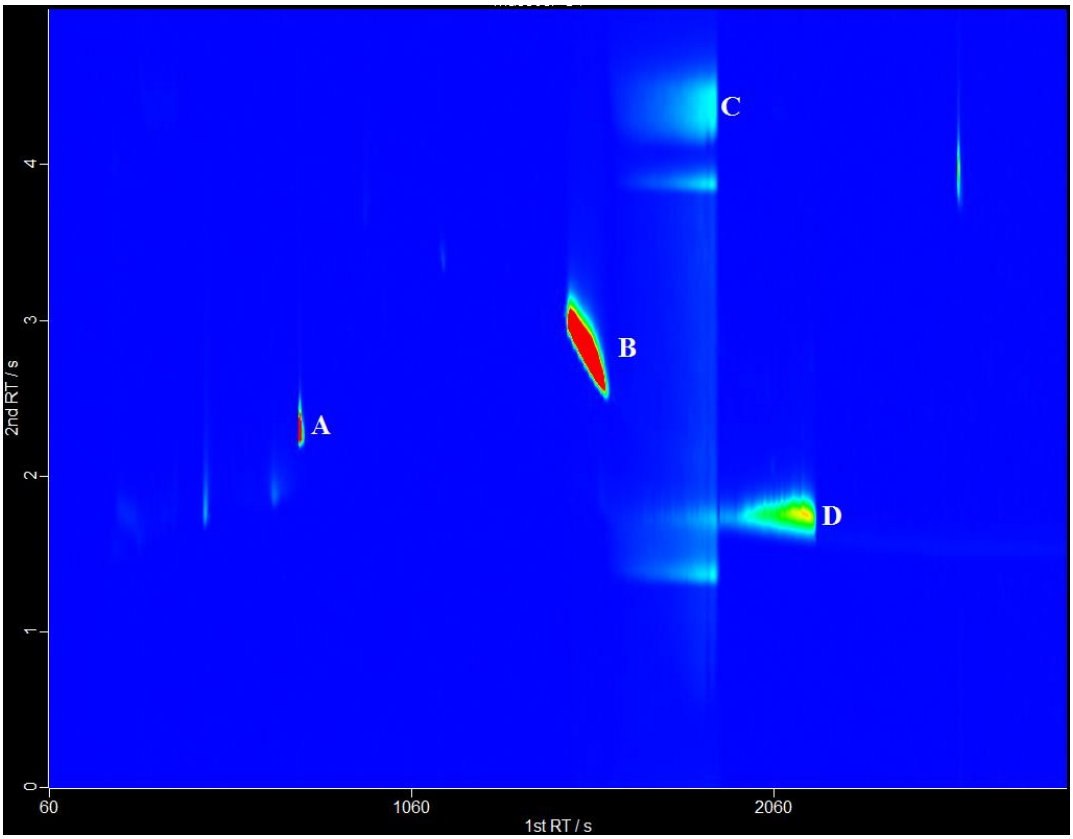

Figure 3.3. GC×GC-NCD chromatogram of a Thermosorb-N air sampling cartridge spiked with *t*BA-NO_2 (20 µL of 500 ppm solution, 10 µg). Peak A: recovered *t*BA-NO_2. Peaks B, C and D: unidentified contaminants from the cartridge that possibly damaged the GC column.

3.3.1.2 Pressurized liquid extraction (PLE) conditions

A PLE method was developed for the analysis of nitrosamines in urban airborne particulate matter,[176] and is included in Chapter 2 (sections 2.2.4 and 2.3.1). The recovery of each nitrosamine is listed in Chapter 2, Table 2.2, and an overall an average recovery level of 91% was obtained, with RSD < 9% for all nitrosamines. Due to the high accuracy and precision associated with this method, the same technique was applied to the target compounds in this study. Evaporating samples to dryness was avoided to prevent the loss of compounds with high vapour pressures. Recoveries of the compounds were calculated by comparing the peak areas obtained from the spiked filters with peak areas acquired by direct injection of the standards. The results obtained are summarised in Table 3.4; recovery levels ranged from 81.8 to 94.9%, with an average recovery level of 88.5%. %RSD remained below 3.5% for all of the target compounds except 1-(4-nitrosopiperazin-1-yl)ethan-1-one and 1-(4-nitropiperazin-1-yl)ethan-1-one, which had %RSD values of 10.95% and 11.35% respectively. The recovery levels for these two compounds were likely to be less precise due to the additional derivatization step that was carried out prior to analysis by GC×GC-NCD.

No further optimisation of the PLE method was carried out as the good recovery levels, coupled with the low standard deviation values, indicated that this method was reliable and capable of accurately quantifying the target compounds. Blanks of the solvent (EtOAc) and the pre-baked blank filter paper were analysed and no detectable amounts of the target compounds were found.

Table 3.4. Recovery levels and %RSD$_{rec}$[a] of the target compounds under the final PLE conditions[b].

Compound	% recovery	% RSD$_{rec}$ (n = 3)
*t*BA-NO_2	86.6	3.52
AMP-NO_2	81.8	3.24
N-nitrosomorpholine	94.1	1.33
N-nitrosopiperidine	92.2	1.82
N-nitromorpholine	94.9	1.97
N-nitropiperidine	83.8	3.24
1,4-dinitrosopiperazine	89.3	0.92
1-(4-nitrosopiperazin-1-yl)ethan-1-one	82.1	11.0
1-(4-nitropiperazin-1-yl)ethan-1-one	91.6	11.4

[a]% Relative standard deviation for the recovery process. [b]PLE conditions: ethyl acetate, 80 °C, 1500 psi, three 5 min cycles, 50% flush volume, 60 s purge time.

3.3.1.3 Derivatization of N-nitrosopiperazine and N-nitropiperazine

The majority of the target compounds were suited to GC×GC, with narrow, symmetric chromatographic peaks and good resolution. However, the peaks produced for N-nitrosopiperazine and N-nitropiperazine were not quantifiable, with peak tailing, reduced response and column carryover observed. It was clear that a method to derivatize the –NH group would need to be developed in order to accurately quantify these compounds. This was achieved by using acetyl chloride in the presence of triethylamine to replace the hydrogen atom in the –NH group with an acetyl group; details of the synthetic procedures and compound characterisation are described overleaf.

1-(4-Nitrosopiperazin-1-yl)ethan-1-one:

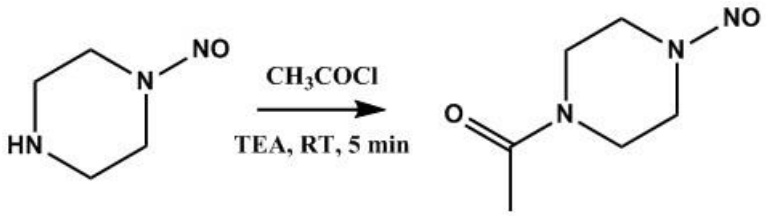

N-nitrosopiperazine (45 mg, 0.39 mmol) was dissolved in EtOAc (3.4 mL) before acetyl chloride (47.4 µL, 0.67 mmol) and triethylamine (124.0 µL, 0.89 mmol,) were added and the mixture stirred at RT for 5 mins. The resulting solution was concentrated *in vacuo* and analysed by ^{1}H NMR spectroscopy: ^{1}H NMR ($CDCl_3$, 400 MHz): δ 4.32–4.23 (m, 2H), 3.83-3.80 (m, 2H), 3.78-3.75 (m, 1H), 3.71-3.68 (m, 1H), 3.61-3.58 (m, 1H), 3.46-3.44 (m, 1H), 2.14 & 2.12 (s, s, 3H, CH_3).

1-(4-Nitropiperazin-1-yl)ethan-1-one:

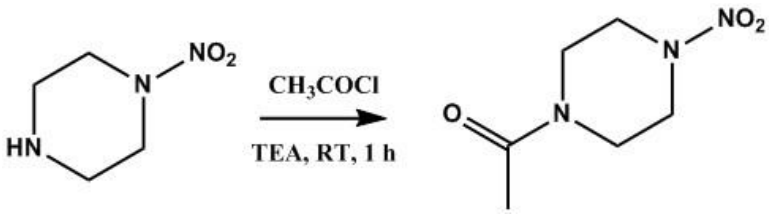

N-nitropiperazine (32 mg, 0.24 mmol) was dissolved in DCM (2.7 mL) before acetyl chloride (29.1 µL, 0.41 mmol) and triethylamine (76.2 µL,0.55 mmol) were added and the mixture stirred at RT for 1 hour. The solvent was evaporated *in vacuo* to give the crude product, which was purified by flash chromatography (EtOAc) to give 1-(4-nitropiperazin-1-yl)ethan-1-one (30.0 mg, 0.17 mmol, 73%). ^{1}H NMR ($CDCl_3$, 400 MHz): δ 3.89-3.60 (m, 8H, CH_2), 2.11 (s, 3H, CH_3); ^{13}C{^{1}H} NMR ($CDCl_3$, 100 MHz): δ 169.1 (C=O), 48.4, 44.4, 39.7, 21.4; HRMS (ESI^{+}): MNa^{+}, found 196.0692 ($C_6H_{11}N_3NaO_3$, error = 0.4 ppm).

Scheme 3.1 shows the mechanism for the derivatization of N-nitropiperazine to form 1-(4-nitropiperazin-1-yl)ethan-1-one. The first step is the addition of the nucleophilic amine to the electrophilic carbonyl group, which leads to the formation of an alkoxide intermediate. As this intermediate is unstable, an elimination reaction occurs in which the chloride ion is removed.[177] The basic conditions of the reaction are achieved by the addition of triethylamine. This removes a proton before the loss of the chloride ion, leading to the formation of triethylamine hydrochloride as a by-product in the reaction. The same procedure was carried out for N-nitrosopiperazine to produce 1-(4-nitrosopiperazin-1-yl)ethan-1-one.

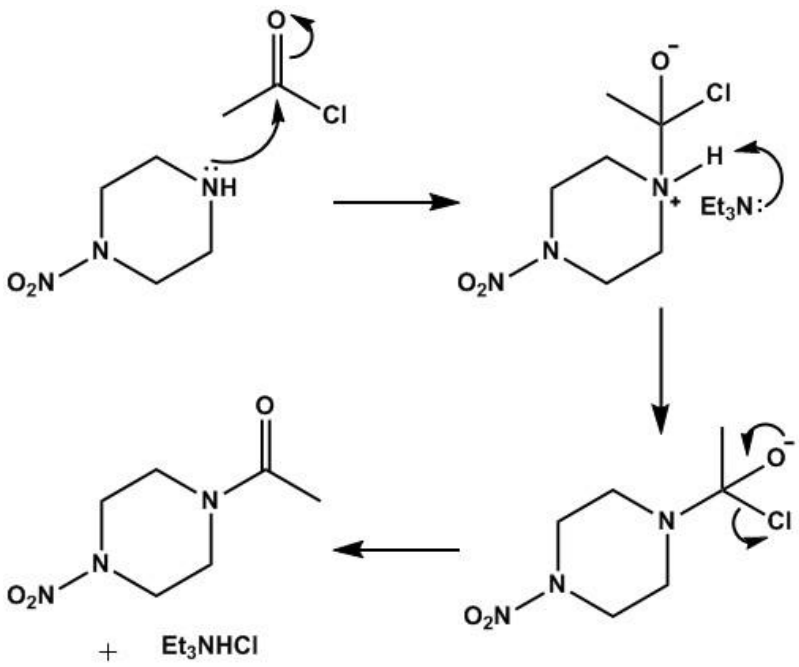

Scheme 3.1. Mechanism for the acylation of N-nitropiperazine to form 1-(4-nitropiperazin-1-yl)ethan-1-one.

The GC×GC-NCD chromatograms shown in Figure 3.4 provide a direct comparison of a 5 ppm solution of N-nitropiperazine (peak A, upper panel, 1st RT = 1755 s, 2nd RT = 2.63 s) and the derivatized product, 1-(4-nitropiperazin-1-yl)ethan-1-one (peak E, lower panel, 1st RT = 2110 s, 2nd RT = 3.21 s). The colour scaling settings are the same for both chromatograms. At 5ppm, N-nitropiperazine had a maximum S/N ratio of 83 and a peak width of *ca*. 125 s. At the same concentration, 1-(4-nitropiperazin-1-yl)ethan-1-one had a higher S/N ratio (max. = 47,438) due to its narrower peak shape (*ca.* 40 s), making it considerably easier to accurately quantify. In addition, unlike N-nitropiperazine, no carryover of this compound was observed. The peak is also separated from other compounds of interest, such as 1,4-dinitrosopiperazine (peak C) and 1-(4-nitrosopiperazine-1-yl)ethan-1-one (peak D). Peak B in the chromatogram is triethylamine left over from the derivatization process. At trace level quantities, it is difficult to remove triethylamine from the solution without significant losses of the target compounds. As it is separated from the compounds of interest and not causing any obvious chromatographic problems, an additional sample clean up step was not carried out.

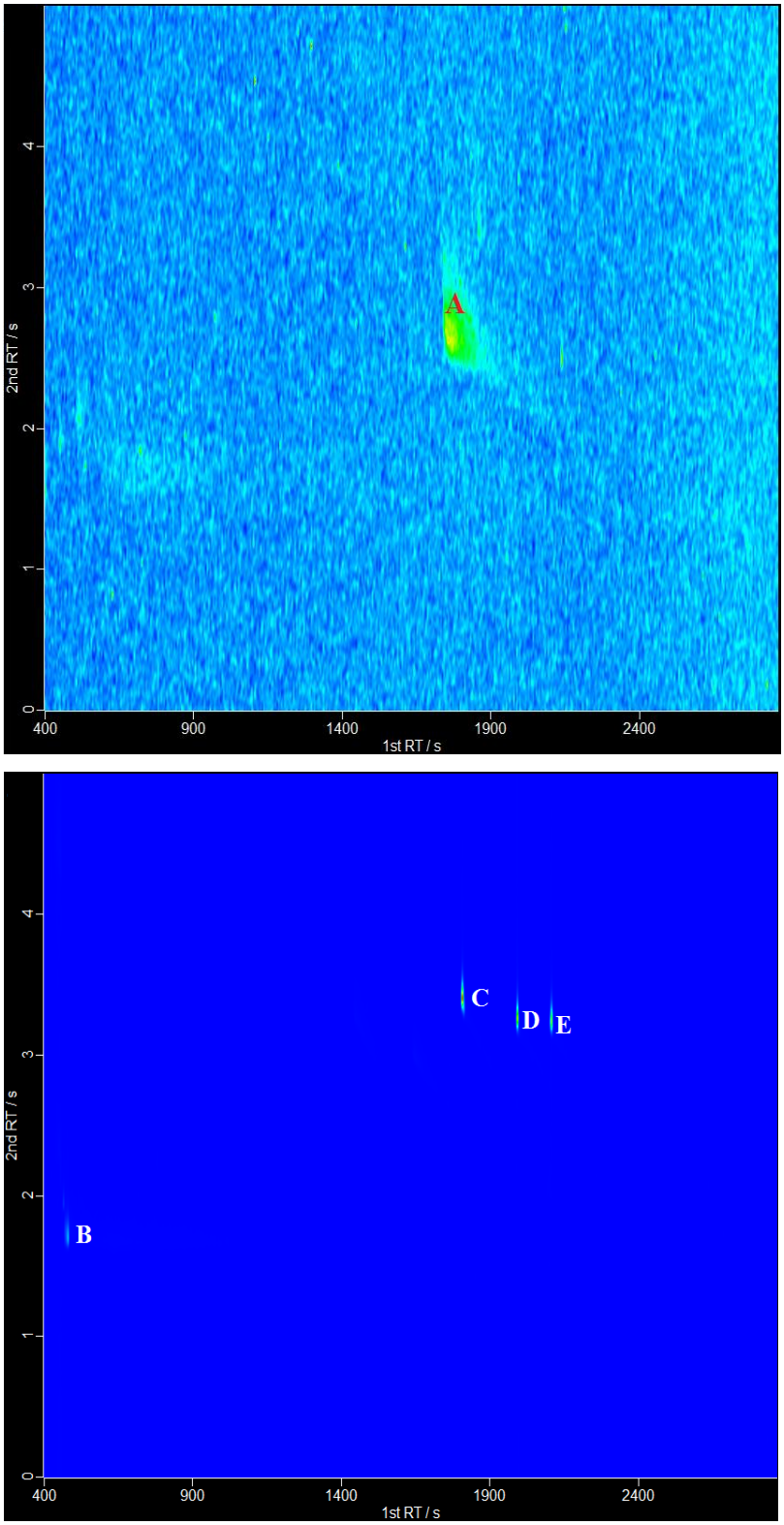

Figure 3.4. The upper chromatogram shows N-nitropiperazine (A), and the lower chromatogram shows triethylamine (B), 1,4-dinitrosopiperazine (C), 1-(4-nitrosopiperazin-1-yl)ethan-1-one (D) and 1-(4-nitropiperazin-1-yl)ethan-1-one (E). All compounds are present at 5 ppm except triethylamine (concentration unknown).

3.3.1.4 Instrumental parameters – GC×GC-NCD

Using the GC×GC-NCD system set up as described in Chapter 2 (sections 2.2.5 and 2.3.2), the main instrumental parameters for the target compounds listed in Table 3.5 were investigated. Although most of the compounds were suited to GC×GC, AMP-NO_2 showed some peak tailing and had a lower response compared to other nitramines. Nevertheless, the identification and quantification of this compound was still possible, and limits of detection were sufficient for the analysis required in this study.

External standards prepared in EtOAc were used to calibrate the GC×GC-NCD system and identification of the compounds was based on 1st and 2nd retention times, as listed in Table 3.5. A linear model was fitted to the calibration data and good R^2 values between 0.9910 and 0.9993 were obtained for the stated linear ranges, confirming that the external standard method can be successfully applied to the quantification of the target compounds.

Replicates of each compound (n = 10, 0.025 – 0.5 ng as indicated in Table 3.5) were injected to the GC×GC-NCD system to monitor instrument repeatability. $\%RSD_{ins}$ for AMP-NO_2 was the highest at 23.0%. This may be due to the interaction of the –OH group with acidic silanol groups present on the column stationary phase. $\%RSD_{ins}$ for the two derivatized compounds, 1-(4-nitrosopiperazin-1-yl)ethan-1-one and 1-(4-nitropiperazin-1-yl)ethan-1-one, were 21.0% and 16.3% respectively. It is possible that these compounds may be slightly susceptible to degradation during pyrolysis, although this has not been confirmed. $\%RSD_{ins}$ for the remaining target compounds remained below 12%, allowing for precise measurements of these compounds to be made.

In order to estimate total errors, the errors associated with the instrument and the recovery process were combined using Equation 3.1. Total errors ($\%RSD_{tot}$) remained below 12.1% with the exception AMP-NO_2 (23.3%), 1-(4-nitrosopiperazin-1-yl)ethan-1-one (23.6%) and 1-(4-nitropiperazin-1-yl)ethan-1-one (19.9%), which had higher errors as previously discussed.

$$\%RSD_{tot} = \sqrt{\%RSD_{rec}^2 + \%RSD_{ins}^2} \quad (3.1)$$

Instrumental LODs and LOQs were calculated according to the U.S. EPA procedure, as previously discussed in Chapter 2, section 2.3.2.[178] Using these guidelines, a suitable spike level was chosen for the recovery tests, and ranged from 0.025 ng to 0.5 ng, as shown in Table 3.5. The compounds with the lowest detection limits were N-nitrosomorpholine, N-nitrosopiperidine, N-nitromorpholine, N-nitropiperidine and 1,4-dinitrosopiperazine, with LOD values ranging from 1.7 to 7.7 pg and LOQ values between 13.0 pg and 27.1 pg. These compounds are well suited to GC×GC analysis and do not contain any –NH or –OH

Table 3.5. Instrumental parameters and associated errors for the GC×GC-NCD system.

Compound	1st RT / s	2nd RT / s	LOD / pg	LOQ / pg	Linear range / ng	R^2	%RSD_{ins} (n = 10)	%RSD_{tot}
*t*BA-NO_2	750	2.27	26.9 ‡	48.9 ‡	0.05 – 5	0.9977	6.09	7.04
AMP-NO_2	1370	3.01	1214.7 *	1474.5 *	0.5 – 50	0.9910	23.04	23.27
N-nitrosomorpholine	1060	4.12	7.2 ≠	20.2 ≠	0.005 – 1.0	0.9927	8.64	8.74
N-nitrosopiperidine	1180	3.82	5.0 ≠	17.2 ≠	0.005 – 1.0	0.9956	6.99	7.23
N-nitromorpholine	1320	3.51	7.3 ≠	16.8 ≠	0.005 – 1.0	0.9973	6.97	7.24
N-nitropiperidine	1425	3.17	1.7 ≠	13.0 ≠	0.005 – 1.0	0.9959	5.62	6.48
1,4-dinitrosopiperazine	1810	3.34	7.7 ≠	27.1 ≠	0.005 - 20	0.9991	12.03	12.06
1-(4-nitrosopiperazin-1-yl)ethan-1-one	1995	3.21	12.6 ≠	58.5 ≠	0.005 – 20	0.9991	20.95	23.63
1-(4-nitropiperazin-1-yl)ethan-1-one	2105	3.21	10.4 ≠	29.1 ≠	0.005 – 20	0.9993	16.33	19.88

Spike levels used to determine LOD and LOQ: 0.05 ng ‡, 0.5 ng *, 0.025 ng ≠.

groups to interact with the GC column. LOD and LOQ values for the two derivatized compounds were slightly higher, at 12.6 pg and 58.5 pg for the nitrosamine, and 10.4 pg and 29.1 pg for the nitramine. The LOD and LOQ for *t*BA-NO_2 were 26.9 pg and 48.9 pg respectively, whilst values for AMP-NO_2 were up to 45 times higher due to the sticky nature of this compound.

In summary, the combined PLE-GC×GC-NCD method is a powerful technique suitable for accurate trace level measurements of nitrosamines and nitramines in aerosol. This method will be used in Chapter 4 to investigate nitrosamine and nitramine formation during a range of amine photo-oxidation experiments at EUPHORE in Valencia, Spain.

3.3.2 Method validation – ion chromatography

3.3.2.1 Ion extraction

A simple and effective approach was adopted to extract amine salts from the spiked filter paper; the sample was dissolved in water, sonicated, and filtered through hydrophilic syringe filters. Recoveries of the target ions were calculated using the same method as the GC×GC-NCD. Two different sets of samples were collected at the chamber during the 2016 campaigns, as described in more detail in Chapter 4, section 4.2.2. One quarter of the 47 mm filters collected using the high volume pump (*ca.* 43 L min^{-1}) was extracted in 2 mL milli-Q water. For the samples collected using the low volume pump (*ca.* 5 L min^{-1}), the entire filter was extracted in 3 mL milli-Q water. As a result, two different recovery tests were carried out to ensure the efficiency of each process was accurately determined. Only one type of recovery test was carried out for the *tert*-butylamine and AMP ions, as these were investigated during the 2015 campaign when samples were collected using the high-volume pump only.

A summary of the results from the recovery tests for the target anions can be found in Table 3.6. All of the reported recoveries have been corrected using procedural blanks; the average contribution was 2.6 % of the total peak area for all ions except phosphate. 56.1% of the total phosphate peak came from background levels present in the blank filter. In general the recovery of the target anions was very high and reproducible. The recovery of the target anions from a whole 47 mm filter dissolved in 3 mL water ranged from 90.5 % to 99.6 % and %RSD was lower than 2.6%. The recoveries from a quarter of a filter were slightly higher, with excellent recovery levels between 99.0 and 100.5%, except for phosphate at 104.7%. Theoretically these levels should not exceed 100%, but in this case it is possible that the higher value for phosphate results from errors associated with the extraction process and the instrument itself.

Table 3.6. Recovery levels and %RSD$_{rec}$ of the target anions under the final extraction conditions[a].

Anion	% recovery (whole filter)[b]	% RSD$_{rec}$ (n = 3)	% recovery (¼ part filter)[c]	%RSD$_{rec}$ (n = 3)
Chloride, Cl^-	99.6	0.26	100.2	0.43
Nitrite, NO_2^-	98.5	0.48	100.3	0.12
Nitrate, NO_3^-	98.8	0.26	99.0	0.32
Phosphate, PO_4^{3-}	90.5	2.52	104.7	5.07
Sulfate, SO_4^{2-}	97.2	0.61	100.5	0.77

[a]Extraction conditions: milli-Q water, RT, 30 min sonication, filtration. [b]47 mm diameter filter dissolved in 3 mL milli-Q water. [c] ¼ part 47 mm filter dissolved in 2 mL milli-Q water.

The results obtained from the cation recovery tests are summarised in Table 3.7. In general, recovery of the *tert*-butylamine and AMP ions (76.6 and 75.2% respectively) are lower than the rest of the cations, which have an average recovery level of 88.0%. These were the two target cations for the 2015 campaign and were tested a year before the rest of the cations. When these tests were carried out, a syringe with less suction was used to remove the water extract from the sonicated filter paper, which would explain why greater losses were observed.

Out of all of the target cations for the 2016 campaigns, the ions of morpholine and piperidine displayed the highest recovery levels, at 94.3% and 98.5% respectively. The recovery levels for the piperazine ion was also relatively high at 86.4%. Overall, the average %RSD across all of the cation recovery tests was 3.1%, with a maximum error of 9.4% for the *tert*-butylamine ion. In summary, the extraction method was not optimised further as a quick and simple technique offering accurate results was obtained. Pre-baked filter papers were analysed for the target cations and no detectable amounts were found.

Table 3.7. Recovery levels and %RSD$_{rec}$ of the target cations under the final extraction conditions[a].

Cation	% recovery (whole filter)[b]	%RSD$_{rec}$ (n = 3)	% recovery (¼ part filter)[c]	% RSD$_{rec}$ (n = 3)
tert-Butylamine ion, $C_4H_{12}N^+$	n/a	n/a	76.6	9.37
Aminomethyl propanol ion, $C_4H_{12}NO^+$	n/a	n/a	75.2	1.21
Morpholine ion, $C_4H_{10}NO^+$	94.4	2.14	94.3	0.66
Piperidine ion, $C_5H_{12}N^+$	98.5	2.70	97.7	5.11
Piperazine ion, $C_4H_{11}N_2^+$	86.4	1.73	86.6	1.76

[a]Extraction conditions: milli-Q water, RT, 30 min sonication, filtration. [b]47 mm diameter filter dissolved in 3 mL milli-Q water. [c] ¼ part 47 mm filter dissolved in 2 mL milli-Q water.

3.3.2.2 Instrumental parameters - IC

The main instrumental parameters for the target anions listed in Table 3.8 were investigated using the IC set up in anion exchange mode, as described in section 3.2.2.3. Using an isocratic elution method with a solution of 8 mM Na_2CO_3 /1 mM $NaHCO_3$ as the eluent, the target anions were successfully separated within 17 minutes, as shown in the anion-exchange chromatogram in Figure 3.5. This method was chosen initially because it is a standard method recommended by Dionex for the isocratic separation of mono- and divalent anions in a single injection.[179] The anions were identified according to their retention times, as listed in Table 3.8. Whilst it is highly unlikely that anions such as methane sulfonate, bromide and oxalate will be present in the chamber samples, they can be present in ambient air and it is useful to observe that they are separated from the target anions for this study. R^2 values were assessed for the stated linear ranges shown in Table 3.8. The values ranged from 0.9968 to 0.9996 and the linear model provided a good fit for the calibration plots. This confirmed that the external standard method is appropriate for quantifying the target anions. In order to check instrument repeatability, replicates of each anion were run on the IC system (n = 10, 5 ng). As shown in Table 3.8, %RSD remained below 9% for all anions except phosphate (20.8%). The phosphate ion peak is relatively small and broad compared to other target anions at the same concentration, as shown in the chromatogram in Figure 3.5. Therefore, it is more difficult to integrate the peak accurately, and as a result a higher amount of variability in the peak area is observed.

Table 3.8. Instrumental parameters and associated errors for the IC system in isocratic anion exchange mode.

Anion	RT / min	LOD / ng	LOQ / ng	Linear range / µg	R^2	$\%RSD_{ins}$ (n = 10)	$\%RSD_{tot}$
Chloride, Cl^-	4.9	11.7	24.1	0.005 – 2.5	0.9985	8.47	8.47
Nitrite, NO_2^-	5.8	11.9	22.2	0.01 – 2.5	0.9994	8.14	8.15
Nitrate, NO_3^-	8.2	9.1	23.5	0.005 – 2.5	0.9968	8.91	8.92
Phosphate, PO_4^{3-}	11.1	19.9	48.3	0.01 – 2.5	0.9994	20.82	21.16
Sulfate, SO_4^{2-}	13.4	4.5	12.5	0.01 – 2.5	0.9996	5.41	5.45

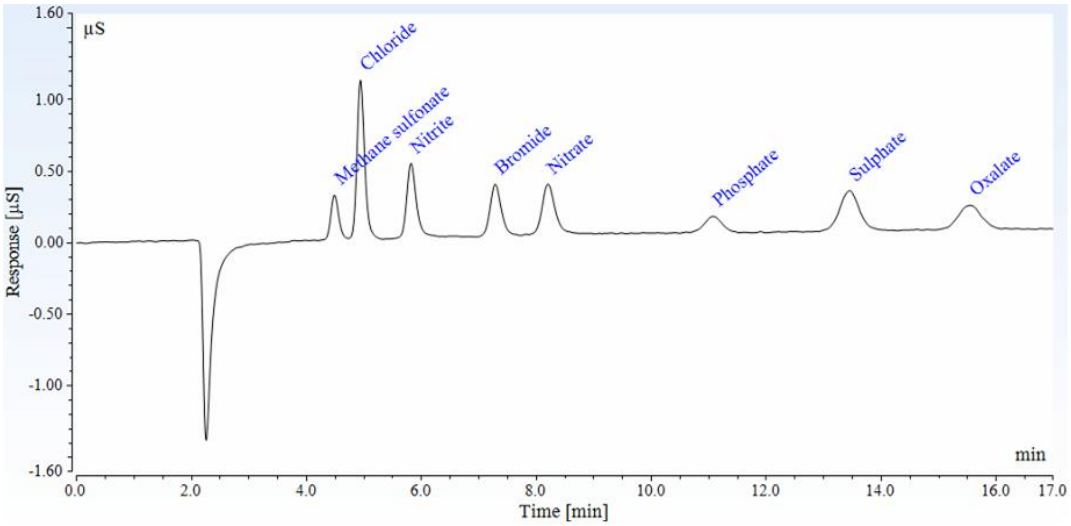

Figure 3.5. Anion chromatogram produced from a 1 ppm mixed anion standard containing methane sulfonate, chloride, nitrite, bromide, nitrate, phosphate, sulfate and oxalate ions.

To estimate total errors associated with both the instrument and the extraction method, the same calculation was carried out as for the GC×GC-NCD system, using Equation 3.1 (section 3.3.1.4). The total errors remained below 9%, with the exception of the phosphate ion (21.1%). The instrumental LODs and LOQs were also calculated using the same method as described in section 3.3.1.3, at a spike level of 0.05 ppm. As expected, the detection limits are considerably higher than the GC×GC-NCD system because IC is generally a much less sensitive technique. Despite this, LODs ranged from 4.5 ng to 19.9 ng for the target anions, and the LOQ values were between 12.5 ng and 48.3 ng; this should provide adequate sensitivity to accurately determine the presence of amine salts in the chamber.

The *tert*-butylamine ion ($C_4H_{12}N^+$) and the aminomethyl propanol ion ($C_4H_{12}ON^+$) were the first two protonated amines to be tested on the cation exchange system. These target cations were for the 2015 ACA campaign and at this stage, the gradient elution system for the IC was not available. However, using the isocratic method shown previously in Table 3.2 (standard method recommended by Dionex),[179] the instrumental parameters for these two cations were assessed and the data is summarised in Table 3.9. A better peak shape was obtained for $C_4H_{12}ON^+$ compared to $C_4H_{12}N^+$. This meant that LOD and LOQ values were lower for $C_4H_{12}ON^+$; 3.6 ng and 13.8 ng respectively, compared to 21.9 ng and 71.1 ng for $C_4H_{12}N^+$. For $C_4H_{12}ON^+$, the total error remained below 3%, and for $C_4H_{12}N^+$ the total error was 15.5%. In summary, it is likely that a slightly more accurate method could have been obtained for $C_4H_{12}N^+$ if the gradient system was employed, but the isocratic method provided accurate measurements nevertheless. The morpholine ion, $C_4H_{10}ON^+$, was also analysed using the isocratic method. As shown in the chromatogram in Figure 3.6, $C_4H_{10}ON^+$ is well separated from the major atmospheric cations. The LOD and LOQ values were 1.3 ng and 3.8 ng respectively, and $\%RSD_{tot}$ was 7.6%.

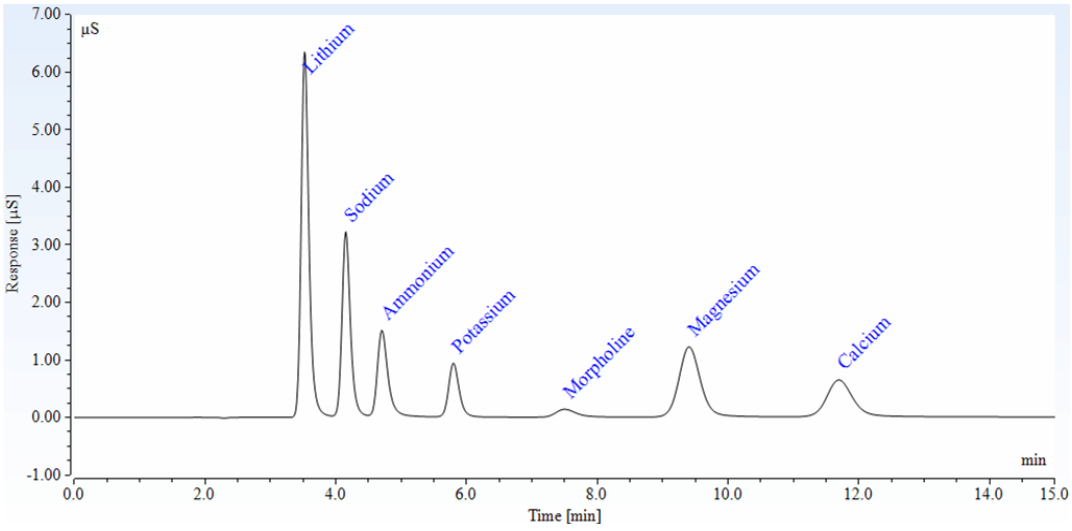

Figure 3.6. Cation chromatogram produced from a 1 ppm mixed cation standard containing ions of lithium, sodium, ammonium, potassium, morpholine, magnesium and calcium.

Table 3.9. Instrumental parameters and associated errors for the IC system in isocratic cation exchange mode.

Cation	RT / min	LOD / ng	LOQ / ng	Linear range / ng	R^2	%RSD_{ins} (n = 10)	%RSD_{tot}
Aminomethyl propanol ion, $C_4H_{12}ON^+$	4.1	3.6	13.8	50 – 5000	0.9999[b]	2.57	2.84
tert-Butylamine ion, $C_4H_{12}N^+$	6.2	21.9	71.1	50 – 5000	0.9993[a]	15.53	15.53
Morpholine ion, $C_4H_{10}ON^+$	7.5	1.3	3.8	1 - 2500	0.9994[b]	7.44	7.57
[a]R^2 values obtained using a linear model. [b]R^2 values obtained using a quadratic model.							

In order to determine whether a linear or quadratic model was the most suitable fit for the calibration data obtained, the adjusted R^2 values were compared for each type of model for each cation. The R^2 value for the *tert*-butylamine ion was 0.9993 and the linear model provided a good fit for the calibration curve. The calibration curves for the AMP and morpholine ions were more suited to a quadratic fit, and respective R^2 values of 0.9999 and 0.9994 were obtained. Figure 3.7 provides a comparison of the linear and quadratic fit for $C_4H_{10}ON^+$; it is clear that the quadratic model (represented by the red line, adjusted $R^2 = 0.9992$) fits the data considerably better than the linear model (blue line, adjusted $R^2 = 0.9799$).

Deviation from the linear relationship between analyte concentration and response can occur for analytes that form weak acids or weak bases in the suppressor.[173] Due to the processes associated with self-regenerating suppressors used in ion chromatography, the analyte *e.g.* $C_4H_{10}ON^+$ enters the suppressor in a 20 mM MSA solution, and leaves the suppressor in H_2O. In response to the increased pH, the equilibrium (shown in Equation 3.2) shifts to the left, and the amount of $C_4H_{10}ON^+$ decreases. This effect is more pronounced at higher analyte concentrations, and as a result the abundance ratio of $C_4H_{10}ON^+$ is decreased, and the linear relationship between analyte concentration and response is no longer observed.

$$C_4H_9ON + H^+ \leftrightarrow C_4H_{10}ON^+ \quad (3.2)$$

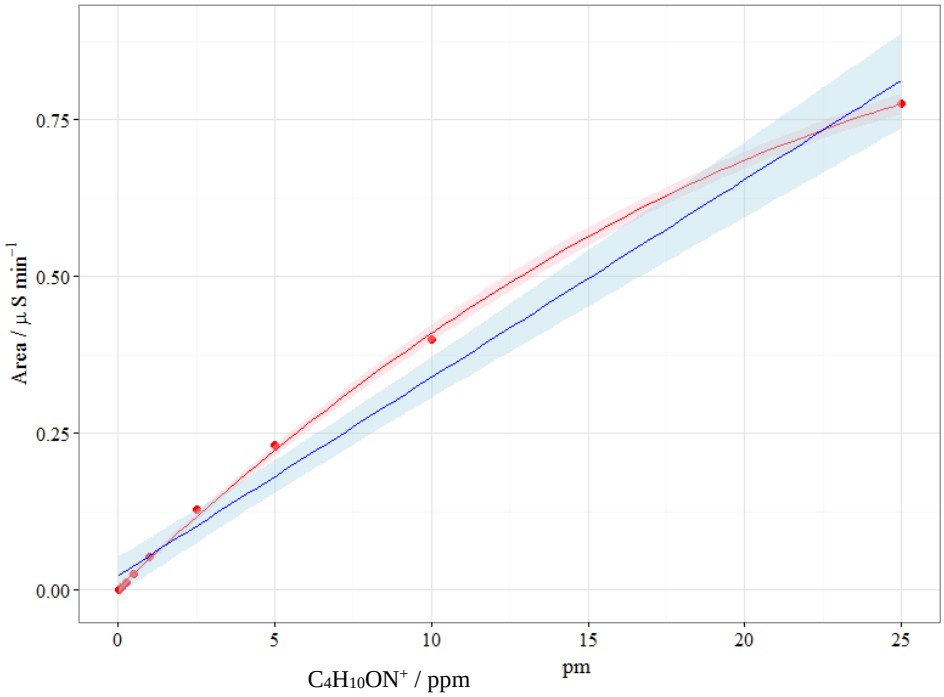

Figure 3.7. Calibration data for $C_4H_{10}ON^+$ fitted to both a linear model (blue line, adjusted R^2 = 0.9799) and a quadratic model (red line, adjusted R^2 = 0.9992). The shaded bands are pointwise 95% confidence intervals on the fitted values.

3.3.2.3 Installation of a gradient system for protonated amines

The rest of the target cations were analysed using a gradient elution system; full details can be found in Table 3.2 and 3.3, section 3.2.2.3. Although it was possible to separate and identify all of the target cations using isocratic elution, the cations took up to 60 minutes to elute and the peak shapes were poor. Gradient elution, where the concentration of the eluent is increased throughout the run, is often introduced in order to obtain higher sensitivity, improved resolution, and more accurate peak integration. It also optimises the analysis time, leading to a more efficient and cost-effective method.[168] Figure 3.8 shows a direct overlay of two cation exchange chromatograms, comparing the piperazine ion ($C_4H_{11}N_2^+$) peak eluted using isocratic mode and gradient mode. $C_4H_{11}N_2^+$ eluted after 46.5 minutes in isocratic mode, and the broad peak took approximately 6.2 minutes to elute. In gradient mode, the retention time was 19.2 minutes and the peak eluted in *ca.* 1.6 minutes. Due to the improved peak shape, it was easier to integrate the peak and determine the peak area more accurately. In gradient mode, after an initial 4 minutes at 20 mM MSA concentration, the concentration of the eluent was increased from 20 to 100 mM over a period of 19 minutes. Although the total run time could have been reduced even further for an earlier elution of $C_4H_{11}N_2^+$, it was important that the peak remained separated from any other interfering ions, such as Na^+ or NH_4^+, which can be present in background levels in the filter paper or the chamber, and may also be present in the extracts. As such, all of the gradient elution methods

provided in Table 3.3 for the target cations were optimised to reach a compromise between the peak shape and retention time of the target cation, and a good separation of the target cation with other cations that may be present. In order to overcome problems associated with gradient elution, such as high background conductivity or difficulty in preparing accurate eluent concentrations, a Dionex reagent free controller (RFC-30) was used in combination with a Dionex EGC 111 MSA eluent generator cartridge and a continuously regenerated trap column. This system allows the user to input their required eluent concentration at a particular time, and the stock MSA solution is combined with the correct amount of deionised water to automatically create the required eluent concentration throughout the entire run. Furthermore, incremental increases in the current supplied to the suppressor are automatically calculated and applied, in order to suppress high background conductivity and baseline drift which can be observed at higher eluent concentrations.[180]

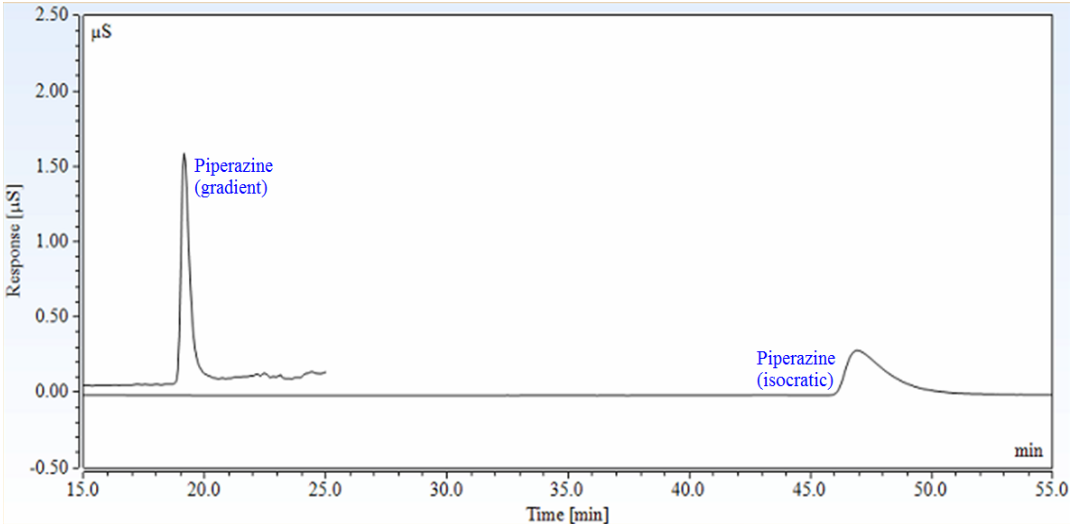

Figure 3.8. Direct overlay of two cation exchange chromatograms to show the reduced retention time and improved peak shape for the piperazine ion ($C_4H_{11}N_2^+$) eluted using a gradient system.

When the appropriate elution method for each cation had been obtained, the instrumental parameters were investigated and are summarised in Table 3.10. Spiked filters were used to determine detection levels, and suitable spike levels ranging from 0.05 ppm to 0.5 ppm were selected, according to the US EPA's detection limit guidance.[178] The LOD for $C_4H_{11}N_2^+$ was 7.8 ng whereas the LOD for $C_5H_{12}N^+$ was 28.5 ng. This is the best result that could be obtained for the piperidine ion without it co-eluting with other cations of interest. The respective LOQs for the piperazine and piperidine ions were 26.8 and 73.7 ng, which provide sufficient sensitivity for the accurate determination of amine salts in the chamber samples. The fit of the calibration data to either a linear or quadratic model was assessed at the stated linear ranges, and R^2 values between 0.9988 and 0.9999 were obtained. Finally, $\%RSD_{ins}$

remained below 15%, and when combined with the errors associated with the recovery process, $\%RSD_{tot}$ ranged from 11.0 to 14.91%. These acceptable error margins would not have been obtained without the use of a gradient system, so this was an essential modification to the original isocratic method.

Table 3.10. Instrumental parameters and associated errors for the IC system in gradient cation exchange mode.

Cation	RT / min	LOD / ng	LOQ / ng	Linear range / ng	R^2	$\%RSD_{ins}$ (n = 10)	$\%RSD_{tot}$
Piperidine ion, $C_5H_{12}N^+$	15.0	28.5	73.7	25 - 2500	0.9988[a]	14.39	14.91
Piperazine ion, $C_4H_{11}N_2^+$	19.4	7.8	26.8	1 - 2500	0.9999[b]	10.86	11.00
[a]R^2 value obtained using a linear model. [b]R^2 value obtained using a quadratic model.							

In summary, a quick and effective sonication and filtration procedure can be carried out to efficiently transfer amine salts present in aerosol samples into deionised water extracts. The liquid extracts can be directly injected into the IC, which can be set up to analyse both anions and cations. The use of carefully selected eluent mixtures and elution settings allows for accurate methods capable of reliably measuring all of the target ions to be obtained.

3.4 Conclusions

The primary objective of this study was to set up and validate a method that can be used to identify and quantify amine degradation products, with a specific focus on measuring potentially carcinogenic nitrosamines and nitramines. This work was carried out in preparation for a number of chamber experiments at the European Photoreactor, as part of the ACA project led by the University of Oslo.

Two extraction methods have been established to analyse particles collected on filter paper – a pressurized liquid extraction technique for the analysis of ON compounds, and a simple sonication and filtration method for the analysis of amine salts. The extraction methods are reliable ($\%RSD_{rec}$ < 11.4% for all compounds of interest) and offer high recovery levels ranging from 81.8 to 104.7%

A highly sensitive and selective technique relying on GC×GC-NCD has been verified for the analysis of ON compounds in the aerosol, focusing specifically on nitrosamines and nitramines. Additional work has been carried out to ensure that all of the target ON compounds are suitable for analysis using this instrument; synthetic work was carried out to derivatise two compounds with a –NH group present, enabling accurate analysis and

avoiding damage to the instrument. Furthermore, the sample extraction technique means that the extracts are suitable for direct analysis on other instruments, such as GC×GC-TOF-MS, which is likely to provide additional information regarding aerosol composition. The technique offers excellent recovery levels at low picogram levels, and total errors for the whole extraction and analysis process remain below 24%. Furthermore, the instrument is easy to calibrate, and compounds can be easily identified according to their first and second retention times.

Additional work beyond the initial objective of this study has been carried out to develop a method for determining the presence of amine salts in the aerosol. Using an isocratic elution method in anion exchange mode, the main atmospheric anions (Cl^-, NO_2^-, NO_3^-, PO_4^{3-}, and SO_4^{2-}) can be detected and accurately quantified. It is likely that NO_3^- will be the main anion of interest due to the reaction between gas phase amines and HNO_3 in the chamber, leading to the formation of aminium nitrate salts. Both isocratic and gradient methods were set up in cation exchange mode to ensure that all of the target cations could be separated and measured accurately. Detection limits in the low nanogram range were achieved, and linear and quadratic models were used to fit the calibration data, depending on the behaviour of each analyte in the suppressor.

In summary, suitable methods have been optimised and validated to ensure that accurate chamber measurements of amine degradation products can be made. This will hopefully provide useful information regarding the photochemical degradation of amines relevant to post-combustion CO_2 capture. Whilst the current methods are suitable for the offline analysis of chamber samples, there is scope to develop the techniques further to allow for online chamber measurements to be made, monitoring both the gas and particle phase. Perhaps more importantly, these techniques could also be developed further to measure these trace level compounds in ambient air, for example at CO_2 capture testing facilities such as TCM in Norway.

4 Atmospheric Chemistry of Amines project: formation of nitramines, nitrosamines and other nitrogen-containing species

4.1 Introduction

A highly sensitive and specific analytical method, relying on GC×GC-NCD, has been developed for the determination of carcinogenic nitrosamines and nitramines formed during the atmospheric degradation of amines relevant to CO_2 capture. An additional method for the measurement of aminium nitrate salts by IC has also been validated, and full details of both methods are provided in Chapter 3. A series of amine photo-oxidation experiments were carried at EUPHORE in Spain throughout June 2015 and July 2016, investigating *tert*-butylamine (*t*BA), aminomethyl propanol (AMP), morpholine, piperidine and piperazine (Figure 4.1). These amines are either potential solvents for amine-based CO_2 capture, or common simple analogues that form from the degradation of more complex amines. These particular amines have been selected as a better understanding of their atmospheric degradation pathways is required. The study builds upon previous work carried out by Nielsen *et al.*, who investigated the photo-oxidation of various aliphatic amines, including methylamine, dimethylamine, trimethylamine and 2-aminoethanol.[50, 181-183] The structures of *t*BA and AMP are different to these amines, as the primary amino group is attached to a tertiary carbon atom. Morpholine, piperidine and piperazine are all secondary amines that have not been extensively studied; whilst previous piperazine experiments were carried out by Nielsen *et al.*, it was not possible to quantify the photo-oxidation products accurately.[182] In this chapter, a full discussion of the results obtained from the offline samples collected during the 2015 and 2016 experiments will be provided. A detailed analysis of nitrosamine and nitramine formation will be included, as well as additional information regarding the formation of both aminium nitrate salts and various other ON compounds.

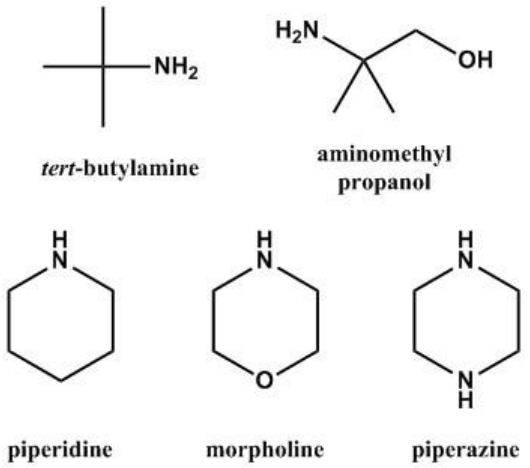

Figure 4.1. Chemical structures of the precursor amines.

4.2 Experimental

4.2.1 The European Photoreactor (EUPHORE)

EUPHORE is located in Valencia, Spain (39°33'05.1"N, 0°27'42.4"W) and is operated by the Mediterranean Centre for Environmental Studies Foundation (CEAM).[171] The facility consists of two hemispherical outdoor atmospheric simulation chambers each with an internal volume of approximately 200 m^3; a detailed description of EUPHORE is available in the literature.[170, 184-185] The fluorine-ethene-propene (FEP) foil used to construct the chambers allows over 80% of sunlight in the near UV and visible range to be transmitted to the chamber, enabling key tropospheric photochemical reactions to be mimicked. The inertness of the FEP foil minimises the likelihood of chemical reactions between trace gases and the chamber walls.

Table 4.1 provides an overview of the typical schedule for a photo oxidation experiment at EUPHORE. Before each experiment, the chamber is flushed with scrubbed air overnight to remove any contaminants from the system. At this stage, the steel canopy used to protect the chamber remains closed. The experiments start at approximately 06:00 UTC, when a sample representative of the chamber background is taken. The necessary reagents are then added to the chamber and when homogenous mixing has been achieved, the canopy is opened, exposing the chamber to sunlight. Images of the chamber when the steel canopy is open and closed are shown in Figure 4.2. The chamber floor is cooled during the photo oxidation experiments to compensate for heating of chamber air by solar radiation, ensuring a stable temperature in the chamber is maintained. Large fans are used to ensure homogenous mixing of chamber air.

Ports on the chamber floor are used to add reagents to the chamber and also to install sampling lines to a suite of analytical instruments. The instruments are used to monitor a range of both gas and particle phase species. Details of both the in-house instrumentation, and the instruments installed by other participants of the ACA project are provided in section 4.2.6. A continuous flow of purified air is supplied to the chamber throughout the photo-oxidation experiment, to compensate for chamber leakage and sampling outflow, and to ensure that the pressure is kept either at or slightly above atmospheric pressure. SF_6 is injected into the chamber at the start of each experiment to monitor the dilution rate. During the photo-oxidation experiments, isopropyl nitrite (IPN) may be added to the chamber to generate OH.

Table 4.1. Typical schedule for a photo oxidation experiment at EUPHORE.

Approximate time (UTC)	Action
06:00	Stop chamber flushing
06:10	Sample chamber background
07:00	Addition of reagents *e.g.* parent amine, NO, O_3, SF_6
08:00	Chamber opened
08:30	Addition of isopropyl nitrite (IPN) if necessary
12:30	Chamber closed
13:00	High volume aerosol collection
14:30	Start chamber flushing

Figure 4.2. Images of the chamber with the canopy open (left) and closed (right).

4.2.2 Chamber sampling

*t*BA and AMP photo-oxidation experiments were carried out in June 2015 and morpholine, piperidine and piperazine were studied in July 2016. The experiments were carried out under different, relevant NO_x conditions and the initial concentration of the parent amine ranged from 90 to 300 ppb. A range of samples were collected to investigate the formation of nitramines, nitrosamines and other nitrogen-containing species.

4.2.2.1 June 2015 sampling

In June 2015, Thermosorb-N air sampling cartridges (Cambridge Scientific Instruments Ltd., U.K.) were collected throughout the duration of each photo-oxidation experiment. The cartridge inlet was connected to the chamber using a 50 cm length of ¼" Sulfinert-treated stainless steel tubing (Swagelok, Teesside, U.K.) with a stainless steel in-line particulate filter (2 μm pore size) and ¼" stainless steel tap installed between the sampling line and the cartridge inlet. Before each experiment, a Thermosorb-N cartridge was collected to represent the chamber background (30 min sampling time). A second cartridge was collected after the addition of the amine precursor, before the chamber canopy had been opened (60 min sampling time). When the chamber canopy was opened, a further 1 – 2 cartridges were collected (60 min per sample). The cartridges were sampled using a low-volume sampling pump operating at 1 L min^{-1}, and typically a total of 3-4 samples were obtained per experiment.

At the end of each experiment, the chamber canopy was closed and additional NO (25 - 500 ppb) was added to the chamber to check for the presence of peroxyacetyl nitrates. The remaining aerosol was collected using a high-volume sampling pump. The aerosol was collected onto 47 mm diameter quartz fibre filters (Whatman, Maidstone, U.K.), which had been prebaked at 550 °C and wrapped in aluminium foil prior to sample collection. Aerosol samples were collected at 48 L min^{-1} for 60 min, giving a total sample volume of 2.88 m^3. After collection, the samples were stored at -18 °C until analysis.

4.2.2.2 July 2016 sampling

The sampling methods were modified for the 2016 experiments. As described in Chapter 3 (section 3.3.1.1), the Thermosorb-N cartridges damaged the GC column installed in the GC×GC-NCD. As a result, only particle sampling was performed in 2016, using quartz fibre filters. Unlike 2015, filters were collected at appropriate intervals throughout the photo-oxidation experiment, in order to obtain time-resolved measurements of aerosol formation and composition.

When the chamber canopy was open the total flow rate available for aerosol filter sampling was 10 L min^{-1}; there were several instruments operating and so flow rates were restricted to avoid excessive chamber dilution. However, when the chamber canopy was closed there were fewer instruments operating and so higher flow rates were allowed for the aerosol sampling. As a result, aerosol sampling flow rates varied throughout the experiment as shown in Table 4.2, allowing for the best compromise between aerosol mass, time resolution and chamber dilution to be achieved.

Table 4.2. Details of aerosol filter sampling during the July 2016 photo-oxidation experiments.

Stage of experiment	Sampling flow rate (L min^{-1})	Sampling time (min)
Chamber background – canopy closed, no reagents added	*ca.* 48	30
Photo oxidation – canopy open, all reagents added	10 (2 × 5)	30 - 120
Remaining aerosol – chamber closed, end of experiment	*ca.* 48	60

For the samples collected using the high-volume sampling pump (*ca*. 48 L min^{-1}), the inlet to the 47 mm filter holder (Cole-Parmer, London, U.K.) was connected to the chamber using a 40 cm length of ¼" PFA tubing (Swagelok, Teesside, U.K.) with an in-line ¼" stainless steel tap installed 10 cm above the filter holder inlet. A further 15 cm of ¼" of PFA tubing was used to connect the filter holder outlet to a mass flow meter (0-50 L min^{-1}, Alicat, Cambridge, U.K.). The mass flow meter outlet was connected to the high volume pump *via* 1.5 m of ½" PFA tubing. A diagram of the high-volume filter sampling set up is shown in Figure 4.3. The low-volume filter sampling was carried out at 10 L min^{-1}, and the air flow was split equally between two 47 mm filter holders, as shown in Figure 4.3. The connections between the chamber, filter holders and mass flow controllers were made using ¼" PFA tubing. After collection, all of the filter samples were stored at -18 °C until analysis. The high-volume filters were divided into two parts; ¼ for analysis by IC and ¾ for analysis by GC×GC. One filter from each pair of low-volume filters was used for analysis by IC and the other one was used for analysis by GC×GC.

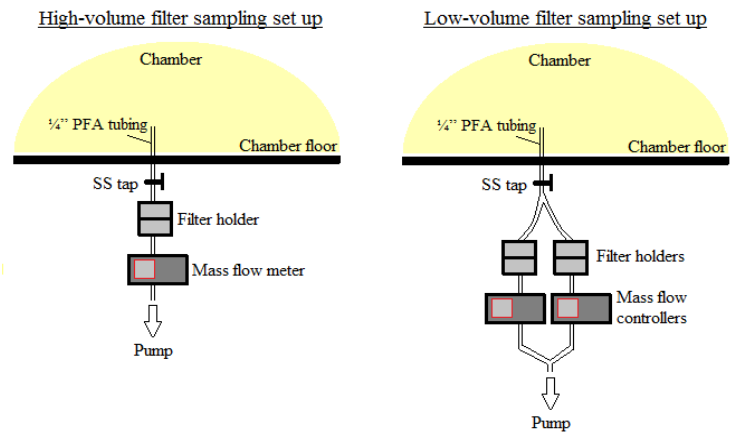

Figure 4.3. Diagrams to show the filter sampling set up for the collection of both the high-volume samples (left) and the low-volume samples (right).

4.2.3 Standards and solutions

The standards used for analysis by GC×GC-NCD and IC were described previously in Chapter 3, sections 3.2.1.1 and 3.2.2.1.

4.2.3.1 Additional standards for GC×GC-TOF-MS

2-methyl-2-nitropropane and N-*tert*-butylformamide were purchased from Sigma-Aldrich Ltd (Dorset, U.K.). N-*tert*-butylacetamide was bought from Alfa Aesar (Lancashire, U.K.), in addition to 2-methyl-2-nitropropanol from Tokyo Chemical Industry Ltd (Oxford, U.K.) and 4,4-dimethyl-1,3-oxazolidinone from Fluorochem (Derbyshire, U.K.). Standard solutions for analysis by GC×GC-TOF-MS were prepared in ethyl acetate (HPLC grade, >99.5% purity) from Fisher Scientific Ltd.

4.2.4 Sample extraction

All of the samples were stored at -18 °C prior to analysis. The method used to extract each sample depended on the sample type, the date of collection, and the instrument used for analysis.

4.2.4.1 Extraction of Thermosorb-N air sampling cartridges (June 2015)

GC×GC analysis: Thermosorb-N cartridges were eluted against the direction of air flow using 3 mL of DCM/ MeOH (75:25), evaporated to near dryness under a gentle stream of nitrogen, and made up to a final volume of 1 mL in EtOAc.

4.2.4.2 Extraction of high-volume aerosol filter samples (June 2015 and July 2016)

GC×GC analysis: three-quarters of each filter sample was extracted using an accelerated solvent extraction system (ASE 350, Dionex, CA, USA). The base of each 5 mL stainless

steel extraction cell was lined with two glass microfibre filter papers (Fisher Scientific, Loughborough, U.K.) and then packed with the sample. Extractions were carried out in EtOAc (HPLC grade, >99.5% purity) at 80 °C and 1500 psi for three consecutive 5 min cycles. A 50% flush volume and 60 s purge time were used. Extracts obtained were stood in an ice bath whilst they were evaporated under nitrogen to a final volume of 1 mL.

IC analysis: the remaining quarter of each filter sample was dissolved in 2 mL ultrapure milli-Q water (18 MΩ cm^{-1}) and sonicated at RT for 30 mins. The extract was filtered using a Millex-GP 33 mm diameter hydrophilic syringe filter with a pore size of 0.22 μm (Millipore UK Limited, Watford, U.K.).

4.2.4.3 Extraction of low-volume aerosol filter samples (July 2016 experiments)

GC×GC analysis: one set of the pair of low-volume aerosol filter samples was extracted using the accelerated solvent extraction system described previously in section 4.2.4.2.

IC analysis: the other set of low-volume aerosol filter samples was extracted by sonication in milli-Q water, as described in section 4.2.4.2. As the whole 47 mm diameter filter was extracted rather than one quarter, 3 mL of milli-Q water was used to ensure a high recovery of the target compounds, as explained in Chapter 3 (section 3.3.2.1).

4.2.5 Sample analysis

The three techniques used to analyse the sample extracts were GC×GC-NCD, IC and GC×GC-TOF-MS. Table 4.3 provides a summary of the analytical techniques applied to particular sets of samples.

Table 4.3. Summary of the extraction method and analytical technique used for each type of sample collected at EUPHORE.

Experiment date	Sample type	Extraction method	Analytical technique
June 2015	Thermosorb-N cartridge	Elution using DCM/ MeOH	GC×GC-NCD
June 2015 and July 2016	High-volume filter sample	¾: accelerated solvent extraction	GC×GC-NCD & GC×GC-TOF-MS
June 2015 and July 2016	High-volume filter sample	¼: aqueous sonication	IC
July 2016	Low-volume filter sample	Set 1: accelerated solvent extraction	GC×GC-NCD
July 2016	Low-volume filter sample	Set 2: aqueous sonication	IC

Details of the chromatographic analysis performed using GC×GC-NCD and IC were described previously in Chapter 3, sections 3.2.1.4 and 3.2.2.3.

4.2.5.1 GC×GC-TOF-MS

The GC×GC-TOF-MS system consisted of an Agilent 6890 gas chromatograph (Agilent Technologies, Palo Alto, CA, USA) and a Pegasus III TOF-MS (LECO, St. Joseph, MI, USA). The first column was a non-polar BPX5 (30 m × 0.32 mm i.d. × 0.25 µm film thickness) and the second column a mid-polarity BPX50 (4 m × 0.18 mm i.d. × 0.20 µm film thickness), both from SGE Analytical Science. The oven temperature ramps for both the main oven and the secondary oven were the same as used for the GC×GC-NCD system. Helium was used as the carrier gas at 1 mL min^{-1}. 1 µL injections were carried out in splitless mode at an injection temperature of 200 °C using a Gerstel automated liquid injector (Gerstel, Mülheim an de Ruhr, Germany). The transfer line temperature and the ion source temperature were set at 280 °C and 250 °C respectively. Mass spectra were obtained between 45 and 500 amu at a spectral acquisition rate of 200 Hz. A liquid nitrogen two-stage cold jet modulation system was used, with a modulation period of 5 s and a +15 °C offset from the primary GC oven temperature.

4.2.6 Additional measurements

4.2.6.1 In-house instrumentation

A range of instruments are installed permanently at the EUPHORE facility to monitor chamber conditions and are operated by staff at CEAM. Measurements of ozone were made using a Serinus 10 ozone analyser (Ecotech) and NO_x measurements were made using a T200UP ultra-sensitive photolytic NO-NO_2 analyser (Teledyne API). A $j(NO_2)$ filter radiometer was used to monitor actinic flux, and a long absorption path optical photometer (LOPAP) was used to determine HONO concentrations in the chamber. The chamber temperature, pressure and humidity were also recorded throughout each experiment. The first order decay of SF_6 (an inert tracer gas) was monitored using a Nicolet 6700 FTIR spectrometer coupled with white multi-reflection mirror systems for *in situ* analyses adjusted to give an optical path length of 553.5 m. FTIR spectra were recorded every 10 mins by co-adding 370 interferograms with a resolution of 0.5 cm^{-1}. This information gave an estimation of the chamber dilution rate, which resulted from replacement of air due to sampling of the connected instruments and minor chamber leaks. First order rate constants for dilution ranged between 7.45×10^{-6} and 1.50×10^{-5} s^{-1}. The number concentration of particles formed in the chamber was measured using a scanning mobility particle sizer (SMPS, model 3080, TSI Inc.) coupled to a differential mobility analyser (DMA,

model 3081). The system can detect particles between 15 and 1000 nm and if the density of the particles are known, the mass loading can be derived.

4.2.6.2 Other instruments used by ACA participants

Four additional online instruments were attached to the chamber by participants from the University of Oslo (Norway), the University of Lyon (France) and the University of Innsbruck (Austria). The instruments used were a high-resolution proton-transfer-reaction time-of-flight mass spectrometer (PTR-TOF-MS), a high-temperature proton-transfer-reaction mass spectrometer (HT-PTR-MS), an aerosol mass spectrometer (AMS), and a chemical analysis of aerosol online system coupled to a proton-transfer-reaction time-of-flight mass spectrometer (CHARON-PTR-TOF-MS). Further details of the instrumentation can be found in the literature.[186-189]

4.3 Results and discussion

4.3.1 Chamber experiments

The EUPHORE facility is an outdoor atmospheric simulation chamber; although there are several restrictions associated with outdoor chamber, (details of which can be found in Seakins' review), they are generally an excellent way of simulating atmospheric processes.[190] For example, the large chamber volume (*ca.* 200 m^3) provides a low surface-to-volume ratio, which minimizes losses and heterogeneous processes on the chamber walls. There is space available to install sensitive monitoring equipment so that gases and particles at ambient concentrations (ppb to ppm range) can be quantitatively analysed. Whilst the use of FEP foil does not completely remove all of the wall effects, it is relatively chemically inert and allows for excellent transmission of solar radiation.

An overview of the experimental conditions and initial reactant concentrations is provided in Table 4.4. The initial parent amine concentrations were determined by PTR-TOF-MS and ranged from approximately 90 to 300 ppb. During the photo-oxidation experiments, the average pressure inside the chamber was 1013.8 mbar; pressures either at or above atmospheric pressure prevent ambient air from outside entering the chamber, and also help to maintain structural integrity. The chamber floor is cooled when the canopy was open to compensate for heating of chamber air by solar radiation, but some variation in temperature was still observed. Over the two campaigns the temperatures ranged from 24.0 °C to 42.5 °C when the canopy was open, with a maximum variation of 14.1 °C during any given experiment.

Table 4.4. Summary of experimental conditions and initial concentrations.

Amine	Date	$j(NO_2)$ / s^{-1} [a]	Initial NO / ppb [b]	Initial NO_2 / ppb [b]	Initial reactant / ppb	Amine: IPN	Amine: NO_x
*t*BA	02-06-15	n/a	15	30	data not available		
	03-06-15	n/a	1	2.5	227	72	high
	04-06-15	n/a	205	70	224	20	low
AMP	09-06-15	9.18×10^{-3}	30	15	102	64	medium
	12-06-15	8.47×10^{-3}	2	1.2	94	59	high
	18-06-15	2.78×10^{-3}	60	60	93	168	low
morpholine	04-07-16	1.61×10^{-2}	90	120	234	no IPN	low
	05-07-16	1.64×10^{-2}	50	0	255	806	low amine: NO high amine: NO_2
	06-07-16	1.67×10^{-2}	5	45	255	806	high amine: NO low amine: NO_2
	07-07-16	9.27×10^{-3}	0.2	0.1	250	790	high
piperidine	11-07-16	1.65×10^{-2}	100	95	181	no IPN	low
	12-07-16	1.59×10^{-2}	0.2	2	170	420	high
	15-07-16	1.63×10^{-2}	145	0	183	543	low amine: NO high amine: NO_2
	18-07-16	1.57×10^{-2}	1	100	191	262	high amine: NO low amine: NO_2
piperazine	20-07-16	1.04×10^{-2}	90	105	305	no IPN	low
	21-07-16	1.58×10^{-2}	80	60	236	no IPN	low
	22-07-16	1.36×10^{-2}	0	0.1	242	765	high
	25-07-16	1.48×10^{-2}	60	0	230	194	low amine: NO high amine: NO_2
	26-07-16	1.06×10^{-2}	0	70	200	no IPN	high amine: NO low amine: NO_2

[a]Average $j(NO_2)$ when the canopy was open. [b]Initial NO and NO_2 concentration prior to canopy opening.

Whilst the solar radiation supplied to outdoor chambers is an ideal way to simulate photolysis in the real atmosphere, it also varies on a daily basis, and is strongly influenced by both local environmental conditions and the solar zenith angle. A direct comparison of experiments must be approached with caution and it is important to consider the atmospheric NO_2 photolysis frequency, $j(NO_2)$, which is monitored continuously throughout each experiment and can be used to assess the strength of solar radiation. This is important because the fast photolysis of NO_2 plays a large role in the formation of tropospheric O_3 and the subsequent formation of OH radicals.[191] Unfortunately there is no $j(NO_2)$ data available for the *t*BA experiments in June 2015, but the average $j(NO_2)$ value for the 2015 AMP experiments was 6.8×10^{-3} s^{-1} and in July 2016 the average $j(NO_2)$ value slightly higher at 1.5×10^{-2} s^{-1}. The estimated annual average NO_2 photolysis frequency in the Mongstad region where the CO_2 capture testing facility is located is 1.25×10^{-3} s^{-1}.[192] Experiments were perfomed under different NO to NO_2 ratios, as well as different VOC to NO_x ratios, as these factors can affect the atmospheric degradation pathways.

HONO can form during the heterogeneous dark reaction of NO_2 and H_2O on the chamber walls and upon exposure to sunlight, can undergo photolysis to form OH.[193] However, in most experiments, IPN was added to the chamber to provide an additional source of OH. IPN is an alkyl nitrite which undergoes photo-dissociation to form an alkoxy radical and NO. As shown in Scheme 4.1, the alkoxy radical can subsequently react with oxygen (in the presence of NO) to form OH radicals.[194] In 2015, the quantities of IPN added to the chamber were significantly higher than in 2016. As shown in Table 4.4, amine to oxidant ratios were between 20 and 168 for the 2015 experiments, and ranged from 194 to 806 in 2016. In order to provide a continuous supply of OH, IPN was added slowly to the chamber, at rates between 0.1 and 5 μL min^{-1}.

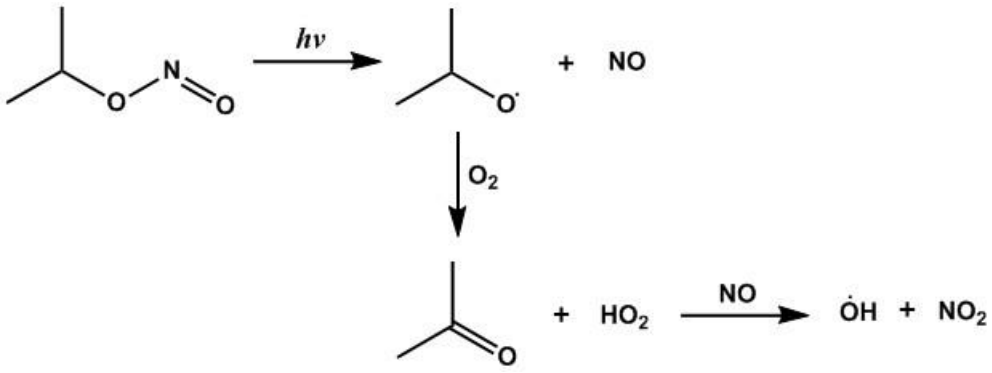

Scheme 4.1. Photolysis of isopropyl nitrite in air to form an alkoxy radical. A series of secondary reactions leads to the formation of OH radicals.

4.3.2 Thermosorb-N air sampling cartridges

Offline sampling techniques, such as Thermosorb-N air sampling, are an important way of validating online measurements. As these methods are independently calibrated they can be used to confirm the analytical quality of online measurements. Thermosorb-N air sampling cartridges were originally designed for the collection of volatile N-nitrosamines, and contain an amine trap and nitrosation inhibitor to prevent the artificial formation of analytes.[195-196] Thermosorb-N cartridges were tested alongside charcoal and Tenax cartridges during the 2010 ACA experiments, when the atmospheric behaviour of methylamine, dimethylamine and trimethylamine was investigated.[50] The study concluded that Thermosorb-N cartridges were the most appropriate offline sampling technique; for example the discrepancy between the Thermosorb-N and PTR-MS data was less than 15% for N-nitrosodimethylamine, but the target nitrosamines were not found on the Tenax cartridges, possibly due to thermal degradation of the compounds during desorption at 300 °C. Significantly higher nitrosamine concentrations were found on the charcoal cartridges, and it was speculated that heterogeneous oxidation of the amines occurred on the charcoal surface.[197] With this information in mind, it was decided that Thermosorb-N cartridges would be deployed during the 2015 *t*BA and AMP experiments. A particulate filter (pore size 2 μm) was installed upstream of the cartridge inlet, which meant that gaseous and particulate species that made it through the sampling line were collected. As a result, the target nitramine concentrations should be systematically higher than the results obtained by PTR-MS.

As primary nitrosamines are highly unstable and decay rapidly in water to form N_2 gas and the corresponding carbocation, only the more stable primary nitramines of *t*BA and AMP were considered.[72, 75, 198] As discussed in Chapter 3 (section 3.3.1.1), the recovery of AMP-NO_2 was poor (*ca*. 4%) and contaminants from the Thermosorb-N cartridge were beginning to cause chromatographic problems, so only the *t*BA-NO_2 results are discussed in this study. Figure 4.4 shows the time profiles for the *t*BA photo-oxidation experiments and provides a comparison of the *t*BA-NO_2 concentrations determined by Thermosorb-N cartridges and PTR-TOF-MS. A Thermosorb-N cartridge was sampled prior to the addition of any reactants or gases to check the chamber background. At this initial stage, any observed nitramine will be from a previous experiment, or will have formed artificially on the cartridge from amine still present in the chamber. As the amine trap and nitrosation inhibitor present in the cartridges is designed to prevent artificial formation of nitrosamines and nitramines, the former is the most likely.

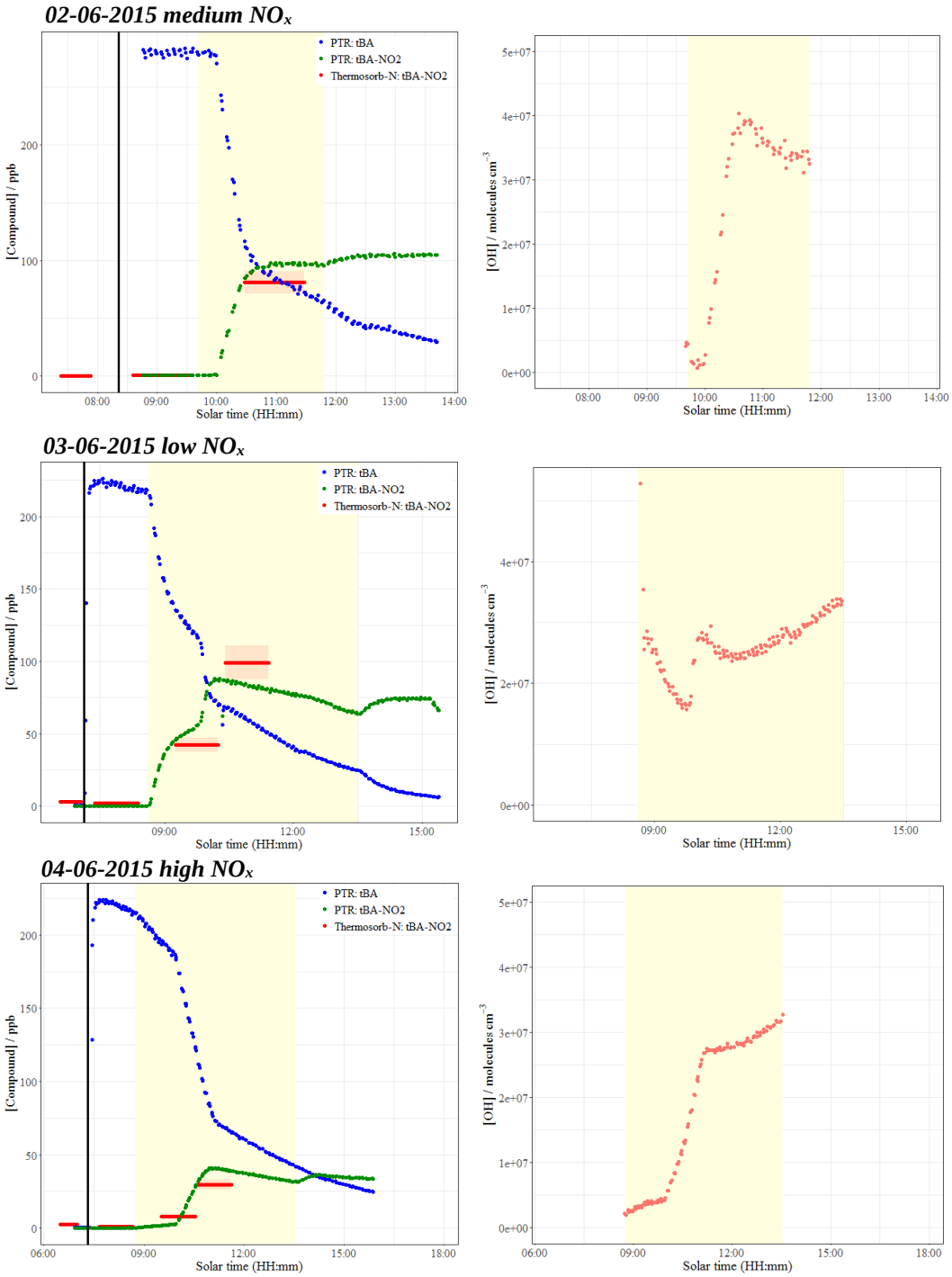

Figure 4.4. Time profiles of the tBA photo-oxidation experiments (left panels) and estimations of the OH concentration in the chamber (right panels). PTR-TOF-MS data for the decay of *t*BA and formation of *t*BA-NO_2 is compared to Thermosorb-N measurements of *t*BA-NO_2. The black vertical line (left panels) indicate the time at which the amine was added to the chamber. %RSD_{tot} = 13.2% for Thermosorb-N measurements.

Table 4.5 provides a summary of the *t*BA-NO_2 results obtained by Thermosorb-N sampling and PTR-MS for 3 different experiments. The first result listed for each day from the Thermosorb-N cartridges is representative of the background tests. For the first experiment (02-06-2015) when no previous *t*BA experiments had been performed, the nitramine was not observed. Nitramine concentrations of 3.09 and 2.32 ppb were recorded for the two consecutive experiments (03-06-2015 and 04-06-2015 respectively). Whilst these nitramines levels are significantly above the detection limit, they are relatively low compared to the observed nitramine levels observed during the photo-oxidation phase of the experiment (canopy open). As it was not possible to quantitatively determine background levels at the start of irradiation, the rest of the reported values have not been background corrected.

Table 4.5. Comparison of the *t*BA-NO_2 results obtained using Thermosorb-N air sampling cartridges and PTR-MS.

Date	Start time (UTC)	End time (UTC)	*tert*-Butyl(nitro)amine / ppb	
			Thermosorb-N cartridge ***(%RSD_{tot} = 13.2%)***	***PTR-MS*** [d]
02-06-2015 'medium NO_x'	07:23[a]	07:53	0.00	n/a
	08:36[b]	09:36	0.23	0.36
	10:28[c]	11:28	80.81	94.56
03-06-2015 'low NO_x'	06:34[a]	07:04	3.09	0.24
	07:23[b]	08:23	2.05	0.31
	09:15[c]	10:15	42.28	62.75
	10:25[c]	11:25	99.19	83.56
04-06-2015 'high NO_x'	06:29[a]	06:59	2.32	0.19
	07:40[b]	08:40	0.88	0.23
	09:32[c]	10:32	7.72	9.29
	10:37[c]	11:37	29.56	38.91

[a]Canopy closed, before addition of reactants. [b]Canopy closed, after addition of reactants. [c]Canopy open, photo-oxidation of amine in progress. [d]Average *tert*-butyl(nitro)amine concentration over the Thermosorb-N cartridge sampling time.

The next Thermosorb-N sample was collected after the amine, SF_6 and NO (if necessary) had been injected into the chamber, but before the canopy was opened. This was to check

again for any artificial formation of the nitramine on the cartridge, or for any nitramine formation in the chamber in the absence of sunlight. The main nitrosating agents of interest in the dark are HONO and the NO_3 radical. Nielsen *et al.* recently reported that amines do not react in the dark with $NO/NO_2/HONO$ in the gas phase to form nitrosamines, but instead heterogenous (or surface assisted) reactions take place and lead to the formation of nitrosamines.[199-200] However, it was also reported that the rate of these surface reactions is low, so they can be neglected under relevant atmospheric conditions. The *t*BA-NO_2 concentrations measured using Thermosorb-N cartridges before the canopy was opened ranged from 0.23 to 2.05 ppb; such levels lie within the background chamber concentration range (<LOD – 3.09 ppb), indicating that nitramine formation in the dark may be insignificant in the chamber.

The remaining Thermosorb-N cartridges were collected during the photo-oxidation stage of the experiment. For each experiment, 1-2 cartridges were collected when the canopy was open, and the sampling duration was 60 minutes per cartridge. Sampling for 60 minutes allowed for nitramine levels above the limit of detection to be collected, whilst also providing limited time resolved data. The reaction scheme for the formation of *t*BA-NO_2 in the sunlit atmosphere, derived from previous theoretical studies, is provided in Scheme 4.2.[182, 201]

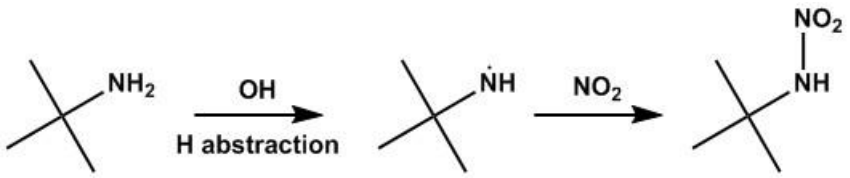

Scheme 4.2. Formation of *t*BA-NO_2 from *t*BA; H-abstraction by an OH radical from the NH_2 group and subsequent reaction with NO_2.[182, 201]

When the canopy was open, the Thermosorb-N *t*BA-NO_2 concentration measured on 02-06-15 was 80.81 ppb; this value was approximately 14 ppb lower than that recorded by PTR-TOF-MS at the same time interval. The *t*BA-NO_2 concentrations determined using Thermosorb-N cartridges were also lower than those measured by PTR-TOF-MS on 04-06-15 (7.72 and 29.56 ppb compared to 9.29 and 38.91 ppb). However on 03-06-15, one recorded Thermosorb-N value was lower than the PTR-TOF-MS value (42.28 ppb *cf.* 62.75 ppb) and one was higher (99.19 ppb *cf.* 83.56 ppb). As previously discussed, it was expected that the measurements obtained using Thermosorb-N cartridges would have been systematically higher than the PTR-MS measurements, but this was not the case. However, the measured concentrations during the photo-oxidation phase of the experiment were accurate to within a factor of 1.5, and for the first time, offline and online time-resolved

measurements of *t*BA-NO_2 by independently calibrated methods have been obtained. Without further testing of Thermosorb-N cartridges, which is not currently an option due to the potential for damage to the GC column (Chapter 3, section 3.3.1.1), it is only possible to speculate why there was a lack of consistency between the measured values. For example, as shown in Figure 4.5, recovery tests were carried out for *t*BA-NO_2 by spiking the Thermosorb-N cartridge with 10 µg of material and a recovery level of 61.5% was achieved (n = 3, %RSD < 12%). However, up to 90 µg of nitramine was collected onto a single cartridge during the photo-oxidation experiments, and additional compounds present in the chamber may have also been trapped on the cartridge. Higher cartridge loadings may have caused breakthrough of the target nitramine, leading to lower concentrations being measured. Alternatively, the higher concentration of nitramine and interferences from other compounds may have affected both the value and reproducibility of the recovery level, which would significantly affect the quality of the results obtained. Furthermore, whilst sensitivity checks and calibrations were regularly performed on the GC×GC-NCD system, the GC column was damaged by impurities from the cartridge sorbent. This has the potential to disrupt the quality of the chromatographic results obtained and can lead to inaccurate measurements. There may also be errors associated with the PTR-TOF-MS measurements, such as compound degradation in the heated sampling lines.

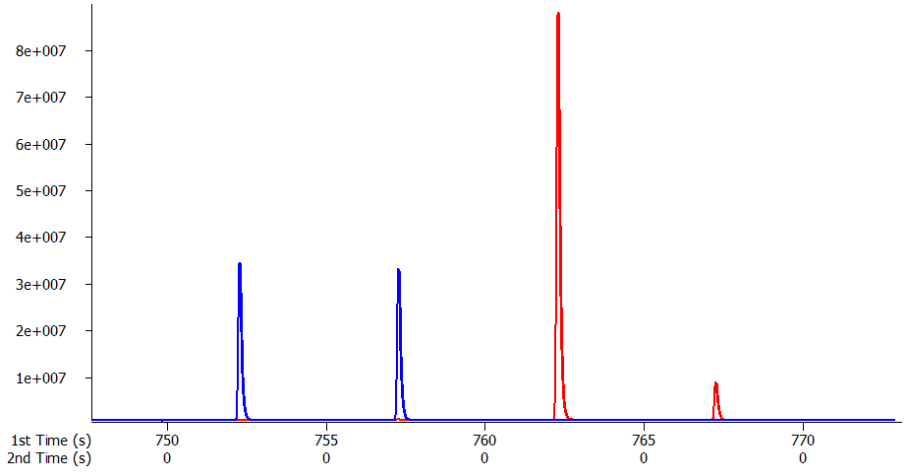

Figure 4.5. GC×GC chromatograms used to calculate the recovery of *t*BA-NO_2 from spiked Thermosorb-N cartridges (61.5%). The red chromatogram shows the peak area for the direct injection of *t*BA-NO_2 and the blue chromatogram shows the peak area for *t*BA-NO_2 recovered from the Thermosorb-N cartridge.

Time profiles for the *t*BA photo-oxidation experiments were shown previously in Figure 4.4. The right panels show the estimated concentration of OH in the chamber for each experiment. OH concentrations were estimated using Equation 4.1;

$$\frac{d[tBA]}{dt} = k_{OH}[tBA][OH] \quad (4.1)$$

where k_{OH} is the rate constant for the reaction of *t*BA with OH (1.30×10^{-11} cm^3 molecule^{-1} s^{-1}). This value was calculated by Nielsen *et al.* after the measurement campaign and has not been published yet. It should be noted that the calculation only provides an approximate OH concentration, and corrections for loss processes such as chamber dilution have not been applied. Whilst there does not appear to be any obvious relationship between the extent of *t*BA-NO_2 formation and the NO_x mixing ratio, the data shown in Figure 4.4 suggests that greater nitramine formation is observed when OH concentrations are higher. This observation may be attributed to the fact that the initial amine reaction with OH radicals (Scheme 4.2, step 1) constitutes the rate-limiting step in the formation of nitramines.[182]

In conclusion, semi-quantitative results have been obtained for *t*BA-NO_2 using Thermosorb-N cartridges, which have been directly compared to online PTR-MS measurements carried out by the University of Oslo. Whilst there is considerable scope for improving these measurements, they have the potential to be used alongside other data to estimate nitramine concentrations at CCS plants under typical atmospheric conditions.

4.3.3 Aerosol filter samples

During amine photo-oxidation experiments there are two major aerosol formation processes; primary salt formation *via* acid-base chemistry, and oxidation of the parent amine.[182] When oxidation of the parent amine occurs, aerosol is formed either by direct partitioning or secondary salt formation. After oxidation, a number of ageing processes may occur in atmosphere, including chemical reactions in the aqueous phase or heterogeneous processes such as the uptake of HNO_3 or O_3.[182] In 1996, Odum *et al.* proposed a method to calculate organic aerosol yield.[52] As shown in Equation 4.2, the fractional aerosol yield (Y) can be defined as the mass of SOA produced (ΔM_{OA}) when a certain mass of precursor amine is oxidised (ΔM_A).

$$Y = \frac{\Delta M_{OA}}{\Delta M_A} \quad (4.2)$$

However in the case of amines, the organic aerosol yield does not account for contribution of salts to the aerosol mass, and therefore it is more suitable to calculate the total aerosol yield. This is achieved by dividing the total mass of aerosol produced (corrected for wall

loss and dilution) by the mass of parent amine reacted. It is challenging to compare all of the aerosol yields obtained for the amine photo-oxidation experiments, as there is a lack of consistency regarding both NO_x conditions and the amount of oxidant present in the chamber, and these factors can dramatically influence the aerosol yield. Instead, three sets of experiments have been selected for comparison and the results are summarised in Table 4.6. Further information regarding the basicity, volatility and reactivity of each amine under consideration is provided in Table 4.7.

Scenario A considers the relationship between NO_x mixing ratio and aerosol yield for morpholine (the amine to oxidant ratio is *ca.* 800 in all three experiments). The total maximum aerosol yield is lowest (1.6%) when no additional NO_x is added to the chamber. On 05-07-2016, NO is added to the chamber before the canopy is opened, and production of NO_2 upon amine photo-oxidation maintains a NO_x mixing ratio of around 50 ppb for up to 2 hours after opening the canopy; the highest maximum aerosol yield is obtained for this experiment (5.6%). On 06-07-16, the NO_x mixing ratio is slightly lower (approximately 30 ppb) because NO and O_3 were added to the chamber initially, converting the NO to NO_2, which was photolysed upon irradiation. As a result a slightly lower aerosol yield of 5.0% is observed. For many VOCs, such as isoprene or α-pinene, the SOA yield decreases as the NO_x level increases.[202-203] This is due to competitive chemistry of peroxy radicals between NO and HO_2; at lower NO_x mixing ratios the RO_2+HO_2 reaction is increasingly favourable and can produce products of lower volatility than the RO_2+NO reaction.[203-204] However, the situation for amines is different due to the occurrence of salts in the aerosol, and the mass of aerosol is related in a complex manner to the rate of formation of nitric acid in the system.[55] If large amounts of nitric acid are formed during photo-oxidation, the majority of the amine will form aminium nitrate salts. However if nitric acid is not formed, nitrate salts are not observed and the aerosol consists of semi- to low-volatility compounds from amine reactions with OH. As amine oxidation products such as amides and imines are also basic, they too can form salts with nitric acid. The results obtained for the 'scenario A' experiments could suggest that at higher NO_x mixing ratios, higher total aerosol yields are observed as a result of increased nitric acid formation.

Table 4.6. Maximum total aerosol yields for different amine photo-oxidation experiments. Aerosol yields for a range of NO_x conditions and amine to oxidant ratios are reported.

Scenario	Date	Amine	NO_x conditions[a]	Amine: oxidant	Maximum total aerosol yield / %
A	05-07-2016	morpholine	NO: 50 ppb NO_2: 0 ppb	806	5.6
	06-07-2016	morpholine	NO: 15 ppb NO_2: 50 ppb	806	5.0
	07-07-2016	morpholine	NO: 0 ppb NO_2: 0 ppb	790	1.6
B	07-07-2016	morpholine	NO: 0 ppb NO_2: 0 ppb	790	1.6
	22-07-2016	piperazine	NO: 0 ppb NO_2: 0 ppb	765	9.7
C	04-07-2016	morpholine	NO: 90 ppb NO_2: 120 ppb	no IPN	3.9
	11-07-2016	piperidine	NO: 100 ppb NO_2: 95 ppb	no IPN	11.7
	20-07-2016	piperazine	NO: 90 ppb NO_2: 105 ppb	no IPN	36.7

[a]Initial NO_x conditions when the canopy was opened.

Table 4.7. Base dissociation constants (logarithmic scale, pKb), vapour pressures and predicted rate constants (k_{OH}) for morpholine, piperidine and piperazine.

Amine	pKb[205]	Vapour pressure / mmHg	k_{OH} / 10^{-11} cm^3 molecule^{-1} s^{-1}
Morpholine	5.51	10.1 (Riddick *et al.*)[206]	9.5 ± 0.95 (Nielsen *et al.*)[182]
Piperidine	2.72	32.1 (Yaws)[207]	7.4 ± 0.7 (Nielsen *et al.*)[182]
Piperazine	4.27	0.16 (Kirk *et al.*)[208]	23.8 ± 0.28 (Onel *et al.*)[209]

In scenario B, the amine to oxidant ratios were approximately the same and no additional NO_x was added to the chamber in either experiment. This allowed for a direct comparison of the total aerosol yield from the photo-oxidation of morpholine and piperazine. A significantly higher total aerosol yield was observed for piperazine (9.7%) compared to morpholine (1.6%). As shown in Table 4.7, the vapour pressure for piperazine (0.16 mmHg)

is considerably lower than that of morpholine (10.1 mmHg), and piperazine also reacts approximately 2.5 times faster with OH than morpholine. Both of these factors are likely to contribute to higher yields from piperazine photo-oxidation than morpholine photo-oxidation.

In scenario C, all experiments were carried out under high NO_x conditions (*ca.* 210 ppb) and no additional oxidant was added to the chamber. The data showed that piperazine also forms more aerosol than morpholine at high NO_x mixing ratios (36.7% and 3.9% respectively), and that piperidine falls between the two amines with an aerosol yield of 11.7% under these conditions. Morpholine and piperidine both have a lower aerosol yield than piperazine, as they are approximately 63-200 times more volatile, and react around 2.5 to 3.2 times slower with OH. It is not immediately obvious why morpholine forms less aerosol than piperidine. Overall morpholine is a stronger base (pKb of 5.51 *c.f.* 2.72, thus expected to form aminium salts more easily), and is three times less volatile than piperidine and reacts with OH slightly quicker (9.5×10^{-11} cm^3 $molecule^{-1}$ s^{-1} compared to 7.4×10^{-11} cm^3 $molecule^{-1}$ s^{-1} for piperidine). This information suggests that morpholine is likely to form more aerosol than piperidine, but this is not the case and it is possible that other factors *e.g.* solubility, hydrogen bonding or other unknown structural effects are affecting aerosol yield.

Whilst it has been possible to observe some important trends regarding amine aerosol formation, the conditions were not controlled enough to draw any valid conclusions about the behaviour of primary amines (*t*BA and AMP), or to make accurate comparisons between primary and secondary amines. Nevertheless a full set of calculated maximum aerosol yields for each experiment is provided in Table A3, Appendix A. In the future, experiments with specific amine to oxidant and VOC to NO_x ratios could be performed to gain further insight. Also, when the data from the AMS becomes available, estimations of the total organic yield for each amine could be made. The rest of this chapter will investigate the composition of the aerosol, focusing on the formation of aminium nitrate salts, nitrosamines and nitramines, and additional ON species in the aerosol.

4.3.3.1 Formation of aminium nitrate salts

The formation of aminium nitrate salts occurs when HNO_3 reacts with gas phase amines in the chamber, as shown in Equation 4.3. The salt will be present as either a solid salt or an aqueous solution of aminium and nitrate ions, depending on the relative humidity in the chamber.[50] The average relative humidity in the chamber during the 2015 and 2016 photo-oxidation experiments was very low (1.7 %) so it is highly likely that the salt existed in the solid form.

$$R_nNH_{3-n\,(g)} + HNO_{3\,(g)} \leftrightarrow R_nNH_{4-n}NO_{3\,(s)} \quad (4.3)$$

Previous studies by Nielsen *et al.* have focused on the atmospheric degradation of 2-aminoethanol, ethylamine, diethylamine and triethylamine.[181-182] The formation of secondary (non-salt) organic aerosol from the photo-oxidation of 2-aminoethanol was less than 6%, which agreed with previous results obtained by Murphy *et al.*, who reported the yield of non-salt particles to be only 2%.[55] Aminium nitrate salts were also a major constituent of the aerosol formed during ethylamine and diethylamine photo-oxidation experiments and higher NO_x mixing ratios led to increased salt formation.[182] However, very different behaviour was observed for the triethylamine photo-oxidation experiments and the formation of salt was independent of the NO_x conditions. Moreover, the aerosol mass was dominated by secondary organic products and the ratio of organic/nitrate increased with time.[182]

In this study, IC was used to determine the formation of salt particles using the validated method described in Chapter 3, sections 3.2.2 and 3.3.2. Figure 4.6 shows example anion and cation chromatograms for the detection of nitrate (NO_3^-) and the *tert*-butylaminium ion ($C_4H_{12}N^+$). The black line represents the chromatogram for the collected aerosol sample and the green line represents the chromatogram for the blank filter paper.

As there is no time resolved data available for the formation of aminium nitrate salts during the photo-oxidation of *t*BA or AMP, only the aerosol composition at the end of each experiment has been investigated. The total yield of aminium nitrate salt has been calculated by dividing the mass of the salt formed by the amount of precursor amine reacted. For the *t*BA experiments, the total salt yield was 70% for the medium NO_x experiment (02-06-15, NO_x ~ 45 ppb) but the total salt yield exceeded 100% for the low NO_x experiment (03-06-15, NO_x ~ 10 ppb). This is thought to be due to problems with chamber air inflow and oxidant injection for this experiment, and the correction factor applied to compensate for chamber losses seems to fail for data points obtained at the end of the experiment. It is therefore difficult to determine any correlation between NO_x mixing ratios and the formation of *tert*-butylaminium nitrate salts.

For the AMP experiments however, the total salt yield ranged from 35.6% to 84.0% and the formation of aminium nitrate salts increased with increasing NO_x mixing ratios; this is likely to be due to increased formation of HNO_3 (from OH and NO_2) at higher NO_x levels.[55] Overall aminium nitrate yields were considerably lower for the secondary amines compared to the primary amines. The yields for the aerosol samples collected at the end of each experiment ranged from 0.4 to 1.1% for morpholine, 2.6 to 7.2% for piperidine, and 0.6 to 9.2% for piperazine.

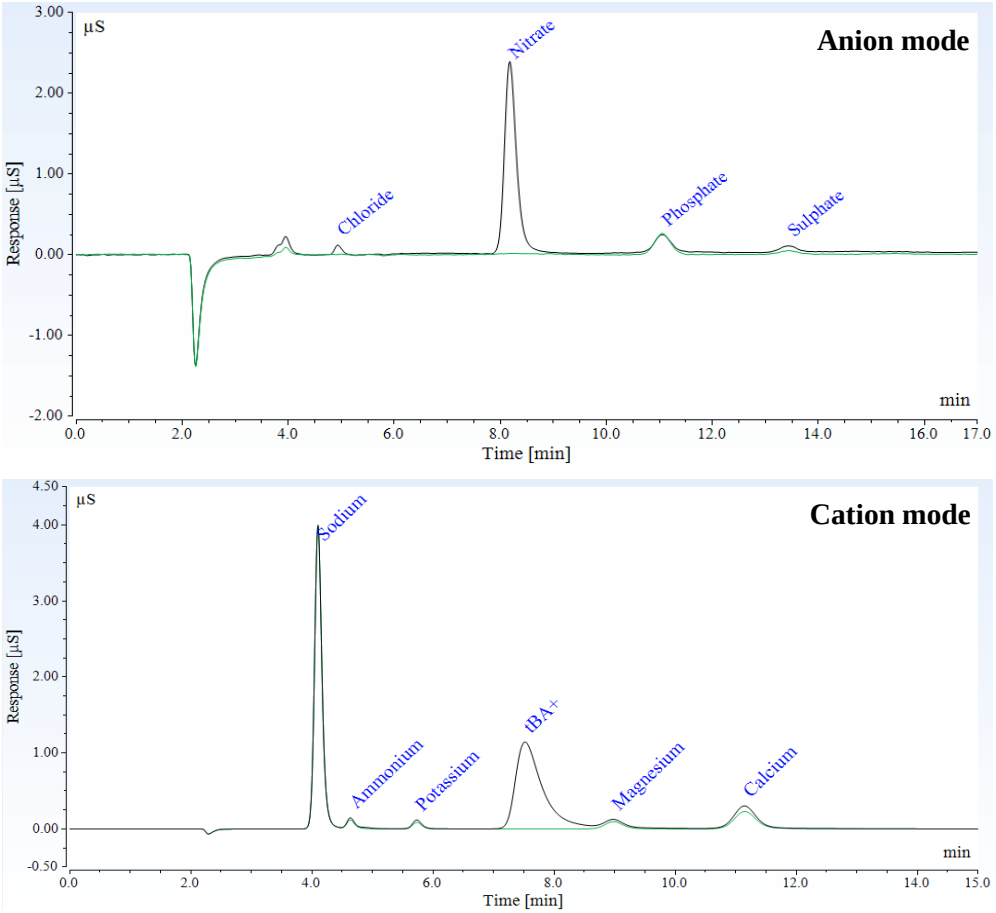

Figure 4.6. Anion and cation chromatograms to show the detection of nitrate (upper panel) and the *tert*-butylamine ion (lower panel). The black line represents the chromatogram for the collected aerosol sample and the green line represents the chromatogram for the blank filter paper.

The time resolution of the data for the secondary amine photo-oxidation experiments (morpholine, piperidine and piperazine) is better, so it is possible to study the salt formation processes of these amines in more detail. Whilst only the key observations are discussed here, Tables A4 – A6 in Appendix A provide full details of the ion concentrations, percentage yields and molar ratios for all the experiments. Figure 4.7 shows concentration time profiles for salt formation during the photochemical degradation of piperidine (11-07-16, NO_x ~ 200 ppb, uncorrected data and data corrected for particle wall loss and dilution are both shown).

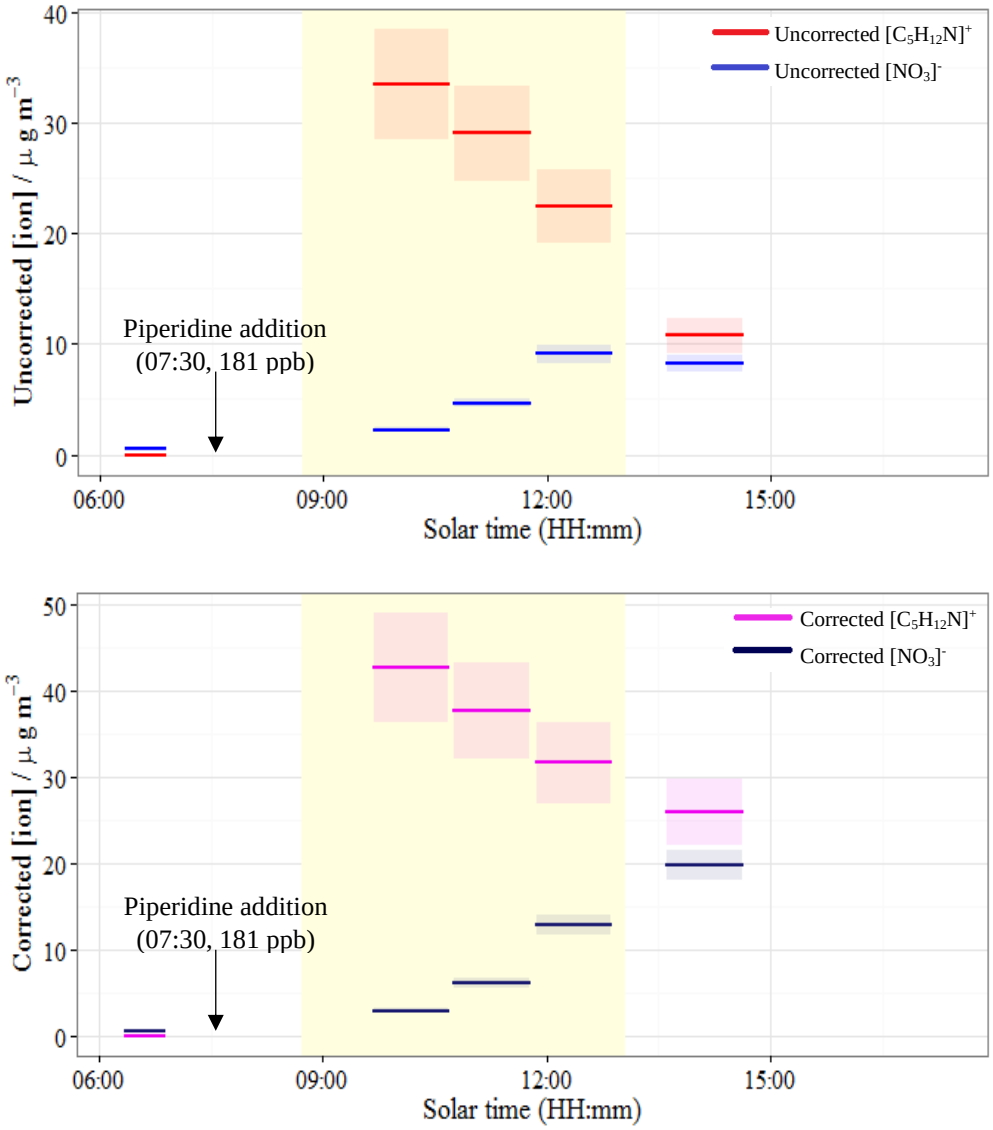

Figure 4.7. Concentration time profiles to show the formation of $C_5H_{12}N^+$ and NO_3^- during the photochemical degradation of piperidine (11-07-16, NO_x ~ 200 ppb). The upper panel shows raw data and the lower panel shows data corrected for particle wall loss and dilution.

Figure 4.7 shows that the concentration of $C_5H_{12}N^+$ was highest during the initial phase of the irradiation period and then subsequently decreased throughout the experiment. The corrected data shows that the maximum measured concentration of $C_5H_{12}N^+$ was 42.7 µg m^{-3}, and the final concentration was 25.9 µg m^{-3}. The behaviour of $C_5H_{12}N^+$ can be explained by considering the equilibrium between the parent amine present in the gas phase and the protonated amine in the particle phase. When particle formation commences at the start of the experiment, the concentration of the parent amine in the gas phase is still relatively high, and so there is a preference for partitioning to the aerosol. However, as

photochemical degradation continues and the levels of gas phase amine are depleted, $C_5H_{12}N^+$ in the aerosol can revolatilize to drive the equilibrium back to the gas phase amine. Additional loss of $C_5H_{12}N^+$ in the aerosol may be observed due to oxidation of the amine; the IC only measured $C_5H_{12}N^+$ in cation-exchange mode and was not set up to detect other oxidised species present in the aerosol.[55]

A different trend was observed for NO_3^-. In this particular experiment, the amount of NO_3^- in the aerosol increased throughout the duration of the photo-oxidation period, from 2.9 μg m^{-3} to 19.7 μg m^{-3}. The amount of NO_3^- in the aerosol is influenced by the rate of formation of HNO_3 in the chamber, which is formed from the reaction of NO_2 and OH. Whilst HNO_3 measurements were not made during these experiments, it is likely that continuous formation of HNO_3 occurs and equilibrium is shifted increasingly towards the particle phase, in an attempt to neutralise the large amounts of protonated amines present in the aerosol. The molar ratio (NO_3^- : $C_5H_{12}N^+$) was 0.07 for the first sample collected when the chamber canopy was opened. This subsequently increased to 0.20 and then 0.54 for the second and third samples. By the end of the experiment, when the canopy was closed, the molar ratio was 1.01. Whilst there are likely to be other acids and bases present in the aerosol, the data indicates that the aged particles collected at the end of the day are relatively neutral compared to the particles formed at the initial stages of photo-oxidation.

The results shown in Figure 4.7, and indeed several other experiments, suggest the formation of highly charged particles at the start of the photo-oxidation period. However, it is possible that there were several other anions present in the aerosol which have not been quantified using IC. Interestingly, small quantities of nitrite (NO_2^-) were found in some of the aerosol samples collected during the piperidine and piperazine photo-oxidation experiments, although the concentrations were not sufficient to completely neutralise the aminium ions. The highest NO_2^- concentrations (*ca.* 8 - 10 μg m^{-3}) were observed during the high NO_x experiments, and the concentration of NO_2^- rapidly decreased as the aerosol aged. By the end of the experiment the NO_2^- had presumably either evaporated back to the gas phase or oxidised to NO_3^-. The most likely source of NO_2^- is nitrous acid (HONO) present in the chamber. Other possible species include hydroxide ions (OH^-), formate (HCO_2^-) and acetate ($C_2H_3O_2^-$). The formation of OH^- cannot be determined using IC. Formic acid and acetic acid are well known chamber artefacts and could potentially form particulate HCO_2^- and $C_2H_3O_2^-$ respectively. Furthermore, Nielsen *et al.* have previously reported the formation of formic acid during the reaction of OH with various nitrosamines, and in fact formic acid was one of the 4 most abundant products of N-nitrosomorpholine photolysis.[182] Some of the anion chromatograms obtained for the aerosol samples collected in this study show the presence of small, unidentified peaks at the start of the chromatogram, which is where ions such as

formate and acetate are known to elute. Whilst the concentrations are unlikely to be as significant as the NO_3^- concentrations, further investigation is necessary to characterise and quantify as many additional species as possible.

It is important to assess how the results displayed in Figure 4.7 compare to other secondary amine photo-oxidation experiments. It is challenging to directly compare all the experiments, due to variations in the conditions *e.g.* amine/oxidant ratio. In general, higher NO_x mixing ratios led to increased salt concentrations, due to the increased formation and subsequent partitioning of gaseous HNO_3. In most experiments, NO_3^- behaved similarly to the example shown in Figure 4.7, and increased throughout the experiment. This happens because gas phase HNO_3 partitions to the aerosol in an attempt to neutralise protonated amines. In some cases, the NO_3^- concentration peaked before the end of the experiment, as sufficient quantities of NO_3^- to neutralise the aminium ion had been reached.

In all but one of the experiments, the concentration of protonated amine in the aerosol was highest at the start of the irradiation period and then subsequently decreased, as seen in the described piperidine experiment (11-07-16, Figure 4.7). It is likely that the anomalous trend observed for one of the morpholine experiments (05-07-16, initial NO ~ 50 ppb, initial NO_2 ~ 0 ppb) was due to a problem with the injection of IPN. A sudden burst of IPN was accidentally added to the chamber, leading to increased photochemistry, causing spikes in the concentrations of HONO, NO_2 and N-nitrosomorpholine, and rapid increases in the decay of morpholine and NO, and in the formation of particles, O_3 and N-nitromorpholine. As the aerosol sample collection period coincided with this event, a high NO_3^- concentration was observed (10.7 µg m^{-3}) due to the rapid formation of HNO_3. Whilst there was also $C_4H_{10}ON^+$ present in the aerosol, the concentration was only 1.6 µg m^{-3} and therefore the NO_3^- : $C_4H_{10}ON^+$ molar ratio was 15.30. Whilst in other experiments the protonated amine has subsequently revolatilized back to the gas phase, in this case further partitioning of the gas phase amine occurred, most likely in an attempt to neutralise the high NO_3^- content. Final NO_3^- and $C_4H_{10}ON^+$ concentrations were 1.7 µg m^{-3} and 4.5 µg m^{-3} respectively, and the final molar ratio was 0.87. The molar ratios (NO_3^- : RNH_3^+) were calculated for the *t*BA and AMP aerosol samples collected at the end of the day. The molar ratio was 1.45 for the *t*BA photo-oxidation performed on 03-06-15, whilst for the remaining *t*BA and AMP experiments the molar ratio ranged from 0.75 to 0.91. A molar ratio of less than 1 indicates that there is more $C_4H_{12}N^+$ or $C_4H_{12}ON^+$ present in the aerosol than NO_3^-. This may occur when there is a lack of HNO_3 available for partitioning to the aerosol, or when the condensation of organic species onto salt particles creates a barrier and prevents equilibrium with the gas phase.[55] The final molar ratios for the secondary amines (NO_3^- : $R_2NH_2^+$) ranged from 0.82 to 1.67 for morpholine, 1.08 to 1.73 for piperidine, and 0.64 to 2.56 for piperazine. When the molar

ratio is greater than 1, there is more NO_3^- in the aerosol than the aminium ion. This may occur when the amine repartitions back to the gas phase and forms a different basic compound, such as an amide or an imine. These compounds can also form salts with NO_3^-, but the new cations were not measured by IC in this study. This type of particle transformation process was recently proposed by Nielsen *et al.*, when it was not possible to confirm the identity of the salt particles present in aerosol formed from the photochemical degradation of 2-aminoethanol. Comparison of the mass spectrum of pure ethanolammonium salt with the aerosol formed showed significant differences for the peaks at *m/z* 18, 28, 29 and 45.[183] Molar ratios of 0.64, 1.98, 2.56 were obtained at the end of the piperazine experiments. A ratio of approximately 1 suggests that the salt exists as mono-nitrate piperazine aminium salt, $[C_4H_{11}N_2]^+[NO_3]^-$, whereas a ratio closer to 2 indicates that the dinitrate piperazine aminium salt has formed, $[C_4H_{12}N_2]^{2+}2[NO_3]^-$. In a previous study by Nielsen *et al.* the low NO_x experiments formed mainly the mono-nitrate salt, while under high NO_x conditions the dinitrate salt was observed.[182] This trend was not observed in this study, and the molar ratio was highest (2.56) during the low NO_x experiment. Further investigation is required to determine the factors influencing the formation of mono-nitrate and dinitrate salts.

In summary, the time-resolved measurements presented in this study provide an interesting insight into the formation of aminium nitrate salts during the photochemical degradation of amines relevant to CO_2 capture. Nevertheless, there are some limitations associated with chamber studies, and these should be taken into consideration if the data is used to model ambient salt formation in aerosols under typical conditions at Mongstad, Norway. For example, the chamber is representative of a dry atmosphere and in the real atmosphere humidity levels are likely to be considerably higher; the presence of H_2O has the potential to change the solubility of oxidants and amine precursors in the aerosol and significantly enhance aerosol formation.[183] In addition, urban atmospheres tend to contain a complex mixture of acidic species such as HNO_3, H_2SO_4 and HCl, which can all react with basic amines to form salts.

4.3.3.2 Nitrosamine and nitramine formation

The main objective of this study was to investigate the suitability of a new analytical method, based on GC×GC-NCD, for the determination of nitrosamines and nitramines formed during atmospheric amine degradation. The methods for sample collection, extraction and analysis were validated (as discussed in Chapter 3), and then the formation of nitrosamines and nitramines in aerosol samples collected during a series of photo-oxidation experiments was investigated. Figure 4.8 shows a typical GC×GC-NCD chromatogram for an aerosol sample collected at the end of a morpholine photo-oxidation experiment. The combination of two-dimensional GC separation and nitrogen-specific detection meant that trace level ON species such as N-nitrosomorpholine and N-nitromorpholine could be easily detected within a complex atmospheric matrix. However, the GC×GC chromatogram shows that N-nitrosomorpholine and N-nitromorpholine were detected amongst hundreds of other ON compounds and made up a very small fraction of the total ON; in the chromatogram shown below for example, the nitrosamine and nitramine made up 0.4% and 1.9% of the total ON respectively (assuming an equimolar response for all ON compounds). In the future, it will be necessary to characterise the ON fraction of the aerosol formed during each photo-oxidation experiment in more detail. Whilst a small number of additional ON compounds have been characterised in this study (see section 4.3.3.3), a considerably more thorough investigation is required.

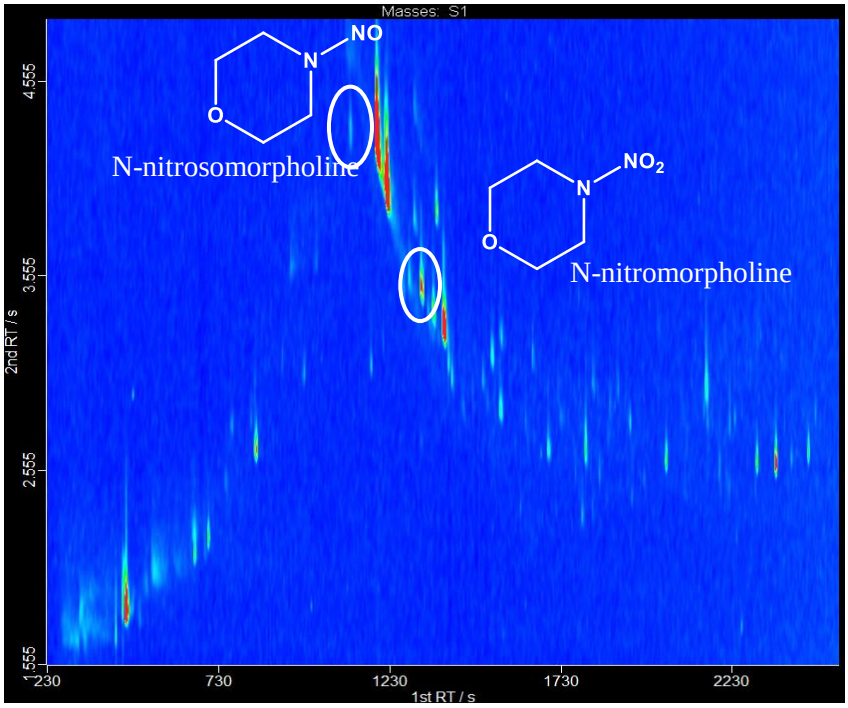

Figure 4.8. GC×GC-NCD chromatogram to show the detection of N-nitrosomorpholine and N-nitromorpholine amongst other ON compounds present in the aerosol.

Several filter samples were collected throughout the duration of each secondary amine photo-oxidation experiment, and for every sample, the particulate concentrations of the nitrosamines and nitramines were successfully quantified (full details are provided in Tables A7 – A10, Appendix A). A summary of the maximum particulate nitrosamine and nitramine concentrations measured during each photo-oxidation experiment is provided in Table 4.8, and a calculation of the % yield from the parent amine is also included.

Morpholine: During the morpholine photo-oxidation experiments, maximum N-nitrosomorpholine concentrations ranged from 0.027 to 0.14 µg m^{-3} (0.004 – 0.018% yield). Maximum N-nitromorpholine concentrations between 0.86 and 13.5 µg m^{-3} were observed, equating to yields of 0.12 – 1.64%.

Piperidine: Maximum N-nitrosopiperidine concentrations ranged from 0.049 to 0.47 µg m^{-3} and maximum N-nitropiperidine concentrations were between 0.34 and 3.26 µg m^{-3}. This equated to maximum % aerosol yields of N-nitrosopiperidine and N-nitropiperidine of 0.01 – 0.18% and 0.11 – 0.58% respectively.

Piperazine: The concentrations of the di-nitrosamine product (1,4-dinitrosopiperazine) were of similar magnitude to those of N-nitrosomorpholine and N-nitrosopiperidine and ranged from 0.14 – 0.30 µg m^{-3}. 1,4-dinitrosopiperazine was not detected during the low NO_x experiment carried out on 22-07-16. The mono-nitrosamine (N-nitrosopiperazine) levels were between 11 and 72 times higher than those of 1,4-dinitrosopiperazine, and maximum concentrations ranged from 1.8 µg m^{-3} to 11.9 µg m^{-3}, which is equivalent to aerosol yields of 0.29 - 2.84% from the parent amine. Nitramine formation during the piperazine photo-oxidation experiments was even more significant, and the maximum N-nitropiperazine concentration recorded was 108.9 µg m^{-3}. At this maximum concentration, 18.9% of the parent amine had been converted to particle phase N-nitropiperazine.

As shown in Figure 4.9, three experiments performed under similar conditions have been used to compare the extent of nitrosamine and nitramine formation for three different secondary amines; morpholine, piperidine and piperazine. Measurements of particulate N-nitrosomorpholine and N-nitromorpholine under high NO_x conditions are shown in the upper panels of Figure 4.9. Under the same NO_x conditions, the formation of N-nitrosopiperidine and N-nitropiperidine are shown in the middle panels, and N-nitrosopiperazine and N-nitropiperazine in the lower panels. In general, the amount of nitrosamine and nitramine formation observed for the 3 different secondary amines under high NO_x conditions showed the same trend as the total aerosol yield measurements *i.e.* piperazine >> piperidine > morpholine. This suggests that the extent of partitioning of

nitrosamines and nitramines to the particle phase is strongly influenced by the amount of absorptive mass present.

Table 4.8. Maximum nitrosamine and nitramine concentrations (and the corresponding % yield from the parent amine) detected in aerosol samples collected during morpholine, piperidine and piperazine photo-oxidation experiments. All reported data has been corrected for particle wall loss and chamber dilution.

Amine	Date	NO_x conditions	Nitrosamine		Nitramine	
			Max. conc. / µg m^{-3}	% OA yield	Max. conc. / µg m^{-3}	% OA yield
morpholine	04-07-16	high	0.053	0.011	0.86	0.614
	05-07-16	medium	0.027	0.004	0.91	0.121
	06-07-16	medium	0.14	0.018	13.5	1.635
	07-07-16	low	0.037	0.005	1.00	0.127
piperidine	11-07-16	high	0.47	0.180	2.15	0.433
	12-07-16	low	0.049	0.011	1.02	0.183
	15-07-16	medium-high	0.13	0.043	0.34	0.109
	18-07-16	medium	0.12	0.022	3.26	0.577
piperazine	20-07-16	high	11.9 0.30*	2.84 0.070≠	88.1	18.35
	21-07-16	medium-high	8.76 0.17*	1.95 0.031≠	108.9	18.89
	22-07-16	low	1.81 0.00*	0.290 0.000≠	55.6	10.67
	25-07-16	medium	5.47 0.14*	0.959 0.024≠	32.3	5.67
	26-07-16	medium	5.90 0.19*	1.62 0.053≠	63.5	17.43

*Concentration of 1,4-dinitrosopiperazine. ≠% yield of 1,4-dinitrosopiperazine.

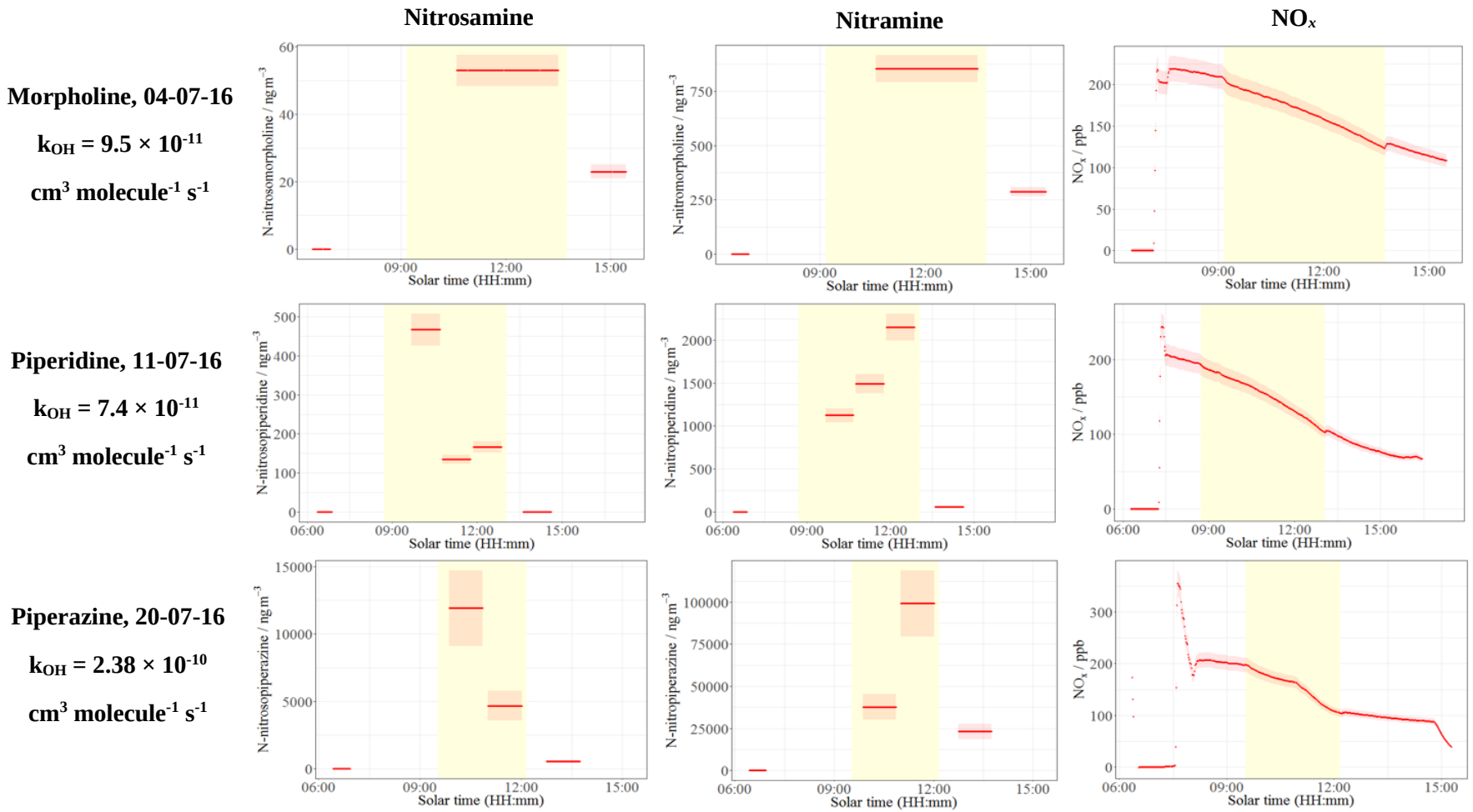

Figure 4.9. Nitrosamine, nitramine and NO_x time series for 3 amine photo-oxidation experiments.

***t*BA and AMP:** It is important to consider nitramine formation from primary amines and whilst there is no time-resolved data available for *t*BA or AMP, it is still possible to consider the high-volume aerosol samples collected at the end of each experiment. Table 4.9 summarises the nitramine concentrations measured during each primary amine photo-oxidation experiment under the specified NO_x conditions and amine: oxidant ratios. The data has been corrected for wall loss and dilution, but unfortunately it was not possible to determine the wall loss rate for some experiments (04-06-15, 15-06-15 and 19-06-15) and so this data has been excluded.

Table 4.9. Average *t*BA-NO_2 and AMP-NO_2 concentrations (and the corresponding % yield from the parent amine) detected in aerosol collected at the end of the photo-oxidation experiments when the chamber was closed. NO_x conditions and amine:oxidant ratios have been provided, and all reported concentrations have been corrected for particle wall loss and chamber dilution.

Amine	Date	NO_x conditions	Amine: oxidant	[nitramine] / µg m^{-3}	% yield from parent amine
*t*BA	02-06-15	low	72	4.01	0.59
	03-06-15	high	20	13.06	1.92
AMP	09-06-15	medium	64	25.48	6.85
	12-06-15	low	59	18.58	5.42
	18-06-15	high	168	45.19	13.33

It is difficult to compare the experiments listed in Table 4.9 directly because of the different amine: oxidant ratios present in the chamber, but overall it seems that the formation of both *t*BA-NO_2 and AMP-NO_2 in the aerosol increased with increasing NO_x mixing ratios. This trend is less consistent for the secondary amines but overall the highest nitrosamine and nitramine yields were obtained under high NO_x conditions when no additional IPN was added to the chamber. For piperazine and piperidine, the lowest yields of the target carcinogens were obtained for the low NO_x experiments, but this trend was not observed for morpholine.

Primary *vs.* secondary amines: Table 4.10 provides a summary of the nitramine concentrations measured at the end of each experiment and allows a comparison of nitramine formation for primary and secondary amines to be made. As previously shown, nitramine formation from secondary amines was higher when the canopy was open, but this data cannot be compared to nitramine formation from primary amines as samples were only collected at the end of the primary amine photo-oxidation experiments. The data shows that the highest

nitramine levels at the end of the experiments formed from AMP oxidation (5.42 – 13.33% yield). However, the formation of nitramines (and nitrosamines) can be affected by factors such as actinic flux or the amount of oxidant in the chamber; significantly larger amounts of oxidant were added to the chamber during the *t*BA and AMP experiments. Nitramine formation from both *t*BA and piperazine oxidation was also relatively high, with respective maximum yields of 1.92 and 3.81%. Nitramine formation from morpholine and piperidine was considerably lower and maximum yields of 0.12 and 0.012% respectively were measured at the end of the experiment.

Table 4.10. Maximum nitramine concentrations (and the corresponding percentage yield from the parent amine) detected in aerosol samples collected at the end of each experiment. All reported data has been corrected for particle wall loss and chamber dilution.

Type of amine	Amine	[nitramine] / μg m^{-3}	% yield from parent amine
Primary	*t*BA	4.01 – 13.06	0.59 – 1.92
	AMP	18.58 – 45.19	5.42 – 13.33
Secondary	morpholine	0.15 – 0.29	0.02 – 0.12
	piperidine	0.03 – 0.08	0.006 – 0.012
	piperazine	2.85 – 23.00	0.32 – 3.81

Nitrosamines from *t*BA and AMP photo-oxidation were not observed in the aerosol, as primary nitrosamines are unstable in the atmosphere and undergo rapid decay to form a carbocation and N_2 (further discussion is provided in section 4.3.3.3).[75] However, secondary nitrosamines are relatively stable and the formation of these carcinogens was observed for morpholine, piperidine and piperazine. In the samples collected at the end of the experiments, the maximum yields of the nitrosamines from these three amines were 2.8, 11.8 and 89.9 ‰ respectively. Whilst the nitrosamine levels are considerably lower than the nitramine levels, these compounds are known to be highly carcinogenic and still may pose a threat to human health at trace level concentrations. In terms of nitramine formation, the secondary amines may seem preferable to the primary amines for use as CO_2 capture solvents, but it is important to consider the total formation of both nitramines and nitrosamines in the aerosol from a particular amine.

Ratio of nitramine to nitrosamine: A key observation in these experiments was that the overall nitramine concentrations in the aerosol were significantly higher than the corresponding nitrosamine concentrations. Pitts *et al.* reported a similar observation for

nitrosamine and nitramine gas phase concentrations during a study of the photo-oxidation of diethylamine.[72] The study stated that whilst the relative concentrations of diethylnitrosamine and diethylnitramine partially depended on the NO:NO_2 ratio, they also depended on the relative stability of the two compounds in sunlight. Diethylnitrosamine can absorb a wide range of actinic UV radiation, whereas diethylnitramine has a lower absorption cross section in sunlight, and therefore the photochemical losses of this compound in the chamber are considerably smaller.[72] The UV spectra of the nitrosamines and nitramines formed from the photochemical degradation of morpholine, piperidine and piperazine are not available in the literature, but it is assumed that the same effect is observed for these secondary amines, and that the nitramines accumulate to higher concentrations as a result of their increased stability in sunlight.

Another important consideration is the fate of the nitrosamine once it has formed. In 1977, Hanst *et al.* reported that the photolysis of dimethylnitrosamine yielded significant amounts of a 'new compound.'[210] Further investigation by Pitts *et al.* revealed that this compound was dimethylnitramine. Although dimethylnitramine can initially form directly from the oxidation of dimethylamine (*via* pathway B), after approximately 1 hour in sunlight, additional dimethylnitramine can form *via* direct, thermal or photochemical oxidation of dimethylnitrosamine, as shown in Scheme 4.3 (pathway C).[72]

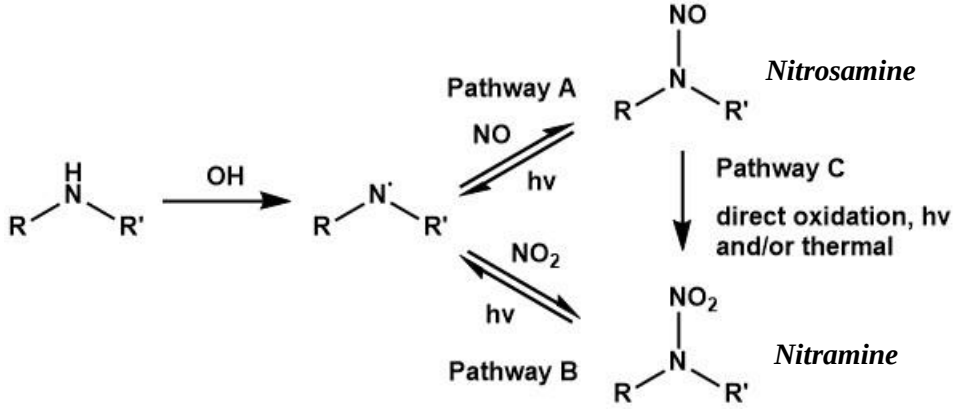

Scheme 4.3. Reaction scheme for the formation of nitrosamines (pathway A) and nitramines (pathway B) *via* amine photo-oxidation. Nitrosamine oxidation can lead to additional nitramine formation (pathway C).[72]

With this knowledge in mind, it is interesting to assess how the nitramine to nitrosamine ratio in aerosol varies with time in this study. All of the collected aerosol samples apart from one (piperidine, 18-07-16, canopy closed, ratio = 0.7) had a nitramine to nitrosamine ratio of greater than 1 *i.e.* there was almost always more nitramine than nitrosamine present in the chamber at any given time. During the different stages of all the photo-oxidation experiments, the nitramine to nitrosamine ratios ranged from 12.4 to 93.6 for morpholine,

1.7 to 91.2 for piperidine, and 3.2 to 42.4 for piperazine. Whilst there is high variability in the relative amounts of nitramine and nitrosamine during each experiment, the ratios calculated for each amine span similar orders of magnitude. Pitts *et al.* described the shape of the time-concentration profile of gaseous diethylnitrosamine formed from triethylamine, and observed a rapid rise to a maximum followed by a decay.[72] It is understood that this profile is characteristic of initial diethylnitrosamine formation by the typical photo-oxidation process (pathway A, Scheme 4.3), followed by the occurrence of competitive photodecomposition processes after about 1 hour in sunlight (pathway C, Scheme 4.3).[72] Figure 4.10 shows the time-concentration profiles for N-nitrosopiperidine and N-nitropiperidine for a low NO_x experiment (12-06-16) as well as the measured NO_x and aerosol concentrations.

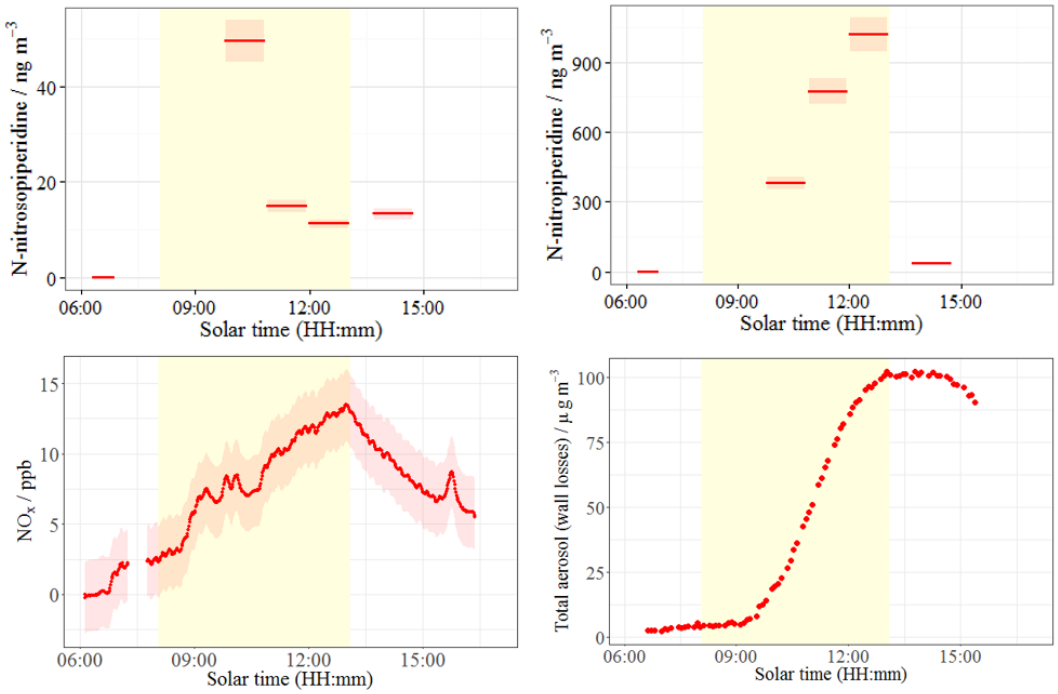

Figure 4.10. Time-concentration profiles of N-nitrosopiperidine (upper left), N-nitropiperidine (upper right), NO_x (lower left) and total aerosol concentration (lower right) during a piperidine photo-oxidation experiment (12-07-16).

The characteristic gas-phase nitrosamine time profile described by Pitts *et al.* is also observed for particulate N-nitrosopiperidine in this experiment, and Figure 4.10 (upper left panel) shows an initial maximum N-nitrosopiperidine concentration of 49.4 ng m^{-3}, followed by decay to levels of *ca.* 13 ng m^{-3} for the remainder of the experiment. Figure 4.10 shows the time-concentration profile for N-nitropiperidine (upper right panel) during the same experiment; when the canopy was open the concentration of N-nitropiperidine increased continuously at a steady pace to reach a maximum of 1017.9 ng m^{-3}. The nitramine to nitrosamine ratios for the three consecutive samples collected when the canopy is open were

7.7, 52.0 and 91.2. This indicated that the difference in the amount of nitramine and nitrosamine increased throughout the irradiation period. The observed trends and ratios support the hypothesis that initial formation of the nitrosamine occurs *via* amine photo-oxidation, and then competitive photodecomposition processes occur, oxidising the nitrosamine to the nitramine. At this stage the extent to which the nitramine is formed *via* pathway B or pathway C (Scheme 4.3) is still unclear and further investigation is required. When the canopy is closed, the N-nitrosopiperidine concentration increases slightly by approximately 2 ng m^{-3}; this may be because decomposition of the nitrosamine (Pathway C) is not favoured in the absence of sunlight, although more evidence is required to support this hypothesis. Interestingly, a large decrease in the amount of N-nitropiperidine occurs when the chamber canopy is closed, and the nitramine concentration drops from 1017.9 ng m^{-3} to 34.0 ng m^{-3}. There could be a number of reasons why this dramatic decline is observed: for example there may be a lack of N-nitropiperidine formation from the photo-oxidation of piperidine in the absence of sunlight; or there may be a reduction in the oxidation of N-nitrosopiperidine to form N-nitropiperidine; or a change in the chamber temperature or gas phase composition, leading to a shift of the gas-particle N-nitropiperidine equilibrium. As a result the nitramine to nitrosamine ratio decreases when the chamber canopy is closed (ratio = 2.6) and the two species become more similar in concentration. It is difficult to investigate the nitrosamine and nitramine trends for every experiment because in some cases fewer aerosol samples were collected per experiment. Nevertheless, in the majority of experiments the nitrosamine and nitramine concentrations reach their maximum concentrations at some stage during the irradiation period and then subsequently decrease when the canopy is closed – this usually means that the nitramine to nitrosamine ratio also decreases when the canopy is closed. There are some exceptions, such as the photo-oxidation of morpholine (05-07-16, initial NO_x ~ 50 ppb) and piperazine (20-07-16, initial NO_x ~ 200 ppb), which exhibit an increase in the nitramine to nitrosamine ratio when the canopy is closed. On 05-07-16 a large amount of IPN was suddenly added to the chamber during the photo-oxidation period, leading to increased photochemical degradation and a sharp rise in the NO_2 levels. On 20-07-16 the NO_x mixing ratios were high and NO_2 levels of approximately 100 ppb were sustained throughout the experiment. It is possible that these conditions were more suitable for nitramine stability in the aerosol, and therefore the concentration did not decline as rapidly when the canopy was closed, leading to higher nitramine to nitrosamines ratios.

In summary, a suitable method has been obtained for the determination of nitrosamines and nitramines formed during the photochemical degradation of amines relevant to CO_2 capture. The analytical technique has allowed for the accurate quantification of these carcinogens in

aerosol collected during a range of photo-oxidation experiments. Although more information is needed to assess the suitability of each amine as a solvent for CO_2 absorption, the data presented in this study shows that piperazine forms high levels of both nitrosamines and nitramines in the particle phase and should be considered as a CO_2 capture solvent with caution. Furthermore, it will be important to account for relative toxicity and carcinogenicity of different nitrosamines and nitramines if such information becomes available in the future.

4.3.3.3 Characterisation of additional ON species in the SOA

Aside from the target nitrosamines and nitramines, the GC×GC-NCD chromatograms highlighted the presence of several other ON species in the SOA as shown previously in Figure 4.8. In an attempt to identify some of these additional compounds, the high-volume aerosol samples from the *t*BA and AMP experiments were analysed by GC×GC-TOF-MS. Five key compounds were selected for further analysis; these species were chosen because they matched the NIST mass spectral library well and were commercially available as analytical standards, allowing for accurate quantification. Furthermore, the compounds demonstrate other important reactions occurring in the photo-oxidation chamber, as discussed later in this section. The structures of these compounds are shown in Figure 4.11, and a series of GC×GC-TOF-MS extracted ion chromatograms (EICs) for each ON compound are shown in Figure 4.12.

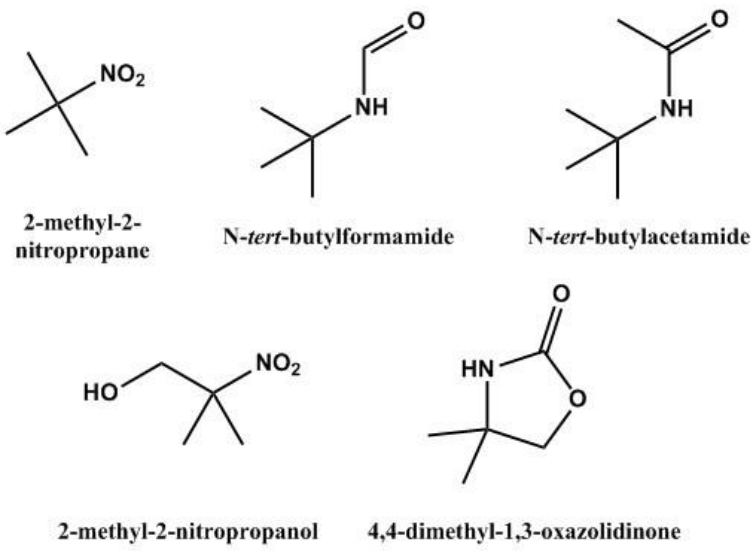

Figure 4.11. Chemical structures of the target compounds analysed by GC×GC-TOF-MS.

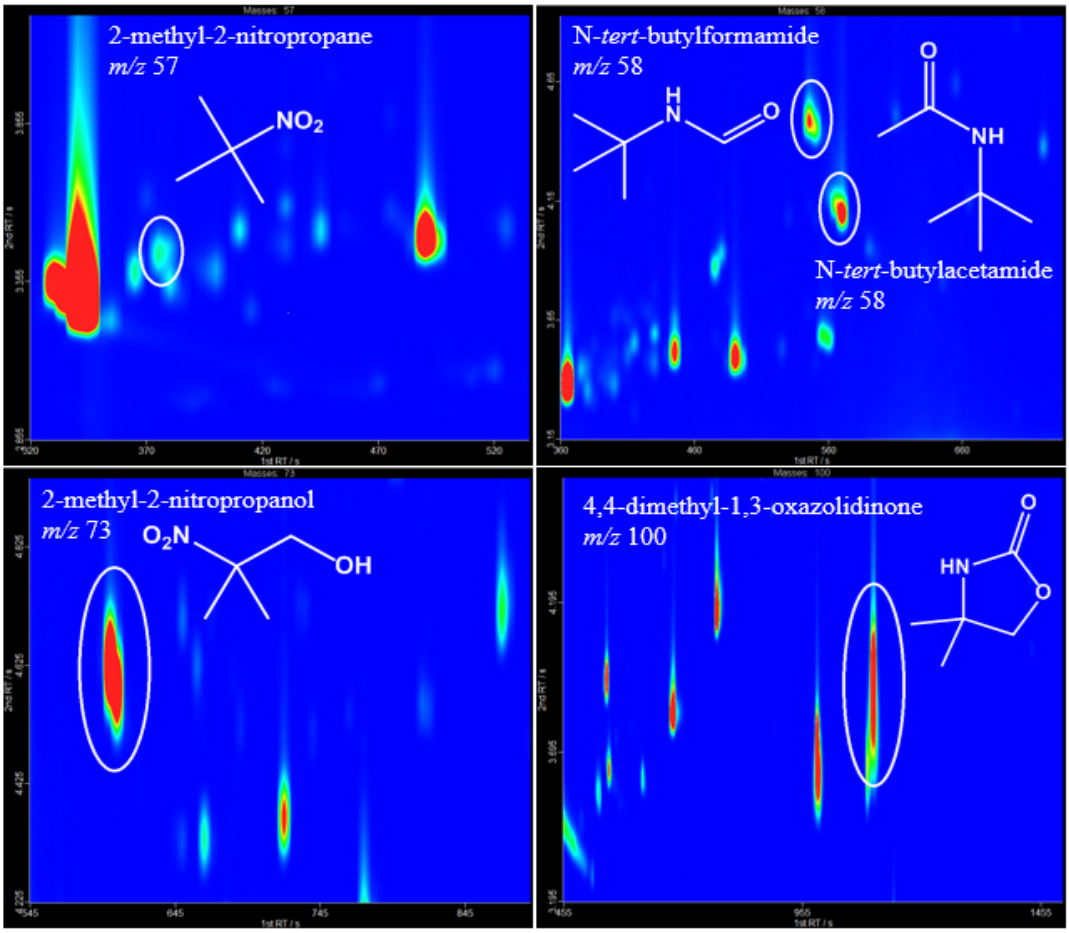

Figure 4.12. GC×GC-TOF-MS EICs for the additional ON compounds measured in the aerosol. *m/z* 57, 2-methyl-2-nitropropane (upper left); *m/z* 58 N-*tert*-butylformamide and N-*tert*-butylacetamide (upper right); *m/z* 73 2-methyl-2-nitropropanol (lower left); *m/z* 100 4,4-dimethyl-1,3-oxazolidinone (lower right).

The concentration of each compound in the aerosol was determined by external calibration of each standard. Table 4.11 summarises the results for the *t*BA aerosol samples, and Table 4.12 provides details of the ON species found in the AMP aerosol samples. The concentration of each compound has been corrected for chamber wall loss and dilution, and the percentage yield of each compound was determined by dividing the mass of the target ON compound observed in the SOA by the mass of the parent amine reacted. Data from experiments performed on the 4th, 15th and 19th June has been excluded due to problems associated with calculating the wall loss rate.

Table 4.11. Chamber concentrations (corrected for wall loss and dilution) and percentage aerosol yield for SOA compounds formed from the photo-oxidation of *t*BA.

Compound		02-06-15 (medium NO_x)	03-06-15 (low NO_x)
2-methyl-2-nitropropane	Conc / μg m^{-3}	15.85	n.d.
	% yield	1.7	n/a
N-*tert*-butylformamide	Conc / μg m^{-3}	1.45	1.97
	% yield	0.16	0.21
N-*tert*-butylacetamide	Conc / μg m^{-3}	1.81	1.34
	% yield	0.17	0.13

Table 4.12. Chamber concentrations (corrected for wall loss and dilution) and percentage aerosol yield for SOA compounds formed from the photo-oxidation of AMP.

Compound		09-06-15 (medium NO_x)	12-06-15 (low NO_x)	18-06-15 (high NO_x)
2-methyl-2-nitropropanol	Conc / μg m^{-3}	0.40	0.27	1.37
	% yield	0.08	0.06	0.30
4,4-dimethyl-1,3-oxazolidinone	Conc / μg m^{-3}	5.40	5.02	2.87
	% yield	1.12	1.14	0.65

The corresponding nitroalkane of each parent amine was observed *i.e.* 2-methyl-2-nitropropane from *t*BA oxidation and 2-methyl-2-nitropropanol from the oxidation of AMP. For *t*BA, the 2-methyl-2-nitropropane was not detected in the low NO_x experiment (03-06-2015), but a concentration of 15.85 μg m^{-3} was determined for the medium NO_x experiment (02-06-2015). This equated to an aerosol yield of 1.7%. In contrast the maximum aerosol yield for 2-methyl-2-nitropropanol from AMP was only 0.30%. The amount of 2-methyl-2-nitropropanol increased with increasing NO_x mixing ratios. Although accurate concentrations cannot be provided, 2-methyl-2-nitropropane was also detected in discounted aerosol samples collected on 04-06-2015, and 2-methyl-2-nitropropanol on 15-06-2015 and 18-06-2015. It is likely that the nitroalkane formation is a result of oxidative processing of the amine by ozone, as shown in Scheme 4.4.[211]

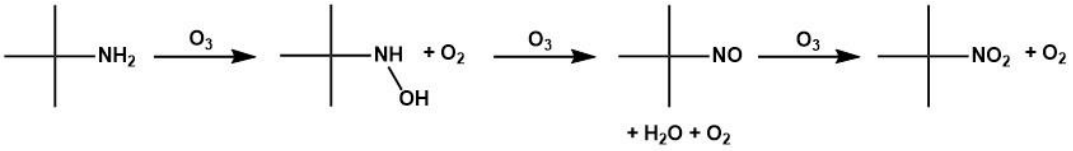

Scheme 4.4. Mechanism for the ozonolysis of *t*BA to form 2-methyl-2-nitropropane.

The formation of 4,4-dimethyl-1,3-oxazolidinone was also observed in the aerosol from the AMP photo-oxidation experiments and the aerosol yield for this compound was between 0.65 % and 1.14 %. The concentrations ranged from 2.87 to 5.40 μg m^{-3}, and there was no obvious trend between the yield of the compound and the NO_x mixing ratio. This is likely to be because the compound is a condensation product, formed from the reaction of AMP with small molecules such as aldehydes, ketones or carboxylic acids formed during the photo-oxidation experiment, and does not depend on the amount of NO_x in the system. Similar results were obtained during a study of the photo-oxidation of 2-aminoethanol; Nielsen *et al.* reported the presence of various condensation products, such as 2-oxazolidinone, which formed by reactions on particles, chamber walls and possibly instrument inlet surfaces.[181] Products with more carbon atoms than their parent amine were also observed in the *t*BA aerosol. For example, the concentrations of N-*tert*-butylformamide ranged from 1.45 to 1.97 μg m^{-3}, and N-*tert*-butylacetamide concentrations were between 1.34 and 1.81 μg m^{-3}. Similar results were obtained when Pitts *et al.* studied the photo-oxidation of diethylamine; four gaseous products from diethylamine were found, and included diethylformamide and diethylacetamide.[72]

Although the investigation of these SOA compounds only accounts for a small fraction of the total aerosol, useful information has been obtained and the results have been compared with relevant previous work. In the future it would be possible to use a combination of GC×GC-TOF-MS and GC×GC-NCD to characterise the *t*BA and AMP aerosol more extensively, and also investigate the aerosol composition for other amines relevant to CO_2 capture in more detail, such as morpholine, piperidine and piperazine.

4.4 Conclusions

The formation of *t*BA-NO_2 was monitored during the photo-oxidation experiments using Thermosorb-N air sampling cartridges, but the cartridges were not suitable for the detection of AMP-NO_2. The *t*BA-NO_2 concentrations determined using Thermosorb-N cartridges and PTR-TOF-MS agreed with each other to within a factor of 1.5, as shown in Table 4.5. It was not possible to investigate the sources of error in more detail as the cartridge extracts were beginning to damage the ultra-inert column installed in the GC×GC-NCD. Although there

was not an obvious relationship between *t*BA-NO_2 formation and NO_x mixing ratio, the data suggested that *t*BA-NO_2 formation was greatest when OH concentrations were highest.

The total aerosol yield was calculated by dividing the mass of aerosol formed (both non-salt and salt contribution) by the amount of precursor amine reacted. By analysing sets of comparable experiments, it was possible to draw some key conclusions regarding aerosol formation resulting from amine photo-oxidation. For example, the total aerosol yield during the morpholine photo-oxidation experiments increased with increasing NO_x levels, and this was most likely due to an increased availability of HNO_3 in the system. At both low and high NO_x levels, piperazine formed more aerosol than morpholine and piperidine, due to its faster rate constant (k_{OH}) and lower volatility.

The presence of aminium nitrate salts in the aerosol was determined by IC. For the *t*BA experiments it was difficult to determine a trend between salt formation and NO_x mixing ratios, but for the AMP experiments the formation of aminium nitrate salts increased with increasing NO_x levels. Time-resolved data for salt formation from the photochemical degradation of secondary amines revealed that in most cases, an initial maximum in aminium ion concentration was observed at the start of irradiation, followed by subsequent revolatilization to the gas phase, or oxidation to other basic species capable of forming nitrate salts. The opposite trend was observed for NO_3^- and concentrations generally increased throughout the experiment, most likely due to the increased availability of $HNO_{3(g)}$ in the reaction system.

The developed GC×GC-NCD technique enabled the accurate quantification of nitrosamines and nitramines in aerosols. The nitramines accumulated to higher levels than nitrosamines in the aerosol, most likely due to their increased stability in sunlight. Whilst nitramine formation was lower for secondary amines than primary amines, additional factors such as lower oxidant concentrations during these experiments must be considered. Furthermore, the overall carcinogenic risk from the degradation of secondary amines may be higher than primary amines due to the substantial nitrosamine formation that is not observed for primary amines. Both the nitramine and nitrosamine concentrations varied throughout the irradiation period, due to photo-oxidation from the parent amines and the occurrence of competing photochemical decomposition processes. In general, the highest levels of nitrosamines and nitramines in the aerosol were observed under high NO_x conditions and when the amount of absorptive mass was highest, but a more systematic approach to the experiments is needed to verify these trends. In the future, the technique could be used to analyse nitrosamine and nitramine concentrations in ambient air, and a cancer risk assessment from exposure *via* inhalation could be performed if more detailed toxicological data becomes available.

Additional ON compounds were identified using GC×GC-TOF-MS and five key compounds were identified for further analysis. The formation of the corresponding nitroalkanes from both *t*BA and AMP was observed, and the highest concentrations were measured at high NO_x levels. It is possible that the nitroalkanes formed as a result of the reaction between NO_2 and the carbocation produced during primary nitrosamine decay. Additional compounds identified contained more carbon atoms than their parent amine, and were likely to be formed from surface-assisted condensation reactions. No clear trends between NO_x mixing ratios and the concentration of these species was identified.

In summary, a range of analytical techniques have successfully been used to investigate the formation of nitrosamines, nitramines and other nitrogen-containing species in the aerosol. More information is required to assess the suitability of each amine as a solvent for CO_2 absorption, but the data from this study suggests that piperazine forms high levels of both nitrosamines and nitramines in the particle phase and should be considered as a CO_2 capture solvent with caution. In the future, it is hoped that this data will be combined with gas phase data and incorporated into models to determine ambient nitrosamine and nitramine concentrations under typical conditions at Mongstad, Norway. In turn, the data will potentially help to determine the most suitable amines to be used for CO_2 capture, and will also allow more accurate environmental impact assessments of amine-based solvents to be carried out.

5 Investigation of the chemical composition of cooking emissions and the impact of cooking with herbs and pepper

The work presented in this chapter was part of a collaborative project with the Paul Scherrer Institute (PSI), Switzerland. A significant amount of the work on gas phase cooking emissions and the impact of cooking with herbs and pepper has been published in two papers:

Felix Klein, Stephen M. Platt, Naomi J. Farren, Anais Detournay, Emily A. Bruns, Carlo Bozzetti, Kaspar R. Daellenbach, Dogushan Kilic, Nivedita K. Kumar, Simone M. Pieber, Jay G. Slowik, Brice Temime-Roussel, Nicolas Marchand, Jacqueline F. Hamilton, Urs Baltensperger, André S. H. Prévôt and Imad El Haddad. Characterization of Gas-Phase Organics Using Proton Transfer Reaction Time-of-Flight Mass Spectrometry: Cooking Emissions. *Environmental Science & Technology,* **2016**, *50* (3), 1243-1250.

Felix Klein, Naomi J. Farren, Carlo Bozzetti, Kaspar R. Daellenbach, Dogushan Kilic, Nivedita K. Kumar, Simone M. Pieber, Jay G. Slowik, Rosemary N. Tuthill, Jacqueline F. Hamilton, Urs Baltensperger, André S. H. Prévôt and Imad El Haddad. Indoor terpene emissions from cooking with herbs and pepper and their secondary organic aerosol production potential. *Scientific Reports,* **2016**, *6*, 36623.

5.1 Introduction

It is estimated that people in developed countries typically spend around 90% of their time indoors,[212] and therefore assessing exposure risks from indoor air pollution is essential for the protection of human health. In the absence of solid fuel burning, cooking is generally recognized as the main source of organic aerosol in indoor environments.[41] Cooking processes can generate large quantities of harmful pollutants (such as PM,[213] PAHs,[214] VOCs[215] and carbonyls[216]), and therefore exposure to cooking fumes can have a negative impact on human health. For example, Ko *et al.* conducted a study on non-smoking Chinese woman and found that cooking activities considerably increased their risk of lung cancer.[217] Other vulnerable groups of people that may be susceptible to the harmful effects of cooking emissions include primary household cooks and professional chefs.[218] Whilst there are numerous studies focusing on the composition of particulate emissions from cooking,[39-40, 219-220] there are only a few studies which have investigated the associated non-methane organic gases (NMOG). For example, Schauer *et al.* reported VOC emissions from meat charbroiling and cooking with seed oils,[221-222] whilst Huang *et al.* investigated VOCs from

residential cooking activities in Hong Kong.[218] Additional studies have focused on measuring stack emissions from restaurants,[223-224] and whilst this is useful for characterizing bulk emissions, it is not a suitable method for comparing emissions from different cooking processes. Experiments designed in this way also make it difficult to distinguish between emissions from the food itself and emissions from the heating source. In many studies, gas phase and particulate species have been identified as markers for the quantification of cooking emissions in ambient air, even though there are large uncertainties related to the relative contribution of these markers. As the composition of the emissions is highly dependent on both the cooking process and the type of food cooked, a systematic characterization of the emissions from different cooking processes is required. In this study, a combination of two-dimensional gas chromatography time-of-flight mass spectrometry (GC×GC-TOF-MS), proton transfer reaction time-of-flight mass spectrometry (PTR-TOF-MS) and high-resolution time-of-flight aerosol mass spectrometry (HR-TOF-AMS) will be used to characterize the chemical composition of both gas and particle phase cooking emissions. A wide variety of cooking techniques, such as boiling, charbroiling, shallow frying and deep frying of different types of food (vegetables and meats) under different cooking conditions will be considered. Furthermore, indoor terpene emissions from cooking with herbs and pepper will be considered, alongside their SOA production potential. Monoterpenes such as limonene are thought to originate primarily from detergent use,[225-226] and are believed to be the main source of indoor SOA.[227] As SOA and aged NMOGs from terpenes may have harmful effects on human health, it is important to identify any other possible terpene sources, such as cooking with condiments. In this study, GC×GC-TOF-MS will be used to characterise the volatile and intermediate volatility compounds released upon heating pepper and herbs. Furthermore, the amount of terpene emissions released during frying meat with different amounts of herbs and pepper will be estimated using PTR-TOF-MS, and the SOA production potential will be predicted using HR-TOF-AMS.

5.2 Experimental

5.2.1 Online studies of cooking emissions

The work described in this section was carried out by research scientists at PSI, Switzerland.

5.2.1.1 Gas phase NMOG emissions

A total of 95 cooking experiments were conducted and included heating vegetable oils, boiling vegetables, charbroiling meat, shallow frying meat and vegetables, and deep frying fish and potato. A list of all experiments and experimental conditions can be found in a study by Klein *et al.* (Tables S1 and S2).[228] The food was cooked in a pan on an electric heating plate and was enclosed within metal housing (60 L capacity). Approximately 2 L min^{-1} of the total flow through the housing (14 L min^{-1}) was diluted with zero air (737-250 series, AADCO Instruments Inc., U.S.) using two sequential temperature controlled ejector dilutors (Dekati Ltd., Kangasala, Finland), giving a final dilution ratio of *ca.* 1:100. Equilibrium was reached quickly within the metal housing, which enabled a fast response time, and the residence times of the gases in the metal housing and sampling inlet were <120 s and <10 s respectively. The gas phase NMOG concentrations were measured by PTR-TOF-MS. Methane, which is not emitted by cooking processes, was measured using cavity ring-down spectroscopy (G2401, Picarro, Inc.) before and after dilution to determine the dilution ratio.

5.2.1.2 Herb and pepper emissions

The pan frying was carried out using the same setup as described in section 5.2.1.1. For each experiment, two pieces of lean beef (~250 g) were seasoned with different amounts of Herbs de Provence (McCormick, Promena AG) and/or grained black pepper (Qualité & Prix, Coop AG). The herbs contained 20% rosemary, 26% savory, 26% oregano, 19% thyme and 3% basil. The pan was heated to 180 °C with 5 g of canola oil and the meat was fried on both sides for 5 min. Gas phase NMOG emissions were sampled using PTR-TOF-MS using the same sequential dilution system as provided in section 5.2.1.1. Additional aging experiments were carried out in which emissions that had been diluted once (dilution ratio ~1:10) were introduced into a 7 m^3 Teflon smog chamber; the smog chamber setup is described in Bruns *et al.*[229] The NMOG, CH_4 and aerosol were measured using PTR-TOF-MS, a CO_2/CO/CH_4/H_2O analyser, and a high resolution time-of-flight aerosol mass spectrometer (HR-TOF-AMS, Aerodyne Research Inc., U.S.A), respectively. Full details of the aging experiments are described in Klein *et al.*[230]

5.2.1.3 Particulate cooking emissions

A total of 11 experiments were carried out to investigate the composition of cooking aerosol and included charbroiling various types of meat, as well as frying beef and heating olive oil; the details of each experiment are shown in Table 5.1. The meat was cooked in a pan on an electric heating plate enclosed within metal housing (60 L capacity). Throughout the duration of each experiment, the particulate emissions were sampled onto 47 mm diameter quartz fibre filters at a flow rate of 20 L min^{-1}. An additional 2 L min^{-1} of air was removed from the container *via* a heated ejector dilutor, and a further 12 L min^{-1} of air was directed to the exhaust to ensure the air within the container was well-mixed. When the blank filters were collected, the pan was heated to 180 °C in the absence of oil or meat. As shown in Table 5.1, an experiment was carried out to investigate emissions from heating olive oil alone. The remaining experiments involved cooking meat and typically lasted between 30 and 60 min, in which time several portions of meat were cooked one after another, and the emissions were sampled continuously. The container was only opened to turn the meat halfway through cooking, or to change the sample. For the frying experiments, the oil was added to the pan approximately 30 s before adding the meat. For the charbroiling experiments, a small amount of olive oil was rubbed onto the surface of the chicken and the beef to stop it sticking to the pan. After sampling, the filters were wrapped in aluminium foil immediately and stored at -18 °C. Small sections of each 47 mm diameter filter (2 – 3 circles of 17 mm diameter) were packed in dry ice and shipped to the University of York, U.K.

5.2.1.4 Instrumentation

A full description of the PTR-TOF-MS instrument used to characterise NMOG emissions is provided in Klein *et al.*[228] The PTR-TOF-MS was operated in H_3O^+ mode in order to measure NMOG with a proton affinity higher than that of water. Although protonation with H_3O^+ is a soft ionization technique, fragmentation of many compounds present in cooking emissions can still occur and therefore fragmentation patterns for the most abundant compounds were determined by headspace measurements of the pure standards.[231] The HR-TOF-AMS was used to measure real time (< 1 min), size-resolved chemical composition and mass loadings of ambient non-refractory aerosol particles.[232] A $PM_{2.5}$ lens designed by Williams *et al.* was used to measure particles with a vacuum aerodynamic diameter up to 2.5 μm.[233]

Table 5.1. Experimental conditions for a range of cooking experiments: charbroiling different types of meat, frying beef in sunflower oil, and heating olive oil.

Experiment	Experiment length / min	Cooking method	Cooking time / min sample^{-1}	Food mass	Oil type	Oil mass / g	Temp. / °C	Air sampled / L	Approximate mass collected / µg
Blank 1	30	Heat pan	-	0	-	-	180	580	0
Beef 1	60	Charbroil	10	4 × ~250 g	(Olive)[a]	-	200	1181	2700
Beef 2	60	Charbroil	10	5 × ~250 g	(Olive)[a]	-	200	1168	3000
Beef burger 1	30	Charbroil	10	3 × ~130 g	-	-	180	579	1200
Beef burger 2	30	Charbroil	10	3 × ~130 g	-	-	180	577	900
Chicken 1	60	Charbroil	10	4 × ~160 g	(Olive)[a]	-	180	1151	300
Chicken 2	60	Charbroil	10	5 × ~160 g	(Olive)[a]	-	180	1171	1200
Beef + oil 1	30	Fry	10	4 × ~220 g	Sunflower	4 × ~25 g	180	587	750
Beef + oil 2	30	Fry	10	4 × ~220 g	Sunflower	4 × ~25 g	180	586	700
Blank 2	30	Heat pan	-	0	-	-	180	580	0
Olive oil 1	105	Heat oil	105	0	Olive	250	180	2064	1000

[a]A small amount of oil was rubbed into the meat using greaseproof paper prior to cooking to avoid the meat sticking to the pan.

5.2.1.5 Emission factors and enhancement factors

Full details of the calculations of both emission factors (EFs) and enhancement factors (EHFs) can be found in Klein *et al.*[228] As shown in Equation 5.1, EFs were calculated by multiplying the average emissions (C, μg m^{-3}) by the cooking time (t, min), the flow from the metal container (F, m^3 min^{-1}) and the dilution ratio (DR), and dividing by the mass of food used (M_{food}, kg).

$$EF = \frac{C \times t \times F \times DR}{M_{food}} \quad (5.1)$$

EHFs were used to determine the additional emissions coming from the cooked food, rather than the oil itself. EHFs were calculated from the ratio of the average emission factor of a compound (X) to the average emission of a compound emitted only from the oil (Y), normalized to the same ratio measured during oil heating experiments (Equation 5.2). Whilst an EHF value of 1 indicates that compound X comes solely from the oil, EHF values above 1 means that some of compound X comes from the cooked food, with increasing EHF values representing a decreasing influence of the oil on the total emissions.

$$EHF_x = \frac{X_{fry}}{Y_{fry}} \times \frac{Y_{oil}}{X_{oil}} \quad (5.2)$$

5.2.2 Offline studies of cooking emissions

The work described in this section was carried out at the University of York, U.K.

5.2.2.1 Emissions from heated cooking oil

Sample preparation: A small plug of glass wool was placed in the bottom of a glass thermal desorption tube (Model 013010, Gerstel) and then the tube was packed with 0.5 g of Tenax. A second glass wool plug was used to hold the Tenax in place, and the tube was heated to 300 °C for 1 hour and sealed until ready for use. A series of experiments were carried out in which 7 mL of cooking oil (either olive, sunflower or canola oil) was placed inside a 49 cm^3 stainless steel reactor with a stirrer; the reactor was encased in a heated unit and the oil was allowed to equilibrate for 3 min at 180 °C. The NMOG emissions were sampled onto the prepared thermal desorption tubes for 1 min using a flow rate of 40 mL min^{-1} of synthetic air and analysed immediately.

Sample analysis: The thermal desorption tubes were analysed using a Gerstel thermal desorption unit (TDU) coupled directly to a Gerstel cooled injection system (CIS). This entire desorption and injection system is attached directly to the inlet of the GC×GC-TOF-MS system. The thermal desorption tube was inserted into the TDU, which was held at 80 °C for 1 min, followed by heating at 60 °C min^{-1} until 220 °C was reached

and held isothermally for a further 5 min. The CIS was held at -80 °C during the desorption process, using liquid nitrogen as the cooling agent. The analytes were transferred to the CIS in splitless mode, with a transfer line temperature of 230 °C. At this stage, the CIS was heated at 10 °C min^{-1} until 280 °C was reached and held isothermally for 30 s. The analytes were transferred to the primary GC column using a split ratio of 20:1 (details of the subsequent GC×GC-TOF-MS analysis are provided in section 5.2.2.4).

5.2.2.2 Emissions from heated herbs and pepper

Sample preparation: The thermal desorption tubes and glass wool were heated to 300 °C for 1 hour, and the tubes were sealed until ready for use. Either 10 mg of Herbs de Provence (McCormick, Promena AG) or 5 mg of grained black pepper (Qualité & Prix, Coop AG) were packed into each thermal desorption tube between 2 pieces of glass wool.

Sample analysis: The thermal desorption tubes were analysed using the same TDU and CIS method as described in 5.2.2.1. However, the herbs and pepper were heated to a lower final temperature in the TDU (180 °C).

5.2.2.3 Cooking aerosol filter samples

Sample preparation: A series of 17 mm diameter filter samples were received in dry ice from PSI, Switzerland (section 5.2.1.3) and were stored at -18 °C prior to analysis. In order to obtain sufficient mass for analysis by GC×GC-TOF-MS, individual filters from each type of experiment were combined together, as shown in Table 5.2. The filters were extracted using an accelerated solvent extraction system (ASE 350, Dionex). The base of each 5 mL stainless steel extraction cell was lined with two clean glass microfibre filter papers (Fisher Scientific, Loughborough, U.K.) and then packed with a batch of filters (Table 5.2). Extractions were carried out in ethyl acetate (GC grade, 99.9% purity) at 80 °C and 1500 psi for three consecutive 5 min cycles. A 50% flush volume and 60 s purge time were used. Extracts obtained were stood in an ice bath whilst evaporated under nitrogen to a final volume of 1 mL, and stored at -18 °C prior to analysis by GC×GC-TOF-MS.

Sample analysis: A liquid injection to the GC×GC-TOF-MS (1 µL) was carried out in splitless mode at an injection temperature of 200 °C using an automated liquid injector (Gerstel, Mülheim an der Ruhr, Germany).

Table 5.2. Cooking aerosol filters grouped according to sample type and cooking technique, in order to achieve sufficient aerosol mass for analysis by GC×GC-TOF-MS.

Sample type	Cooking technique	Filters analysed
Blank	Heat pan only	1 × 21 mm, 2 × 17 mm
Beef	Charbroil	5 × 17 mm
Beef burger	Charbroil	3 × 17 mm
Chicken	Charbroil	5 × 17 mm
Beef + oil	Fry	3 × 17 mm
Olive oil	Heat oil in pan	1 × 17 mm

5.2.2.4 GC×GC-TOF-MS

The GC×GC-TOF-MS system consisted of an Agilent 6890 gas chromatograph (Agilent Technologies, CA, USA) and a Pegasus III TOF-MS (LECO, MI, USA). The first column was a non-polar BPX5 (30 m × 0.32 mm i.d. × 0.25 μm film thickness) and the second column was a mid-polarity BPX50 (4 m × 0.10 mm i.d. × 0.10 μm film thickness), both from SGE Analytical Science (Milton Keynes, U.K.). The initial temperature of the first dimension column was 60 °C for 2 min, followed by heating at 10 °C min^{-1} until 260 °C was reached and held isothermally for a further 3 min. A temperature offset of 20 °C was applied to the second dimension column throughout the GC temperature program. A liquid nitrogen two-stage cold jet modulation system was used, with a modulation period of 5 s and a +15 °C offset from the primary GC oven temperature. Helium was used as a carrier gas with a flow rate of 1 mL min^{-1}, the transfer line temperature was 280 °C and the ion source temperature was 250 °C. The analysis was performed using electron ionisation at 70 eV. The spectra were collected at 200 Hz between *m/z* 45-500, and analysed using LECO ChromaTOF software.

5.3 Results and discussion

5.3.1 Gas phase compounds from heated cooking oils

A series of experiments were carried out at PSI to investigate the composition of gas phase NMOGs released from different cooking oils using PTR-TOF-MS. A summary of the experimental setup is provided in section 5.2.1.1 and the experimental conditions are provided in Table S2 of the study by Klein et *al.*[228] Alongside these experiments, the characterisation of gaseous NMOG emissions from heated cooking oils using GC×GC-TOF-MS was carried out at the University of York, as shown in section 5.2.2.1. Figure 5.1 shows the relative contributions of different compounds to the total NMOG emissions from canola, sunflower and olive oil; the oils were heated to high temperatures (180 – 200 °C) and the measurements were made using PTR-TOF-MS. Figure 5.2 shows the corresponding GC×GC-TOF-MS measurements for each oil; each green spot on the 2D chromatogram represents a different compound present in the NMOG emissions, and the main compounds of interest have been labelled. A full list of the compounds identified by GC×GC-TOF-MS when canola, sunflower and olive oil were heated to 180 °C in the stainless steel reactor can be found in Tables A11 – A13, Appendix A.

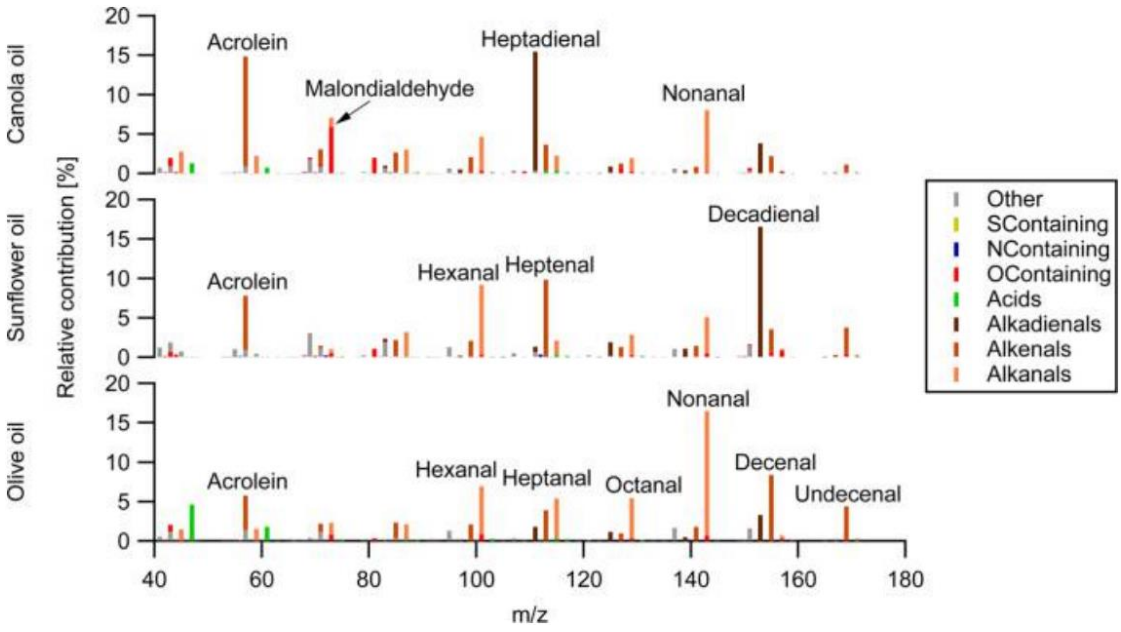

Figure 5.1. Relative contributions of different compounds to the total NMOG emissions from canola, sunflower and olive oil at high temperatures (180 – 200 °C), measured using PTR-TOF-MS.[223]

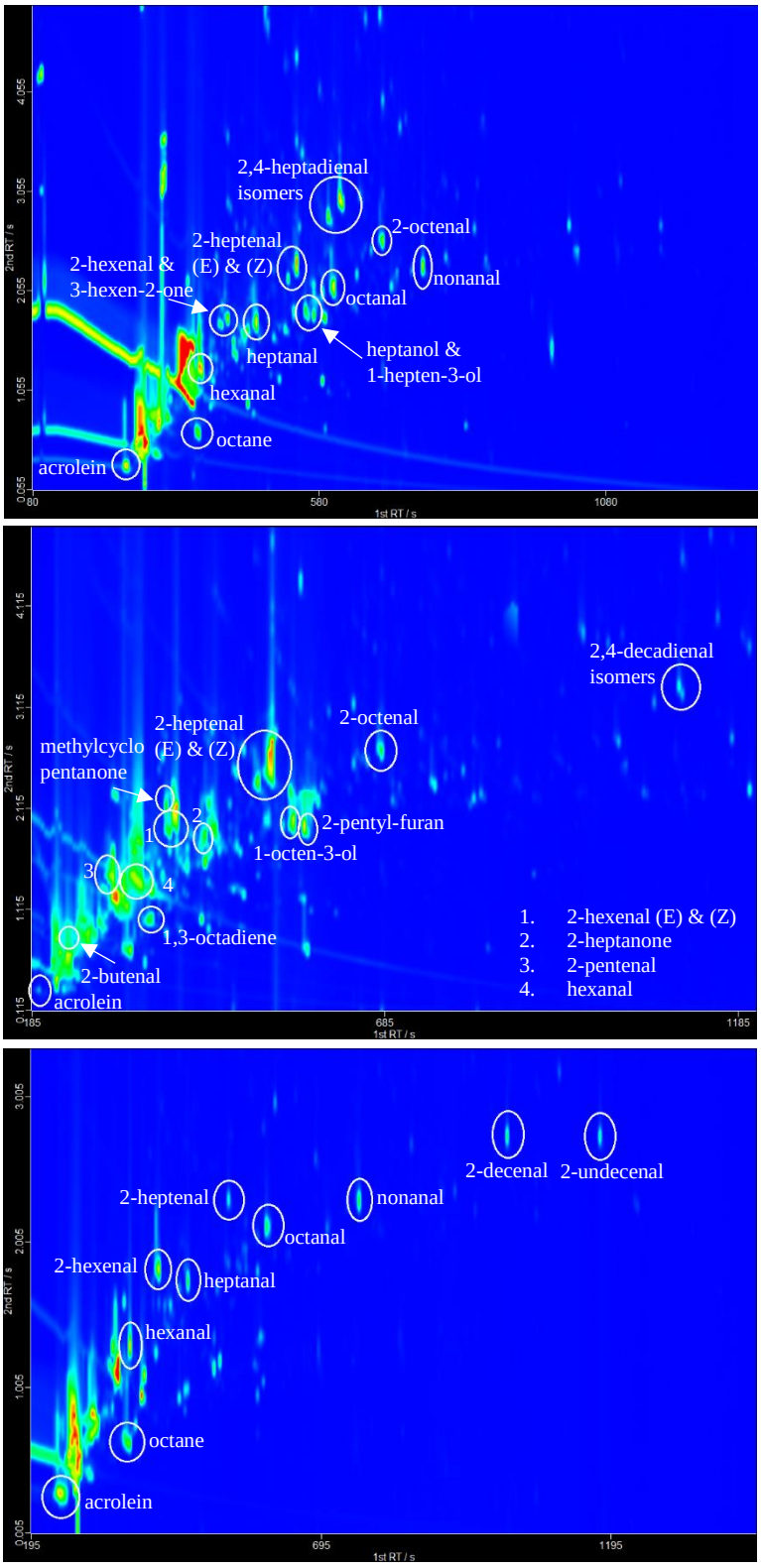

Figure 5.2. GC×GC-TOF-MS measurements of the compounds emitted from cooking oil heated to 180 °C. 2D chromatograms for canola oil (upper panel), sunflower oil (middle panel) and olive oil (lower panel) are shown.

The compounds measured by PTR-TOF-MS were classified into eight families: alkanals, alkenals, alkadienals, carboxylic acids, O-containing, N-containing, S-containing and unknown. Analysis of the PTR-TOF-MS data using the Tofware post processing software and comparison with the literature allowed for many ions to be attributed to their families, and also revealed that saturated and unsaturated carbonyls dominated the NMOG emissions. However, it was not possible to distinguish between aldehydes and ketones using the PTR-TOF-MS data alone, and therefore the GC×GC-TOF-MS measurements were used to identify the carbonyl compounds. The analysis revealed that the NMOG emissions were dominated by aldehydes, which is consistent with previous work carried out by Fullana *et al.* and Katragadda *et al.*[234-235] The measurements obtained by PTR-TOF-MS and GC×GC-TOF-MS exhibited several similarities. For example, all of the samples contained acrolein, which is formed through the dehydration of glycerol as shown in Scheme 5.1.[236] Glycerol links fatty acids together to form triglycerides, which are the main constituents of cooking oil.

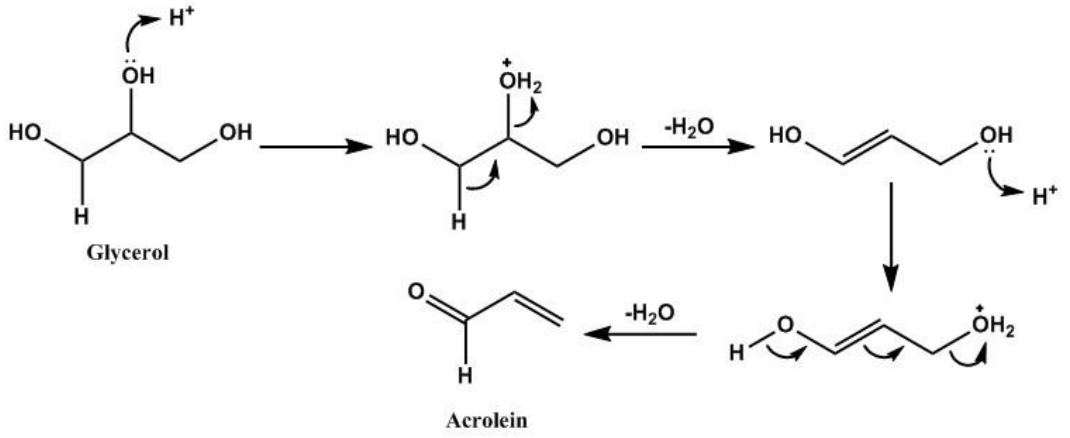

Scheme 5.1. Mechanism for the dehydration of glycerol to form acrolein.

The PTR-TOF-MS data in Figure 5.1 shows that the most abundant species present in the canola oil emissions were acrolein (C_3H_4O, *m/z* 57.069), malondialdehyde ($C_3H_4O_2$, *m/z* 73.064), 2,4-heptadienal ($C_7H_{10}O$, *m/z* 111.117) and nonanal ($C_9H_{18}O$, *m/z* 143.143). The highest signals for sunflower oil were at *m/z* 57.069, 101.096, 113.096 and 153.127, which corresponds to acrolein, hexanal ($C_6H_{12}O$), 2-heptenal ($C_7H_{12}O$) and 2,4-decadienal ($C_{10}H_{16}O$), respectively. For olive oil, the dominant species identified by PTR-TOF-MS were acrolein, hexanal, heptanal ($C_7H_{14}O$, *m/z* 115.112), octanal ($C_8H_{16}O$, *m/z* 129.127), nonanal, 2-decenal ($C_{10}H_{18}O$, *m/z* 155.143) and 2-undecenal ($C_{11}H_{20}O$, *m/z* 169.159). With the exception of malondialdehyde, all of these compounds were identified in the GC×GC chromatograms; compound identification was achieved using a combination of retention indices and reference to the NIST mass spectral library. Although malondialdehyde is likely

to be present in the canola oil emissions sample, it was not possible to accurately identify this compound without the use of an analytical standard because the compound is not listed in the NIST mass spectral library. Aside from the most abundant compounds identified, there were various other species emitted from heated cooking oil. The key compounds are labelled on the GC×GC chromatograms shown in Figure 5.2, and a full list of compounds identified by GC×GC-TOF-MS can be found in Appendix A (Tables A11 – A13). A large proportion of the emissions were comprised of aldehydes; apart from acrolein, aldehydes present in cooking emissions are formed *via* peroxy radical reactions of the fatty acids.[237] This means that the position of the double bonds in the triglycerides and the location of fracture determines which hydroperoxides are produced. In turn, this determines which alkanals, alkenals and alkadienals are formed as a result of decomposition. In this study, the different emission patterns of the oils are consistent with the varying composition of the triglycerides present in the oils. In order to explain this observation further, it is important to consider the relative proportions of three major C_{18} unsaturated fatty acids found in canola, sunflower and olive oil (Table 5.3). Table 5.3 shows that olive oil contains the highest proportion of oleic acid (~78%), followed by canola oil (~60%) and sunflower oil (~18%).[238-239]

Table 5.3. Typical amounts of C_{18} unsaturated fatty acids (oleic, linoleic and linolenic acid) found in canola, sunflower and olive oil.[238-239]

Cooking oil	% Oleic acid ($C_{18}H_{34}O_2$)	% Linoleic acid ($C_{18}H_{32}O_2$)	% Linolenic acid ($C_{18}H_{30}O_2$)
Canola oil	60	20	10
Sunflower oil	18	69	0
Olive oil	78	7	1

During the oxidation of oleic acid, hydrogen abstraction from the allyl group produces allylic radicals in which the electrons are delocalised across a three-carbon system.[240] Reaction with oxygen at the end positions of these delocalized systems produces well-defined mixtures of isomeric hydroperoxides. As shown in Scheme 5.2, the oxidation of oleic acid can lead to the formation of a hydroperoxide at the C_8 (~26 - 28%), C_9 (~22 - 25%), C_{10} (~22 - 24%) or C_{11} (~26 - 28%) position.[241] At this stage, homolytic cleavage between the oxygen-oxygen bond occurs and alkoxy and hydroxyl radicals are produced. The alkoxy radical undergoes β-scission of the carbon-carbon bond and produces a series of secondary oxidation products.[241] Scheme 5.3 shows the decomposition of the hydroperoxide formed at the C_8 position of oleic acid as an example, and the secondary products predicted to form are decanal, decene, 8-oxooctanoic acid, 2-undecenal and heptanoic acid.

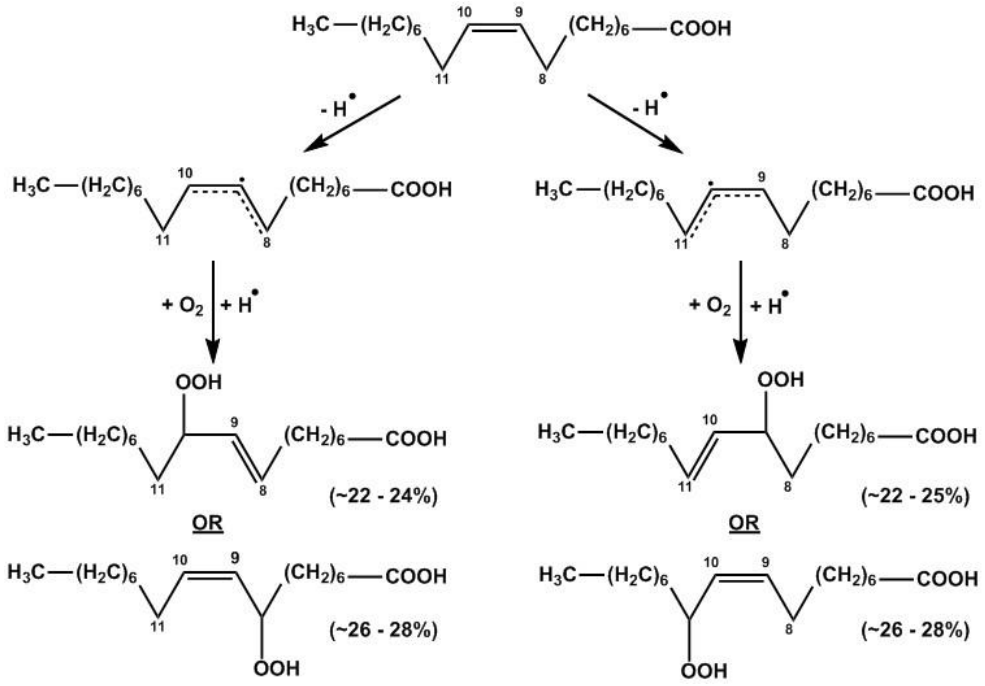

Scheme 5.2. Autoxidation of oleic acid to form various hydroperoxides (C_8, C_9, C_{10}, C_{11}).[240-241]

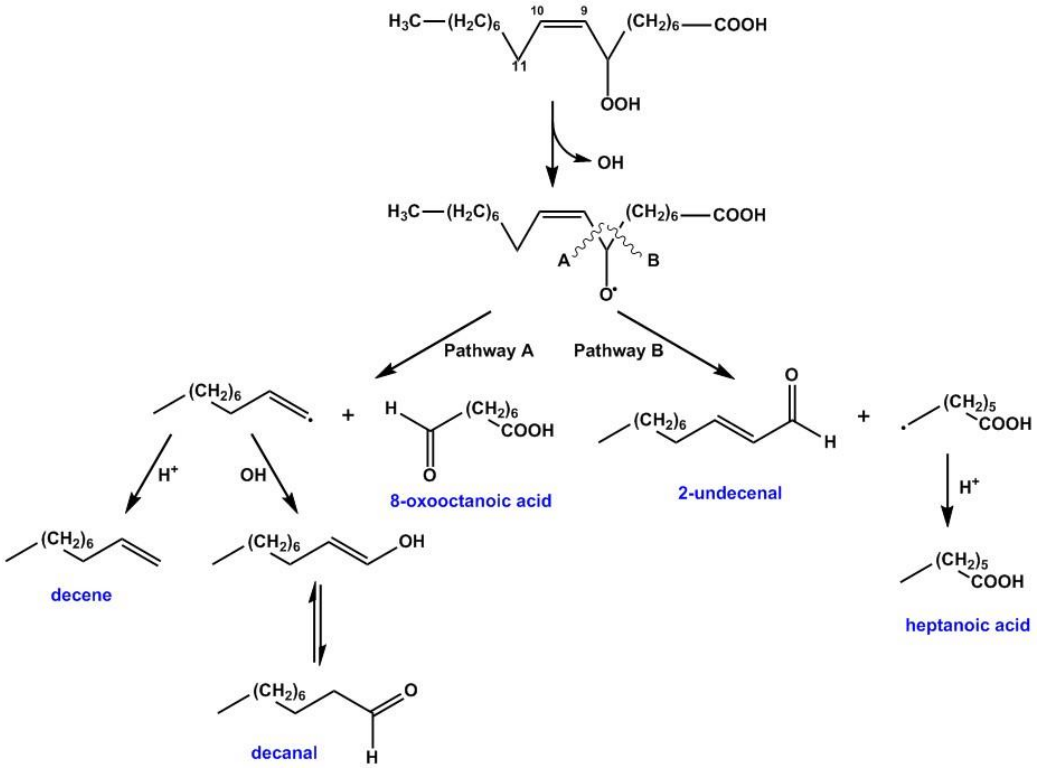

Scheme 5.3. Decomposition of C_8 hydroperoxide (from oleic acid) to form secondary oxidation products (decene, decanal, 8-oxooctanoic acid, 2-undecenal, heptanoic acid).

By applying a similar mechanism to that shown in Scheme 5.3 to each of the four hydroperoxides formed as a result of the autoxidation of oleic acid, it is possible to predict the formation of a range of secondary oxidation products, as shown in Table 5.4. The chemical formula of each compound is included, and the compounds are grouped according to the position at which the hydroperoxide attached itself to the oleic acid molecule in the first oxidation step (Scheme 5.2).

Table 5.4. Secondary oxidation products formed as a result of oleic acid degradation, grouped according to the position at which the hydroperoxide formed on the oleic acid molecule. The chemical formula and 1st and 2nd GC×GC retention time of each compound detected in the olive oil sample is provided.

Compound	Parent hydroperoxide	1st RT / s	2nd RT / s	Chemical formula
Decene	C_8	580	1.17	$C_{10}H_{20}$
Heptanoic acid		710	2.15	$C_7H_{14}O_2$
Decanal		925	2.36	$C_{10}H_{20}O$
2-undecenal		1175	2.74	$C_{11}H_{20}O$
8-oxooctanoic acid		n.d.	n.d.	$C_8H_{14}O_3$
Nonene	C_9	450	0.94	C_9H_{18}
Nonanal		760	2.30	$C_9H_{18}O$
Octanoic acid		865	2.32	$C_8H_{14}O_2$
2-decenal		1015	2.74	$C_{10}H_{18}O$
9-oxononanoic acid		n.d.	n.d.	$C_9H_{16}O_3$
Octane	C_{10}	365	0.63	C_8H_{18}
Nonanal		760	2.30	$C_9H_{18}O$
8-nonenoic acid		n.d.	n.d.	$C_9H_{16}O_2$
9-oxononanoic acid		n.d.	n.d.	$C_9H_{16}O_3$
10-oxo-8-decenoic acid		n.d.	n.d.	$C_{10}H_{16}O_3$
Heptane	C_{11}	295	0.41	C_7H_{16}
Octanal		600	2.12	$C_8H_{16}O$
9-decenoic acid		n.d.	n.d.	$C_{10}H_{18}O_2$
10-oxo-8-decenoic acid		n.d.	n.d.	$C_{10}H_{16}O_3$
11-oxo-9-undecenoic acid		n.d.	n.d.	$C_{11}H_{18}O_3$

The GC×GC-TOF-MS data was analysed in order to determine whether the predicted secondary oxidation products from oleic acid degradation were present in the cooking oil emissions. As shown in Table 5.4, 11 out of the total 17 compounds were successfully identified in the olive oil emissions. It was not possible to identify the $C_8 – C_{10}$ alkenoic and oxo acids; the poor chromatographic response of these species is most likely due to their low volatility and the interaction between active sites on the GC column with active hydrogens on the acid functional groups. It is highly likely that these compounds are still present in the olive oil emissions. All of the 11 compounds identified in the olive oil emissions were also found in the canola and sunflower oil emissions, but they were not the most dominant species. These results agree with the fact that canola and sunflower oil contain lower proportions of oleic acid (~ 60% and ~ 18% respectively) compared to olive oil (~ 78%). According to the PTR-TOF-MS data, two of the most abundant compounds in canola oil emissions were heptadienal and malondialdehyde, but these two species were not present in significant amounts in the olive or sunflower oil emissions. These results can be explained by the fact that heptadienal and malondialdehyde are specific secondary oxidation products of linolenic acid,[242] which makes up approximately 10% of canola oil, but only 0 – 1% of olive and sunflower oil. Three of the most dominant compounds identified in sunflower oil emissions were specific markers of linoleic acid (hexanal, heptenal and decadienal).[242] These compounds were present in lower quantities in the canola and olive oil emissions, which agrees with the fact that sunflower oil contains the highest proportion of linoleic acid (~69% compared to ~20% and ~7% for canola and olive oil respectively). In conclusion, the analysis of cooking oil emissions by a combination of PTR-TOF-MS and GC×GC-TOF-MS has allowed for the accurate identification and quantification of various compounds formed in the gas phase when cooking oil is heated. It is clear that the emissions are dominated by aldehydes, and that the different emission patterns of the oils are consistent with the varying composition of the triglycerides present in the oils.

5.3.2 Gas phase emissions from cooking vegetables and meats

As the GC×GC-TOF-MS measurements allowed for aldehydes and ketones measured by PTR-TOF-MS to be distinguished from each other, it was possible to use this information to characterise the NMOG emissions for all of the 95 cooking experiments carried out at PSI. The experiments involved cooking various types of food using different techniques - the results were published in the study by Klein *et al.*[228] and a summary of this work will be discussed herein.

5.3.2.1 Emissions from frying food

When food was shallow fried in a pan, aldehydes made up more than 60% of the total NMOG emissions, and the contribution of smaller ($\leq C_5$) aldehydes to the total emissions increased when frying food in oil, rather than just heating the oil alone. Furthermore, the proportion of smaller aldehydes decreased with increasing oil temperature. Overall, the total NMOG emission factors for shallow frying of meat in sunflower oil ranged from 3 mg kg^{-1} for chicken to 42 mg kg^{-1} for beef. For deep frying, the total NMOG emissions factors were 59 mg kg^{-1} for potato and 39 mg kg^{-1} for fish. These amounts were similar to those expected from heating pure oil, and the composition of the emissions was similar too. The only differences observed were increased alcohol emissions for potato frying, and increased O-containing compounds for fish frying. Carbonyl emission factors from the oils depended on both cooking temperature and the surface area of the oil. Using enhancement factors, it was possible to separate oil emissions from those originating from the food itself. Interestingly for shallow frying, the enhancement factors for larger ($\geq C_5$) aldehydes were around 1, whereas smaller aldehydes showed significant enhancement factors ranging from 5 to *ca.* 1000. It is likely that the small aldehydes originated from the decomposition of fatty acids in the meat.[243]

5.3.2.2 Emissions from charbroiling food

The total emission factors for charbroiling were lower than for frying because less oil was used to cook the food (which is where the majority of the emissions came from). Total emission factors for charbroiling beef and chicken were 11 mg kg^{-1} and 4 mg kg^{-1} respectively. The charbroiling of beef burgers released total NMOG emissions of 58 mg kg^{-1}, which was thought to be due to the high fat content of the burgers. Emissions from beef charbroiling (without oil) were dominated by small aldehydes, which confirmed that these compounds originated from the meat rather than the heated oils.

5.3.2.3 Markers for cooking emissions

It was found that hexanal and nonanal were present in all emissions from frying and charbroiling. As these compounds have relatively long atmospheric lifetimes, they may be potentially suitable markers for identifying gas and particle phase cooking emissions in ambient air and future studies should investigate this possibility.

5.3.3 Implications for indoor air quality

Using calculated emissions factors, Klein *et al.* estimated the potential concentrations of individual aldehydes in a 40 m^3 kitchen without ventilation after cooking 1 kg of food for 10 min and compared them to exposure limits reported in the literature.[228] At high

concentrations, aldehydes can irritate the eyes and respiratory tract.[244] For example, the US EPA's level 1 acute exposure level guideline (AEGL-1) for acrolein is 0.07 mg m^{-3}; this limit is the level at which notable discomfort or irritation occurs, yet the effects are reversible upon cessation of exposure.[245] Klein *et al.* found that this limit for acrolein can be readily exceeded by most of the frying processes. It was also found that deep frying in sunflower oil would lead to a concentration of 0.25 mg m^{-3} of 2,4-decadienal, which could potentially increase the risk of lung cancer.[246] It is clear that further systematic studies of the health effects of cooking emissions are required, and through the installation of proper ventilation systems it is highly likely that the adverse health effects can be significantly reduced.

5.3.4 Gas phase compounds from herbs and pepper

The chemical composition of the gas phase emissions from herbs and pepper heated to 180 °C were characterised using GC×GC-TOF-MS. Figure 5.3 shows the GC×GC chromatograms obtained for both the herb emissions and the pepper emissions, and a full list of the compounds identified can be found in Table 5.5 and Table 5.6 respectively. Whilst monoterpenes, sesquiterpenes and oxygenated VOCs were detected in emissions from both herbs and pepper, diterpenes were only detected in the herb emissions. Monoterpenes are compounds found in the essential oils extracted from many plants, including fruits, vegetables, spices and herbs.[247] They consist of two isoprene units and their chemical formula is $C_{10}H_{16}$. As shown in Table 5.5, it was possible to identify *p*-cymene ($C_{10}H_{14}$) and 10 monoterpenes in the herb emissions using GC×GC-TOF-MS. The compounds were identified by reference to the NIST library and consideration of retention indices; the 1st and 2nd retention times of each compound, as well as its similarity to the reference spectra is shown in Table 5.5. The herb mixture contained rosemary, savory, oregano, thyme and basil. All of the monoterpenes identified in this study have been previously detected in the essential oils of at least one of these herbs.[248-252] For example, Bolechowski *et al.* studied the composition of oregano essential oil, and amongst the 10 monoterpenes identified were α-pinene, sabinene, myrcene, α-phellandrene, α-terpinene and d-limonene.[250] Although the monoterpene concentrations were not quantified using analytical standards, comparison of the relative peak intensities revealed that camphene, d-limonene and γ-terpinene were the most abundant monoterpenes in this study. The data also suggested that high levels of *p*-cymene were present in the herb emissions, but co-elution with another compound means that it is difficult to confirm this observation. A total of 12 sesquiterpenes (three isoprene units, $C_{15}H_{24}$) were identified and the 3 most abundant compounds were β-caryophyllene, α-bisabolene and cadinene. Some of these compounds have been previously found in herbs; for example, Salido *et al.* report the presence of β-caryophyllene, humulene, muurolene and cadinene in rosemary oil.[248] Furthermore, it has been reported that thyme contains

β-caryophyllene, humulene and α-bisabolene,[251] oregano contains β-caryophyllene and farnesene,[250] basil contains *trans*-bergamotene and muurolene,[252] and savory contains α-bisabolene.[249]

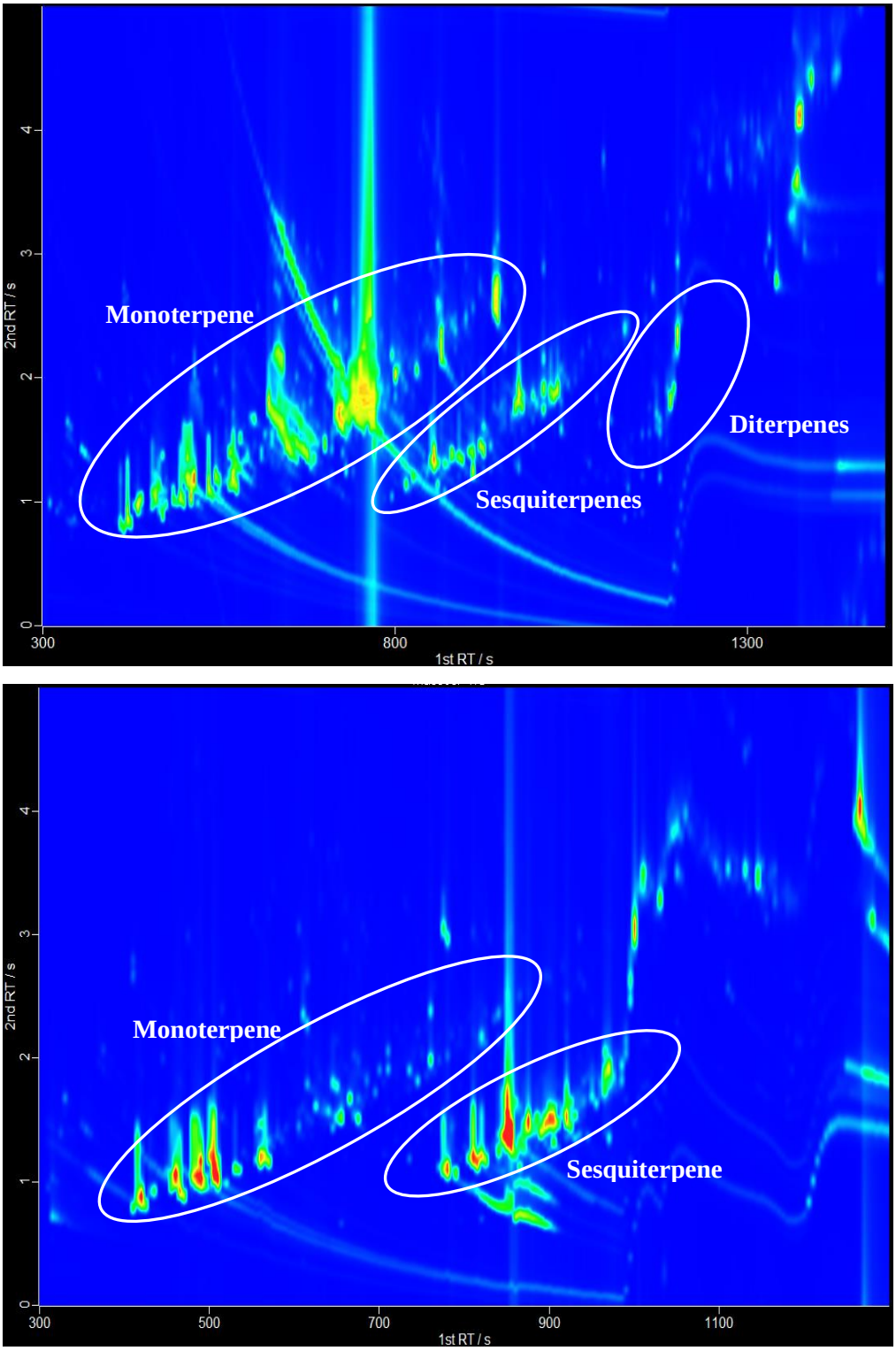

Figure 5.3. GC×GC chromatograms to show the compounds emitted from herbs (upper panel) and black pepper (lower panel) heated to 180 °C.

Table 5.5. Compounds identified by GC×GC-TOF-MS upon heating herbs to 180 °C. 1st RT and 2nd RT represent first and second retention time, and similarity is the extent to which the spectra matches the reference spectra (out of 1000). *Peak coelution prevented similarity match in MS. MT = monoterpene, SQT = sesquiterpene, and DIT = diterpene, OVOC = oxygenated volatile organic compound, and HC = hydrocarbon.

Compound	1st RT / s	2nd RT / s	Similarity	Formula	Type
α-pinene	420	0.82	936	$C_{10}H_{16}$	MT
camphene	435	0.95	887	$C_{10}H_{16}$	MT
sabinene	460	1.01	896	$C_{10}H_{16}$	MT
myrcene	470	0.89	902	$C_{10}H_{16}$	MT
α-phellandrene	485	1.01	937	$C_{10}H_{16}$	MT
α-terpinene	495	1.02	894	$C_{10}H_{16}$	MT
p-cymene*	495	1.25	na	$C_{10}H_{14}$	HC
d-limonene	505	1.07	908	$C_{10}H_{16}$	MT
eucalyptol	515	1.14	958	$C_{10}H_{18}O$	OVOC
ocimene	520	0.99	904	$C_{10}H_{16}$	MT
benzyl alcohol	520	1.96	931	C_7H_8O	OVOC
γ-terpinene	535	1.10	842	$C_{10}H_{16}$	MT
terpinolene	560	1.17	903	$C_{10}H_{16}$	MT
linalool	570	1.16	865	$C_{10}H_{18}O$	OVOC
camphor	620	1.77	916	$C_{10}H_{16}O$	OVOC
isoborneol	640	1.53	904	$C_{10}H_{18}O$	OVOC
terpinen-4-ol	645	1.44	886	$C_{10}H_{18}O$	OVOC
octanoic acid	650	1.10	848	$C_8H_{16}O_2$	Acid
α-terpineol	655	1.52	933	$C_{10}H_{18}O$	OVOC
estragole	660	1.72	841	$C_{10}H_{12}O$	OVOC
methyl salicylate	660	1.98	869	$C_8H_8O_3$	OVOC
α-santolina alcohol	670	1.44	779	$C_{10}H_{18}O$	OVOC
verbenone	685	1.97	944	$C_{10}H_{14}O$	OVOC
2-furan carboxyaldehyde	715	2.59	919	$C_5H_4O_2$	OVOC
carvacrol	725	1.80	891	$C_{10}H_{14}O$	OVOC
thymoquinone	725	1.79	868	$C_{10}H_{12}O_2$	OVOC
dihydroxyacetophenone	735	2.34	850	$C_8H_8O_3$	OVOC
nonanoic acid	740	1.27	868	$C_9H_{18}O_2$	Acid
2-methoxyvinylphenol	765	2.15	947	$C_9H_{10}O_2$	OVOC
α-cubenene	790	1.06	861	$C_{15}H_{24}$	SQT
decanoic acid	795	1.22	849	$C_{10}H_{20}O_3$	Acid
eugenol	800	2.03	896	$C_{10}H_{12}O_2$	OVOC

Table 5.5 continued. Compounds identified by GC×GC-TOF-MS upon heating herbs to 180 °C. 1st RT and 2nd RT represent first and second retention time, and similarity is the extent to which the spectra matches the reference spectra (out of 1000). MT = monoterpene, SQT = sesquiterpene, and DIT = diterpene, OVOC = oxygenated volatile organic compound, and HC = hydrocarbon.

Compound	1st RT / s	2nd RT / s	Similarity	Formula	Type
4-hydroxybenzaldehyde	800	2.85	956	$C_7H_6O_2$	OVOC
o-thymol	805	1.73	894	$C_{10}HO$	OVOC
α-copaene	815	1.15	888	$C_{15}H_{24}$	SQT
α-bourbonene	825	1.20	877	$C_{15}H_{24}$	SQT
methyl eugenol	830	2.07	914	$C_{11}H_{14}O_2$	OVOC
niacinamide	835	3.83	953	$C_6H_6N_2O$	Amide
β-caryophyllene	850	1.34	900	$C_{15}H_{24}$	SQT
trans-bergamotene	855	1.14	916	$C_{15}H_{24}$	SQT
farnesene	855	1.32	783	$C_{15}H_{24}$	SQT
humulene	875	1.41	907	$C_{15}H_{24}$	SQT
α-amorphene	890	1.36	887	$C_{15}H_{24}$	SQT
α-longipene	890	1.20	810	$C_{15}H_{24}$	SQT
muurolene	905	1.40	878	$C_{15}H_{24}$	SQT
α-bisabolene	910	1.22	895	$C_{15}H_{24}$	SQT
cadinene	925	1.41	880	$C_{15}H_{24}$	SQT
caryophyllene alcohol	965	1.70	821	$C_{15}H_{26}O$	OVOC
caryophyllene oxide	975	1.80	879	$C_{15}H_{24}O$	OVOC
cadinol	1010	1.71	834	$C_{15}H_{26}O$	OVOC
methyl-jasmonate	1010	2.16	922	$C_{13}H_{20}O_3$	OVOC
α-bisabolol	1035	1.58	875	$C_{15}H_{26}O$	OVOC
tetradecanoic acid	1075	1.31	882	$C_{14}H_{28}O_2$	Acid
pentadecanoic acid	1135	1.32	848	$C_{15}H_{30}O_2$	Acid
rimuene	1190	1.88	711	$C_{20}H_{32}$	DIT
hexadecanoic acid	1200	2.36	853	$C_{16}H_{32}O_2$	Acid
cembrene	1270	3.87	777	$C_{20}H_{32}$	DIT
phytol	1350	2.42	900	$C_{20}H_{40}O$	OVOC
linolenic acid	1365	3.57	894	$C_{18}H_{30}O_2$	Acid
octadecanoic acid	1380	3.05	850	$C_{18}H_{36}O_2$	Acid

Table 5.6. Compounds identified by GC×GC-TOF-MS upon heating pepper to 180 °C. 1st RT and 2nd RT represent first and second retention time, and similarity is the extent to which the spectra matches the reference spectra (out of 1000). MT = monoterpene, SQT = sesquiterpene, and DIT = diterpene, OVOC = oxygenated volatile organic compound, and HC = hydrocarbon.

Compound	1st RT / s	2nd RT / s	Similarity	Formula	Type
α-thujene	410	0.80	867	$C_{10}H_{16}$	MT
α-pinene	425	0.82	948	$C_{10}H_{16}$	MT
camphene	435	0.94	951	$C_{10}H_{16}$	MT
sabinene	455	0.96	912	$C_{10}H_{16}$	MT
carene	480	0.98	910	$C_{10}H_{16}$	MT
α-phellandrene	485	0.99	793	$C_{10}H_{16}$	MT
d-limonene	505	1.12	862	$C_{10}H_{16}$	MT
cis- α-ocimene	520	1.00	922	$C_{10}H_{16}$	MT
γ-terpinene	530	1.15	886	$C_{10}H_{16}$	MT
dimethylstyrene	560	1.48	945	$C_{10}H_{12}$	HC
linalool	565	1.21	890	$C_{10}H_{18}O$	OVOC
1,3,8-*p*-methatriene	580	1.38	919	$C_{10}H_{14}$	HC
camphor	615	1.80	942	$C_{10}H_{16}O$	OVOC
octanoic acid	625	1.25	617	$C_8H_{16}O_2$	Acid
geranaldehyde	635	1.58	746	$C_{10}H_{18}O$	OVOC
terpinen-4-ol	645	1.44	879	$C_{10}H_{18}O$	OVOC
3-pinanone	645	1.77	822	$C_{10}H_{16}O$	OVOC
p-cymen-8-ol	650	1.78	897	$C_{10}H_{14}O$	OVOC
4(10)-thujen-3-ol acetate	665	1.68	878	$C_{10}H_{18}O_2$	OVOC
cis-geraniol	675	1.52	791	$C_{10}H_{18}O$	OVOC
E-3(10)-caren-4-ol	675	1.68	838	$C_{10}H_{16}O$	OVOC
p-cuminic aldehyde	700	1.92	829	$C_{10}H_{12}O$	OVOC
p-menth-1-en-3-one	710	1.92	919	$C_{10}H_{16}O$	OVOC
eucarvone	710	2.06	852	$C_{10}H_{14}O$	OVOC
nonanoic acid	710	1.23	827	$C_9H_{18}O_2$	Acid
isoestragole	735	1.91	804	$C_{10}H_{12}O$	OVOC
2-undecanone	735	1.19	893	$C_{11}H_{22}O$	OVOC
thymol	745	1.82	859	$C_{10}H_{14}O$	OVOC
cis-verbenone	760	2.39	883	$C_{10}H_{14}O$	OVOC
piperonal	775	3.06	956	$C_8H_6O_3$	OVOC
elemene	780	1.05	755	$C_{15}H_{24}$	SQT
α-cubenene	790	1.05	868	$C_{15}H_{24}$	SQT

Table 5.6 continued. Compounds identified by GC×GC-TOF-MS upon heating pepper to 180 °C. 1st RT and 2nd RT represent first and second retention time, and similarity is the extent to which the spectra matches the reference spectra (out of 1000). MT = monoterpene, SQT = sesquiterpene, and DIT = diterpene, OVOC = oxygenated volatile organic compound, and HC = hydrocarbon.

Compound	1st RT / s	2nd RT / s	Similarity	Formula	Type
decanoic acid	790	1.25	843	$C_{10}H_{20}O_2$	Acid
copaene	805	1.20	890	$C_{15}H_{24}$	SQT
2,3-epoxycarane	820	2.19	772	$C_{10}H_{16}O$	OVOC
α-gurjunene	840	1.25	873	$C_{15}H_{24}$	SQT
β-caryophyllene	855	1.36	908	$C_{15}H_{24}$	SQT
α-farsenene	865	1.13	928	$C_{15}H_{24}$	SQT
humulene	875	1.50	720	$C_{15}H_{24}$	SQT
α-bisabolene	905	1.32	902	$C_{15}H_{24}$	SQT
cadinene	920	1.52	878	$C_{15}H_{24}$	SQT
undecanoic acid	935	1.39	871	$C_{11}H_{22}O_2$	Acid
caryophyllene oxide	965	1.86	781	$C_{15}H_{24}O$	OVOC
cubenol	985	1.83	798	$C_{15}H_{26}O$	OVOC
lanceol	995	2.61	801	$C_{15}H_{24}O$	OVOC
farsenene epoxide	1000	3.05	760	$C_{15}H_{24}O$	OVOC
trans-2- α-bisabolene epoxide	1045	3.82	833	$C_{15}H_{24}O$	OVOC
hexadecanoic acid	1280	3.12	846	$C_{16}H_{32}O_2$	Acid

In addition, 26 OVOCs were also identified in the herb emissions, and the majority were either oxygenated monoterpenes or oxygenated sesquiterpenes. Similar to the monoterpenes and sesquiterpenes, many of these oxygenated compounds have also been previously identified; estragole, linanool and terpin-4-ol are volatiles from basil,[252] whilst eucalyptol, camphor, verbenone and linalool can be found in rosemary.[253] Thymol is a volatile compound released from thyme and oregano, and carvacrol comes from oregano and savory.[249-251] In terms of oxygenated sesquiterpenes, caryophyllene oxide has been found in rosemary, thyme and oregano, and cadinol comes from basil.[250-253] Diterpenes were also present in the herb emissions, as indicated in the GC×GC chromatogram (Figure 5.3, upper panel) and two diterpenes, rimuene and cembrene, were successfully identified. The black pepper emissions did not contain any diterpenes (Figure 5.3, lower panel).

A total of 9 monoterpenes were found in the pepper emissions, all of which have been previously identified as black pepper volatiles.[254-256] The most abundant compounds were

α-pinene, camphene, α-phellandrene and cis-α-ocimene. A total of 23 OVOCs were identified; these included well-reported species such as linalool, terpinen-4-ol and piperonal,[255] as well as more unusual compounds such as *p*-menth-1-en-3-one and *p*-cymen-9-ol. Piperonal comes from the degradation of piperine ($C_{17}H_{19}O_3N$), which is one of the major constituents of black pepper.[257] Eleven sesquiterpenes were found, including copaene and β-caryophyllene, which are well known constituents of ground black pepper oils.[255] In summary, whilst many of the compounds identified using GC×GC-TOF-MS have previously been reported as constituents of the essential oils of herbs and pepper, this study has also identified several new compounds released from herbs and black pepper.

Although many literature studies report the same compounds to be present in herbs and black pepper, the proportions of individual compounds are highly variable across the range of studies that have been carried out. For example, a study by Menon *et al.* shows wide variation in the essential oil composition of four black pepper varieties; the sabinene content ranged from 0.2% to 30%, whilst the β-caryophyllene fraction was between 19.8% and 47.5%.[254] The variation in the chemical composition of volatiles from herbs and pepper can be attributed to a number of factors, including different plant cultivation methods, agroclimatic conditions, and variation in the maturity of the raw material.[258] Furthermore, the method of obtaining the oil may also influence the chemical composition. Parthasarathy *et al.* report that steam-distilled pepper oils usually contain approximately 70-80% monoterpenes, 20-30% sesquiterpenes, and less than 4% of oxygenated components.[258] On the other hand, oils prepared by vacuum distillation of oleoresin generally contain fewer monoterpenes, and high levels of sesquiterpenes and oxygenated species. In this study, extraction of the oil from herbs and pepper was avoided and the condiments were simply heated to 180 °C to simulate cooking and immediately analysed by GC×GC-TOF-MS. The results matched well with the PTR-TOF-MS data obtained when a series of experiments that involved cooking lean beef seasoned with different amounts of herbs and pepper were carried out. This indicates that analysis of herb and pepper emissions by thermal desorption coupled directly to GC×GC-TOF-MS is a good technique for replicating real-life cooking with condiments. However, it is worth noting that the herb mixture used in this study was not homogenous, and each 10 mg sample may contain different amounts of individual herbs. Therefore, in the future it would be useful to either analyse replicate samples, or to study the emissions from each herb individually.

Figure 5.4 shows the relative contribution of different compounds to the total NMOG emissions from frying lean beef with either herbs or pepper at 180 °C, measured using PTR-TOF-MS. The compounds were classified in the same way as described in Klein *et al.*,[228] with an additional 'terpenes' class, which includes *p*-cymene ($C_{10}H_{14}$),

monoterpenes ($C_{10}H_{16}$), terpenoids ($C_{10}H_{14}O$, $C_{10}H_{16}O$) and sesquiterpenes ($C_{15}H_{24}$). The addition of 2, 4 and 6 g of condiments to the meat before frying for 10 minutes led to terpene emissions of 2.6, 6.8 and 12 mg kg^{-1}_{meat} respectively.

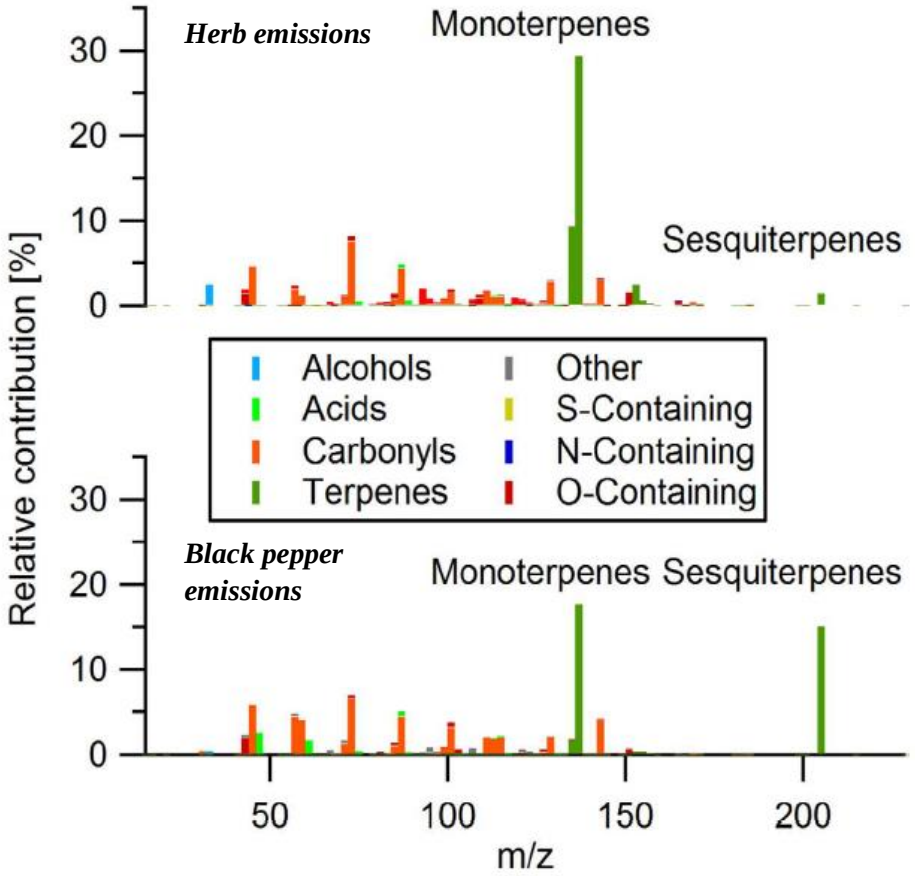

Figure 5.4. Relative contributions of different compounds to the total NMOG emissions from frying lean beef with herbs (upper panel) and pepper (lower panel) at 180 °C, measured using PTR-TOF-MS.[223]

The GC×GC-TOF-MS results shown in Figure 5.3 compare very well with the PTR-TOF-MS measurements shown in Figure 5.4, and therefore it was possible to identify the dominant contributors to the bulk signal measured by PTR-TOF-MS. Both of the techniques revealed that the herbs emit mainly *p*-cymene and monoterpenes, but only small amounts of sesquiterpenes. However, significant quantities of oxygenated sesquiterpenes (such as caryophyllene oxide and cadinol) and diterpenes (*e.g.* cembrene) were detected in the herb emissions by GC×GC-TOF-MS, but could not be detected by PTR-TOF-MS. As a result, the C_{10}/C_{15} compound ratios were very different for the PTR-TOF-MS and GC×GC-TOF-MS, with ratios of 20 and 2.5 found respectively. Both of the techniques showed that black pepper primarily emits sesquiterpenes, with lower amounts of monoterpenes and almost no *p*-cymene. The C_{10}/C_{15} ratio was 1.4 from the PTR-TOF-MS measurements and 1.25 from the GC×GC-TOF-MS measurements. With the exclusion of

the diterpenes and the oxygenated sesquiterpenes, the PTR-TOF-MS measurements show that herbs and pepper emit similar amounts of 'terpenes', 46 ± 5 μg $g^{-1}_{seasoning}$ min^{-1}.[230]

5.3.5 Aerosol formation from cooking with herbs and pepper

To perform the aging experiments (described in section 5.2.1.2), the NMOG emissions were diluted by a factor of ~1:10 and were introduced into a 7 m^3 Teflon smog chamber and exposed to UV light. The studies revealed that the primary organic aerosol (POA) formation was mainly attributed to meat frying; POA concentrations in the chamber were around 6.0 ± 3.3 μg m^{-3} for all experiments, regardless of the amount of seasoning added to the meat. However, rapid SOA production was observed and the total amount of SOA formed ranged from 4.9 to 64.4 μg m^{-3}. The amount of SOA was strongly dependent on the initial mass of terpenes present in the chamber ($R^2 = 0.93$, slope = 0.4). The SOA formed due to the addition of condiments (SOA_{cond}) was calculated by subtracting the average SOA formed by the emissions from frying meat with oil alone from SOA_{tot} for each experiment. The effective SOA yield was then calculated by dividing the mass SOA_{cond} by the mass of terpenes reacted. The effective yield from the terpenes was found to be 45% for herbs and 29% for pepper. As previously mentioned, additional diterpenes and oxygenated sesquiterpenes (which were not detected by PTR-TOF-MS) were identified in the herb emissions using GC×GC-TOF-MS. It is possible that these compounds acted as efficient intermediate volatility SOA precursors, and made a significant contribution to the effective SOA yield from the terpenes in the herb emissions. This hypothesis can be shown by the fact that if known SOA yields are used, the terpenes measured by PTR-TOF-MS would account for approximately 105-120% of the total SOA for cooking with pepper, but only ~50-75% of the total SOA for cooking with herbs. Whilst there will be uncertainties arising from the PTR-TOF-MS measurements and the literature yields used to predict the contribution of individual terpene families to SOA_{tot}, there is a higher fraction of unexplained SOA_{tot} for the herb experiments compared to the pepper experiments. It is highly likely that the unexplained SOA_{tot} can originate from other SOA producing compounds, such as the diterpenes and oxygenated sesquiterpenes.

In summary, the terpene concentrations released upon cooking with condiments are substantial and are likely to have a significant influence on terpene concentrations measured in indoor environments, which are currently mostly attributed to cleaning detergents. In the future, it is important that a range of monoterpenes, sesquiterpenes, diterpenes and terpenoids are used to estimate the total terpene load and subsequent SOA formation indoors, as currently it is often only α-pinene and limonene that are considered.[227, 259] Overall, cooking

with herbs and pepper is likely to be an important yet overlooked source of terpenes and SOA indoors and should be taken into consideration in future indoor air quality studies.

5.3.6 Composition of cooking aerosol

Aerosol filters were collected from a series of cooking experiments (details in section 5.2.1.3 and 5.2.2.3), and the chemical composition of the particulate emissions was investigated using GC×GC-TOF-MS. The experiments included heating olive oil in a pan, frying beef in sunflower oil, and charbroiling beef, chicken and beef burgers. Aerosol filter samples representative of background conditions were also collected by heating an empty pan, and the compounds present were blank subtracted from the cooking emission samples.

5.3.6.1 Particulate compounds from heated cooking oils

The main compounds found in the particulate emissions from heating olive oil are listed in Table 5.7. Compound identification was achieved using a combination of retention indices and reference to the NIST mass spectral library. At this stage, there are still several compounds present in the aerosol that have not been identified, but the use of external standards will allow for further characterisation and quantification of the emissions in the future. The particulate emissions from olive oil were dominated by three groups of compounds; fatty acids, γ-lactones and δ-lactones. The fatty acids identified by GC×GC-TOF-MS are shown in the upper panel of Figure 5.5. The relative peak intensities reveal a clear even-to-odd carbon number preference, and the most abundant fatty acids in the olive oil emissions are oleic acid ($C_{18}H_{34}O_2$), linoleic acid ($C_{18}H_{32}O_2$), stearic acid ($C_{18}H_{36}O_2$) and palmitic acid ($C_{16}H_{32}O_2$). These are typically the most dominant compounds found in olive oil.[260] The GC×GC chromatogram in the middle panel of Figure 5.5 shows a series of long-chain alkyl γ-lactones detected in the olive oil emissions, whilst the lower panel shows several long-chain alkyl δ-lactones. With the exception of 4,8,12,16-tetramethylheptadecan-4-olide, the alkyl chain length ranged from C_8 to C_{18} for the γ-lactones, and from C_{13} to C_{18} for the δ-lactones. According to Rogge *et al.*, such compounds can form during the lactonization of γ- and δ-hydroxy fatty acids, or alternatively by the oxidation of alkenals and oleic acid.[39]

Several reports in the literature have highlighted the potential of lactones as suitable tracers for cooking emissions. For example, Rogge *et al.* investigated the chemical composition of meat smoke aerosol in Los Angeles and identified a series of higher lactones,[39] whilst Schauer *et al.* have reported lactones to be emitted from both meat charbroiling and seed oil cooking operations.[221-222] More recently, McDonald *et al.* investigated emissions of speciated organic compounds (PAHs, cholesterol and long-chain γ-lactones) from charbroiling and grilling of chicken and beef, and found that only the lactones were unique

to the cooking emissions.[219] Whilst the studies conclude that lactone species are not emitted in great quantities and may be difficult to detect in ambient air, there seems to be a good agreement that if detected, lactones can be used as unique markers for cooking emissions.

Table 5.7. GC×GC-TOF-MS measurements of SOA compounds present in emissions from heating olive oil to 180 °C. 1st and 2nd RT represent first and second retention time, and similarity is out of 1000. ≠ denotes compounds detected in urban atmospheric $PM_{2.5}$ collected during the ClearfLo campaign.

Compound	1st RT / s	2nd RT / s	Similarity	Molecular formula	Type
glycerol≠	655	2.53	533	$C_3H_8O_3$	triol
2,4-decadienal	1485	2.19	822	$C_{10}H_{16}O$	aldehyde
niacinamide	1605	0.29	792	$C_6H_6N_2O$	amide
dodecanoic (lauric) acid≠	1840	1.19	NA	$C_{12}H_{24}O_2$	fatty acid
tetradecanoic (myristic) acid≠	2040	1.16	NA	$C_{14}H_{28}O_2$	fatty acid
pentadecanoic acid≠	2135	1.15	NA	$C_{15}H_{30}O_2$	fatty acid
hexadecenoic (palmitic) acid≠	2220	1.17	908	$C_{16}H_{32}O_2$	fatty acid
heptadecanoic (margaric) acid≠	2305	1.15	NA	$C_{17}H_{34}O_2$	fatty acid
linoleic acid≠	2360	1.45	935	$C_{18}H_{32}O_2$	fatty acid
oleic acid≠	2365	1.33	935	$C_{18}H_{34}O_2$	fatty acid
linolenic acid≠	2365	1.57	843	$C_{18}H_{30}O_2$	fatty acid
octadecanoic (stearic) acid≠	2380	1.17	879	$C_{18}H_{36}O_2$	fatty acid
5-butyldihydro-2(3H)-furanone≠	1350	4.36	NA	$C_8H_{14}O_2$	γ-lactone
5-pentyldihydro-2(3H)-furanone≠	1555	2.97	NA	$C_9H_{16}O_2$	γ-lactone
5-hexyldihydro-2(3H)-furanone≠	1715	2.41	NA	$C_{10}H_{18}O_2$	γ-lactone
5-heptyldihydro-2(3H)-furanone≠	1845	2.16	NA	$C_{11}H_{20}O_2$	γ-lactone
5-octyldihydro-2(3H)-furanone≠	1960	2.02	NA	$C_{12}H_{22}O_2$	γ-lactone
5-nonyldihydro-2(3H)-furanone≠	2065	1.93	NA	$C_{13}H_{24}O_2$	γ-lactone
5-decyldihydro-2(3H)-furanone≠	2165	1.85	NA	$C_{14}H_{26}O_2$	γ-lactone
5-undecyldihydro-2(3H)-furanone≠	2255	1.82	NA	$C_{15}H_{28}O_2$	γ-lactone
5-dodecyldihydro-2(3H)-furanone≠	2340	1.79	NA	$C_{16}H_{30}O_2$	γ-lactone
5-tridecyldihydro-2(3H)-furanone≠	2420	1.78	NA	$C_{17}H_{32}O_2$	γ-lactone
5-tetradecyldihydro-2(3H)-furanone≠	2500	1.74	NA	$C_{18}H_{34}O_2$	γ-lactone
4,8,12,16-tetramethylheptadecan-4-olide	2520	1.52	834	$C_{21}H_{40}O_2$	γ-lactone
tetrahydro-6H-octyl-2H-pyran-2-one≠	2085	2.03	NA	$C_{13}H_{24}O_2$	δ-lactone
tetrahydro-6-nonyl-2H-pyran-2-one≠	2190	2.02	NA	$C_{14}H_{26}O_2$	δ-lactone
tetrahydro-6-decyl-2H-pyran-2-one≠	2280	1.98	NA	$C_{15}H_{28}O_2$	δ-lactone
tetrahydro-6-undecyl-2H-pyran-2-one≠	2365	1.96	NA	$C_{16}H_{30}O_2$	δ-lactone
tetrahydro-6-dodecyl-2H-pyran-2-one≠	2445	1.92	NA	$C_{17}H_{32}O_2$	δ-lactone
tetrahydro-6-tridecyl-2H-pyran-2-one≠	2525	1.87	NA	$C_{18}H_{34}O_2$	δ-lactone

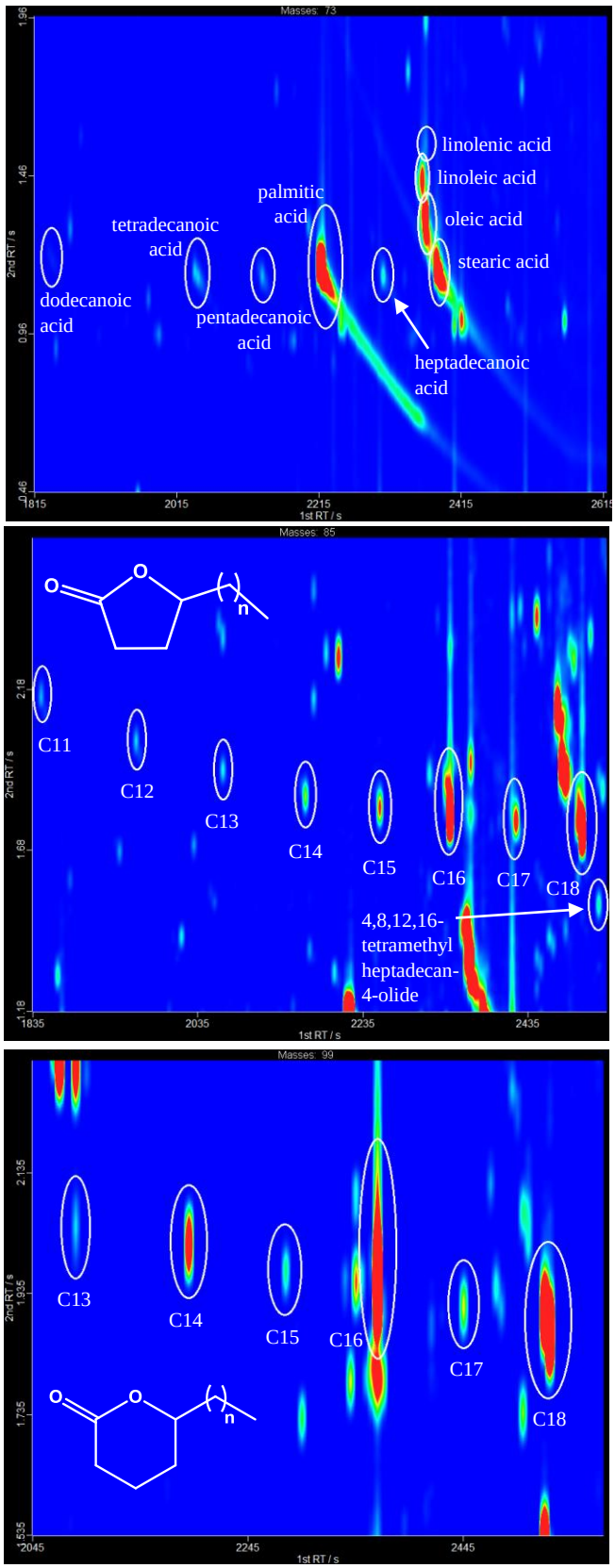

Figure 5.5. GC×GC-TOF-MS measurements of compounds present in the aerosol formed during olive oil heating to 180 °C. 2D chromatograms for fatty acids (*m/z* 73, upper panel), γ-lactones (*m/z* 85, middle panel) and δ-lactones (*m/z* 99, lower panel).

Furthermore, Zhao *et al.* reported that lactones with carbon number greater than 14 are particularly useful tracers of both Western and Chinese-style cooking, as they are emitted in higher concentrations than the smaller lactones.[261] Although Zhao *et al.* found that significantly higher quantities of lactones are released during Western-style cooking than Chinese-style cooking,[261-262] and Schaeur *et al.* investigated the effect of cooking temperature on the extent of lactone emissions,[222] there remains a lack of knowledge regarding the impact of different cooking styles and geographical location on the emission of lactones. To investigate whether the lactones identified in the study can be detected in ambient air, a $PM_{2.5}$ sample from an urban background site (North Kensington, London) was analysed using the described GC×GC-TOF-MS method. The $PM_{2.5}$ sample was collected as part of the ClearfLo project and was extracted into ethyl acetate using the pressurised liquid extraction process described in Chapter 2, section 2.2.4. Interestingly, the $C_8 - C_{18}$ γ-lactones listed in Table 5.7 were all detected in the atmospheric PM, as well as a series of δ-lactones ranging from C_{13} to C_{18}. In the future, it will be useful to assess the temporal variability of the lactones by quantifying the daily lactone concentrations throughout the entire measurement campaign; assessing the correlation with the cooking organic aerosol (COA) factor, which was derived from aerosol mass spectrometry measurements carried out during the ClearfLo project,[263] will allow us to assess the viability of lactones as tracers for cooking emissions. The fatty acids listed in Table 5.7 were also detected in urban atmospheric PM, but it is likely that these compounds have other sources in the environment. For example, Robinson *et al.* reported that whilst palmitic, stearic, palmitoleic and oleic acid are important markers for cooking emissions, there are also non-cooking related sources of these compounds, such as biomass smoke, motor vehicle exhaust and road dust.[264] As shown in Table 5.7, three other compounds were also identified in the olive oil emissions: glycerol, niacinamide and 2,4-decadienal. During cooking, glycerol is emitted as a result of the hydrolysis of thermal oxidation of triglycerides, which are present in cooking oils and consist of three fatty acids esterified to a glycerol backbone.[265] Niacinamide is a key constituent of niacin, which is a vitamin that is either naturally present in the food or is added as an essential nutrient supplement.[266] 2,4-decadienal was also detected in the gas-phase emissions from heated cooking oil and is a specific marker of linoleic acid emissions.[242] The presence of 2,4-decadienal in both the gas and particle phase is potentially of concern as exposure to this compound can increase the risk of lung cancer.[246]

5.3.6.2 Particulate compounds from cooking meat

The SOA compounds present in the emissions from cooking various types of meat using different techniques are listed in Tables A14 – A17, Appendix A. Without the use of analytical standards, it can be challenging to assign the compound identities accurately and

therefore the best prediction of the compound identity has been provided, as well as the similarity to the NIST mass spectral library (score out of 1000). Most of the compounds identified in the olive oil emissions can also be found in the emissions from meat cooking. During the charbroiling of chicken and beef, a small amount of oil was rubbed into the meat prior to cooking to avoid the meat sticking to the pan; it is apparent that this small quantity of cooking oil was sufficient for the emissions to be dominated by compounds from the oil. When the beef burgers were cooked, no additional oil was added but the high fat content of the burgers means that compounds characteristic of oil emissions are likely to be observed. During the frying experiments, the beef was fried in *ca.* 25 g of sunflower oil, and therefore emissions characteristic of cooking oil can be expected. Nevertheless, there were several compounds found in the emissions from the meat cooking experiments that were not detected in the olive oil emissions, and are therefore likely to be from the meat itself. Between 14 and 16 additional compounds were identified in the emissions from charbroiling chicken/ beef burgers and frying beef, whilst 32 extra compounds were found in the emissions from charbroiling beef. The emissions from charbroiling beef also contained a higher number of nitrogen-containing species; 20 of the additional 32 compounds contained nitrogen, compared to between 3 and 7 nitrogen-containing species in the emissions from charbroiling chicken/ beef burgers and frying beef. As shown in Figure 5.6, these findings compare well with the AMS measurements carried out at PSI during the different cooking experiments. The mass spectra for the emissions from charbroiled chicken (upper left panel), charbroiled beef burger (upper right panel) and fried beef (lower left panel) are all very similar with N:C ratios between 0.02 and 0.03, whereas the mass spectra for the emissions from charbroiled beef (lower right panel) shows a higher contribution of ON species and the N:C ratio is 0.10.

Many of the additional compounds found in the meat cooking emissions were fatty acids, including C_5-C_9, C_{11} and C_{13} alkanoic acids and 3,5,5-trimethyl-hexanoic acid. E-11-tetradecenoic acid was also present in the emissions from charbroiled chicken and beef burger. Figure 5.7 shows the non-nitrogen containing compounds found in the meat cooking emissions, except for the series of long-chain alkanoic acids, γ-lactones and δ-lactones. During the cooking process, it is possible for fatty acids in raw meat (which are bound chemically as triglycerides and phospholipids) to be liberated by bacterial enzymes or by hydrolysis and thermal oxidation.[39] There were also two additional δ-lactones found in the emissions from chicken, beef burgers and fried beef, namely the C_9 and the C_{12} δ-lactone, which can form *via* the lactonization of fatty acids. Two dicarboxylic acids, citraconic acid and 2-propylmalonic acid, were found in the beef and beef burger emissions but were not present in the chicken emissions. It is likely that the citraconic acid comes from the degradation of citric acid, which is used as a food additive. Citric acid acts as a preservative

and antioxidant, and prevents discoloration, flavour changes and rancidity during food processing.[267]

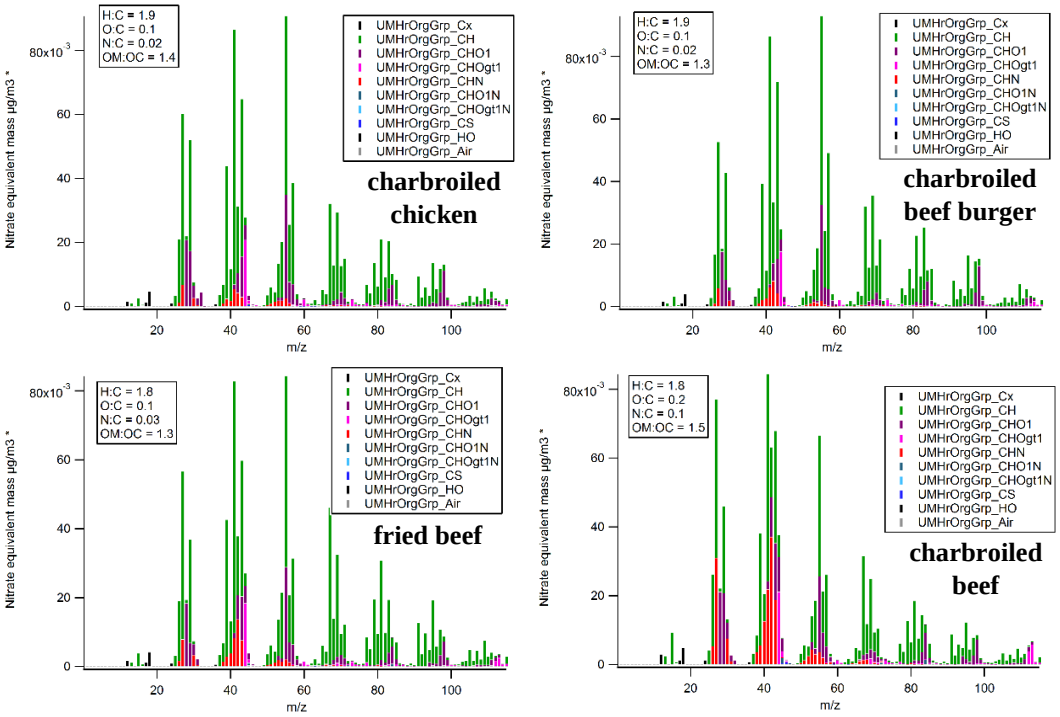

Figure 5.6. AMS mass spectra of the emissions from charbroiled chicken (upper left panel), charbroiled beef burger (upper right panel), fried beef (lower left panel) and charbroiled beef (lower right panel).[223]

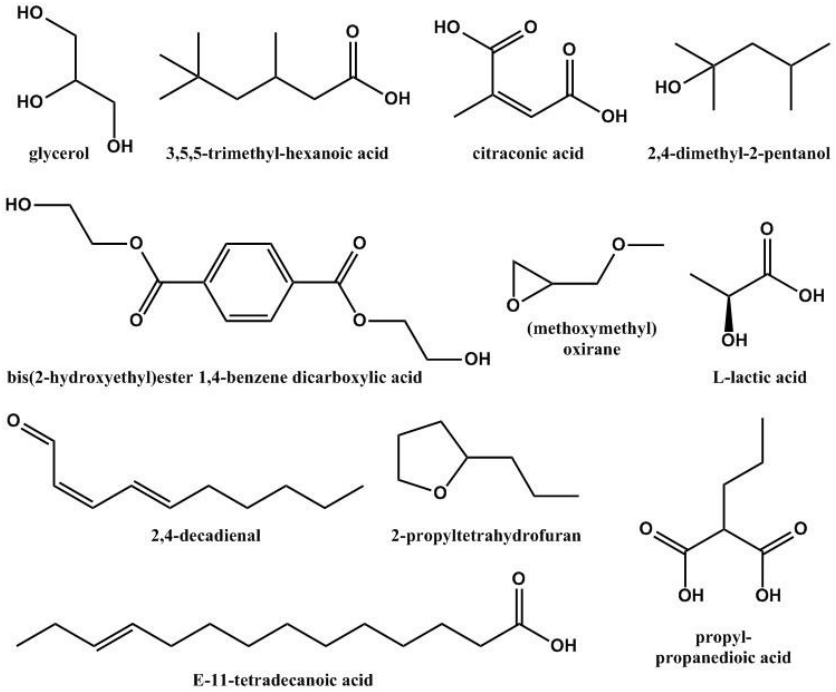

Figure 5.7. Non-nitrogen containing species present in the meat cooking emissions. The long-chain alkanoic acids, γ-lactones and δ-lactones are not included.

Other additional compounds present in the meat cooking emissions included 5-ethyl-4-tridecanone (chicken), 2,4-dimethyl-pentanol (chicken, beef burger, fried beef), (methoxymethyl)oxirane (all beef samples), bis(2-hydroxyethyl)ester-1,4-benzene dicarboxylic acid (all beef samples) and lactic acid (chicken). Many organic compounds such as ketones, alcohols and esters can form during the oxidation composition of fatty acids,[39] whilst lactic acid is often added to meat in order to extend the shelf life and avoid microbial growth.[268] There were also several ON species present in the meat cooking emissions; the addition of nitrogen to an organic structure can significantly increase the carcinogenic and mutagenic effects of a compound,[269] and therefore exposure to these species can potentially pose a threat to human health. The ON species common to all the meat cooking emissions were niacinamide, 2-nitrobutane and hexahydropyrrolizin-3-one, as shown in Figure 5.8. Creatinine was emitted from charbroiled beef and chicken, as well as fried beef.

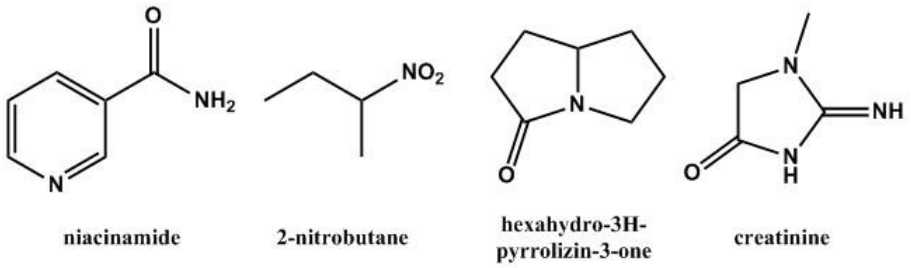

Figure 5.8. Key ON species present in the meat cooking emissions.

Niacinamide was also present in the olive oil emissions, and as previously discussed is a key constituent of niacin.[266] Although further investigation is required, it is possible that the presence of nitroalkanes such as 2-nitrobutane are linked to the presence of sodium nitrite in meat – this is added to various foods to prevent the growth of bacteria and prevent spoilage.[270] Creatinine is from the non-proteinogenic amino acid creatine, which exists as creatine phosphate in the muscle of vertebrates and serves as an energy store.[271] Upon heating, it is converted to the physiologically inert cyclization product creatinine, which is an important precursor to a range of heterocyclic aromatic amines (HAAs).[272] HAAs are compounds which contain at least one heterocyclic ring in which at least one amine group is present, and form when meat is cooked using high-temperature methods such as pan frying or grilling over an open flame.[273] Several HAAs are been found to have mutagenic and carcinogenic effects,[274] and therefore exposure *via* both ingestion and inhalation is of concern to human health. In addition to hexahydropyrrolozin-3-one, which was present in all meat emissions, an additional 6 HAAs were found in the emissions from charbroiled chicken and a further 18 HAAs were found in the charbroiled beef emissions. One of the most important processes in the formation of several HAAs is the Maillard reaction; this is

a series of complex reactions between reducing sugars and amino acids, and can also be referred to as non-enzymatic browning.[275] The most important intermediates formed during the course of the Maillard reaction are α-dicarbonyl structures; these compounds can undergo a series of complex reactions, many of which are not yet fully understood, to form various meat flavour impact compounds such as pyrazines, N-, S- and O-heterocycles, and sulphides.[276] In this study, there were three pyrazine compounds detected in the lean meat emissions: 2-methyl-5-propyl-pyrazine, 2-isoamylpyrazine and 2-isoamyl-6-methylpyrazine. It is possible to predict mechanisms for their formation by considering the Strecker degradation, which is a key aspect of the Maillard reaction. At the start of the series of reactions referred to as the 'Maillard reaction', the carbonyl of an aldose monosaccharide can react with a free amino group and undergo an Amadori rearrangement to form a ketosamine.[277-278] Decomposition of the ketosamine eventually leads to the formation of an α-dicarbonyl intermediate, and through a series of Strecker reactions a variety of aminocarbonyl compounds can be formed.[276] Pyrazine formation occurs as a result of the condensation of two α-aminocarbonyls, which forms a dihydropyrazine that spontaneously oxidises to produce the corresponding pyrazine.[276] For example, Scheme 5.4 shows the proposed mechanism for the formation of 2-isoamyl-6-methylpyrazine.

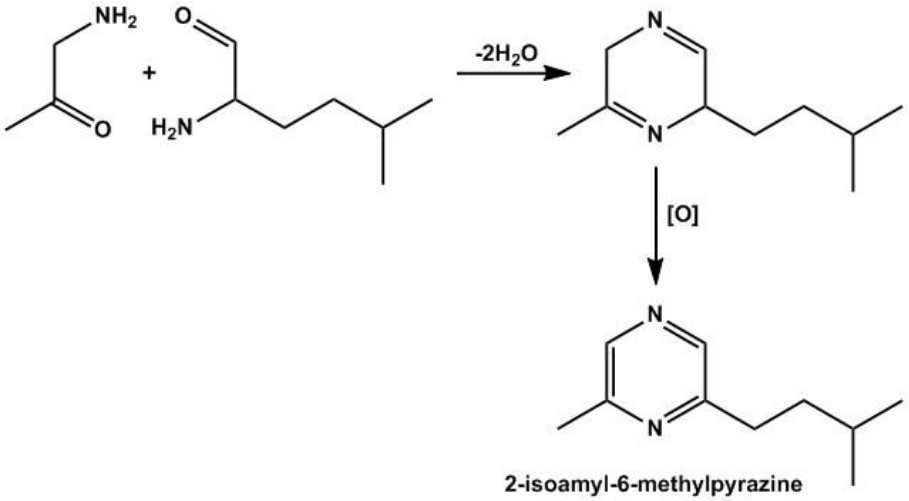

Scheme 5.4. Condensation of two α-aminocarbonyls, 1-amino-2-propanone and 2-amino-5-methylhexanal, followed by spontaneous oxidation to form 2-isoamyl-6-methylpyrazine.[271]

Other HAAs detected in the meat cooking emissions during this study included various imidazolidine and creatinine derivatives, as well as purine and piperazine structures. Whilst the mechanisms for their formation are complex and beyond the scope of this study, the Maillard reaction and Strecker degradation processes are likely to have played an important role in their formation. Additional ON species measured by GC×GC-TOF-MS in the

charbroiled lean meat emissions included Nε-acetyl-L-lysine and dl-alanyl-l-leucine. Dl-alanyl-l-leucine consists of two amino acids, alanine and leucine, whilst Nε-acetyl-L-lysine is the acetylated version of the amino acid L-lysine. According to the US Department of Agriculture, these three amino acids are some of the most abundant amino acids found in charbroiled lean meat.[279]

Some of the compounds found in the cooked meat emissions that were not present in the olive oil emissions were also identified in the urban $PM_{2.5}$ sample collected at the North Kensington site in London (compounds detected are highlighted in Tables A14 – A17, Appendix A). Four of the compounds found in atmospheric PM were present in all of the cooked meat emissions (2,3-dimethyl-pyridine, 3,5,5-trimethyl-hexanoic acid, 2,4-dimethyl-2-pentanol and 2-nitrobutane), whilst 5-isobutyl-2,4-imidazolidinedione was exclusively from the charbroiled lean meat emissions. In order to determine the suitability of these compounds as atmospheric tracers of cooking emissions, it is necessary to investigate whether any other environmental sources of these compounds exist. For example, other HAAs have been detected in rain water, tobacco smoke and diesel exhaust fumes.[280-281] If these compounds are exclusively from cooking, they would be useful for distinguishing between different cooking techniques, as well as the type of food cooked.

In summary, a wide variety of compounds have been identified in the particulate emissions from heated olive oil, fried beef and charbroiled chicken, beef and beef burgers. Many of the compounds, such as glycerol, niacinamide, 2,4-decadienal, as well as series of fatty acids, γ-lactones and δ-lactones were detected in the olive oil emissions and also dominated the cooked meat emissions. Nevertheless, there were additional compounds identified in the cooked meat emissions, including shorter chain fatty acids and δ-lactones, ketones, alcohols, esters and an array of ON compounds. Analysis of atmospheric $PM_{2.5}$ in London revealed that many of the compounds were also present in the urban atmosphere, and it was proposed that the γ- and δ-lactones detected would be particularly suitable cooking tracers as no other environmental sources have yet been reported in the literature. In the future, it will be useful to fully quantify the emissions of compounds emitted during cooking, and further investigate their formation mechanisms and potential toxicity. It will be important to determine whether any other classes of toxic or carcinogenic compounds are present in the cooking emissions; for example, it has been reported that nitrite present in meat can react with amines and amides to form N-nitrosamines, and their presence in the meat itself has been extensively reported.[282-284] Although there were not any N-nitrosamines detected in the gas or particle phase emissions in this study, it is possible that they were present in trace level concentrations and below the detection limits of the instrument, therefore analysis of more concentrated samples is required.

5.4 Conclusions

In collaboration with PSI, a series of experiments were carried out to investigate the chemical composition of cooking emissions and the impact of cooking with herbs and pepper. Gas phase emissions were characterised by a combination of PTR-TOF-MS and GC×GC-TOF-MS, whilst particulate emissions were investigated using GC×GC-TOF-MS and HR-TOF-AMS. Using PTR-TOF-MS measurements, the gas phase emissions from canola, sunflower and olive oil were categorised into eight different families. The use of GC×GC-TOF-MS allowed for the aldehyde and ketones to be distinguished from each other, and led to the identification of 37, 47 and 56 compounds in the canola, sunflower and olive oil emissions respectively. The different emissions patterns of the oils were consistent with the varying composition of the triglycerides present in the oils. Furthermore, the secondary oxidation products from oleic acid degradation were predicted using mechanistic studies and the majority of the compounds were successfully identified in the olive oil emissions.

The gas phase emissions from cooked vegetables and meats were characterised by PTR-TOF-MS. It was found that when food was shallow fried, aldehydes made up more than 60% of the total NMOG, and the contribution of smaller aldehydes to the total emissions increased when frying food in oil, rather than just heating the oil alone. Interestingly the proportion of smaller aldehydes decreased with increasing oil temperature. The gas phase emissions from charbroiling food were lower than for frying as less oil was used to cook the food, and from these studies it was deduced that hexanal and nonanal, which have relatively long atmospheric lifetimes, may potentially be suitable markers for cooking emissions. Klein *et al.* investigated the impact on indoor air quality and concluded that many aldehydes such as acrolein, which can irritate the eyes and respiratory tract, would exceed the recommended levels in a typical kitchen environment.[228]

Gas phase emissions from herbs and pepper heated to 180 °C were characterised by GC×GC-TOF-MS and whilst monoterpenes, sesquiterpenes and oxygenated VOCs were detected in emissions from both herbs and pepper, diterpenes were only detected in the herb emissions. Analysis of the herb and pepper emissions by PTR-TOF-MS reveled that the addition of 2, 4 and 6 g of condiments to the meat before frying for 10 minutes led to total terpene emissions of 2.6, 6.8 and 12 mg kg^{-1}_{meat} respectively. Significant quantities of oxygenated sesquiterpenes and diterpenes were detected in the herb emissions by GC×GC-TOF-MS, but could not be detected by PTR-TOF-MS. It is possible that these compounds acted as efficient intermediate volatility SOA precursors, and made a significant contribution to the effective SOA yield from the terpenes in the herb emissions; this would account for the fact that there is a higher fraction of unexplained SOA_{tot} for the herb

experiments compared to the pepper experiments. The terpene concentrations released upon cooking with condiments were substantial and will likely make a significant contribution to terpene concentrations measured in indoor environments, which are currently mostly attributed to cleaning detergents. It is important therefore, that this additional source of terpenes is taken into consideration in future indoor air quality studies.

Particulate emissions from heated olive oil, fried beef and charbroiled chicken, beef and beef burgers were investigated. The emissions from olive oil were dominated by fatty acids, γ-lactones and δ-lactones. It is likely that the lactones would be suitable tracers for cooking emissions, as there are no other environmental sources reported in the literature, and these compounds were detected in atmospheric $PM_{2.5}$ samples from an urban environment. The emissions from cooked meat were dominated by compounds from oil emissions, but between 14 and 16 additional compounds were identified in the emissions from charbroiling chicken/ beef burgers and frying beef, whilst 32 extra compounds were found in the emissions from charbroiling beef. Additional non-nitrogen-containing species included shorter chain fatty acids, as well as various dicarboxylic acids, ketones, alcohols and esters. There was a higher fraction of additional nitrogen-containing species in the lean meat emissions than the other cooked meat emissions, and this observation agreed with the measurements obtained by HR-TOF-AMS. Examples of ON species detected were creatinine, niacinamide and a range of heterocyclic aromatic amines (HAAs). Many HAAs have been reported to have carcinogenic and mutagenic properties, and therefore exposure *via* inhalation and ingestion is of concern to human health. A mechanism for the formation of the observed pyrazines was proposed, involving the Maillard reaction and the Strecker degradation, both of which are important processes in the formation of HAAs. Although some of the additional compounds exclusive to the meat emissions were also identified in atmospheric PM, further investigation is required to determine whether these compounds are exclusively from cooking. In summary, this study provides a detailed description of the composition of gas and particle phase emissions from various types of food cooked using different techniques. In the future, it will be useful to quantify the individual compounds present in the emissions, and further investigate their formation mechanisms and potential toxicity.

6 Chemical Characterisation of Water-soluble Ions in Atmospheric Particulate Matter on the East Coast of Peninsular Malaysia

6.1 Introduction

The Bachok Marine and Atmospheric Research Station (6.00892° N, 102.42504° E), which forms part of the Institute of Ocean and Earth Sciences at the University of Malaya (UM), lies on the eastern coast of Peninsular Malaysia approximately 30 km away from Kota Bharu.[285] An atmospheric observation tower facing the South China Sea has been constructed at the research station; this has been built for the specific purpose of monitoring long-range transported pollution, air sea exchange, and coastal meteorology. The research station is working towards designation as a regional Global Atmospheric Watch (GAW) centre, which will be a valuable addition to the network of other global and regional GAW sites in the Maritime Continent, as shown in Figure 6.1.[286]

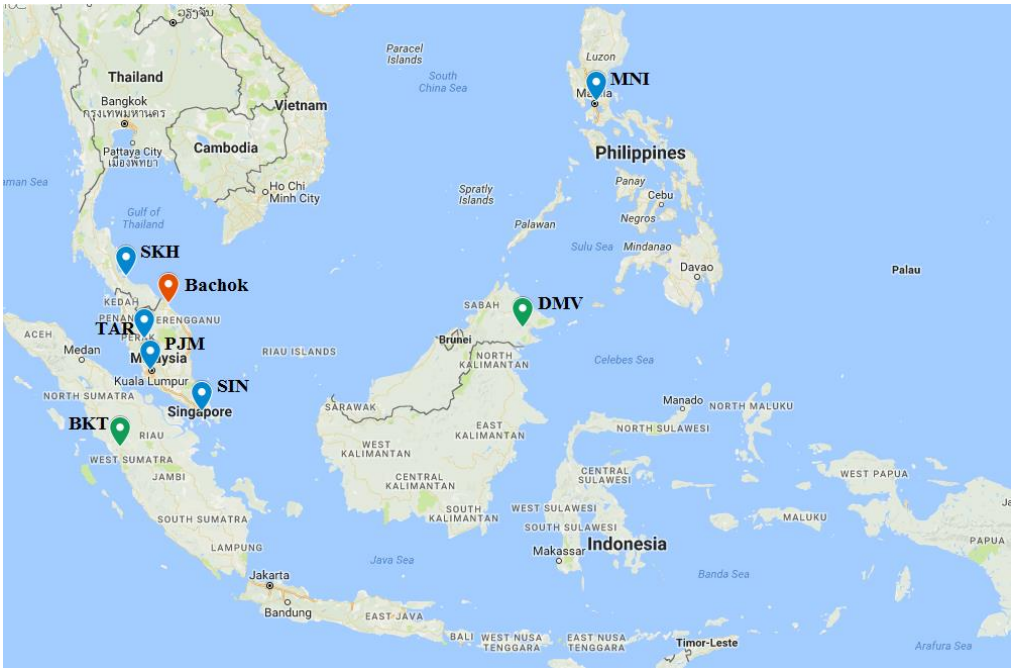

Figure 6.1. Location of global (green pins) and regional (blue pins) GAW sites in the Maritime Continent: Danum Valley in Malaysia (DMV), Bukit Kototabang in Indonesia (BKT), Manila in Philippines (MNI), Songkhla in Thailand (SKH), Tanah Rata in Malaysia (TAR), Petaling Jaya in Malaysia (PJM) and Singapore (SIN). The red pin shows the location of the Bachok Marine and Atmospheric Research Station.[286]

The tropical Maritime Continent, a region in Southeast Asia between 10° S – 20 °N and 90° - 150° E, is a complex distribution of islands and peninsulas, and incorporates countries such as Malaysia, Indonesia, Philippines and Papua New Guinea.[287] It lies within a tropical warm pool that extends eastwards from the Indian Ocean to the Western Pacific, and is home to some of the warmest ocean temperatures in the world. Tropical regions such as the Maritime Continent are of central importance for the chemistry-climate system for various reasons.[288] For example, high photochemical activity in these regions means that global atmospheric lifetimes of key atmospheric species, such as methane and ozone, are controlled by destruction rates in the tropics.[289-290] In terms of ocean productivity, the observed decrease in primary productivity in low-latitude oceans has been linked to a reduced availability of nutrients for phytoplankton growth, caused by changes in upper-ocean temperature and stratification.[291] Furthermore, the wind circulation system in the Maritime Continent is influenced by seasonal Asian monsoons, which are controlled by the natural oscillation of the intertropical convergence zone (ITCZ). During the winter monsoon season, strong north-easterly winds transport atmospheric species from rapidly developing Southeast Asian countries (*e.g.* China, Japan, Taiwan, Vietnam, North and South Korea) across the South China Sea to the Maritime Continent. This means that rural areas, such as the Bachok district in Malaysia, are potentially at an elevated risk of the detrimental effects of poor air quality, such as damage to human health, and disruption of aquatic and terrestrial ecosystems.

Although it is clear that tropical regions are highly important for atmospheric research, there is a lack of long-term observations compared to middle and high-latitudes.[288] This is primarily due to the limited number of countries with sufficient scientific infrastructure to support atmospheric measurement networks. Nevertheless, the Bachok research station has been set up on the east coast of Peninsular Malaysia and is ideally located for studying the outflow of these highly industrialised regions, and for investigating the interaction with cleaner air in the Southern hemisphere. In January and February 2014, an instrument demonstration campaign was carried out to assess the capabilities of the new research station. This was funded by the Natural Environment Research Council (NERC) and UM and involved several UK universities, as well as the National Centre for Atmospheric Science (NCAS), UM and the Malaysian Meteorological Department. As part of this campaign, Dunmore *et al.* used a specialised multi-dimensional GC technique to accurately measure atmospheric mixing ratios of C_5-C_{13} VOC species with a wide range of functionalities.[292] Furthermore, Dominick *et al.* characterised particulate matter in Bachok by studying the influence of north-easterly winds on the patterns of particle mass and particle number concentration size distributions.[293] Both studies highlighted the fact that the site is influenced by a mixture of local anthropogenic and biogenic emissions, clean marine air

masses, and aged emissions transported from Southeast Asia. To extend upon these studies, it would be useful to gain further insight into the composition of atmospheric aerosol in the Bachok region. A better understanding of chemical composition is essential as aerosols play an important role in atmospheric processes and climate change. For example, aerosols can modify the global radiation budget both directly, by scattering and absorbing solar radiation, and indirectly, by altering cloud properties and lifetime.[294] The strength of these direct and indirect effects depends partly on the chemical composition, but also on the particle concentration and size distribution.[295]

There are a limited number of studies that focus on particulate matter composition on the east coast of Peninsular Malaysia, and to our knowledge the composition of ionic species has not been determined at any rural locations along this coastline. For example, Tahir *et al.* studied the composition of major elements and water-soluble ionic species in $PM_{2.5}$ and PM_{10} samples on the east coast of Peninsular Malaysia, but the samples were collected at an urban coastal city (Kuala Terengganu), rather than a rural area.[296] Using principal component analysis, it was possible to determine that the main sources of both fine and coarse particles were soil dust, marine aerosol, vehicle exhaust, secondary aerosol, road dust and biomass burning. In addition, Ismail *et al.* studied PM_{10} concentrations in three major cities (Kota Bahru, Kuala Terengganu and Kuantan) on the east coast of Peninsular Malaysia between 2006 and 2012.[297] The study showed that during the North East Monsoon the air masses originated from China and the Philippines and travelled over the South China Sea, and that during the South West Monsoon the air masses travelled through the Straits of Malacca from Indonesia. Over the 6-year period, it was found that the atmospheric PM_{10} mass was directly proportional to the rate of urbanization.

In this study, measurements of water-soluble ions in atmospheric aerosol at a rural coastal location on the east coast of Peninsular Malaysia are presented. Analysis of the temporal variation of different ionic species has been carried out, and backward air mass trajectories have been used to determine the influence of air mass origin on aerosol composition. Correlation analyses among ionic species, and assessment of the ratios between different ions has helped to obtain information regarding common ion sources and formation pathways, as well as the extent of atmospheric mixing with anthropogenic pollutants.

6.2 Experimental

6.2.1 Eluents and analytical standards

Ultrapure milli-Q water from an ELGA LabWater purification system (18 MΩ cm^{-1}) was used to prepare all of the required eluents and analytical standards. A 20 mM solution of methanesulfonic acid was used as the eluent for cation-exchange chromatography and for anion-exchange chromatography, a solution of 8 mM Na_2CO_3 /1 mM $NaHCO_3$ was prepared. Details of the compounds used to prepare the analytical standards for both cation and anion chromatography are provided in Table 6.1. All of the compounds were purchased from either Sigma-Aldrich Ltd. (Dorset, U.K.) or Fisher Scientific Ltd. (Loughborough, U.K.).

Table 6.1. Compounds used to prepare stock solutions for both anion and cation exchange chromatography and their respective ion concentrations.

Stock solutions for anion exchange chromatography		
Compound	**Target anion**	**[anion] / ppm**
Sodium chloride, NaCl	Cl^-	540.7
Sodium nitrite, $NaNO_2$	NO_2^-	514.0
Sodium nitrate, $NaNO_3$	NO_3^-	493.9
Sodium dihydrogen phosphate, H_2NaPO_4	PO_4^{3-}	502.6
Sodium sulfate, Na_2SO_4	SO_4^{2-}	467.7
Methanesulfonic acid, CH_3SO_3H	$CH_3SO_3^-$	511.6
Oxalic acid, $C_2H_2O_4$	$C_2O_4^{2-}$	511.1
Stock solutions for cation exchange chromatography		
Compound	**Target cation**	**[cation] / ppm**
Sodium nitrate, $NaNO_3$	Na^+	532.1
Ammonium chloride, NH_4Cl	NH_4^+	512.4
Potassium nitrate, KNO_3	K^+	519.1
Magnesium nitrate, $Mg(NO_3)_2$	Mg^{2+}	532.1
Calcium carbonate, $CaCO_3$	Ca^{2+}	459.7

6.2.2 Method validation

The stock solutions listed in Table 6.1 were diluted with milli-Q water to prepare two mixed analytical standards; one contained all of the target anions at 50 ppm and the other contained all of the target cations at 50 ppm. Stepwise dilutions of the mixed analytical standards were carried out to obtain standards at 25, 10, 5, 2.5, 1, 0.5, 0.25, 0.1, 0.05 and 0.01 ppm. These solutions were used to obtain external calibration curves for each target ion, and to assess the detection limits and intra-day precision of the IC. Recovery tests were performed by spiking 5.7 cm^2 of a quartz fibre filter (Whatman, Maidstone, U.K.) with 1 μg of each target ion. Prior to spiking, the filters were pre-baked at 550 °C for 6 hours and then wrapped in aluminium foil and stored at -18 °C until required. The spiked filters were dissolved in 2 mL of milli-Q water and sonicated at room temperature for 30 mins. The extract was filtered using a Millex-GP 33 mm diameter hydrophilic syringe filter with a pore size of 0.22 μm (Millipore UK Limited, Watford, U.K.) and made up to a final volume of 2.5 mL. Procedural blanks were also carried out using quartz fibre filters (5.7 cm^2) and blank subtractions were applied to any target ions found in detectable amounts.

6.2.3 Sample collection and extraction

30 $PM_{2.5}$ filter samples were collected at the Bachok Marine and Atmospheric Research Station (6.00892° N, 102.42504° E) between 18/01/2014 and 06/02/2014. The site is owned and operated by the University of Malaya as part of the Institute of Ocean and Earth Sciences (IOES). The samples were collected at the top of an atmospheric observation tower (height *ca.* 15 m) using a High Volume Air Sampler (Ecotech HiVol 3000, Victoria, Australia) operating at 1.13 m^3 min^{-1} over 24 h sampling intervals. The tower is located on the coastline of the South China Sea and is within 100 m of the shore, as shown in Figure 6.2. A 3-day intensive measurement period was also in operation between 30/01/2014 and 02/02/2014, in which filters were collected every 4-8 hours. The quartz fibre filters (20.3 × 25.4 cm) supplied by Whatman (Maidstone, U.K.) were prebaked at 550 °C for a minimum of 12 h prior to sample collection. After sample collection the filters were wrapped in aluminium foil and stored at -18 °C until analysis. To prepare the samples for analysis, 5.7 cm^2 of each sample was dissolved in 2 mL milli-Q water and sonicated for 30 mins at room temperature. The extract was filtered using a Millex-GP 33 mm diameter hydrophilic syringe filter with a pore size of 0.22 μm (Millipore UK Limited, Watford, U.K.) and made up to a final volume of 2.5 mL.

Figure 6.2. Image to show the atmospheric observation tower at the Bachok Marine and Atmospheric Research Station.

6.2.4 Chromatographic analysis

Chromatographic analysis was carried out using an ICS-110 integrated IC system equipped with an AS-DV autosampler (Dionex Corporation, CA, United States). The column configuration used for anion-exchange consisted of an IonPac AG14A guard column (4 × 50 mm) and an IonPac AS14A analytical column (4 × 250 mm). Cation exchange chromatography was performed using an IonPac CG12A guard column (4 × 50 mm) and an IonPac CS12A analytical column (4 × 250 mm). ASRS 300 and CSRS 300 self-regenerating suppressors (4 mm) were used for anion- and cation-exchange respectively. All columns and suppressors were supplied from Dionex Corporation. The system used a DS6 heated conductivity cell for ion detection. A summary of the separation methods for anion and cation chromatography is provided in Table 6.2. All data obtained was analysed using the Chromeleon v7.1 software package.

Table 6.2. Method parameters used for both anion and cation chromatography.

method parameter	anion-exchange	cation-exchange
run time	18 min	15 min
flow type	isocratic	Isocratic
flow rate	1 mL min^{-1}	1 mL min^{-1}
injection volume	100 µL	100 µL
data collection rate	5 Hz	5 Hz
column temperature	30 °C	30 °C
suppressor current	45 mA	59 mA

6.2.5 Backward air mass trajectories

10-day backward air mass trajectories arriving at the sampling site were run every 3 hours throughout the entire measurement period. A receptor height of 10 m was chosen to represent the measurements made on the sampling tower. The trajectories were computed by D. Carslaw using the HYSPLIT model,[298] and the data was analysed using the openair package in RStudio.[299-300]

6.2.6 Additional data

Meteorological data was accessed from the NOAA Integrated Surface Database.[301] The data was taken from measurements made at the nearest meteorological station, which is approximately 23 km away from the site at the Sultan Ismail Petra Airport (6.17208° N, 102.29288° E). Hourly measurements of wind direction, wind speed, temperature, pressure, dew point and relative humidity were obtained. SO_2 measurements were made by the University of East Anglia at the Bachok observation tower using a Thermo Scientific Model 43i SO_2 analyser.

6.3 Results and discussion

6.3.1 Method validation

Using isocratic elution methods in both cation and anion-exchange mode, the target ions were successfully separated. Recovery tests were performed by spiking 5.7 cm^2 sections of filter paper with mixed standards (1 µg of each ion) and extracting the filter under the conditions described in section 6.2.3. Recovery levels and the associated errors are provided in Table 6.3 (all of the values have been corrected using procedural blanks).

Table 6.3. Recovery levels and %RSD$_{rec}$ of the target ions (extracted from the filters by sonication in water[a] and analysed by ion chromatography).

ion	% recovery	%RSD$_{rec}$
Cl^-	79.5	2.9
NO_2^-	81.5	3.2
NO_3^-	78.8	5.3
PO_4^{3-}	98.2	5.6
SO_4^{2-}	80.4	7.9
$CH_3SO_3^-$	74.5	2.8
$C_2O_4^{2-}$	82.5	2.9
Na^+	87.3	6.0
NH_4^+	80.0	4.6
K^+	78.3	5.3
Mg^{2+}	83.3	4.8
Ca^{2+}	123.3	7.6

[a]Filter extraction: ultrasonication in 2mL milli-Q water (30 min, room temperature) and filtration (0.22 µm pore size).

As shown in Table 6.3, the recovery levels ranged from 74.5% to 98.2% for the target anions, and 78.3% to 87.3% for the target cations, with the exception of Ca^{2+} where a recovery level of 123.3% was calculated. %RSD remained below 8% for recovery of all of the ions. In general the recovery levels of the target ions were lower than the levels calculated in Chapter 3 (section 3.3.2.1, Table 3.6 and Table 3.7). The reduced efficiency is thought to be due to the fact that a syringe with less suction was used to separate the aqueous extract from the sonicated filter paper. The recovery of Ca^{2+} should not exceed 100% and may have been due to errors associated with blank correcting the data for levels of Ca^{2+} already present in the blank filter. For example, it is possible that the amount of calcium present on the blank filters prior to spiking was not always consistent, and the background levels of Ca^{2+} on the filters used for spiking were higher than the levels on the procedural blank filters. The other possibility for this result is that Ca^{2+} contamination occurred at some stage during the recovery tests. All of the reported ion concentrations in this study have been corrected for

procedural blanks, and Table 6.4 provides a summary of the blank contribution of each ion; the average contribution was 18.5% during the sampling period.

Table 6.4. Procedural blank peak areas for each ion (μS min^{-1}) and average blank contribution to field samples over the entire sampling period.

ion	blank peak area / μS min^{-1}	average blank contribution / %
Cl^-	3.31×10^{-3}	2.7
NO_2^-	not detected	0
NO_3^-	6.19×10^{-3}	7.6
PO_4^{3-}	2.38×10^{-2}	52.0
SO_4^{2-}	1.31×10^{-2}	1.0
$CH_3SO_3^-$	not detected	0
$C_2O_4^{2-}$	not detected	0
Na^+	6.51×10^{-1}	53.8
NH_4^+	2.03×10^{-2}	4.9
K^+	1.31×10^{-2}	12.5
Mg^{2+}	3.76×10^{-2}	26.1
Ca^{2+}	5.21×10^{-2}	34.0

The main instrumental parameters of the IC system were evaluated and are described in Table 6.5. The intra-day precision associated with both retention times and peak area was assessed by running triplicate calibration curves of prepared standard solutions on three consecutive days. The $\%RSD_{ins}$ for retention time ranged from 0.13 to 0.72% depending on the ion, and average $\%RSD_{ins}$ for peak area was 4.2% for cations and 12.8% for anions. Instrumental LODs and LOQs were calculated using the same method as described in Chapter 2 (section 2.3.2). The filters were spiked with 5 ng of each cation and 25 ng of each anion. For anion-exchange chromatography LODs and LOQs were in the range 5.5 – 21.0 ng and 25.3 – 144.2 ng respectively. The LODs ranged from 0.5 to 2.1 ng and the LOQs ranged from 2.5 to 6.1 ng for cation exchange chromatography. In summary, the described method provided an accurate way to quantify water-soluble ions in atmospheric aerosol.

Table 6.5. Instrumental parameters and associated errors for the IC.

ion	RT range / mins	RT %RSD	Area %RSD	LOD / ng	LOQ / ng
Cl^-	4.97 - 5.00	0.16	7.97	9.61	46.01
NO_2^-	5.86 - 5.89	0.15	22.36	5.47	25.25
NO_3^-	8.16 - 8.31	0.46	13.31	8.70	36.18
PO_4^{3-}	11.23 - 11.38	0.28	14.40	13.96	42.91
SO_4^{2-}	13.61 - 13.70	0.18	8.02	20.98	66.46
$CH_3SO_3^-$	4.50 - 4.53	0.13	10.26	6.16	29.47
$C_2O_4^{2-}$	15.72 - 15.85	0.21	13.58	9.99	144.18
Na^+	4.10 - 4.14	0.29	3.32	1.01	2.51
NH_4^+	4.64 - 4.68	0.23	4.38	0.77	2.96
K^+	5.71 - 5.77	0.27	3.55	1.65	2.79
Mg^{2+}	8.84 - 9.06	0.72	4.73	2.11	3.67
Ca^{2+}	10.99 - 11.28	0.72	5.32	0.47	6.14

6.3.2 Bachok demonstration campaign

The measurements were carried out at the Bachok Marine and Atmospheric Research Station between 18/01/2014 and 06/02/2014, during an instrument demonstration campaign that was set up to assess the potential of the new research station. The atmospheric observation tower is located within 100m of the South China Sea on the eastern coast of Peninsular Malaysia. The site is located in the state of Kelantan, which along with Terengganu, Pahang and the district of Mersing in Johor, is part of the East Coast Economic Region (ECER). A socio-economic development programme has been set up in this region with the aim of creating an equitable distribution of wealth in Malaysia, as part of the national aspiration to become a developed high income nation by 2020.[302] The Bachok district is a rural area, and the primary economic activity comes from tobacco and kenaf plantations. Other agrarian activities in the wider Kelantan district include the production of rice and rubber, as well as additional economic activities such as livestock rearing and fishing.[303]

The 10-day backward air mass trajectories arriving at the measurement site during the demonstration campaign are shown in Figure 6.3. During the winter months, a strong anticyclone system known as the Siberian High can bring north-easterly onshore winds to

the east coast of Peninsular Malaysia. Some of the air masses had a significant continental influence from highly industrialised countries such as China, Japan, Taiwan and North and South Korea, whilst other air masses had a stronger marine influence from both the East China Sea and the South China Sea.

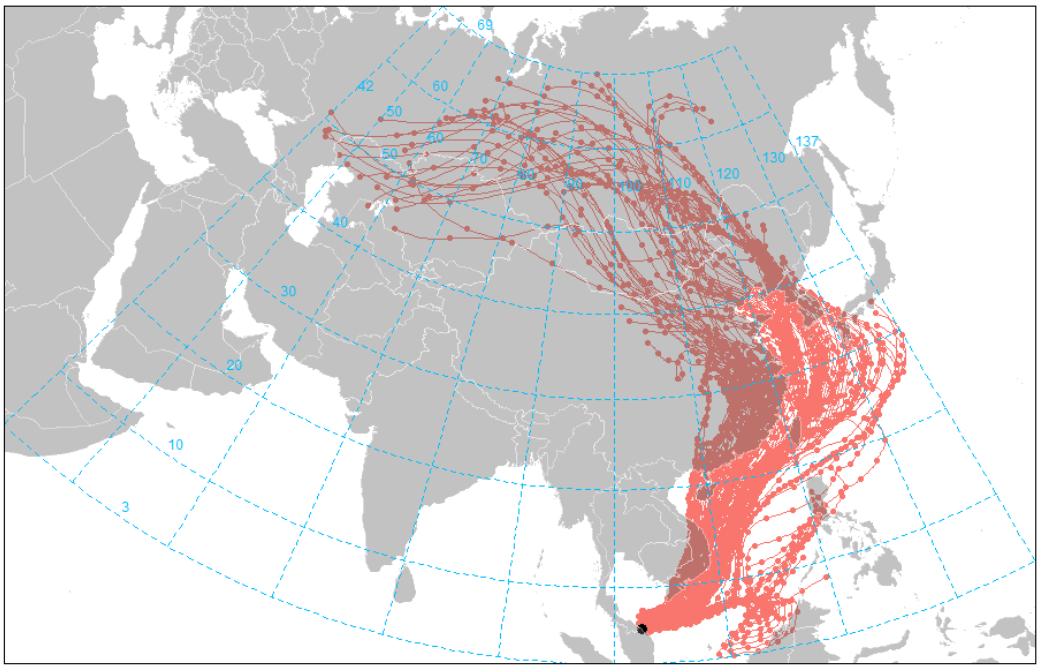

Figure 6.3. 10-day HYSPLIT backward air mass trajectories centred on the Bachok Marine and Atmospheric research station between 18-01-2014 and 07-02-2014.

Although there was no reliable meteorological data obtained at the measurement site during the demonstration campaign, it was possible to consider data from a nearby meteorological station, located approximately 23 km away at the Sultan Ismail Petra airport (Figure 6.4).

Whilst the meteorological data from the airport will not be exactly representative of the measurement site, the patterns in wind direction are consistent with observations made by the field scientists during the campaign. Figure 6.5 shows how wind speed and wind direction conditions varied over a typical 24-hour period during the measurement campaign (01-02-2014). Gentle south westerlies coming from the land (Peninsular Malaysia) were observed between 03:00 and 11:00 local time on 01-02-2014 (Figure 6.5, upper right panel). As shown in the lower left panel of Figure 6.5 a dramatic shift in wind direction occurred at approximately midday, and until approximately 20:00 a strong onshore breeze from the north east (South China Sea) was observed. From 21:00 to the early hours of each morning, a calmer sea breeze predominantly from the east was seen. This daily pattern was observed

throughout the majority of the campaign, with the exception of three 24-hour periods (19-20, 23-24, 26-27 Jan), when the sea breeze dominated throughout the entire day and night.

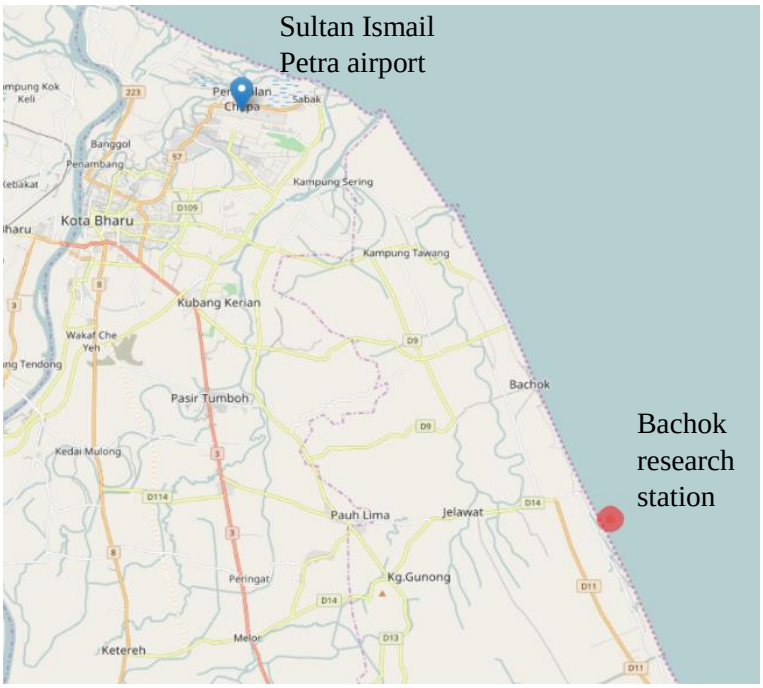

Figure 6.4. Map to show the location of the Sultan Ismail Petra airport, which is located 23 km away from the Bachok research station.

A previous study by Dunmore *et al.* describes the development of a new combined heart-cut GC and GC×GC instrument (GC-GC×GC) used to accurately measure C_5-C_{13} VOC species with a wide range of functionalities.[292] Hourly VOC measurements were conducted at the remote Bachok measurement site, and the development of a sea breeze at approximately midday dramatically influenced the diurnal profiles of the measured species. In the morning, when the air being sampled was coming over the land, very high levels of NO, NO_2 and anthropogenic VOCs such as toluene, *n*-pentane and C_{10} aliphatic species were observed; the main source of these species was local burning of waste.[292] When the sea breeze developed at approximately midday, the concentrations of these species dropped significantly.

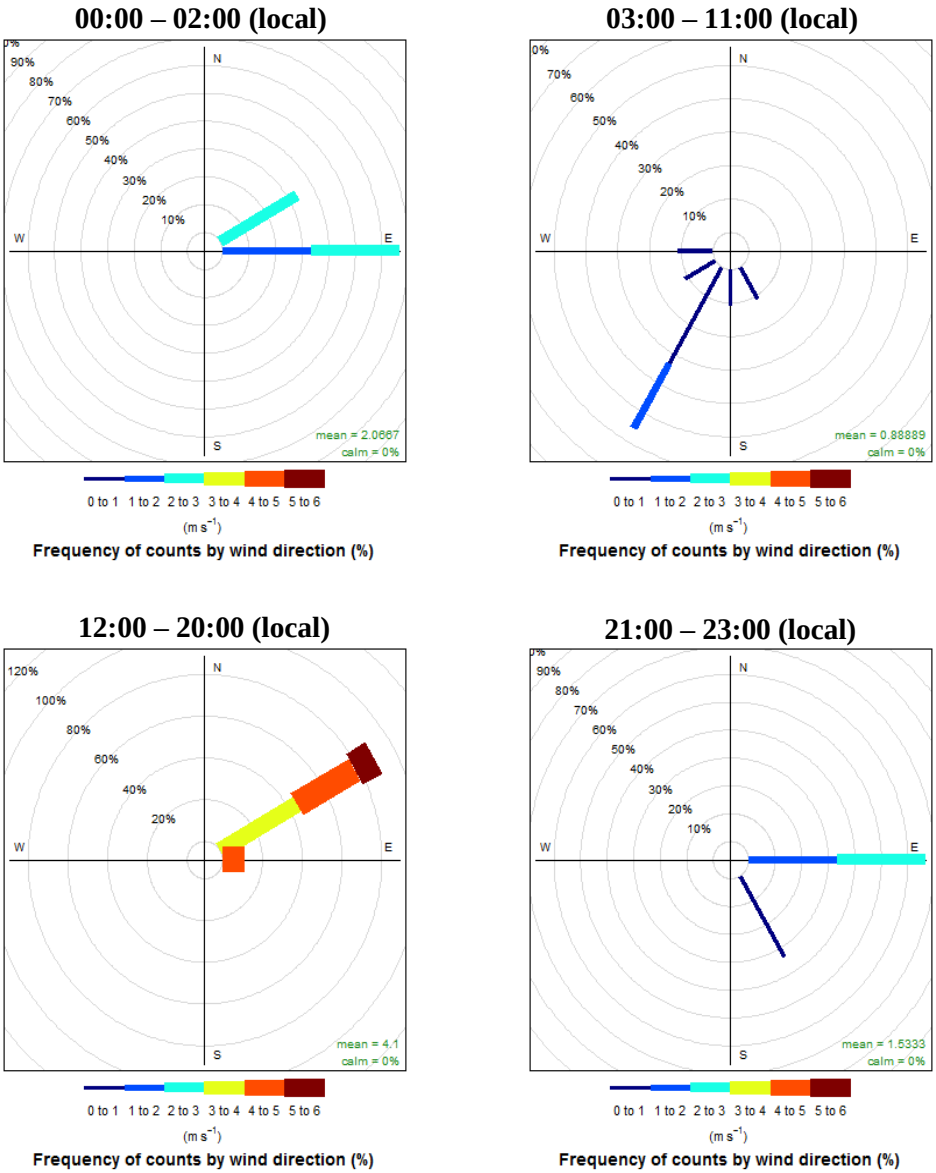

Figure 6.5. Wind rose plots to show the variation in wind speed and wind direction over a typical 24-hour period during the measurement campaign (01-02-2014).

6.3.3 Composition of water-soluble ions in atmospheric aerosol

6.3.3.1 Aerosol composition and determination of non-sea salt and sea salt components

Table 6.6 shows the mean and maximum water-soluble ion concentrations measured throughout the campaign, and Figures 6.6 and 6.7 show time series for all of the ions measured in the aerosol. The total concentration of measured water-soluble ions in the $PM_{2.5}$ during the campaign ranged from 8.06 to 27.0 μg m^{-3}, with an average concentration of 16.2 μg m^{-3}. A study of particle mass and number concentration at the Bachok measurement

site was carried out by Dominick *et al.* and reported that the average $PM_{2.5}$ and PM_{10} concentrations between 09-01-2014 and 24-03-2014 were 30 μg m^{-3} and 31 μg m^{-3} respectively.[293] This data suggests that the measured water-soluble ions in this study made up approximately half of the total aerosol, and the remainder was likely comprised of a range of organic species. During the measurement campaign, the PM levels in the region were of concern to human health, and regularly exceeded the WHO recommended limit of 25 μg m^{-3}.[304]

Table 6.6. Mean and maximum ion concentrations measured throughout the demonstration campaign. Average % mass contribution to the total ions and % of samples in which each target ion was found are also included.

ion	Mean [ion] / μg m^{-3}	Maximum [ion] / μg m^{-3}	Mean % mass of total measured ion content	%Qt[a]	%RSD[b]
SO_4^{2-}	10.7	20.8	65.6	100	11.2
NH_4^+	1.69	4.73	10.4	100	6.38
Na^+	1.13	2.60	6.95	100	6.88
Cl^-	0.67	2.38	4.14	100	8.49
NO_3^-	0.61	1.52	3.76	100	22.6
$C_2O_4^{2-}$	0.42	0.65	2.57	97	13.9
PO_4^{3-}	0.36	2.34	2.22	93	15.4
K^+	0.38	0.67	0.67	100	6.35
Ca^{2+}	0.10	0.35	0.64	100	9.26
Mg^{2+}	0.10	0.21	0.61	100	6.72
$CH_3SO_3^-$	0.08	0.22	0.47	67	10.6
NO_2^-	0.05	0.16	0.33	23	14.3
Total	*16.2*	*27.0*	*n/a*	*n/a*	*n/a*

[a]Percentage of samples in which the target ion was above the LOQ. [b]Total error associated with each ion.

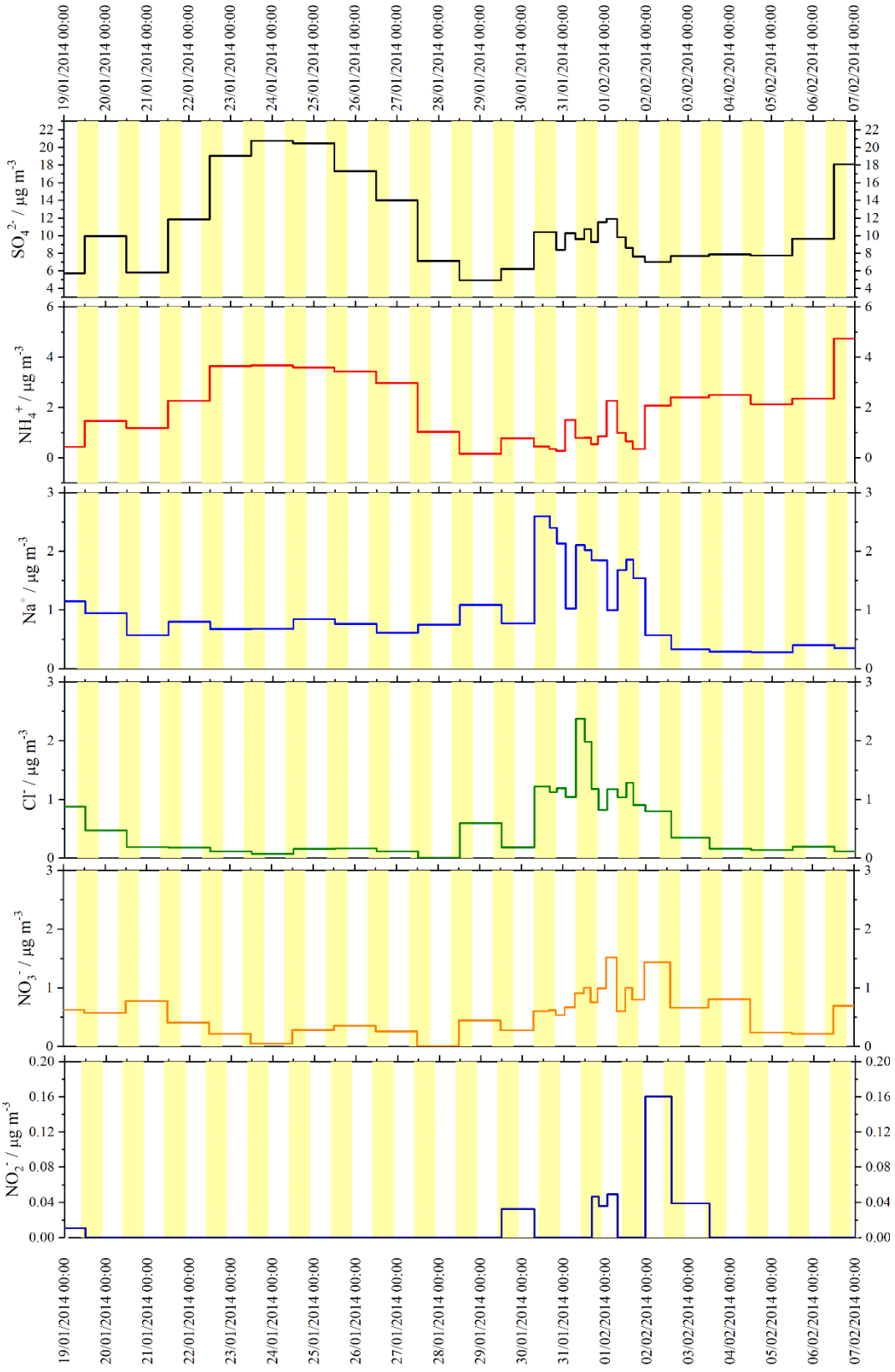

Figure 6.6. Time series of SO_4^{2-}, NH_4^+, Na^+, Cl^-, NO_3^- and NO_2^- concentration (µg m^{-3}) during the Bachok demonstration campaign (18-01-2014 to 07-02-2014).

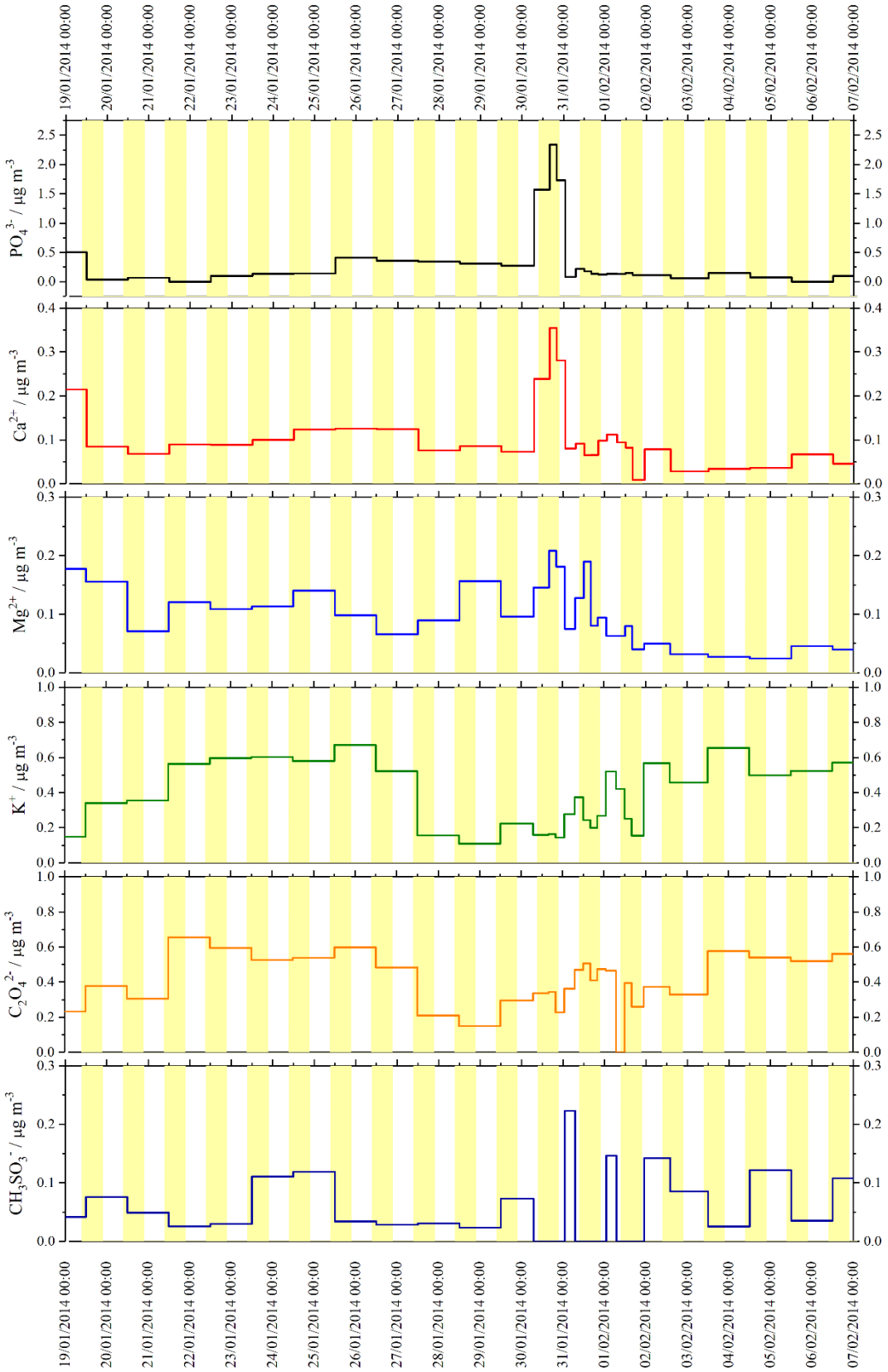

Figure 6.7. Time series of PO_4^{3-}, Ca^{2+}, Mg^{2+}, K^+, $C_2O_4^{2-}$ and $CH_3SO_3^-$ concentration (µg m^{-3}) during the Bachok demonstration campaign (18-01-2014 to 07-02-2014).

As the composition of the water-soluble ions present in aerosol collected at the Bachok site was influenced by both marine and continental sources, it is useful to make an estimation of non-sea salt (nss) and sea salt (ss) components, as shown in Equations 6.1 – 6.4. As total Na^+ and total Ca^{2+} are known, and the mean Na^+/Ca^{2+} ratio in the crust and mean Ca^{2+}/Na^+ ratio in seawater have been estimated by Bowen *et al.* as 1.78 *w/w* and 0.038 *w/w* respectively, it is possible to solve the equations simultaneously for $ssNa^+$, $nssNa^+$, $ssCa^{2+}$ and $nssCa^{2+}$.[305-306] The resulting estimate of $ssNa^+$, which can be used as a sea spray marker, can also be used to predict the contribution of $nssSO_4^{2-}$ and $nssK^+$ in the aerosol, as shown in Equations 6.5 and 6.6.

$$ssNa^+ = Na^+ - nssNa^+ \tag{6.1}$$

$$nssNa^+ = nssCa^{2+} \cdot \left(\frac{Na^+}{Ca^{2+}}\right)_{crust} \tag{6.2}$$

$$nssCa^{2+} = Ca^{2+} - ssCa^{2+} \tag{6.3}$$

$$ssCa^{2+} = ssNa^+ \cdot \left(\frac{Ca^{2+}}{Na^+}\right)_{sea\ water} \tag{6.4}$$

$$nssSO_4^{2-} = SO_4^{2-} - 0.253 \cdot ssNa^+ \tag{6.5}$$

$$nssK^+ = K^+ - 0.037 \cdot ssNa^+ \tag{6.6}$$

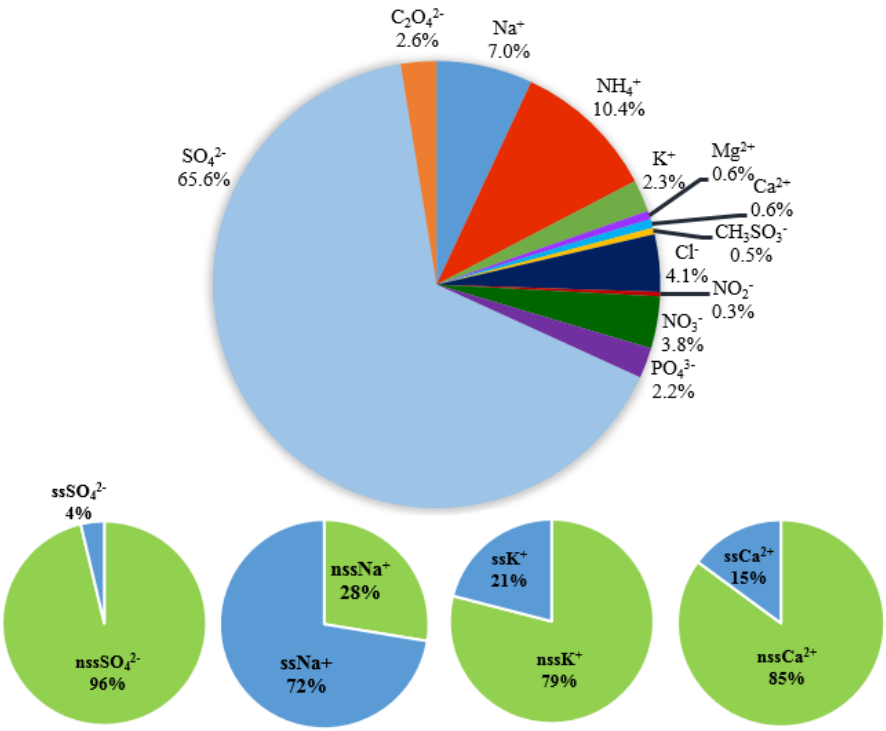

Figure 6.8. Pie chart to show the average composition of water-soluble ions in aerosol at the Bachok research station (upper panel) and pie charts to show the percentage of non-sea salt and sea salt fractions of Na^+, SO_4^{2-}, K^+, Ca^{2+} (lower panel, left to right).

Figure 6.8 shows a series of pie charts to summarise the average composition of water-soluble ions in atmospheric aerosol, and the distribution of non-sea salt and sea salt components. The results show that the water-soluble ion fraction of the aerosol is dominated by sulfate (SO_4^{2-}), which on average made up 65.6% of the total ion content by mass. NH_4^+ and NO_3^- concentrations were significantly lower, with mean concentrations of 1.69 and 0.61 μg m^{-3} respectively. Na^+ and Cl^- made up 11.1% of the total ion content, and 75% of the measured Na^+ was attributed to $ssNa^+$. The concentrations of $nssK^+$ and $nssCa^{2+}$ were 0.30 and 0.09 μg m^{-3} respectively; these ions can be used as tracers for biomass burning ($nssK^+$) and atmospheric dust ($nssCa^{2+}$). NO_2^- and $CH_3SO_3^-$ were the least abundant ions, with average concentrations of 0.05 and 0.08 μg m^{-3}. The two ions were only observed in a subset of samples; $CH_3SO_3^-$ was quantified in 67% of samples and quantification of NO_2^- was only achieved in 23% of samples.

6.3.3.2 Sources and formation of sulfate, SO_4^{2-}

The average SO_4^{2-} concentration during the measurement campaign was 10.7 μg m^{-3}, with a maximum concentration of 20.8 μg m^{-3} recorded. The formation of sulfate in the particle phase occurs when emitted SO_2 is oxidised by OH in the gas phase, or by O_3 or H_2O_2 in the aqueous phase.[307] The most dominant anthropogenic sources of SO_2 include fuel and industrial emissions, as well as open biomass burning. Natural sources of SO_2 arise from both the oxidation of biogenic dimethyl sulphide (DMS) and volcanic activity.[307]

By using $ssNa^+$ as a sea spray marker to determine non-sea salt and sea salt components of the aerosol, it was found that 96% of the measured SO_4^{2-} was $nssSO_4^{2-}$, and only 4% of the SO_4^{2-} was from sea salt. As a potential source of $nssSO_4^{2-}$ is DMS emissions from marine biota, and the main atmospheric source of MSA is the oxidation of DMS, it is possible to use the $MSA^-/nssSO_4^{2-}$ ratio as a tracer to assess the contribution of biogenic sources to $nssSO_4^{2-}$ in the atmosphere.[308] In this study, MSA^- concentrations ranged from 0.02 to 0.22 μg m^{-3}, with an average concentration of 0.08 μg m^{-3}. As a result, the $MSA^-/nssSO_4^{2-}$ ratio ranged from 2.5×10^{-4} to 2.3×10^{-3}, with an average value of 7.8×10^{-4}. These values are very low compared to $MSA/nssSO_4^{2-}$ ratios recorded at remote sites; for example, the mean $MSA/nssSO_4^{2-}$ mass ratio recorded on Fanning Island and American Samoa was 0.065.[309] The considerably lower ratios recorded in Bachok suggest that the majority of $nssSO_4^{2-}$ at the site originates from anthropogenic sources.

As previously discussed, a study by Dunmore *et al.* revealed that levels of NO_x and anthropogenic VOCs at the Bachok measurement site were significantly higher when the air being sampled had passed over land, and dropped significantly at midday when a sea breeze developed.[292] This indicated that air quality in Bachok is influenced by local sources of

pollution, such as vehicle emissions and burning domestic waste. A pollution rose diagram is shown in Figure 6.9 to show the relationship between SO_2 and wind direction. SO_2 concentrations below 10 ppb have been excluded in order to investigate the wind conditions when the spikes in SO_2 concentration occur in more detail. It is clear that the majority of higher SO_2 events are recorded when the air has passed over the land; this provides further evidence that the site is influenced by local sources of pollution. Despite this, there is no obvious relationship between SO_2 and SO_4^{2-} concentration, or between SO_4^{2-} concentration and wind direction. This is probably because it takes time for SO_2 to oxidise to SO_4^{2-}, and that the sulfate fraction of the aerosol is more heavily influenced by long-range transport of aged emissions from Southeast Asia. To investigate this further, the backward air mass trajectories were coloured by the concentration of SO_4^{2-}, as shown in Figure 6.10. The plot clearly shows that the SO_4^{2-} content of the aerosol is highest (*ca.* 14 – 20 µg m^{-3}) when the site is influenced by continental air masses from regions of Southeast Asia, and lowest when the air masses have a more significant marine influence. With this information in mind, it was possible to perform cluster analysis on the back trajectories; this type of analysis groups air masses with a similar origin together, which provides more information on pollutant species with similar chemical histories. Figure 6.11 shows the 10-cluster solution to back trajectories calculated for the Bachok site during the measurement campaign.

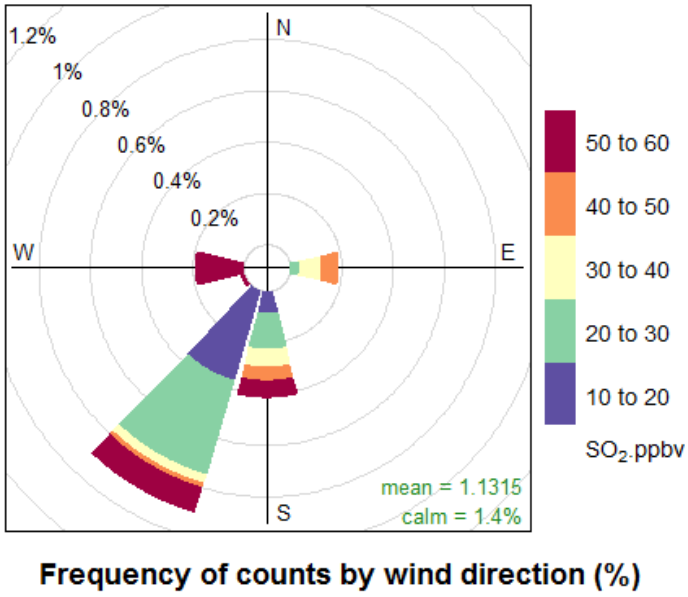

Figure 6.9. Pollution rose diagram to show the relationship between SO_2 levels above 10 ppb and wind direction at the Bachok measurement site.

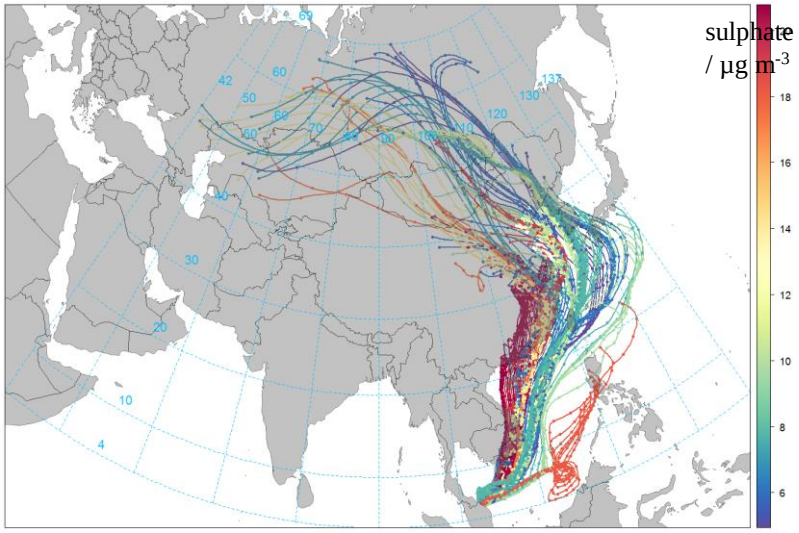

Figure 6.10. 10-day HYSPLIT back trajectories centred on the Bachok research station, between 18-01-2014 and 07-02-2014. The back trajectories are coloured by the concentration of SO_4^{2-} (µg m^{-3}).

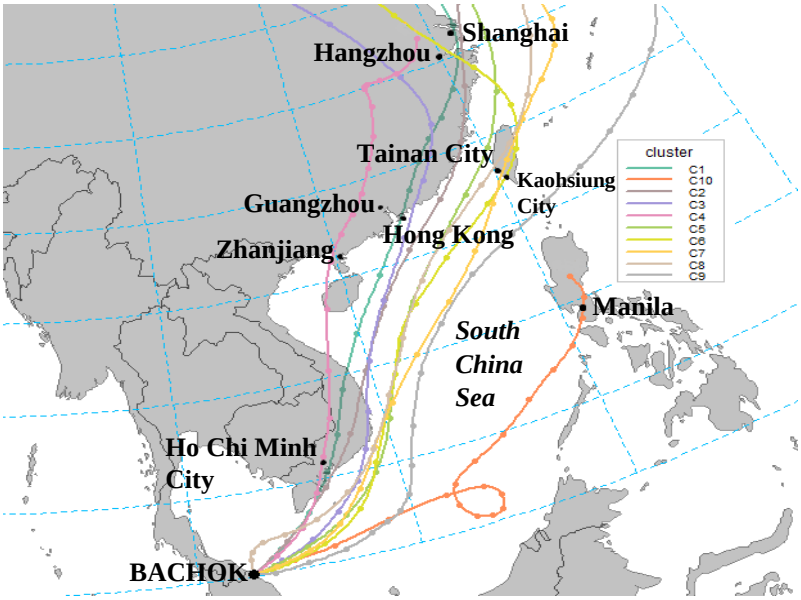

Figure 6.11. 10-cluster solution to back trajectories calculated for the Bachok research station during the measurement campaign.

The air masses associated with the lowest SO_4^{2-} content are represented by clusters 5 – 9 (Figure 6.11). Although air masses in clusters 6 – 8 experience some continental influence from Taiwan, the air masses mainly pass over the South China Sea before arriving at Bachok. However, background levels of SO_4^{2-} at the site when these air masses arrive are still relatively high, at approximately 5 to 11 µg m^{-3}. Air masses with the highest sulfate content (*ca.* 14 to 20 µg m^{-3}, clusters 1 – 4, 10) have passed over several highly industrialised regions, including megacities such as Shanghai, Guangzhou and Manila. Whilst air masses arriving

at Bachok from highly industrialised regions contain higher sulfate levels, the SO_4^{2-} concentration remains above 5 μg m^{-3} throughout the entire measurement period. This shows that the rural location is influenced by emissions from local sources of pollution, but also that continental anthropogenic species such as $nssSO_4^{2-}$ can be transported to the coastal measurement site, potentially perturbing marine background conditions en route.

6.3.3.3 Correlation of SO_4^{2-} with NH_4^+ and implications for aerosol acidity

Ammonium (NH_4^+) was the second most abundant ion in the aerosol; on average NH_4^+ made up 10.4% of the total ion content, and mean and maximum concentrations were 1.69 and 4.73 μg m^{-3} respectively. Strong positive correlation between SO_4^{2-} and NH_4^+ was observed ($R = 0.76$, $p < 0.001$). A similar observation was reported by Keywood *et al.*, when they investigated the sources of particles contributing to haze in the Klang Valley, Malaysia.[310] The strong relationship between these species is due to the neutralisation of SO_4^{2-} by NH_4^+. The results show the occurrence of secondary aerosol formation, resulting from the oxidation of SO_2 to SO_4^{2-} in the atmosphere, followed by subsequent uptake of NH_3, which is ubiquitous in the atmosphere. It is likely that NH_3 emissions in the rural Bachok region come predominantly from agricultural practices such as animal husbandry, fertilizer use and agricultural waste burning. The measurement site is possibly influenced by other key NH_3 sources included in the Emissions Database for Global Atmospheric Research (EDGAR), such as direct soil emissions and road transport, but it is difficult to ascertain which sources are most dominant, as the database does not provide local/ regional scale NH_3 emissions data for Malaysia.[311]

The uptake of SO_4^{2-} is preferential to the uptake of NO_3^- because sulfuric acid has a lower vapour pressure than nitric acid, and aqueous or solid $(NH_4)_2SO_4$ is the preferred form of sulfate.[8] The average NH_4^+/SO_4^{2-} molar ratio is 0.81, which indicates that there was insufficient gaseous NH_3 in the atmosphere to neutralise SO_4^{2-}. Although measurements of the total amounts of ammonia and sulfate in the gas, aqueous and solid phase would provide a better prediction of the aerosol acidity, the results presented in this study indicated that an ammonia-poor regime exists, and the aerosol is likely to be acidic. In these scenarios, the NH_3 partial pressure is low, and therefore the NH_3-HNO_3 partial pressure product will also be low, meaning that the concentrations of ammonium nitrate are low or zero.[8] This hypothesis can be supported by the fact that NO_3^- concentrations in this study were very low and ranged from 0.005 to 1.52 μg m^{-3}. As a result, NO_3^- made up a significantly smaller

fraction of the total ion content compared to SO_4^{2-}; average percentage composition of the total ion content was 3.8% for NO_3^- and 65.6% for SO_4^{2-}.

To estimate proton loading in atmospheric particles, the strong acidity approach can be used, as shown in Equation 6.7. This approach assumes that any deficit in measured cation charge compared to measured anion charge can be attributed to H^+. Total anion and total cation equivalents can be estimated using Equations 6.8 and 6.9.

$$strong\ acidity\ (eq.m^{-3}) = \sum anion\ equivalents - \sum cation\ equivalents \quad (6.7)$$

$$\sum anions = \frac{SO_4^{2-}}{48} + \frac{NO_3^-}{62} + \frac{Cl^-}{35.5} + \frac{PO_4^{3-}}{31.6} + \frac{C_2O_4^{2-}}{44} + \frac{NO_2^-}{46} + \frac{CH_3SO_3^-}{95} \quad (6.8)$$

$$\sum cations = \frac{Na^+}{23} + \frac{NH_4^+}{18} + \frac{K^+}{39} + \frac{Mg^{2+}}{12} + \frac{Ca^{2+}}{20} \quad (6.9)$$

As shown in Figure 6.12, the strong acidity values in this study ranged from 0.03 to 0.19 ueq. m^{-3}, with an average value of 0.11 ueq. m^{-3}. The positive strong acidity values provide an initial indication that the aerosol is acidic and allows us to estimate the proton loading (average H^+ = 0.11 µg m^{-3}), but it is not possible to accurately predict aerosol pH without the liquid water content of the aerosol.

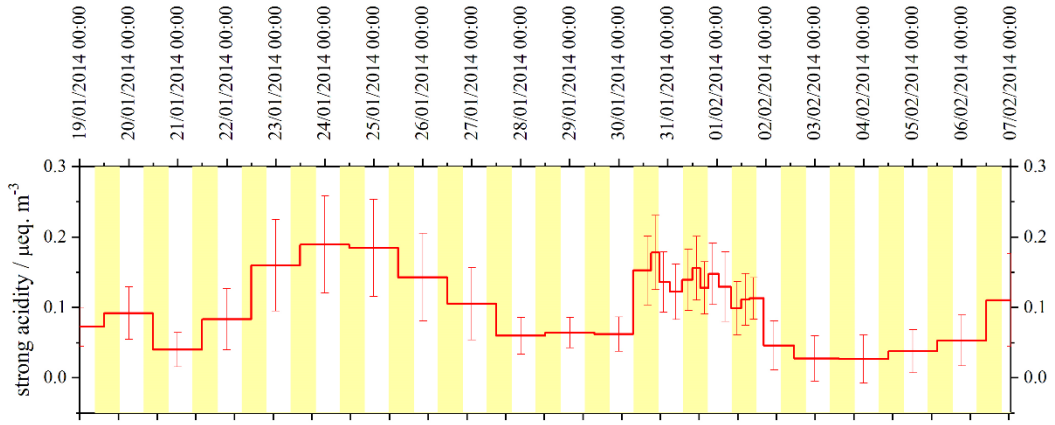

Figure 6.12. Particle strong acidity and associated error predictions for the aerosol collected during the Bachok 2012 measurement campaign.

To obtain error bars for the strong acidity predictions (Figure 6.12), H^+_{max} and H^+_{min} were calculated according to Equations 6.10 and 6.11 respectively. For H^+_{max} the anions were adjusted up to within their uncertainties (*i.e.* +%RSD_{tot}) and the cations were adjusted down to within their uncertainties (*i.e.* -%RSD_{tot}).[312] For H^+_{min} the anions were adjusted down and the cations were adjusted up. %RSD_{tot} was estimated by combining the error of the recovery

process for each ion (%RSD$_{rec}$, Table 6.3) and the error of the instrument for each ion (%RSD$_{ins}$, Table 6.5).

$$H^+_{max} = \sum max.\, anion\ equivalents - \sum min.\ \ cation\ equivalents \quad (6.10)$$

$$H^+_{min} = \sum min.\, anion\ equivalents - \sum max.\, cation\ equivalents \quad (6.11)$$

In most cases, H^+_{min} remains above zero. However, on 03-02-2014 and 04-02-2014, negative H^+_{min} values are calculated, which are physically implausible.[312] These results highlight the possible sources of error associated with the strong acidity approach for estimating aerosol acidity. For example, Hennigan *et al.* report that organic acids (which are excluded from this study, with the exception of MSA and oxalic acid) can have an important influence on aerosol acidity, especially at relatively low acidities where organic acids dissociate and contribute to the ion balance.[313] Furthermore, they can form salt complexes with inorganic species *e.g.* ammonium oxalate. Neglecting organic acids, as well as other species such as HCO_3^- and basic amines, will lead to inaccuracies in the calculated H^+. Whilst thermodynamic models such as ISOROPPIA or E-AIM can be used as alternative methods for predicting aerosol pH, these methods generally require an input of relative humidity and temperature and produce better results when gas phase measurements such as NH_3 and HNO_3 are available. It is not possible to use these models in this study as sufficient data is not available.

Acidic particles can have detrimental effects on human health, air quality, and the health of aquatic and terrestrial ecosystems.[313] For example, Gwynn *et al.* performed a time-series analysis of acidic PM and daily mortality and morbidity in Buffalo, New York; several significant pollutant-health effect associations were identified, the strongest being the correlation between atmospheric SO_4^{2-} concentration and respiratory hospital admissions.[314] Deposition of acidic gases and particles can affect the acid-neutralizing capacity of freshwater ecosystems, leading to biological damage and loss of invertebrates in worst-case scenarios.[315] The extent to which sulfate aerosol is neutralized also has important implications for aerosol radiative forcing and ice cloud nucleation.[316] For example, estimates of the radiative forcing for anthropogenic sulfate aerosol range from -0.26 to -0.82 W m^{-2}.[317-319] Furthermore, particle acidity can influence various atmospheric chemical processes, including SO_2 oxidation, halogen chemistry, and the partitioning of ammonia, nitric acid and organic acids.[313] In summary, whilst some of the risks associated with aerosol acidity in Bachok originate from local sources of pollution, it is possible that people living in these

rural areas are also exposed to an additional risk, as the region is sensitive to the effects of industrialisation further afield in Southeast Asia.

6.3.3.4 Sources and formation of oxalate, $C_2O_4^{2-}$

Oxalic acid is the most abundant dicarboxylic acid in tropospheric aerosol.[320] This major water-soluble organic component can alter the hygroscopicity of aerosols,[321] and can either act as CCN, or reduce the surface tension of particles to form CCN.[322-324] In this study, oxalate made up 2.57% of the total measured water-soluble ion content. The average concentration was 0.42 μg m^{-3}, and throughout the measurement period the concentration ranged from 0.15 to 0.65 μg m^{-3}. Interestingly, such levels of oxalate in atmospheric aerosol are more comparable to typical oxalate levels found in urban PM, despite the fact that the Bachok research station is located in a rural coastal region. For example, Freitas *et al.* report average oxalate concentrations in TSP at an urban site and a rural site in Londrina City, Brazil of 0.57 and 0.03 μg m^{-3} respectively.[325] Other reported oxalate concentrations in urban TSP include measurements of 0.10 – 0.48 μg m^{-3} in Shanghai (China),[326] 0.27 μg m^{-3} in Tokyo (Japan),[327] and 0.38 μg m^{-3} in Chiba (Japan).[328] Direct emissions of oxalate come from biomass burning and fossil fuel combustion,[326] and it can also form *via* secondary pathways such as homogenous photochemical oxidation of VOCs, and in-cloud and heterogeneous formation.[325]

In order to investigate possible sources and formation pathways, it is necessary to consider the correlation of oxalate with different atmospheric species. Jiang *et al.* report using NO_2^- as the indicator for vehicular emissions, $nssSO_4^{2-}$ and NO_3^- for secondary formation through different pathways, and K^+ for biomass burning.[326] In this study, there was a relatively strong correlation between oxalate and $nssSO_4^{2-}$ ($R = 0.60$, $p < 0.001$), suggesting a common formation pathway of the two species. It is well know that SO_4^{2-} forms *via* aqueous oxidation,[8] and modelling studies also suggest that aqueous chemistry is a large contributor of oxalate formation globally.[329] Furthermore, Carlton *et al.* report that whilst there are likely to be many sources of oxalate, oxidation of pyruvate in the aqueous phase is known to form oxalate at dilute (cloud-relevant) concentrations.[330] Tan *et al.* also state that aqueous acetate oxidation is a key source of oxalate.[331] A positive correlation between oxalate and NH_4^+ was also observed ($R = 0.66$, $p < 0.001$). A similar observation was reported by Jiang *et al.* in a study of aerosol oxalate in Shanghai.[326] Using size distribution data, they were able to propose that the correlation was due to the presence of ammonium oxalate in aerosol. In this study there is no size distribution data available, and therefore it is necessary to consider the fact that the correlation may be linked to the influence of sulfate on both NH_4^+ and oxalate in aerosol; NH_4^+ partitions to the aerosol from gaseous NH_3 in an attempt to neutralise acidic sulfate particles, whilst oxalate exhibits similar formation pathways to SO_4^{2-}.

A study carried out by Huang *et al.* in the urban area of Shenzhen (Southern China) reported that whilst good correlation of droplet oxalate with K^+ was observed ($R^2 = 0.75$), there was poor correlation between oxalate and K^+ in the condensation mode ($R^2 = 0.10$).[332] This implied that whilst biomass burning was probably not an important primary source of condensation mode oxalate, it is likely that biomass burning particles act as effective CCN, promoting in-cloud sulfate and oxalate formation. In this study, oxalate correlated strongly with $nssK^+$ ($R = 0.65$, $p < 0.001$). The oxalate/$nssK^+$ ratio was used to predict whether biomass burning was an important primary or secondary source of oxalate. The oxalate/$nssK^+$ ratio ranged from 0.49 to 0.99 during the Bachok demonstration campaign; these values were significantly higher than those found in aerosol directly emitted from vegetation fires in the Amazon Basin (0.02 – 0.10).[333] This information provided an initial indication that biomass burning is an important secondary source of oxalate in the Bachok region, rather than a significant primary source. A similar hypothesis was proposed by Huang *et al.*, who measured ambient $PM_{2.5}$ in an urban environment in the Pearl River Delta Region of China, and reported oxalate/K^+ ratios of 0.57 and 0.33 in the summer and winter respectively.[334] However, it is worth noting that whilst the higher ratios reported in both studies indicate that biomass burning is not a major primary source of oxalate, measurements of oxalate and K^+ in local biomass burning aerosols (rather than aerosol in the Amazon Basin) would provide a better indication of the source contribution by biomass burning.

There was no significant correlation observed between oxalate and NO_3^-, or between oxalate and NO_2^-. The lack of correlation with NO_3^- suggests that the two species do not have similar formation pathways, and that vehicle emissions are not an important secondary source of oxalate. It is also unlikely that vehicle emissions contribute to the primary sources of oxalate, due to the lack of correlation between oxalate and NO_2^-. However, NO_2^- was only detected in 7 out of the 30 samples collected, so it is difficult to ascertain whether there is a relationship between these two species or not.

6.3.3.5 Sea salt aerosol and factors affecting chloride depletion

On average, Na^+ and Cl^- contributed 7.0% and 4.1% to the total measured water-soluble ion content respectively, and 72% of the measured Na^+ was attributed to $ssNa^+$. The concentration of $ssNa^+$ ranged from 0.24 to 2.35 μg m^{-3}, whilst the concentration of Cl^- ranged from 0.003 to 2.38 μg m^{-3}. There was no correlation between $nssNa^+$ and Cl^-, but a strong positive correlation between $ssNa^+$ and Cl^- was observed ($R = 0.83$, $p < 0.001$). Figure 6.13 shows time series plots for $ssNa^+$ and Cl^-.

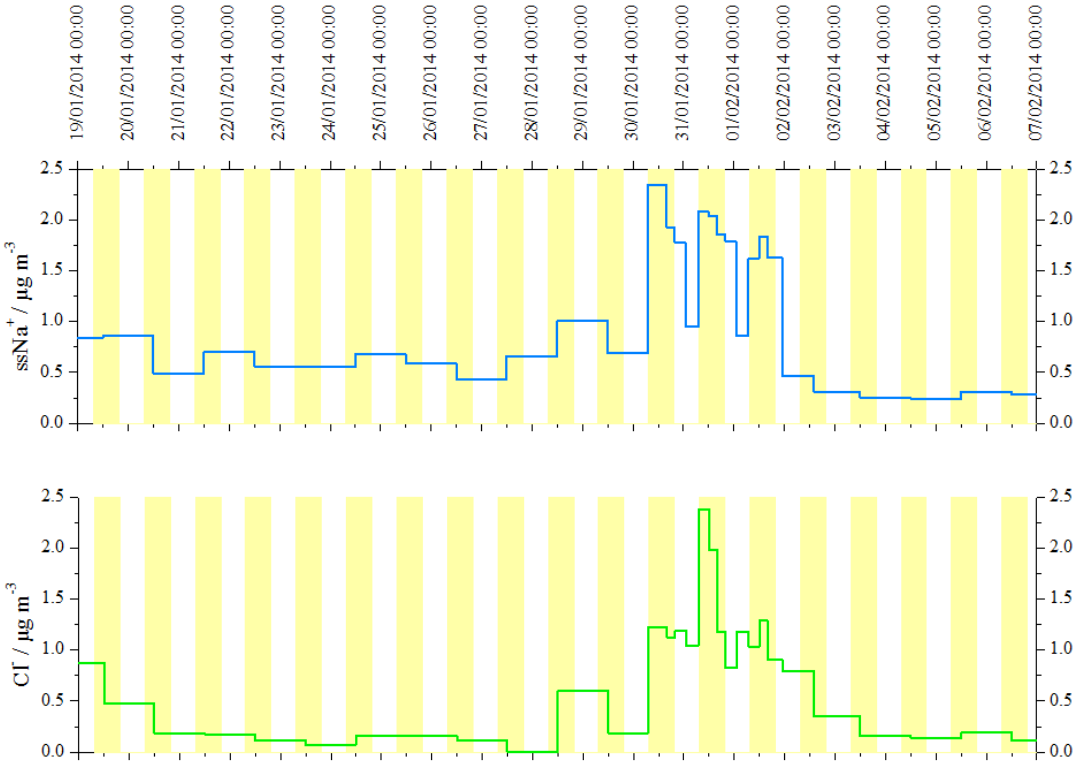

Figure 6.13. Time series of $ssNa^+$ and Cl^- concentration (µg m^{-3}) during the Bachok demonstration campaign (18-01-2014 to 07-02-2014).

During the measurement period, the $Cl^-/ssNa^+$ molar ratio ranged from 0.003 to 1.10 with an average value of 0.40. All of the ratios recorded were lower than that of bulk seawater (1.18).[306] Figure 6.14 shows backward air mass trajectories from the Bachok site, coloured by the $Cl^-/ssNa^+$ molar ratio. The plot shows that the lowest $Cl^-/ssNa^+$ ratios are found when continental air masses from highly industrialised countries such as China and Vietnam arrive at the site, and higher $Cl^-/ssNa^+$ ratios are found when marine air masses from the South China Sea arrive.

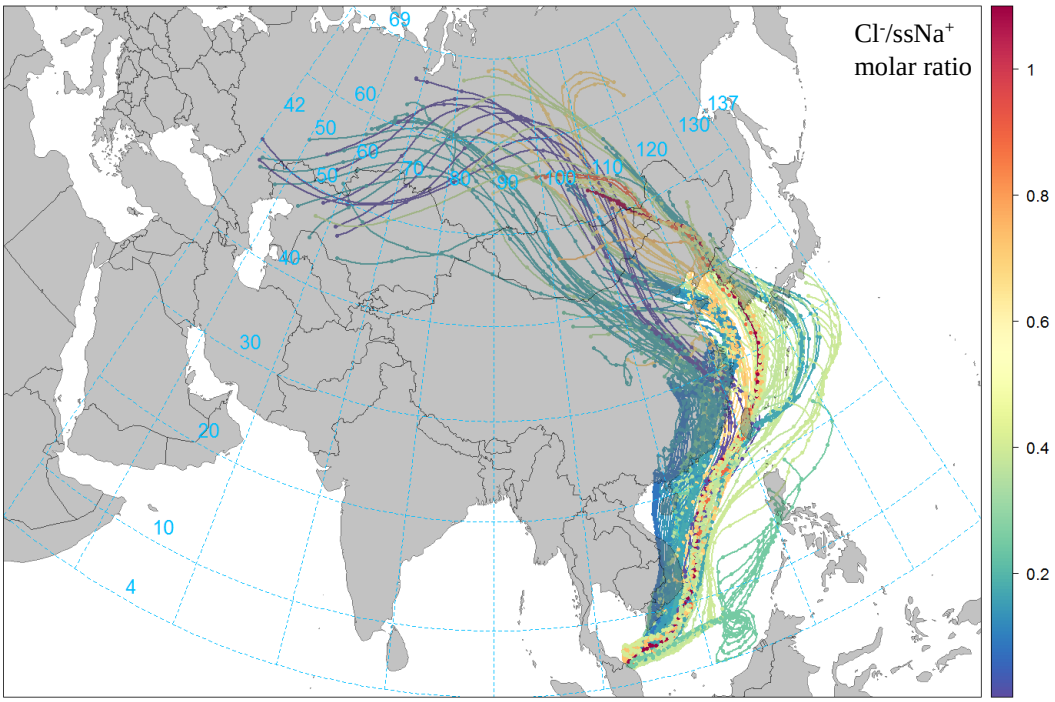

Figure 6.14. 10-day HYSPLIT back trajectories centred on the Bachok research station, between 18-01-2014 and 07-02-2014. The back trajectories are coloured by the $Cl^-/ssNa^+$ molar ratio.

The relationship between $Cl^-/ssNa^+$ molar ratio and air mass origin shown in Figure 6.14 clearly indicates that the extent of chloride depletion is greater when the aerosol has been more influenced by anthropogenic sources of pollution. A study of marine aerosol at remote Chichijima Island in the western North Pacific during 2001 and 2002 reported that mean Cl^-/Na^+ molar ratios were highest (1.34) in September 2001 and lowest (0.30) in May 2002, and the mean ratio across the 2-year period was 1.10.[335] Boreddy *et al.* reported that the observed chloride depletion was likely due to acid displacement occurring as a result of atmospheric mixing of anthropogenic pollutants such as SO_2 and NO_3.[335] Acid displacement can occur when sea salt particles react with acids such as H_2SO_4, HNO_3, oxalic acid ($C_2H_2O_4$) and methanesulfonic acid (CH_3SO_3H) in the atmosphere, as shown in Equations 6.13 – 6.16.[306]

$$2NaCl + H_2SO_4 \rightarrow Na_2SO_4 + 2HCl \quad (6.13)$$

$$NaCl + HNO_3 \rightarrow NaNO_3 + HCl \quad (6.14)$$

$$2NaCl + C_2H_2O_4 \rightarrow Na_2C_2O_4 + 2HCl \quad (6.15)$$

$$NaCl + CH_3SO_3H \rightarrow CH_3SO_3Na + HCl \quad (6.16)$$

In a more recent study, Boreddy *et al.* performed a regression analysis between the Cl^-/Na^+ mass ratio and various acidic species ($nssSO_4^{2-}$, NO_3^-, MSA^- and oxalic acid).[306] They found

a moderate negative correlation between Cl^-/Na^+ mass ratio and $nssSO_4^{2-}$, and a moderate to weak negative correlation with NO_3^-; this suggested that sulfate had a higher influence on chloride depletion than nitrate. Furthermore, whilst MSA^- moderately correlated with the mass ratio in the summer, there was significant negative correlation between oxalic acid and the mass ratio in the other three seasons, confirming that oxalic acid plays an important role in chlorine loss at Chichijima Island.[306] As previously shown in Equation 6.15, sea salt can react with oxalic acid to form sodium oxalate ($Na_2C_2O_4$) and HCl. A similar regression analysis was carried out on the measurements obtained during the Bachok demonstration campaign, and whilst a weak negative correlation was found between SO_4^{2-} and the $Cl^-/ssNa^+$ mass ratio ($R = 0.41$, $p < 0.025$), there was no correlation of the $Cl^-/ssNa^+$ mass ratio with oxalate or MSA^-. Interestingly, a strong positive correlation was observed between NO_3^- and $Cl^-/ssNa^+$ mass ratio ($R = 0.78$, $p < 0.001$). These results imply that H_2SO_4 played an important role in chloride depletion, whilst methanesulfonic acid and oxalic acid did not. The positive correlation between NO_3^- and Cl^-/Na^+ mass ratio may be explained by the fact that the high sulfate content of the aerosol in Bachok is capable of suppressing both NO_3^- and Cl^- levels.

6.3.3.6 Using Ca^{2+} as a potential tracer for dust episodes

The concentration of Ca^{2+}, which can be used as a tracer for dust,[313] ranged from 0.009 to 0.35 μg m^{-3}, with an average concentration of 0.10 μg m^{-3}. Strong positive correlation was observed between Ca^{2+} and PO_4^{3-} ($R = 0.91$, $p < 0.001$), Ca^{2+} and Mg^{2+} ($R = 0.70$, $p < 0.001$), and Ca^{2+} and $nssNa^+$ ($R = 0.95$, $p < 0.001$). Figure 6.15 shows time series plots for Ca^{2+}, PO_4^{3-}, Mg^{2+} and $nssNa^+$ during the Bachok demonstration campaign. On most days, the Ca^{2+} concentration was approximately 0.05 – 0.10 μg m^{-3}, but between midday on 30-01-2014 and midnight on 31-01-2014, elevated Ca^{2+} levels were observed, and the average concentration during this period was 0.29 μg m^{-3}. The same trend is observed for PO_4^{3-}; the average concentration across the entire measurement period was 0.34 μg m^{-3}, but during this 12-hour episode the PO_4^{3-} concentration increased to 1.88 μg m^{-3}. The increase in ion concentration was less obvious for $nssNa^+$ and Mg^{2+}, but the concentrations were still 0.26 and 0.08 μg m^{-3} above the average for the whole measurement period respectively.

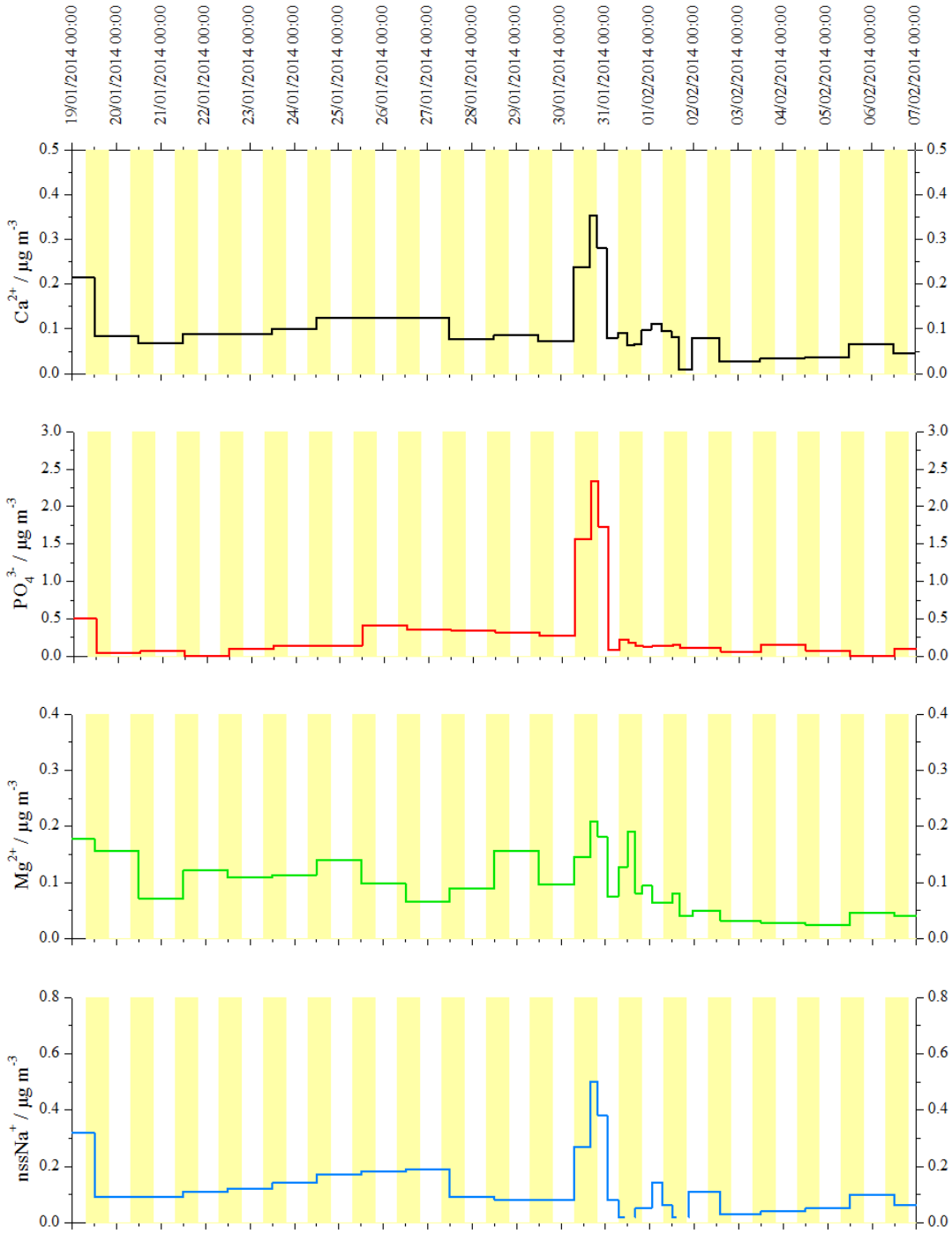

Figure 6.15. Time series of Ca^{2+}, PO_4^{3-}, Mg^{2+} and $nssNa^{+}$ concentration (µg m^{-3}) during the Bachok demonstration campaign (18-01-2014 to 07-02-2014).

It is possible that the elevated levels of these ions was due to a dust episode, and therefore it is important to consider where the air masses originated from during this period. Figure 6.16 shows backward air mass trajectories from the Bachok site between midday on 30-01-2014 and midnight on 31-01-2014, coloured by the Ca^{2+} concentration. The plot shows that the air masses have originated from the North China Plains and the Horqin sandy land.[336] Although more information is required to confirm that dust episodes in these regions are

responsible for the elevated levels of Ca^{2+} at the Bachok research station, it is important to consider such sources of pollutants in the future as they can have damaging effects on human health, agricultural land, infrastructure and transport.[337]

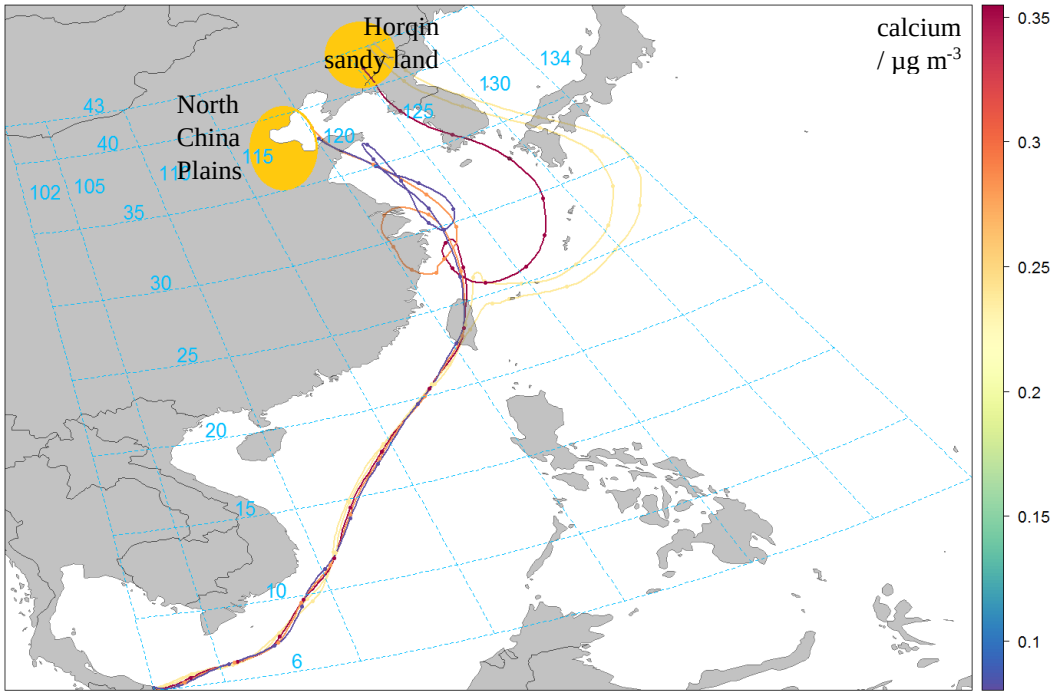

Figure 6.16. 10-day HYSPLIT back trajectories centred on the Bachok research station, between 30-01-2014 12:00 and 31-01-2014 00:00. The back trajectories are coloured by the concentration of Ca^{2+} (µg m^{-3}) and the North China Plains and Horqin sandy land regions are highlighted.[336]

6.4 Conclusions

An accurate and reliable technique, using IC, was used for the determination of water-soluble ions in atmospheric aerosol collected at the Bachok Marine and Atmospheric Research Station. Average recovery levels of the target anions and cations from the collected aerosol filters were 82.2% and 90.4% respectively. Excellent instrument intra-day precision was observed (%RSD < 5%) and limits of detection and limits of quantification for the target ions ranged from 0.5 – 21.0 ng and 2.5 – 144.2 ng respectively.

Using meteorological data from the nearby airport, or HYSPLIT backward air mass trajectories centred on the Bachok research station, it was possible to observe both the diurnal wind pattern behaviour, and assess where the air masses arriving at the site originated from. In general, the site was dominated by south westerlies coming from the land from the early hours of the morning until approximately midday, and then a dramatic shift in wind direction occurred and a sea breeze from the South China Sea was present for the remainder

of the day. This was accompanied by a drop in the concentrations of NO_x and anthropogenic VOCs.[292] 10-day back trajectories showed that air masses originated from the South China Sea and Asian countries such as China, Japan, Taiwan, Vietnam and North and South Korea.

Twelve major atmospheric ions were measured in this study and the water-soluble ion fraction of the aerosol was dominated by sulfate (66% of the total ion content). The non-sea salt and sea salt components of SO_4^{2-}, Na^+, K^+ and Ca^{2+} were determined, and it was found that 96% of the measured SO_4^{2-} was non-sea salt SO_4^{2-}. By combining the aerosol measurements with back trajectory data, it was clear that SO_4^{2-} concentrations were higher when the air masses originated from highly industrialised cities and regions of high biomass burning activity. An analysis of aerosol acidity revealed that the aerosol was highly likely to be acidic, potentially impacting human health and the health of ecosystems at this remote coastal location.

Oxalate concentrations were also measured and found to be more comparable to other studies of urban locations, rather than rural ones. A strong correlation with SO_4^{2-} suggested a common aqueous oxidation formation pathway. Strong correlation between oxalate and K^+ coupled with high oxalate/nssK^+ ratios indicated that biomass burning was an important secondary source of oxalate in the Bachok region, whereas lack of correlation with NO_2^- and NO_3^- suggested that vehicular emissions were not an important source.

The average Cl^-/ssNa^+ molar ratio during the measurement campaign was 0.40, significantly lower than that of bulk seawater (1.18).[306] Analysis of back trajectories revealed that chloride depletion was greater when the aerosol was more influenced by anthropogenic sources of pollution. In addition, the time profile of Ca^{2+} and its correlation with other species was investigated, as Ca^{2+} can be used as a potential tracer for atmospheric dust. Strong positive correlation with other species such as PO_4^{3-}, Mg^{2+} and Na^+ was observed, and significantly elevated concentrations of Ca^{2+} and PO_4^{3-} were recorded between 30-01-2014 12:00 and 31-01-2014 00:00. The air arriving at the site during this time had originated from two regions where dust storm events occur frequently, the Horqin sandy land and the North China Plains. Further investigation is required to determine the potential effects of dust storms on human health, agricultural land and infrastructure.

In summary, whilst this information has demonstrated the capabilities of the Bachok Marine and Atmospheric Research Station in terms of aerosol composition studies, a longer study with increased time-resolved sampling and particle size fractionation would provide a better insight into the factors affecting the composition of major atmospheric ions in aerosol. Both seasonal and diurnal patterns could be investigated, and more extensive meteorological measurements at the sampling site would allow for a more in-depth analysis. Nevertheless,

it is clear that this remote coastal location is susceptible to the effects of local, regional and national air pollution, and it is becoming increasingly evident that remote locations such as the east coast of Peninsular Malaysia are vulnerable to the effects of poor air quality.

7 Conclusions and future work

Human activities have drastically enhanced the amount of reactive nitrogen in the atmosphere and in the last few decades, the amount of reactive nitrogen produced by anthropogenic activities has exceeded the amount produced by natural processes. ON is ubiquitous in both the gas and particle phase in the atmosphere, and incorporates a vast number of species that span a wide range of polarities and volatilities. ON compounds, which can be emitted from various biogenic and anthropogenic sources and undergo long-range transport in the atmosphere, are often found in trace level quantities amongst a complex mixture of species. As such, it is challenging to measure ON in the atmosphere; this thesis has relied on the use of a powerful separation technique (GC×GC) coupled to an element-specific detector (NCD) to allow for trace level measurements of ON compounds in complex matrices to be made. In the future, it is important to expand upon the existing library of ON compounds that can be characterised by GC×GC-NCD. This could be achieved by gaining access to a wider range of analytical standards - some are commercially available whilst others would require custom synthesis. Once a more extensive library of ON compounds has been created, it would be useful to improve the time-resolution of the measurements (*i.e.* hourly rather than 12-hourly) and then make measurements at a wide variety of locations across the globe, examining diurnal, weekly, seasonal and annual trends. It would also be beneficial to develop a second GC×GC-NCD system which is coupled to a thermal desorption unit, allowing for measurements of gaseous ON species to be made alongside the compounds in the particle phase. Furthermore, and perhaps most importantly, any ON measurements obtained need to be supported with simultaneous measurements of meteorological conditions and other key components of the atmospheric nitrogen cycle, such as inorganic nitrogen compounds and gaseous N_R species such as NO_x and NH_3. Inorganic nitrogen compounds, *e.g.* NH_4^+, NO_3^- and NO_2^-, can be measured using the ion chromatography method described in Chapter 6. In summary, making synchronized measurements of a wider range of atmospheric nitrogen-containing species at various locations and during different seasons will allow for a much better understanding of the atmospheric nitrogen cycle.

Nitrosamines are a class of ON compounds known to be highly carcinogenic, but prior to this study there were no detailed time-resolved estimates of their abundance in ambient air. A highly sensitive analytical method capable of separating hundreds of ON compounds has been described in this thesis, and used to determine daily variability in nicotine, and 8 non-specific and 4 tobacco-specific nitrosamines in ambient PM from central London. The lifetime cancer risk from nitrosamines in urban PM exceeded the US EPA guideline of

10 excess cancer cases per 1 million population exposed after 1-3 h of exposure to observed concentrations per day over the duration of an adult lifetime. However, a key limitation of this study was the lack of data available for indoor air, which meant that indoor exposure was assumed to be zero and only the outdoor air contribution was included in the exposure assessment. As a result, the risk assessment does not account for the full 24-hour period of each day, and is therefore most certainly an underestimate of true exposure. Indoor nitrosamine measurements both in homes and workplaces should be made a priority, considering that it has been estimated that people in developed countries spend around 90% of their time indoors. Furthermore, it is important that a wider range of nitrosamines and other trace level carcinogens are measured; hopefully this will be accompanied by progression in the availability of toxicological information for these compounds, allowing for more comprehensive cancer risk assessments to be made. In the future, attention must also be paid to exposure from third hand smoke, which is a term used to describe residual tobacco smoke gases and particles that are deposited to surfaces and dust. Studies have shown that nitrosamines present in house dust pose a significant cancer risk from exposure *via* ingestion and dermal absorption.[62, 73] It would be useful to carry out more extensive studies of nitrosamine exposure from house dust, and compare the resulting estimates of cancer risk *via* ingestion and dermal absorption with estimates of cancer risk *via* inhalation. This would help to gain a better understanding the overall cancer risk and the importance of different exposure routes.

The described GC×GC-NCD system was also used in the Atmospheric Chemistry of Amines project; this project was set up by the University of Oslo to investigate the atmospheric degradation of amines emitted to the atmosphere from CO_2 capture plants. In preparation for a series of photo-oxidation experiments at the outdoor atmospheric simulation chamber in Spain, two methods were developed for the identification and quantification of amine degradation products. The first method relied on GC×GC-NCD and was developed for the determination of carcinogenic nitrosamines and nitramines; this technique offered excellent recovery of the target analytes at low picogram levels, and total errors for the extraction and analysis process remained below 24%. Synthetic work was carried out to derivatise compounds which were not otherwise amenable to GC analysis. The nature of the sample extraction technique meant that the samples were also suitable for direct analysis by GC×GC-TOF-MS, providing additional mass spectral information to help characterise other ON species in the aerosol. A method relying on IC was also developed to determine the presence of aminium nitrate salts in the aerosol, formed through reactions of gaseous amines with nitric acid. A gradient elution method was set up in cation-exchange mode to allow for various protonated amines to be accurately measured. A series of photo-oxidation

experiments were carried out to investigate the atmospheric degradation of *t*BA, AMP, morpholine, piperidine and piperazine. Comparison of various morpholine photo-oxidation experiments revealed that the total aerosol yield increased with increasing NO_x levels; this was most likely due to an increased availability of HNO_3 in the system, leading to increased salt formation. Piperazine formed more aerosol than piperidine and morpholine due to its lower volatility and faster rate of reaction with OH. Maximum aerosol yields under high NO_x conditions were 36.7% for piperazine, 11.7% for piperidine and 3.9% for morpholine. The particulate nitrosamines and nitramines formed during amine photo-oxidation were successfully quantified using GC×GC-NCD. Nitramines accumulated to higher levels than nitrosamines in the aerosol, most likely due to their increased stability in sunlight. Nitramine formation was lower for secondary amines than primary amines, but the overall carcinogenic risk from the degradation of secondary amines may be higher than that of primary amines, as substantial nitrosamine formation is also observed. For example, although more information is needed to assess the suitability of each amine as a solvent for CO_2 absorption, piperazine forms high levels of both nitrosamines (0.3 – 2.8% chamber yield) and nitramines (5.7 – 18.9% chamber yield) in the particle phase and should be considered as a CO_2 capture solvent with caution. Additional organic nitrogen compounds were identified using GC×GC-TOF-MS, many of which formed by surface-assisted condensation reactions. In the future, it will be possible to characterise the organic fraction of the aerosol in more detail by using a wider range of analytical standards. The presence of aminium nitrate salts were determined by IC; in most experiments an initial maximum aminium ion concentration was observed, followed by subsequent revolatilization to the gas phase, or oxidation to other basic species. NO_3^- concentrations increased throughout the experiment in an attempt to neutralise the protonated amines.

The overall objective of the Atmospheric Chemistry of Amines project was to improve the understanding of the atmospheric degradation of amines emitted to the atmosphere from CO_2 capture plants, as degradation can lead to the formation of potentially carcinogenic nitrosamines and nitramines. In the future, it is important that the data obtained is used to perform 'worst case studies', which essentially evaluate the possible risks to human health and the environment, and eliminate the effects that are not relevant to investigate. To achieve this, it is necessary to establish gas phase chemical reaction schemes for each amine under consideration, and to gain a full understanding of the corresponding aerosol chemistry. Gaseous chemical reaction schemes are currently being developed for *t*BA, AMP, morpholine, piperidine and piperazine using the data obtained using proton-transfer-reaction time-of-flight mass spectrometry (PTR-TOF-MS), alongside theoretical calculations. Analysis of this data will allow for branching ratios and atmospheric lifetimes of each amine

to be estimated. To better understand the aerosol chemistry, the information obtained in this study (offline aerosol measurements) will need to be combined with the online aerosol measurements as soon as they are available. In future chamber studies, it would be useful to adopt a more systematic approach to chamber conditions so that intercomparing between amines is more accurate. Increasing the time-resolution of the aerosol filter sampling would also allow for aerosol formation and ageing to be studied in more detail. The information from the photo-oxidation experiments can be used to improve future atmospheric chemical transport models, which are used to model the atmospheric dispersion of amine emissions from the exhaust plume of CO_2 capture plants. The models also allow for different emission scenarios to be tested and derive predictions for the future. Whilst photo-oxidation experiments allow us to study the chemical degradation pathway of a specific amine, atmospheric monitoring in the local vicinity of CO_2 capture plants would also provide valuable information and be a useful way to validate model predictions. It is possible that the methods developed for aerosol filter sampling in this study could be applicable to ambient air if necessary modifications were carried out. This would allow trace level measurements of nitrosamines and nitramines in ambient air to be made at the CO_2 capture testing facility in Mongstad for example. For such studies to be successful, it would be important to optimise a technique that offers a good compromise between the time-resolution of the sampling, and collecting sufficient mass for detailed aerosol composition analysis. Furthermore, various tests would be required to ensure there are no species present in ambient air interfering with the target compounds, as the real atmosphere is inherently more complex than an atmospheric simulation chamber. Overall it is hoped that the data from this thesis will incorporated with all of the data obtained during the Atmospheric Chemistry of Amines project, and used to better predict the feasibility of different amines as solvents for CO_2 absorption. This is important because large scale CCS facilities have the potential to capture up to 800,000 tonnes of CO_2 per annum, and are likely to prove an essential way of reducing atmospheric CO_2 levels and mitigating global temperature rise.

Cooking is widely recognised as an important source of indoor and outdoor gaseous and particulate emissions which can have detrimental impacts on human health. The composition of cooking emissions can vary significantly, depending on the type of food, type of cooking oil, style of cooking and cooking temperature. Using a combination of GC×GC-TOF-MS and PTR-TOF-MS, a collaborative project was carried out with the Paul Scherrer Institute to investigate the chemical composition of gas phase and particulate emissions from a broad variety of cooking styles and techniques. By adopting a systematic approach, emissions from various heated vegetable oils and cooked vegetables and meat were individually characterized, as well as terpene emissions from cooking with herbs and pepper. The use of

GC×GC-TOF-MS allowed aldehydes and ketones to be distinguished from each other, revealing that the gaseous emissions were dominated by aldehydes, which can have a negative impact on indoor air quality and irritate the eyes and respiratory tract. In the future, it is important that harmful pollutants, such as acetaldehyde, hexanal, acrolein and 2,4-decadienal are monitored in a range of cooking environments, as they have the potential to exceed the recommended workplace limits reported in the literature. Some of these compounds, such as acetaldehyde, are known carcinogens and therefore the risk from exposure *via* inhalation needs to be minimised. Furthermore, the cooking emission studies revealed that cooking with herbs and pepper led to significant terpene emissions; monoterpenes and sesquiterpenes were detected in emissions from both herbs and pepper, whilst oxygenated sesquiterpenes and diterpenes were only detected in the herb emissions and acted as efficient intermediate volatility SOA precursors. Current indoor air quality studies often only measure α-pinene and limonene, yet this study highlights the potential importance of a range of other monoterpenes, sesquiterpenes, diterpenes and terpenoids. It is important that future indoor air quality studies do not focus solely on cleaning products as a source of terpenes, and consider the fact that cooking emissions are an important yet overlooked source of terpenes and SOA indoors. The composition of particulate cooking emissions was also studied and emissions were dominated by fatty acids, γ-lactones and δ-lactones. Additional ON compounds were also identified, particularly during the charbroiling of lean meat. Many of these species belonged to the heterocyclic aromatic amine family, and are therefore likely to have carcinogenic and mutagenic properties. Most of the γ- and δ-lactones, as well as several ON species, were detected in ambient PM samples, and further investigation is required to assess whether these compounds are exclusively from cooking and the suitability of these species as cooking emission tracers. If these tracers can be verified, it would be important to investigate how they vary with geographical location and culinary technique. Due to the ability of cooking aerosol to deposit in the human respiratory tract, improvements in the capture of cooking emissions by fume extraction and filtration is necessary; this would drastically reduce human exposure and lead to improvements in both indoor and outdoor air quality.

Ion chromatography was used to measure water-soluble ions in $PM_{2.5}$ collected at a rural coastal location on the East coast of Peninsular Malaysia. Analysis of backward air mass trajectories showed that the air masses arriving at the site originated from the South China Sea and countries such as China, Japan, Taiwan, Vietnam and North and South Korea. Combining the water-soluble ion measurements with back trajectory data showed that sulfate concentrations were higher in Bachok when the air masses had passed over highly industrialised cities such as Shanghai and Guangzhou in China. An estimation of strong

acidity revealed that the aerosol was likely to be acidic, potentially impacting human health and the health of ecosystems at remote locations such as Bachok in Malaysia. In the future, more accurate predictions of aerosol pH would be useful, and could be achieved using thermodynamic models such as ISORROPIA and E-AIM. This is only possible if complementary measurements of relative humidity, temperature and gaseous species such as NO_x and NH_3 are recorded at the site. Other particulate measurements, such as organic aerosol composition, EC/OC and total PM would also provide further information regarding aerosol behaviour. The back trajectories showed that chloride depletion was greater when the aerosol was more influenced by anthropogenic sources of pollution, and that elevated concentrations of Ca^{2+}, PO_4^{3-}, Mg^{2+} and $nssNa^{+}$ were recorded when the air arriving at the measurement site had originated from regions susceptible to frequent dust storms. This rural location is vulnerable to the effects of local and regional pollution and in the future, it would be useful to make aerosol measurements with higher time-resolution over longer periods of time, to assess the daily, seasonal and annual variability in aerosol composition. Furthermore, distinguishing different size fractions of aerosol and measuring at a greater number of locations would help to improve our knowledge of the influence of highly industrialised regions on air quality in the Maritime Continent.

Appendix A: Supplementary Figures and Tables

Table A1. Normalized cancer risk estimations for the inhalation of NDMA, NDEA, NDPA, NPyr, NMor, NPip, NDBA, NDPhA and NNN, by age group, expressed as the number of excess cancer cases per 1 million population exposed in winter. The bracketed values represent the minimum risk estimations when concentration values below the LODs and LOQs are zero.

Winter	Exposure Time (ET) / hours							
Age group / years	**1**	**2**	**3**	**4**	**5**	**6**	**7**	**8**
0 to < 2	0.682 (0.681)	1.363 (1.362)	2.045 (2.043)	2.726 (2.724)	3.408 (3.404)	4.089 (4.085)	4.771 (4.766)	5.453 (5.447)
2 to < 16	1.439 (1.437)	2.878 (2.874)	4.317 (4.310)	5.756 (5.747)	7.195 (7.184)	8.634 (8.621)	10.073 (10.058)	11.512 (11.495)
16 to 70	1.878 (1.873)	3.757 (3.746)	5.635 (5.619)	7.513 (7.492)	9.392 (9.365)	11.270 (11.237)	13.148 (13.110)	15.027 (14.983)
Total	**3.999 (3.991)**	**7.998 (7.981)**	**11.997 (11.972)**	**15.995 (15.962)**	**19.994 (19.953)**	**23.993 (23.944)**	**27.992 (27.934)**	**31.991 (31.925)**

Table A2. Normalized cancer risk estimations for the inhalation of NDMA, NDEA, NDPA, NPyr, NMor, NPip, NDBA, NDPhA and NNN, by age group, expressed as the number of excess cancer cases per 1 million population exposed in summer. The bracketed values represent the minimum risk estimations when concentration values below the LODs and LOQs are zero.

Summer	Exposure Time (ET) / hours							
Age group / years	**1**	**2**	**3**	**4**	**5**	**6**	**7**	**8**
0 to < 2	1.147 (1.146)	2.294 (2.292)	3.441 (3.438)	4.588 (4.584)	5.735 (5.730)	6.882 (6.876)	8.029 (8.022)	9.176 (9.168)
2 to < 16	2.416 (2.414)	4.833 (4.828)	7.249 (7.242)	9.665 (9.656)	12.082 (12.070)	14.498 (14.484)	16.914 (16.898)	19.331 (19.312)
16 to 70	3.135 (3.131)	6.269 (6.263)	9.404 (9.394)	12.539 (12.525)	15.673 (15.657)	18.808 (18.788)	21.943 (21.919)	25.078 (25.051)
Total	6.698 (6.691)	13.396 (13.383)	20.094 (20.074)	26.792 (26.765)	33.490 (33.456)	40.188 (40.148)	46.886 (46.839)	53.584 (53.530)

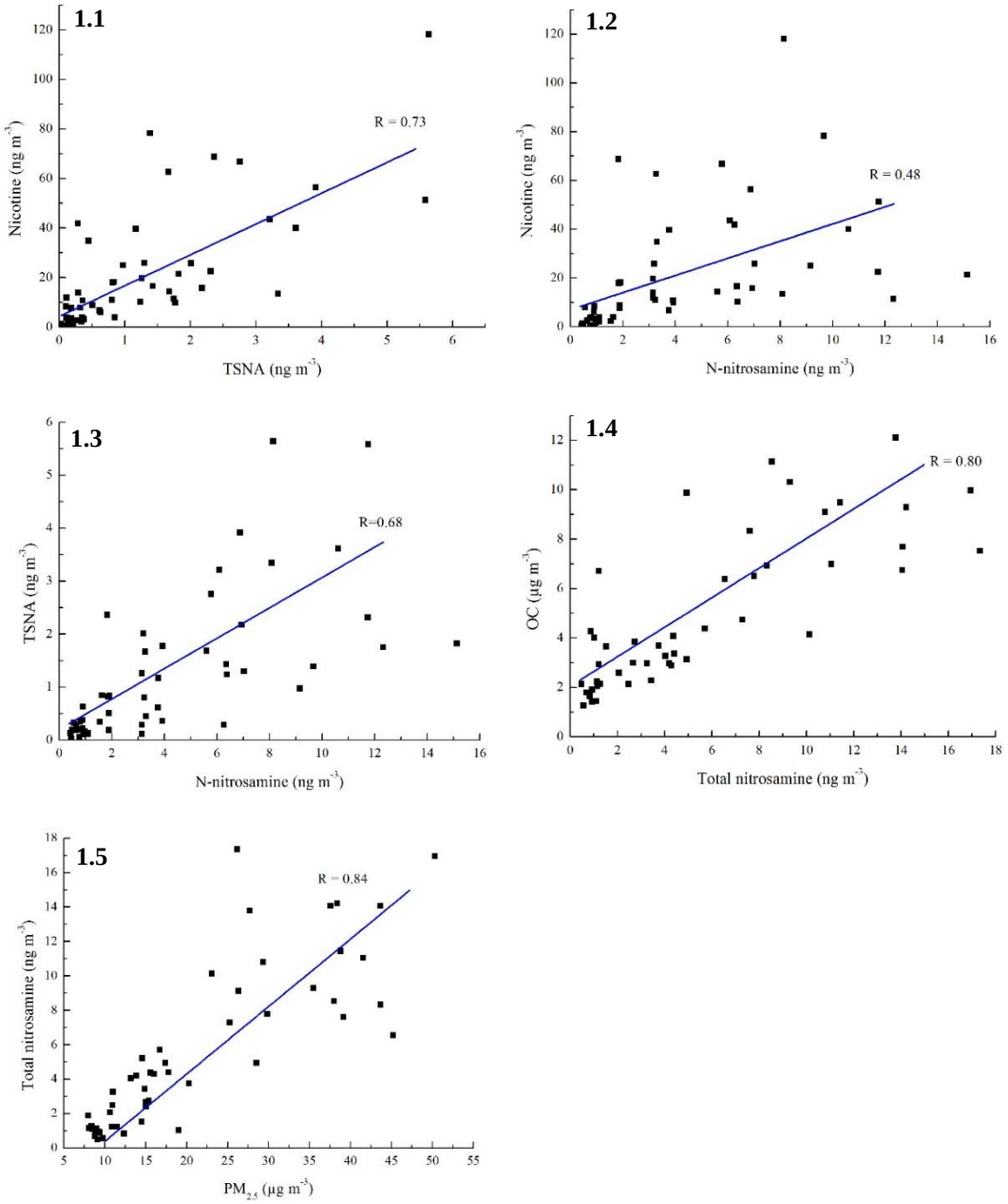

Figure A1. Correlations for winter 2012 measurements. TSNA vs. nicotine (1.1); N-nitrosamine vs. nicotine (1.2); N-nitrosamine vs. TSNA (1.3); Total nitrosamine vs. OC (1.4); $PM_{2.5}$ vs. total nitrosamine (1.5).

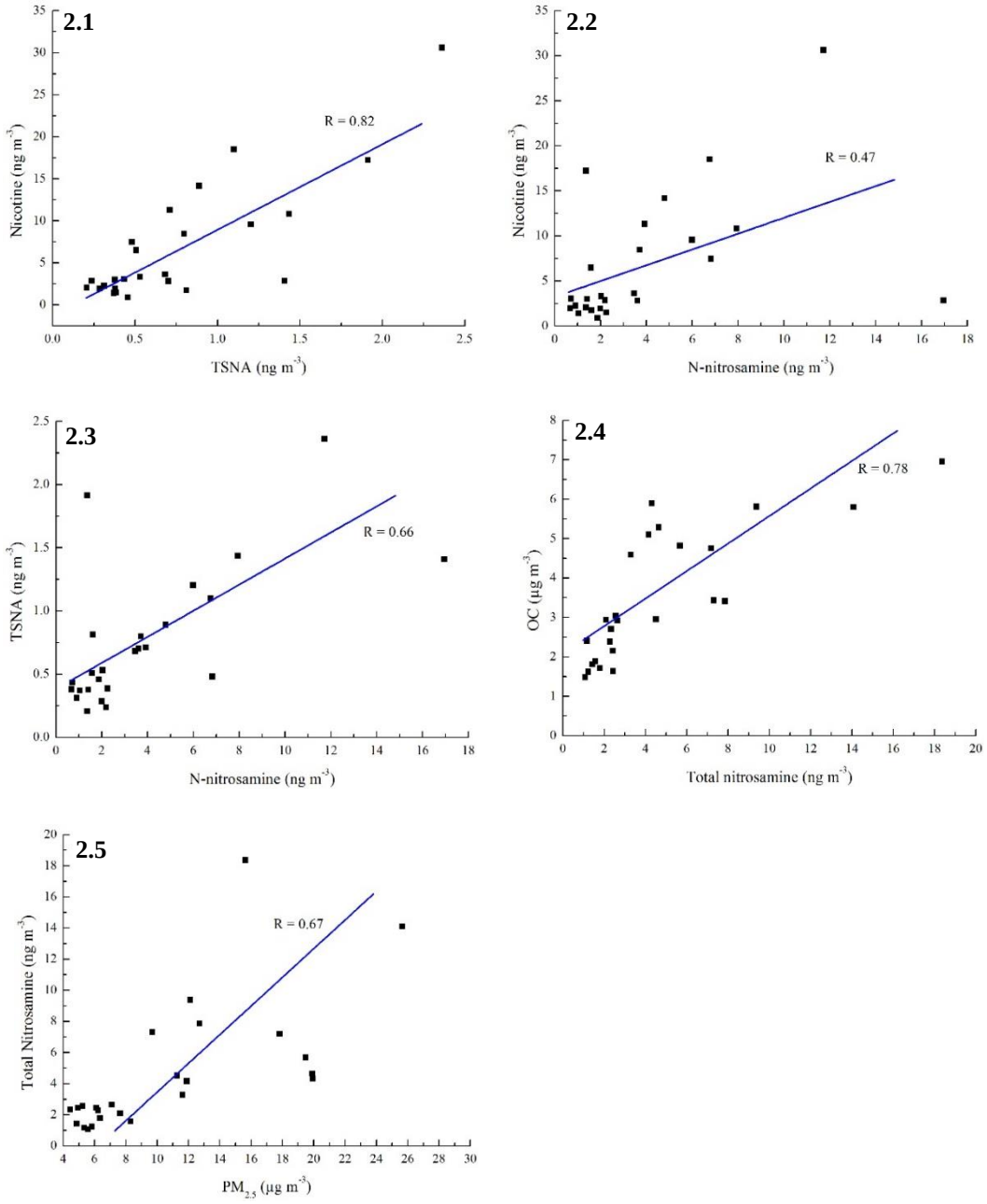

Figure A2. Correlations for summer 2012 measurements. TSNA vs. nicotine (2.1); N-nitrosamine vs. nicotine (2.2); N-nitrosamine vs. TSNA (2.3); Total nitrosamine vs. OC (2.4); $PM_{2.5}$ vs. total nitrosamine (2.5).

Table A3. Maximum % aerosol yield observed during each amine photo-oxidation experiment. Aerosol concentrations were corrected for particle wall loss and dilution. Data from experiments carried out on 4th, 15th and 19th June 2015 have been excluded as it was not possible to calculate the wall loss rate. It was not possible to calculate the aerosol yield on 02-06-15 as the PTR-MS data was not provided.

Amine	Date	Maximum % aerosol yield
*t*BA	03-06-2015	124.4
AMP	09-06-2015	101.6
	12-06-2015	55.7
	18-06-2015	135.5
Morpholine	04-07-2016	3.85
	05-07-2016	5.60
	06-07-2016	4.96
	07-07-2016	1.59
Piperidine	11-07-2016	11.7
	12-07-2016	18.0
	15-07-2016	8.11
	18-07-2016	18.0
Piperazine	20-07-2016	36.7
	21-07-2016	10.5
	22-07-2016	9.73
	25-07-2016	35.4
	26-07-2016	37.9

Table A4. Average NO_3^- and $C_4H_{10}NO^+$ concentrations (and the corresponding average percentage yields from the parent amine) detected in aerosol collected throughout the morpholine photo-oxidation experiments. The NO_3^- : $C_4H_{10}NO^+$ molar ratios are also reported. All reported concentrations have been corrected for particle wall loss and chamber dilution. *denotes sampling intervals during which the chamber canopy was open.

Date	Sampling time (HH:mm, UTC)	NO_3^- / µg m^{-3}	Average % NO_3^- yield	$C_4H_{10}NO^+$ / µg m^{-3}	Average % $C_4H_{10}NO^+$ yield	Molar NO_3^- : $C_4H_{10}NO^+$
04-07-2016	06:29 – 06:59	0.000	n/a	0.000	n/a	n/a
	10:36 – 13:30*	3.480	0.701	7.560	1.524	0.65
	14:26 – 15:26	3.504	0.417	5.480	0.651	0.91
05-07-2016	06:31 – 07:01	0.112	n/a	0.318	n/a	n/a
	11:07 – 13:10*	10.842	1.443	1.468	0.195	10.48
	13:47 – 14:47	3.036	0.332	5.284	0.578	0.82
06-07-2016	06:21 – 06:51	0.100	n/a	0.174	n/a	n/a
	09:51 – 11:51*	4.986	0.970	10.538	2.050	0.67
	12:11 – 13:11*	3.859	0.467	2.301	0.278	1.39
	13:55 – 14:55	3.401	0.376	2.892	0.320	1.67
07-07-2016	06:20 – 06:50	0.000	n/a	0.225	n/a	n/a
	12:05 – 14:05*	1.532	0.195	4.185	0.533	0.52
	15:07 – 16:07	2.278	0.255	2.043	0.229	1.58

Table A5. Average NO_3^- and $C_5H_{12}N^+$ concentrations (and the corresponding average percentage yields from the parent amine) detected in aerosol collected throughout the piperidine photo-oxidation experiments. The NO_3^- : $C_5H_{12}N^+$ molar ratios are also reported. All reported concentrations have been corrected for particle wall loss and chamber dilution. *denotes sampling intervals during which the chamber canopy was open.

Date	Sampling time (HH:mm, UTC)	NO_3^- / μg m^{-3}	Average % NO_3^- yield	$C_5H_{12}N^+$ / μg m^{-3}	Average % $C_5H_{12}N^+$ yield	Molar NO_3^- : $C_5H_{12}N^+$
11-07-2016	06:22 – 06:52	0.571	n/a	0.000	n/a	n/a
	09:41 - 10:41*	2.868	1.104	42.658	16.415	0.09
	10:46 - 11:46*	6.063	1.469	37.735	9.142	0.22
	11:52 – 12:52*	12.884	2.491	37.715	6.131	0.56
	13:37 – 14:37	19.724	3.114	25.872	4.085	1.06
12-07-2016	06:20 – 06:50	0.090	n/a	0.000	n/a	n/a
	09:48 – 10:48*	2.420	0.569	24.531	5.770	0.14
	10:55 – 11:55*	6.939	1.309	9.653	1.822	1.00
	12:01 – 13:01*	9.159	1.650	7.893	1.422	1.61
	13:42 – 14:42	9.030	1.572	8.632	1.502	1.45
15-07-2016	11:04 – 13:06*	3.105	0.994	24.793	7.933	0.17
	14:01 – 15:01	7.704	1.205	9.234	1.444	1.16
18-07-2016	06:28 – 06:58	0.000	n/a	0.000	n/a	n/a
	09:44 – 10:44*	7.633	2.392	32.659	10.240	0.32
	10:50 – 11:50*	19.692	3.491	20.470	3.629	1.33
	12:41 – 13:41	20.272	3.050	16.643	2.504	1.69

Table A6. Average NO_3^- and $C_4H_{12}N_2^{2+}$ concentrations (and the corresponding average percentage yields from the parent amine) detected in aerosol collected throughout the piperazine photo-oxidation experiments. The NO_3^- : $C_4H_{12}N_2^{2+}$ molar ratios are also reported. All reported concentrations have been corrected for particle wall loss and chamber dilution. *denotes sampling intervals during which the chamber canopy was open.

Date	Sampling time (HH:mm, UTC)	NO_3^- / µg m^{-3}	Average % NO_3^- yield	$C_4H_{12}N_2^{2+}$ / µg m^{-3}	Average % $C_4H_{12}N_2^{2+}$ yield	Molar NO_3^- : $C_4H_{12}N_2^{2+}$
20-07-2016	06:26 – 06:56	0.205	n/a	0.389	n/a	n/a
	09:52 – 10:52*	4.923	1.172	75.766	18.037	0.09
	11:01 – 12:01*	18.967	3.510	45.453	8.412	0.59
	12:45 – 13:45	32.199	5.339	23.073	3.826	1.96
21-07-2016	06:22 – 06:52	0.031	n/a	0.357	n/a	n/a
	11:42 – 12:27*	5.995	1.734	87.010	25.172	0.10
	12:32 – 13:02*	8.184	1.399	72.192	12.339	0.16
	13:07 – 13:19*	7.412	1.158	67.767	10.590	0.15
	13:37 – 14:37	8.503	1.201	18.858	2.663	0.63
22-07-2016	06:35 – 07:05	0.000	n/a	0.349	n/a	n/a
	09:30 – 10:30*	3.805	0.606	142.113	22.631	0.04
	10:44 – 11:15*	8.691	1.047	19.255	2.319	0.63
	11:49 – 12:49	3.350	0.376	1.860	0.209	2.53

Table A6 continued. *denotes sampling intervals during which the chamber canopy was open.

Date	Sampling time (HH:mm, UTC)	NO_3^- / µg m^{-3}	Average % NO_3^- yield	$C_4H_{12}N_2^{2+}$ / µg m^{-3}	Average % $C_4H_{12}N_2^{2+}$ yield	Molar NO_3^- : $C_4H_{12}N_2^{2+}$
25-07-2016	06:31 – 07:01	0.000	n/a	0.000	n/a	n/a
	08:35 – 09:15*	19.719	3.458	47.106	8.261	0.59
	09:54 – 10:54	44.245	5.177	13.621	1.594	4.56
26-07-16	06:29 – 06:59	0.000	n/a	0.000	n/a	n/a
	08:55 – 09:30*	16.920	4.645	63.003	17.297	0.38
	10:06 – 10:51	36.488	5.424	18.543	2.756	2.76
*Sampling intervals during which the chamber canopy was open.						

Table A7. Average N-nitromorpholine and N-nitrosomorpholine concentrations (and the corresponding average percentage yields from the parent amine) detected in aerosol collected throughout the morpholine photo-oxidation experiments. The nitramine: nitrosamine mass ratios are also reported. All reported concentrations have been corrected for particle wall loss and chamber dilution. *denotes sampling intervals during which the chamber canopy was open.

Date	Sampling time (HH:mm, UTC)	[N-nitromorpholine] / μg m^{-3}	Average % nitramine yield	[N-nitrosomorpholine] / μg m^{-3}	Average % nitrosamine yield	Nitramine: nitrosamine
04-07-2016	06:29 – 06:59	0.000	n/a	0.000	n/a	n/a
	10:36 – 13:30*	0.855	0.173	0.053	0.011	16.3
	14:26 – 15:26	0.288	0.034	0.023	0.003	12.4
05-07-2016	06:31 – 07:01	0.188	n/a	0.003	n/a	n/a
	11:07 – 13:10*	0.839	0.121	0.027	0.004	30.8
	13:47 – 14:47	0.319	0.035	0.006	0.001	53.6
06-07-2016	06:21 – 06:51	0.054	n/a	0.000	n/a	n/a
	09:51 – 11:51*	1.184	0.230	0.054	0.010	22.1
	12:11 – 13:11*	13.510	1.635	0.144	0.017	93.6
	13:55 – 14:55	0.154	0.017	0.007	0.001	23.0
07-07-2016	06:20 – 06:50	0.000	n/a	0.016	n/a	n/a
	12:05 – 14:05*	0.998	0.127	0.037	0.005	27.0
	15:07 – 16:07	0.168	0.019	0.009	0.001	17.7

Table A8. Average N-nitropiperidine and N-nitrosopiperidine concentrations (and the corresponding average percentage yields from the parent amine) detected in aerosol collected throughout the piperidine photo-oxidation experiments. The nitramine: nitrosamine mass ratios are also reported. All reported concentrations have been corrected for particle wall loss and chamber dilution. *denotes sampling intervals during which the chamber canopy was open.

Date	Sampling time (HH:mm, UTC)	[N-nitropiperidine] / µg m^{-3}	Average % nitramine yield	[N-nitrosopiperidine] / µg m^{-3}	Average % nitrosamine yield	Nitramine: nitrosamine
11-07-2016	06:22 – 06:52	0.000	n/a	0.000	n/a	n/a
	09:41 - 10:41*	1.125	0.433	0.467	0.180	2.41
	10:46 - 11:46*	1.491	0.361	0.135	0.033	11.0
	11:52 – 12:52*	2.152	0.416	0.166	0.032	12.9
	13:37 – 14:37	0.058	0.009	0.000	0.000	n/a
12-07-2016	06:20 – 06:50	0.095	n/a	0.000	n/a	n/a
	09:48 – 10:48*	0.380	0.089	0.050	0.012	7.69
	10:55 – 11:55*	0.775	0.146	0.015	0.003	52.0
	12:01 – 13:01*	1.018	0.183	0.011	0.002	91.2
	13:42 – 14:42	0.034	0.006	0.013	0.002	2.55
15-07-2016	11:04 – 13:06*	0.340	0.109	0.133	0.043	2.56
	14:01 – 15:01	0.075	0.012	0.045	0.007	1.68

Table A8 continued. *denotes sampling intervals during which the chamber canopy was open.

Date	Sampling time (HH:mm, UTC)	[N-nitropiperidine] / µg m^{-3}	Average % nitramine yield	[N-nitrosopiperidine] / µg m^{-3}	Average % nitrosamine yield	Nitramine: nitrosamine
18-07-2016	06:28 – 06:58	0.007	n/a	0.000	n/a	n/a
	09:44 – 10:44*	0.000	0.000	0.040	0.012	n/a
	10:50 – 11:50*	3.256	0.577	0.124	0.022	26.3
	12:41 – 13:41	0.050	0.008	0.073	0.011	0.68

Table A9. Average N-nitropiperazine and N-nitrosopiperazine concentrations (and the corresponding average percentage yields from the parent amine) detected in aerosol collected throughout the piperazine photo-oxidation experiments. The nitramine: nitrosamine mass ratios are also reported. All reported concentrations have been corrected for particle wall loss and chamber dilution. *denotes sampling intervals during which the chamber canopy was open.

Date	Sampling time (HH:mm, UTC)	[N-nitropiperazine] / µg m^{-3}	Average % nitramine yield	[N-nitrosopiperazine] / µg m^{-3}	Average % nitrosamine yield	Nitramine: nitrosamine
20-07-2016	06:26 – 06:56	0.059	n/a	0.017	n/a	n/a
	09:52 – 10:52*	37.736	8.983	11.908	2.835	3.2
	11:01 – 12:01*	99.152	18.349	4.673	0.865	21.2
	12:45 – 13:45	22.999	3.813	0.542	0.090	42.4
21-07-2016	06:22 – 06:52	0.069	n/a	0.046	n/a	n/a
	11:42 – 12:27*	65.279	18.885	6.732	1.947	9.7
	12:32 – 13:02*	84.265	14.403	5.656	0.967	14.9
	13:07 – 13:19*	108.877	17.015	8.756	1.368	12.4
	13:37 – 14:37	9.344	1.320	0.509	0.072	18.4
22-07-2016	06:35 – 07:05	0.234	n/a	0.046	n/a	n/a
	09:30 – 10:30*	55.623	10.669	1.510	0.290	36.8
	10:44 – 11:15*	16.806	2.012	0.659	0.079	25.5
	11:49 – 12:49	2.846	0.320	0.194	0.022	14.7

Table A9 continued. *denotes sampling intervals during which the chamber canopy was open.

Date	Sampling time (HH:mm, UTC)	[N-nitropiperazine] / µg m^{-3}	Average % nitramine yield	[N-nitrosopiperazine] / µg m^{-3}	Average % nitrosamine yield	Nitramine: nitrosamine
25-07-2016	06:31 – 07:01	0.142	n/a	0.436	n/a	n/a
	08:35 – 09:15*	32.321	5.668	5.466	0.959	5.9
	09:54 – 10:54	5.140	0.601	0.176	0.021	29.2
26-07-16	06:29 – 06:59	0.057	n/a	0.309	n/a	n/a
	08:55 – 09:30*	63.469	17.425	5.903	1.621	10.8
	10:06 – 10:51	6.254	0.930	0.192	0.028	32.6

Table A10. Average 1,4-dinitrosopiperazine concentrations (and the corresponding average percentage yield from the parent amine) detected in aerosol collected throughout the piperazine photo-oxidation experiments. The nitramine: dinitrosamine ratio and the mono-nitrosamine: dinitrosamine ratio are also reported. All reported concentrations have been corrected for particle wall loss and chamber dilution. *denotes sampling intervals during which the chamber canopy was open.

Date	Sampling time (HH:mm, UTC)	[1,4-dinitrosopiperazine] / μg m^{-3}	Average % dinitrosamine yield	Nitramine: dinitrosamine	Mono-nitrosamine: dinitrosamine
20-07-2016	06:26 – 06:56	0.000	n/a	n/a	n/a
	09:52 – 10:52*	0.295	0.070	127.9	40.4
	11:01 – 12:01*	0.095	0.018	1046.1	49.3
	12:45 – 13:45	0.009	0.001	2654.5	62.6
21-07-2016	06:22 – 06:52	0.005	n/a	n/a	n/a
	11:42 – 12:27*	0.106	0.031	616.0	63.5
	12:32 – 13:02*	0.078	0.013	1077.3	72.3
	13:07 – 13:19*	0.173	0.027	629.1	50.6
	13:37 – 14:37	0.010	0.001	963.0	52.5
22-07-2016	06:35 – 07:05	0.000	n/a	n/a	n/a
	09:30 – 10:30*	0.000	0.000	n/a	n/a
	10:44 – 11:15*	0.000	0.000	n/a	n/a
	11:49 – 12:49	0.000	0.000	n/a	n/a

Table A10 continued. *denotes sampling intervals during which the chamber canopy was open.

Date	Sampling time (HH:mm, UTC)	[1,4-dinitrosopiperazine] / µg m^{-3}	Average % dinitrosamine yield	Nitramine: dinitrosamine	Mono-nitrosamine: dinitrosamine
25-07-2016	06:31 – 07:01	0.035	n/a	n/a	n/a
	08:35 – 09:15*	0.138	0.024	234.3	39.6
	09:54 – 10:54	0.012	0.001	438.9	15.0
26-07-16	06:29 – 06:59	0.000	n/a	n/a	n/a
	08:55 – 09:30*	0.192	0.053	330.4	30.7
	10:06 – 10:51	0.017	0.003	365.2	11.2

Table A11. Compounds identified from TDU-GC×GC-TOF-MS measurements for heating canola oil to 180 °C. 1st RT and 2nd RT represent first and second retention time, and similarity is out of 1000.

Compound	1st RT / s	2nd RT / s	Molecular formula	Similarity
propanal	245	0.29	C_3H_6O	918
acrolein	245	0.32	C_3H_4O	967
heptane	295	0.42	C_7H_{16}	923
5-hydroxymethyl-2[5H]-furanone	350	2.16	$C_6H_6O_3$	831
octane	370	0.63	C_8H_{18}	914
hexanal	375	1.28	$C_6H_{12}O$	854
3-hexen-2-one	405	1.74	$C_6H_{10}O$	936
maelic anhydride	420	3.60	$C_4H_2O_3$	953
2-hexenal (E)	420	1.78	$C_6H_{10}O$	949
1-nonene	455	0.93	C_9H_{18}	942
nonane	465	0.84	C_9H_{20}	927
heptanal	470	1.76	$C_7H_{14}O$	923
butyrolactone	485	4.78	$C_4H_6O_2$	967
1-butyl-cyclopentene	495	1.22	C_9H_{16}	853
butyl-cyclopentane	510	1.17	C_9H_{18}	963
2-heptenal (Z)	525	2.18	$C_7H_{12}O$	830
5-methyldihydro-2(3H)-furanone	535	4.42	$C_5H_8O_2$	963
5-ethyl-2(5H)-furanone	540	3.54	C_6H_8O	856
2-heptenal (E)	540	2.36	$C_7H_{12}O$	886
benzaldehyde	550	3.44	C_7H_6O	946
1-heptanol	555	1.87	$C_7H_{16}O$	912
1-hepten-3-ol	570	1.87	$C_7H_{14}O$	810
1-decene	585	1.16	$C_{10}H_{20}$	962
2-pentyl-furan	585	1.81	$C_9H_{14}O$	932
2,4-heptadienal – 1	595	2.81	$C_7H_{10}O$	906
octanal	605	2.11	$C_8H_{16}O$	935
2,4-heptadienal – 2	615	3.00	$C_7H_{10}O$	892
5-ethyl-dihydro-2(3H)-furanone	685	4.83	$C_6H_{10}O_2$	936
2-octenal	690	2.56	$C_8H_{14}O$	939
heptanoic acid	710	2.20	$C_7H_{14}O_2$	898
nonanal	760	2.31	$C_9H_{18}O$	936
2-nonenal	850	2.69	$C_9H_{16}O$	927
octanoic acid	865	2.32	$C_8H_{16}O_2$	887
decanal	925	2.35	$C_{10}H_{20}O$	856
isophthalaldehyde	985	1.49	$C_8H_6O_2$	947
2-decenal	1015	2.72	$C_{10}H_{18}O$	926
2-undecenal	1175	2.72	$C_{11}H_{20}O$	896

Table A12. Compounds identified from TDU-GC×GC-TOF-MS measurements for heating sunflower oil to 180 °C. 1st RT and 2nd RT represent first and second retention time, and similarity is out of 1000.

Compound	1st RT / s	2nd RT / s	Molecular formula	Similarity
acrolein	195	0.32	C_3H_4O	979
2-methylpropanal	240	0.65	C_4H_8O	936
2-butenal	240	0.92	C_4H_6O	924
heptane	250	0.46	C_7H_{16}	939
2-pentenal	295	1.45	C_5H_8O	930
2-methylbutenal	305	2.24	C_5H_8O	851
octane	325	0.72	C_8H_{18}	893
3-octene	330	0.88	C_8H_{16}	948
hexanal	330	1.70	$C_6H_{12}O$	859
cyclopentanone	335	2.22	C_5H_8O	924
2-octene	340	0.97	C_8H_{16}	887
1,3-octadiene	350	1.02	C_8H_{14}	964
methylcyclopentanone	375	2.15	$C_6H_{10}O$	951
2-hexenal (Z)	380	1.89	$C_6H_{10}O$	881
2-hexenal (E)	390	2.14	$C_6H_{10}O$	950
1-nonene	425	1.02	C_9H_{18}	958
2-butyl-furan	430	1.59	$C_8H_{12}O$	919
2-heptanone	430	1.86	C_7H14_4O	942
heptanal	440	1.84	$C_7H_{14}O$	891
butyrolactone	470	0.14	$C_4H_6O_2$	971
2-heptenal (Z)	505	2.39	$C_7H_{12}O$	858
2-heptenal (E)	520	2.66	$C_7H_{12}O$	936
dihydro-5-methyl-2(3H)-furanone	525	4.76	$C_5H_8O_2$	946
ethylcyclopentanone	525	3.09	$C_7H_{12}O$	848
1-hepten-3-one	550	2.29	$C_7H_{12}O$	831
1-octen-3-ol	555	2.01	$C_8H_{16}O$	915
hexanoic acid	560	2.21	$C_6H_{12}O_2$	941
dihydro-dimethyl-2(3H)-furanone	565	4.38	$C_6H_{10}O_2$	NA
2-pentyl-furan	570	1.95	$C_9H_{14}O$	877
1-decene	570	1.23	$C_{10}H_{20}$	957
3-octanol	580	1.82	$C_8H_{18}O$	844
octanal	590	2.15	$C_8H_{16}O$	964
2-octenal	680	2.69	$C_8H_{14}O$	921
dihydro-5-ethyl-2(3H)-furanone	680	0.07	$C_6H_{10}O_2$	919
1-octanol	695	2.20	$C_8H_{18}O$	940
heptanoic acid	705	2.34	$C_7H_{14}O_2$	949
nonanal	755	2.34	$C_9H_{18}O$	960
benzoic acid	860	4.07	$C_7H_6O_2$	927

Table A12 continued.

Compound	1st RT / s	2nd RT / s	Molecular formula	Similarity
octanoic acid	870	2.40	$C_8H_{16}O_2$	892
decanal	920	2.45	$C_{10}H_{20}O$	889
2-decenal	1015	2.78	$C_{10}H_{18}O$	933
2,4-decadienal – 1	1100	3.30	$C_{10}H_{16}O$	931
2,4-decadienal – 2	1105	3.25	$C_{10}H_{16}O$	946
2-undecenal	1175	2.82	$C_{11}H20O$	915
cyclododecane	1410	2.29	$C_{12}H_{24}$	925
hexadecenoic acid	1970	2.86	$C_{16}H_{32}O_2$	887
octadecanoic acid	2215	4.16	$C_{18}H_{36}O_2$	910

Table A13. Compounds identified from TDU-GC×GC-TOF-MS measurements for heating olive oil to 180 °C. 1st RT and 2nd RT represent first and second retention time, and similarity is out of 1000.

Compound	1st RT / s	2nd RT / s	Molecular formula	Similarity
propanal	240	0.29	C_3H_6O	NA
acrolein	240	0.30	C_3H_4O	NA
hexane	295	0.41	C_7H_{16}	NA
2-ethylfuran	295	0.72	C_6H_8O	934
2-pentanone	300	0.77	$C_5H_{10}O$	865
2-methylbutanal	305	0.82	$C_5H_{10}O$	850
2-methyl-1-butanol	325	0.85	$C_5H_{12}O$	890
3-methyl-2-butenal	335	1.29	C_5H_8O	909
2-methylpropanoic acid, ethyl ester	335	0.88	$C_6H_{12}O_2$	895
2-hexanone	355	1.22	$C_{10}H_{12}O$	924
octane	365	0.63	C_8H_{18}	966
hexanal	365	1.30	$C_6H_{12}O$	827
1-methoxyhexane	385	0.96	$C_7H_{16}O$	940
1-methoxy-3-hexene	390	1.09	$C_7H_{14}O$	947
2-hexenal (Z)	405	1.73	$C_6H_{10}O$	889
3-methylbutanoic acid, ethyl ester	410	1.25	$C_7H_{14}O_2$	951
2-hexenal (E)	415	1.83	$C_6H_{10}O$	945
pentanoic acid	440	1.52	$C_5H_{10}O_2$	962
1-nonene	450	0.94	C_9H_{18}	944
2-heptanone	450	1.69	$C_7H_{14}O$	939
nonane	460	0.86	C_9H_{20}	922
heptanal	465	1.74	$C_7H_{14}O$	951
butyrolactone	485	4.78	$C_4H_6O_2$	956
α-pinene	510	1.35	$C_{10}H_{16}$	937
5-methyl-dihydro-2(3H)-furanone	535	4.42	$C_5H_8O_2$	956
6-methyl-2-heptanone	535	1.86	$C_6H_{16}O$	916
2-heptenal (E)	535	2.30	$C_7H_{12}O$	926
2-ethyl-2(5H)-furanone	540	3.51	$C_6H_8O_2$	862
hexanoic acid	565	1.96	$C_6H_{12}O_2$	925
1-decene	580	1.17	$C_{10}H_{20}$	939
2-pentylfuran	585	1.81	$C_9H_{14}O$	922
2-octanone	585	2.05	$C_8H_{16}O$	933
decane	595	1.05	$C_{10}H_{22}$	949
octanal	600	2.12	$C_8H_{16}O$	960
2,4-heptadienal	615	2.97	$C_7H_{10}O$	896
5-ethyl-dihydro-2(3H)-furanone	685	4.83	$C_6H_{10}O_2$	932
2-octenal	685	2.58	$C_8H_{14}O$	929
tetrahydro-2H-pyran-2-one	690	1.27	$C_5H_8O_2$	885

Table A13 continued.

Compound	1st RT / s	2nd RT / s	Molecular formula	Similarity
heptanoic acid	710	2.15	$C_7H_{14}O_2$	785
2-nonanone	740	2.27	$C_9H_{18}O$	886
undecane	750	1.19	$C_{11}H_{24}$	908
nonanal	760	2.30	$C_9H_{18}O$	957
5-propyl-dihydro-2(3H)-furanone	845	4.84	$C_7H_{12}O_2$	922
2-nonenal	850	2.68	$C_9H_{16}O$	935
benzoic acid	860	3.90	$C_7H_6O_2$	926
octanoic acid	865	2.32	$C_8H_{14}O_2$	859
2-decanone	905	2.35	$C_{10}H_{20}O$	943
decanal	925	2.36	$C_{10}H_{20}O$	914
5-butyl-dihydro-2(3H)-furanone	1015	4.78	$C_8H_{14}O_2$	912
2-decenal	1015	2.74	$C_{10}H_{18}O$	928
nonanoic acid	1020	2.42	$C_9H_{18}O_2$	799
2,4-decadienal	1105	3.18	$C_{10}H_{16}O$	906
2-undecenal	1175	2.74	$C_{11}H_{20}O$	914
5-pentyl-dihydro-2(3H)-furanone	1180	4.60	$C_9H_{16}O_2$	937
6,10-dimethyl-2-undecanone	1240	2.25	$C_{13}H_{26}O$	847
hexadecanoic acid	1965	2.64	$C_{16}H_{32}O_2$	854

Table A14. GC×GC-TOF-MS measurements of SOA compounds present in emissions from charbroiling chicken in a small amount of oil at 180 °C. 1st and 2nd RT represent first and second retention time, and similarity is out of 1000. * denotes compounds present in oil emissions, and ≠ represents compounds detected in urban atmospheric $PM_{2.5}$.

Compound	1st RT / s	2nd RT / s	Similarity	Molecular formula	Type
2,3-dimethyl-pyridine*≠	540	1.48	938	C_7H_9N	pyridine
glycerol≠	650	2.57	650	$C_3H_8O_3$	triol
3,5,5-trimethyl-hexanoic acid*≠	975	2.64	814	$C_9H_{18}O_2$	fatty acid
2,4-dimethyl-2-pentanol*≠	990	2.74	715	$C_7H_{16}O$	alcohol
creatinine*	1360	2.09	912	$C_4H_7N_3O$	N-heteroc.
2,4-decadienal	1485	2.19	735	$C_{10}H_{16}O$	aldehyde
niacinamide	1605	0.30	927	$C_6H_6N_2O$	amide
2-nitrobutane*≠	1650	1.53	763	$C_4H_9NO_2$	nitroalkane
hexahydropyrrolizin-3-one*	1835	4.33	687	$C_7H_{11}NO$	N-heteroc.
2-isoamylpyridine*	1840	3.50	NA	$C_9H_{14}N_2$	pyridine
6-amino-3-methylpurine*	2015	3.36	687	$C_6H_7N_2$	purine
E-11-tetradecenoic acid*	2030	1.31	787	$C_{14}H_{26}O_2$	alken. acid
hexahydro-pyrrolo[1,2-α]pyrazine-1,4-dione*	2045	0.41	544	$C_7H_{10}N_2O_2$	diketo pz.
5-ethyl-4-tridecanone*	2100	1.55	607	$C_{15}H_{30}O$	ketone
nonanoic acid*≠	1375	2.03	NA	$C_9H_{18}O_2$	fatty acid
decanoic acid*≠	1560	1.54	NA	$C_{10}H_{20}O_2$	fatty acid
undecanoic acid*≠	1705	1.34	NA	$C_{11}H_{22}O_2$	fatty acid
dodecanoic (lauric) acid≠	1835	1.23	NA	$C_{12}H_{24}O_2$	fatty acid
tridecanoic acid*≠	1940	1.19	NA	$C_{13}H_{26}O_2$	fatty acid
tetradecanoic (myristic) acid≠	2035	1.18	852	$C_{14}H_{28}O_2$	fatty acid
pentadecanoic acid≠	2130	1.17	NA	$C_{15}H_{30}O_2$	fatty acid
hexadecenoic (palmitic) acid≠	2220	1.17	910	$C_{16}H_{32}O_2$	fatty acid
heptadecanoic (margaric) acid≠	2305	1.14	NA	$C_{17}H_{34}O_2$	fatty acid
linoleic acid≠	2360	1.42	NA	$C_{18}H_{32}O_2$	fatty acid
oleic acid≠	2365	1.29	912	$C_{18}H_{34}O_2$	fatty acid
linolenic acid≠	2360	1.57	867	$C_{18}H_{30}O_2$	fatty acid
octadecanoic (stearic) acid≠	2380	1.17	857	$C_{18}H_{36}O_2$	fatty acid

Table A14 continued.

Compound	1st RT / s	2nd RT / s	Similarity	Molecular formula	Type
5-butyldihydro-2(3H)-furanone≠	1355	4.255	NA	$C_8H_{14}O_2$	γ-lactone
5-pentyldihydro-2(3H)-furanone≠	1555	2.97	NA	$C_9H_{16}O_2$	γ-lactone
5-hexyldihydro-2(3H)-furanone≠	1715	2.41	NA	$C_{10}H_{18}O_2$	γ-lactone
5-heptyldihydro-2(3H)-furanone≠	1845	2.16	NA	$C_{11}H_{20}O_2$	γ-lactone
5-octyldihydro-2(3H)-furanone≠	1960	2.02	NA	$C_{12}H_{22}O_2$	γ-lactone
5-nonyldihydro-2(3H)-furanone≠	2065	1.93	NA	$C_{13}H_{24}O_2$	γ-lactone
5-decyldihydro-2(3H)-furanone≠	2165	1.85	NA	$C_{14}H_{26}O_2$	γ-lactone
5-undecyldihydro-2(3H)-furanone≠	2255	1.81	NA	$C_{15}H_{28}O_2$	γ-lactone
5-dodecyldihydro-2(3H)-furanone≠	2340	1.79	NA	$C_{16}H_{30}O_2$	γ-lactone
5-tridecyldihydro-2(3H)-furanone≠	2420	1.77	NA	$C_{17}H_{32}O_2$	γ-lactone
5-tetradecyldihydro-2(3H)-furanone≠	2500	1.74	NA	$C_{18}H_{34}O_2$	γ-lactone
tetrahydro-6-butyl-2H-pyran-2-one*≠	1600	3.12	NA	$C_9H_{16}O_2$	δ-lactone
tetrahydro-6-heptyl-2H-pyran-2-one*≠	1990	2.19	NA	$C_{12}H_{22}O_2$	δ-lactone
tetrahydro-6-octyl-2H-pyran-2-one≠	2095	2.08	NA	$C_{13}H_{24}O_2$	δ-lactone
tetrahydro-6-nonyl-2H-pyran-2-one≠	2190	2.02	NA	$C_{14}H_{26}O_2$	δ-lactone
tetrahydro-6-decyl-2H-pyran-2-one≠	2280	1.97	NA	$C_{15}H_{28}O_2$	δ-lactone
tetrahydro-6-undecyl-2H-pyran-2-one≠	2365	1.94	NA	$C_{16}H_{30}O_2$	δ-lactone
tetrahydro-6-dodecyl-2H-pyran-2-one≠	2445	1.92	NA	$C_{17}H_{32}O_2$	δ-lactone
tetrahydro-6-tridecyl-2H-pyran-2-one≠	2525	1.87	NA	$C_{18}H_{34}O_2$	δ-lactone

Table A15. GC×GC-TOF-MS measurements of SOA compounds present in emissions from charbroiling beef burgers at 200°C. 1st and 2nd RT represent first and second retention time, and similarity is out of 1000. * denotes compounds present in oil emissions, and ≠ represents compounds detected in urban atmospheric $PM_{2.5}$.

Compound	1st RT / s	2nd RT / s	Similarity	Molecular formula	Type
glycerol≠	650	2.56	930	$C_3H_8O_3$	triol
3,5,5-trimethyl-hexanoic acid*≠	975	2.64	817	$C_9H_{18}O_2$	fatty acid
2,4-dimethyl-2-pentanol*≠	990	2.75	719	$C_7H_{16}O$	alcohol
citraconic acid*	1050	1.96	859	$C_5H_6O_4$	dicarb acid
2,4-decadienal	1485	2.19	NA	$C_{10}H_{16}O$	aldehyde
(methoxymethyl)oxirane*	1485	3.91	675	$C_4H_8O_2$	O-heteroc.
niacinamide	1605	0.29	931	$C_6H_6N_2O$	amide
2-nitrobutane*≠	1650	1.53	872	$C_4H_9NO_2$	nitroalkane
hexahydropyrrolizin-3-one*	1835	4.33	588	$C_7H_{11}NO$	N-heteroc.
2-propyltetrahydrofuran*	1890	1.08	700	$C_7H_{14}O$	O-heteroc.
E-11-tetradecenoic acid*	2025	1.33	771	$C_{14}H_{26}O_2$	alken. acid
bis(2-hydroxyethyl)ester 1,4-benzene dicarboxylic acid*	2405	3.60	690	$C_{12}H_{14}O_6$	ester/diol
octanoic acid*≠	1090	3.46	NA	$C_8H_{16}O_2$	fatty acid
nonanoic acid*≠	1375	2.03	NA	$C_9H_{18}O_2$	fatty acid
undecanoic acid*≠	1705	1.34	NA	$C_{11}H_{22}O_2$	fatty acid
dodecanoic (lauric) acid≠	1830	1.23	NA	$C_{12}H_{24}O_2$	fatty acid
tridecanoic acid*≠	1940	1.18	NA	$C_{13}H_{26}O_2$	fatty acid
tetradecanoic (myristic) acid≠	2035	1.19	NA	$C_{14}H_{28}O_2$	fatty acid
pentadecanoic acid≠	2130	1.17	824	$C_{15}H_{30}O_2$	fatty acid
hexadecenoic (palmitic) acid≠	2220	1.16	901	$C_{16}H_{32}O_2$	fatty acid
heptadecanoic (margaric) acid≠	2305	1.14	NA	$C_{17}H_{34}O_2$	fatty acid
linoleic acid≠	2360	1.43	900	$C_{18}H_{32}O_2$	fatty acid
oleic acid≠	2365	1.30	902	$C_{18}H_{34}O_2$	fatty acid
linolenic acid≠	2360	1.58	840	$C_{18}H_{30}O_2$	fatty acid
octadecanoic (stearic) acid≠	2380	1.17	872	$C_{18}H_{36}O_2$	fatty acid

Table A15 continued.

Compound	1st RT / s	2nd RT / s	Similarity	Molecular formula	Type
5-butyldihydro-2(3H)-furanone≠	1350	4.34	887	$C_8H_{14}O_2$	γ-lactone
5-pentyldihydro-2(3H)-furanone≠	1555	2.97	NA	$C_9H_{16}O_2$	γ-lactone
5-hexyldihydro-2(3H)-furanone≠	1715	2.41	NA	$C_{10}H_{18}O_2$	γ-lactone
5-heptyldihydro-2(3H)-furanone≠	1845	2.16	NA	$C_{11}H_{20}O_2$	γ-lactone
5-octyldihydro-2(3H)-furanone≠	1960	2.02	NA	$C_{12}H_{22}O_2$	γ-lactone
5-nonyldihydro-2(3H)-furanone≠	2065	1.93	NA	$C_{13}H_{24}O_2$	γ-lactone
5-decyldihydro-2(3H)-furanone≠	2165	1.85	NA	$C_{14}H_{26}O_2$	γ-lactone
5-undecyldihydro-2(3H)-furanone≠	2255	1.82	NA	$C_{15}H_{28}O_2$	γ-lactone
5-dodecyldihydro-2(3H)-furanone≠	2340	1.79	NA	$C_{16}H_{30}O_2$	γ-lactone
5-tridecyldihydro-2(3H)-furanone≠	2420	1.77	NA	$C_{17}H_{32}O_2$	γ-lactone
5-tetradecyldihydro-2(3H)-furanone≠	2500	1.74	NA	$C_{18}H_{34}O_2$	γ-lactone
tetrahydro-6-butyl-2H-pyran-2-one*≠	1600	3.11	NA	$C_9H_{16}O_2$	δ-lactone
tetrahydro-6-heptyl-2H-pyran-2-one*≠	1990	2.19	NA	$C_{12}H_{22}O_2$	δ-lactone
tetrahydro-6-octyl-2H-pyran-2-one≠	2095	2.08	NA	$C_{13}H_{24}O_2$	δ-lactone
tetrahydro-6-nonyl-2H-pyran-2-one≠	2190	2.02	844	$C_{14}H_{26}O_2$	δ-lactone
tetrahydro-6-decyl-2H-pyran-2-one≠	2280	1.97	NA	$C_{15}H_{28}O_2$	δ-lactone
tetrahydro-6-undecyl-2H-pyran-2-one≠	2365	1.94	NA	$C_{16}H_{30}O_2$	δ-lactone
tetrahydro-6-dodecyl-2H-pyran-2-one≠	2445	1.91	NA	$C_{17}H_{32}O_2$	δ-lactone
tetrahydro-6-tridecyl-2H-pyran-2-one≠	2525	1.87	NA	$C_{18}H_{34}O_2$	δ-lactone

Table A16. GC×GC-TOF-MS measurements of SOA compounds present in emissions from frying beef in *ca.* 25 g of sunflower oil at 180 °C. 1st and 2nd RT represent first and second retention time, and similarity is out of 1000. * denotes compounds present in oil emissions, and ≠ represents compounds detected in urban atmospheric $PM_{2.5}$.

Compound	1st RT / s	2nd RT / s	Similarity	Molecular formula	Type
glycerol≠	650	2.58	927	$C_3H_8O_3$	triol
propyl-propanedioic acid*	660	1.25	824	$C_6H_{10}O_4$	dicarb acid
3,5,5-trimethyl-hexanoic acid*≠	975	2.63	778	$C_9H_{18}O_2$	fatty acid
2,4-dimethyl-2-pentanol*≠	990	2.74	697	$C_7H_{16}O$	alcohol
citraconic acid*	1050	1.96	NA	$C_5H_6O_4$	dicarb acid
creatinine*	1360	2.10	898	$C_4H_7N_3O$	N-heteroc.
2,4-decadienal	1485	2.19	820	$C_{10}H_{16}O$	aldehyde
(methoxymethyl)oxirane*	1490	3.90	733	$C_4H_8O_2$	oxirane
niacinamide	1600	0.40	932	$C_6H_6N_2O$	amide
2-nitrobutane*≠	1650	1.54	NA	$C_4H_9NO_2$	nitroalkane
hexahydropyrrolizin-3-one*	1835	4.34	617	$C_7H_{11}NO$	N-heteroc.
bis(2-hydroxyethyl)ester 1,4-benzene dicarboxylic acid*	2405	3.60	NA	$C_{12}H_{14}O_6$	ester/diol
octanoic acid*≠	1095	3.48	NA	$C_8H_{16}O_2$	fatty acid
nonanoic acid*≠	1375	2.03	NA	$C_9H_{18}O_2$	fatty acid
decanoic acid*≠	1560	1.54	NA	$C_{10}H_{20}O_2$	fatty acid
undecanoic acid*≠	1705	1.35	NA	$C_{11}H_{22}O_2$	fatty acid
dodecanoic (lauric) acid≠	1830	1.24	NA	$C_{12}H_{24}O_2$	fatty acid
tridecanoic acid*≠	1940	1.19	NA	$C_{13}H_{26}O_2$	fatty acid
tetradecanoic (myristic) acid≠	2040	1.16	767	$C_{14}H_{28}O_2$	fatty acid
pentadecanoic acid≠	2135	1.14	NA	$C_{15}H_{30}O_2$	fatty acid
hexadecenoic (palmitic) acid≠	2215	1.18	875	$C_{16}H_{32}O_2$	fatty acid
heptadecanoic (margaric) acid≠	2305	1.15	NA	$C_{17}H_{34}O_2$	fatty acid
linoleic acid≠	2360	1.41	861	$C_{18}H_{32}O_2$	fatty acid
oleic acid≠	2365	1.29	859	$C_{18}H_{34}O_2$	fatty acid
linolenic acid≠	2365	1.54	815	$C_{18}H_{30}O_2$	fatty acid
octadecanoic (stearic) acid≠	2380	1.16	806	$C_{18}H_{36}O_2$	fatty acid

Table A16 continued.

Compound	1st RT / s	2nd RT / s	Similarity	Molecular formula	Type
5-butyldihydro-2(3H)-furanone≠	1350	4.34	887	$C_8H_{14}O_2$	γ-lactone
5-pentyldihydro-2(3H)-furanone≠	1555	2.97	NA	$C_9H_{16}O_2$	γ-lactone
5-hexyldihydro-2(3H)-furanone≠	1715	2.41	NA	$C_{10}H_{18}O_2$	γ-lactone
5-heptyldihydro-2(3H)-furanone≠	1845	2.16	NA	$C_{11}H_{20}O_2$	γ-lactone
5-octyldihydro-2(3H)-furanone≠	1960	2.02	NA	$C_{12}H_{22}O_2$	γ-lactone
5-nonyldihydro-2(3H)-furanone≠	2065	1.93	NA	$C_{13}H_{24}O_2$	γ-lactone
5-decyldihydro-2(3H)-furanone≠	2165	1.85	NA	$C_{14}H_{26}O_2$	γ-lactone
5-undecyldihydro-2(3H)-furanone≠	2255	1.82	NA	$C_{15}H_{28}O_2$	γ-lactone
5-dodecyldihydro-2(3H)-furanone≠	2340	1.79	692	$C_{16}H_{30}O_2$	γ-lactone
5-tridecyldihydro-2(3H)-furanone≠	2420	1.77	NA	$C_{17}H_{32}O_2$	γ-lactone
5-tetradecyldihydro-2(3H)-furanone≠	2500	1.74	727	$C_{18}H_{34}O_2$	γ-lactone
tetrahydro-6-butyl-2H-pyran-2-one*≠	1600	3.11	NA	$C_9H_{16}O_2$	δ-lactone
tetrahydro-6-heptyl-2H-pyran-2-one*≠	1990	2.19	NA	$C_{12}H_{22}O_2$	δ-lactone
tetrahydro-6-octyl-2H-pyran-2-one≠	2095	2.08	844	$C_{13}H_{24}O_2$	δ-lactone
tetrahydro-6-nonyl-2H-pyran-2-one≠	2190	2.02	NA	$C_{14}H_{26}O_2$	δ-lactone
tetrahydro-6-decyl-2H-pyran-2-one≠	2280	1.97	NA	$C_{15}H_{28}O_2$	δ-lactone
tetrahydro-6-undecyl-2H-pyran-2-one≠	2365	1.94	NA	$C_{16}H_{30}O_2$	δ-lactone
tetrahydro-6-dodecyl-2H-pyran-2-one≠	2445	1.91	NA	$C_{17}H_{32}O_2$	δ-lactone
tetrahydro-6-tridecyl-2H-pyran-2-one≠	2525	1.87	NA	$C_{18}H_{34}O_2$	δ-lactone

Table A17. GC×GC-TOF-MS measurements of SOA compounds present in emissions from charbroiling beef in a small amount of oil at 180 °C. 1st and 2nd RT represent first and second retention time, and similarity is out of 1000. * denotes compounds present in olive oil emissions, and ≠ represents compounds detected in urban atmospheric $PM_{2.5}$.

Compound	1st RT / s	2nd RT / s	Similarity	Molecular formula	Type
L-lactic acid*	510	1.41	958	$C_3H_6O_3$	carb acid
2,3-dimethyl-pyridine*≠	540	1.45	861	C_7H_9N	pyridine
glycerol≠	650	2.63	904	$C_3H_8O_3$	triol
propyl-propanedioic acid*	650	1.24	903	$C_6H_{10}O_4$	dicarb acid
3,5,5-trimethyl-hexanoic acid*≠	975	2.64	848	$C_9H_{18}O_2$	fatty acid
creatinine*	1360	2.14	888	$C_4H_7N_3O$	N-heteroc.
(methoxymethyl)oxirane*	1490	3.86	652	$C_4H_8O_2$	oxirane
creatinine derivative*	1515	0.24	818	NA	N-heteroc.
Nε-acetyl-L-lysine*	1575	4.53	976	$C_8H_{16}N_2O_3$	amino acid
niacinamide	1605	0.43	958	$C_6H_6N_2O$	amide
2-nitrobutane*≠	1650	1.54	816	$C_4H_9NO_2$	nitroalkane
4-amino-4,5(1H)-dihydro-1,2,4-triazole-5-one*	1700	3.76	891	$C_2H_4N_4O$	N-heteroc.
l-acetyl-creatinine*	1720	4.06	806	$C_6H_9N_3O_2$	N-heteroc.
2-methyl-5-propyl-pyrazine*	1770	3.31	717	$C_8H_{12}N_2$	pyrazine
3,6-dimethylpiperazine-2,5-dione*	1775	4.90	820	$C_6H_{10}N_2O_2$	diketopz
5-isobutyl-2,4-imidazolidinedione*≠	1820	3.29	829	$C_7H_{12}N_2O_2$	N-heteroc.
hexahydropyrrolizin-3-one*	1835	4.34	684	$C_7H_{11}NO$	N-heteroc.
2-isoamylpyrazine*	1840	3.50	724	$C_9H_{14}N_2$	pyrazine
2-isoamyl-6-methylpyrazine*	1910	3.27	695	$C_{10}H_{16}N_2$	pyrazine
D-pyroglutamic acid*	1915	0.89	942	$C_5H_7NO_3$	cyc a. acid
imidazolidinedione derivative*	1955	4.48	735	$C_4H_6N_2O_2$	N-heteroc.
dl-alanyl-l-leucine*	2010	3.54	702	$C_9H_{18}N_2O_3$	peptide
6-amino-3-methylpurine*	2015	3.36	715	$C_6H_7N_5$	purine
3,6-diisopropylpiperazin-2,5-dione*	2040	3.25	763	$C_{10}H_{18}N_2O_2$	diketopz
hexahydro-pyrrolo[1,2-α] pyrazine-1,4-dione*	2045	0.42	769	$C_7H_{10}N_2O_2$	diketopz.
3-methyl-4-amino-4,5(1H)-dihydro-1,2,4-triazole-5-one*	2045	4.08	775	$C_3H_6N_4O$	N-heteroc.
2-adamantylamine*	2085	3.60	750	$C_{10}H_{17}N$	amine
bis(2-hydroxyethyl)ester 1,4-benzene dicarboxylic acid*	2405	3.60	818	$C_{12}H_{14}O_6$	ester/diol

Table A17 continued.

Compound	1st RT / s	2nd RT / s	Similarity	Molecular formula	Type
pentanoic acid*≠	520	1.13	933	$C_5H_{10}O_2$	fatty acid
hexanoic acid*≠	650	1.24	938	$C_6H_{12}O_2$	fatty acid
nonanoic acid*≠	1370	2.07	760	$C_9H_{18}O_2$	fatty acid
decanoic acid≠	1555	1.57	NA	$C_{10}H_{20}O_2$	fatty acid
undecanoic acid*≠	1705	1.34	NA	$C_{11}H_{22}O_2$	fatty acid
dodecanoic (lauric) acid≠	1830	1.23	701	$C_{12}H_{24}O_2$	fatty acid
tridecanoic acid*≠	1940	1.19	NA	$C_{13}H_{26}O_2$	fatty acid
tetradecanoic (myristic) acid≠	2035	1.18	803	$C_{14}H_{28}O_2$	fatty acid
pentadecanoic acid≠	2130	1.16	NA	$C_{15}H_{30}O_2$	fatty acid
hexadecenoic (palmitic) acid≠	2215	1.18	895	$C_{16}H_{32}O_2$	fatty acid
heptadecanoic (margaric) acid≠	2300	1.17	NA	$C_{17}H_{34}O_2$	fatty acid
linoleic acid≠	2360	1.42	902	$C_{18}H_{32}O_2$	fatty acid
oleic acid≠	2365	1.29	867	$C_{18}H_{34}O_2$	fatty acid
linolenic acid≠	2365	1.53	825	$C_{18}H_{30}O_2$	fatty acid
octadecanoic (stearic) acid≠	2380	1.17	NA	$C_{18}H_{36}O_2$	fatty acid
5-pentyldihydro-2(3H)-furanone≠	1550	2.97	NA	$C_9H_{16}O_2$	γ-lactone
5-hexyldihydro-2(3H)-furanone≠	1715	2.41	NA	$C_{10}H_{18}O_2$	γ-lactone
5-heptyldihydro-2(3H)-furanone≠	1845	2.16	NA	$C_{11}H_{20}O_2$	γ-lactone
5-octyldihydro-2(3H)-furanone≠	1960	2.02	NA	$C_{12}H_{22}O_2$	γ-lactone
5-nonyldihydro-2(3H)-furanone≠	2065	1.92	NA	$C_{13}H_{24}O_2$	γ-lactone
5-decyldihydro-2(3H)-furanone≠	2165	1.85	NA	$C_{14}H_{26}O_2$	γ-lactone
5-undecyldihydro-2(3H)-furanone≠	2255	1.82	NA	$C_{15}H_{28}O_2$	γ-lactone
5-dodecyldihydro-2(3H)-furanone≠	2340	1.79	NA	$C_{16}H_{30}O_2$	γ-lactone
5-tridecyldihydro-2(3H)-furanone≠	NA	NA	coelution	$C_{17}H_{32}O_2$	γ-lactone
5-tetradecyldihydro-2(3H)-furanone≠	2500	1.74	NA	$C_{18}H_{34}O_2$	γ-lactone
tetrahydro-6-nonyl-2H-pyran-2-one≠	2190	2.02	NA	$C_{14}H_{26}O_2$	δ-lactone
tetrahydro-6-undecyl-2H-pyran-2-one≠	2365	1.94	NA	$C_{16}H_{30}O_2$	δ-lactone
tetrahydro-6-tridecyl-2H-pyran-2-one≠	2525	1.87	NA	$C_{18}H_{34}O_2$	δ-lactone

Abbreviations

ACA	Atmospheric Chemistry of Amines
ADAF	Age-Dependent Adjustment Factor
AMP	Aminomethyl Propanol
AMP-NO_2	2-methyl-2-(nitroamino)propan-2-ol
ASE	Accelerated Solvent Extraction
BaP	Benzo(a)pyrene
BNF	Biological Nitrogen Fixation
CCN	Cloud Condensation Nuclei
CCS	Carbon Capture and Storage
CHARON	Chemical Analysis of Aerosol Online system
CIS	Cooled Injection System
ClearfLo	Clean Air for London
COA	Cooking Organic Aerosol
DEA	Diethylamine
DIT	Diterpene
DMA	Dimethylamine
EC	Elemental Carbon
EF	Emission Factor
EHF	Enhancement Factor
EUPHORE	European Photochemical Reactor
FID	Flame Ionization Detector
FTIR	Fourier Transform Infrared Spectroscopy
GC	Gas Chromatography
GC×GC	Comprehensive Two-Dimensional Gas Chromatography
HAA	Heterocyclic Aromatic Amine
HC	Hydrocarbon
HEC	Human Equivalent Concentration
HR-TOF-AMS	High Resolution Time of Flight Aerosol Mass Spectrometer
IARC	International Agency for Research on Cancer
IC	Ion Chromatography

IDM	Inhalation Dosimetry Methodology
IN	Inorganic Nitrogen
IPN	Isopropyl Nitrite
IRIS	Integration Risk Information System
IUR	Inhalation Unit Risk
LC	Liquid Chromatography
LOD	Limit of Detection
LOQ	Limit of Quantification
MT	Monoterpene
NAB	N-nitrosoanabasine
NAT	N-nitrosoanatabine
NCD	Nitrogen Chemiluminescence Detector
NDBA	N-nitrosodibutylamine
NDEA	N-nitrosodiethylamine
NDMA	N-nitrosodimethylamine
NDPA	N-nitrosodipropylamine
NDPhA	N-nitrosodiphenylamine
NERC	Natural Environment Research Council
NH_4NO_3	Ammonium Nitrate
$[NH_4]_2SO_4$	Ammonium Sulfate
Nitro-PAH	Nitrated Polycyclic Aromatic Hydrocarbon
NIPH	Norwegian Institute of Public Health
NMEA	N-nitrosomethylamine
NMOG	Non-Methane Organic Gas
NMor	N-nitrosomorpholine
NNAL	4-(methylnitrosoamino)-1-(3-pyridyl)-1-butanol
NNK	4-(methylnitrosoamino)-1-(3-pyridyl)-1-butanone
NNN	N-nitrosonornicotine
NO_x	$NO + NO_2$
NO_y	All oxides of nitrogen
NPD	Nitrogen Phosphorus Detector
NPip	N-nitrosopiperidine

NPyr	N-nitrosopyrrolidine
NWSON	Non-Water Soluble Organic Nitrogen
OC	Organic Carbon
OEHHA	Office of Environmental Health Hazard Assessment
ON	Organic Nitrogen
OVOC	Oxygenated Volatile Organic Compound
PAH	Polycyclic Aromatic Hydrocarbon
PAN	Peroxyacetyl Nitrate
PLE	Pressurized Liquid Extraction
PM	Particulate Matter
$PM_{2.5}$	Particulate Matter with a diameter ≤ 2.5 μm
POA	Primary Organic Aerosol
PSI	Paul Scherrer Institute
PTR-TOF-MS	Proton Transfer Reaction Time of Flight Mass Spectrometer
QMS	Quadrupole Mass Spectrometer
RSD	Relative Standard Deviation
SMPS	Scanning Mobility Particle Sizer Spectrometer
SOA	Secondary Organic Aerosol
SQT	Sesquiterpene
***t*BA**	*Tert*-Butylamine
***t*BA-NO_2**	*Tert*-Butyl(nitro)amine
TCM	Technology Centre Mongstad
TDU	Thermal Desorption Unit
TEA	Thermal Energy Analyzer
TN	Total Nitrogen
TOF-MS	Time of Flight Mass Spectrometer
TSNA	Tobacco-Specific Nitrosamine
TSP	Total Suspended Particles
US EPA	United States Environmental Protection Agency
VOC	Volatile Organic Compound
WHO	World Health Organisation
WSON	Water Soluble Organic Nitrogen

References

1. Beijerinck, M. W., Über oligonitrophile Mikroben. *Zbl. Backt.* **1901,** *7*, 561-582.

2. Fowler, D.; Coyle, M.; Skiba, U.; Sutton, M. A.; Cape, J. N.; Reis, S.; Sheppard, L. J.; Jenkins, A.; Grizzetti, B.; Galloway, J. N.; Vitousek, P.; Leach, A.; Bouwman, A. F.; Butterbach-Bahl, K.; Dentener, F.; Stevenson, D.; Amann, M.; Voss, M., The global nitrogen cycle in the twenty-first century. *Philos T R Soc B* **2013,** *368* (1621).

3. Vitousek, P. M.; Menge, D. N. L.; Reed, S. C.; Cleveland, C. C., Biological nitrogen fixation: rates, patterns and ecological controls in terrestrial ecosystems. *Philos T R Soc B* **2013,** *368* (1621).

4. Stoltzenberg, D., *Fritz Haber: Chemist, Nobel Laureate, German, Jew*. 1st ed.; Chemical Heritage Foundation: Philadelphia, PA, USA, 2004.

5. Galloway, J. N.; Townsend, A. R.; Erisman, J. W.; Bekunda, M.; Cai, Z. C.; Freney, J. R.; Martinelli, L. A.; Seitzinger, S. P.; Sutton, M. A., Transformation of the nitrogen cycle: Recent trends, questions, and potential solutions. *Science* **2008,** *320* (5878), 889-892.

6. Herridge, D. F.; Peoples, M. B.; Boddey, R. M., Global inputs of biological nitrogen fixation in agricultural systems. *Plant Soil* **2008,** *311* (1-2), 1-18.

7. van Vuuren, D. P.; Bouwman, L. F.; Smith, S. J.; Dentener, F., Global projections for anthropogenic reactive nitrogen emissions to the atmosphere: an assessment of scenarios in the scientific literature. *Curr Opin Env Sust* **2011,** *3* (5), 359-369.

8. Seinfeld, J. H.; Pandis, S. N., *Atmospheric chemistry and physics : from air pollution to climate change*. 2nd ed.; J. Wiley: Hoboken, N.J., 2006; p 1-1203.

9. Behera, S. N.; Sharma, M.; Aneja, V. P.; Balasubramanian, R., Ammonia in the atmosphere: a review on emission sources, atmospheric chemistry and deposition on terrestrial bodies. *Environ. Sci. Pollut. Res.* **2013,** *20* (11), 8092-8131.

10. Talbot, R. W.; Dibb, J. E.; Scheuer, E. M.; Bradshaw, J. D.; Sandholm, S. T.; Singh, H. B.; Blake, D. R.; Blake, N. J.; Atlas, E.; Flocke, F., Tropospheric reactive odd nitrogen over the South Pacific in austral springtime. *J Geophys Res-Atmos* **2000,** *105* (D5), 6681-6694.

11. Wayne, R. P.; Barnes, I.; Biggs, P.; Burrows, J. P.; Canosamas, C. E.; Hjorth, J.; Lebras, G.; Moortgat, G. K.; Perner, D.; Poulet, G.; Restelli, G.; Sidebottom, H., The Nitrate Radical - Physics, Chemistry, and the Atmosphere. *Atmos Environ a-Gen* **1991,** *25* (1), 1-203.

12. Kleffmann, J., Daytime sources of nitrous acid (HONO) in the atmospheric boundary layer. *Chemphyschem* **2007,** *8* (8), 1137-1144.

13. Broske, R.; Kleffmann, J.; Wiesen, P., Heterogeneous conversion of NO2 on secondary organic aerosol surfaces: A possible source of nitrous acid (HONO) in the atmosphere? *Atmos Chem Phys* **2003,** *3*, 469-474.

14. Rappengluck, B.; Lubertino, G.; Alvarez, S.; Golovko, J.; Czader, B.; Ackermann, L., Radical precursors and related species from traffic as observed and modeled at an urban highway junction. *J Air Waste Manage* **2013,** *63* (11), 1270-1286.

15. Lee, B. H.; Santoni, G. W.; Wood, E. C.; Herndon, S. C.; Miake-Lye, R. C.; Zahniser, M. S.; Wofsy, S. C.; Munger, J. W., Measurements of Nitrous Acid in Commercial Aircraft Exhaust at the Alternative Aviation Fuel Experiment. *Environ. Sci. Technol.* **2011,** *45* (18), 7648-7654.

16. Roberts, J. M.; Veres, P.; Warneke, C.; Neuman, J. A.; Washenfelder, R. A.; Brown, S. S.; Baasandorj, M.; Burkholder, J. B.; Burling, I. R.; Johnson, T. J.; Yokelson, R. J.; de Gouw, J., Measurement of HONO, HNCO, and other inorganic acids by negative-ion proton-transfer chemical-ionization mass spectrometry (NI-PT-CIMS): application to biomass burning emissions. *Atmos. Meas. Tech.* **2010,** *3* (4), 981-990.

17. Song, C. H.; Park, M. E.; Lee, E. J.; Lee, J. H.; Lee, B. K.; Lee, D. S.; Kim, J.; Han, J. S.; Moon, K. J.; Kondo, Y., Possible particulate nitrite formation and its atmospheric implications inferred from the observations in Seoul, Korea. *Atmos. Environ.* **2009,** *43* (13), 2168-2173.

18. VandenBoer, T. C.; Young, C. J.; Talukdar, R. K.; Markovic, M. Z.; Brown, S. S.; Roberts, J. M.; Murphy, J. G., Nocturnal loss and daytime source of nitrous acid through reactive uptake and displacement. *Nat Geosci* **2015,** *8* (1), 55-60.

19. Wang, L. W.; Wen, L.; Xu, C. H.; Chen, J. M.; Wang, X. F.; Yang, L. X.; Wang, W. X.; Yang, X.; Sui, X.; Yao, L.; Zhang, Q. Z., HONO and its potential source particulate nitrite at an urban site in North China during the cold season. *Sci Total Environ* **2015,** *538*, 93-101.

20. Galloway, J. N.; Aber, J. D.; Erisman, J. W.; Seitzinger, S. P.; Howarth, R. W.; Cowling, E. B.; Cosby, B. J., The nitrogen cascade. *Bioscience* **2003,** *53* (4), 341-356.

21. Forster, P.; Ramaswamy, V.; Artaxo, P.; Berntsen, T.; Betts, R.; Fahey, D. W.; Haywood, J.; Lean, J.; Lowe, D. C.; Myhre, G.; Nganga, J.; Prinn, R.; Raga, G. B.; Schulz, M.; Van Dorland, R., Changes in Atmospheric Constituents and in Radiative Forcing. In *Climate Change 2007: The Physical Science Basis. Contribution of Working Group 1 to the Fourth Assessment Report of the Intergovernmental Panel on Climate Change*, Solomon, S.; Qin, D.; Manning, M.; Chen, Z.; Marquis, M.; Averyt, K. B.; Tignor, M.; Miller, H. L., Eds. Cambridge University Press: Cambridge, United Kingdom and New York, NY, USA, 2007; pp 131-234.

22. UNECE Conventions and Protocols. http://www.unece.org/env/treaties/welcome.html (accessed 30-05-2017).

23. IRIS (Integrated Risk Information System) A-Z List of Substances. http://cfpub.epa.gov/ncea/iris/index.cfm?fuseaction=iris.showSubstanceList (accessed 31-05-2017).

24. Cape, J. N.; Cornell, S. E.; Jickells, T. D.; Nemitz, E., Organic nitrogen in the atmosphere - Where does it come from? A review of sources and methods. *Atmos Res* **2011,** *102* (1-2), 30-48.

25. Renbaum, L. H.; Smith, G. D., Organic nitrate formation in the radical-initiated oxidation of model aerosol particles in the presence of NOx. *Phys Chem Chem Phys* **2009,** *11* (36), 8040-8047.

26. Ge, X. L.; Wexler, A. S.; Clegg, S. L., Atmospheric amines - Part I. A review. *Atmos. Environ.* **2011,** *45* (3), 524-546.

27. Cornell, S. E.; Jickells, T. D.; Thornton, C. A., Urea in rainwater and atmospheric aerosol. *Atmos. Environ.* **1998,** *32* (11), 1903-1910.

28. Mace, K. A.; Duce, R. A.; Tindale, N. W., Organic nitrogen in rain and aerosol at Cape Grim, Tasmania, Australia. *J Geophys Res-Atmos* **2003,** *108* (D11).

29. Paglione, M.; Saarikoski, S.; Carbone, S.; Hillamo, R.; Facchini, M. C.; Finessi, E.; Giulianelli, L.; Carbone, C.; Fuzzi, S.; Moretti, F.; Tagliavini, E.; Swietlicki, E.; Stenstrom, K. E.; Prevot, A. S. H.; Massoli, P.; Canaragatna, M.; Worsnop, D.; Decesari, S., Primary and secondary biomass burning aerosols determined by proton nuclear magnetic resonance (H-1-NMR) spectroscopy during the 2008 EUCAARI campaign in the Po Valley (Italy). *Atmos Chem Phys* **2014,** *14* (10), 5089-5110.

30. Simoneit, B. R. T.; Rushdi, A. I.; Bin Abas, M. R.; Didyk, B. M., Alkyl amides and nitriles as novel tracers for biomass burning. *Environ. Sci. Technol.* **2003,** *37* (1), 16-21.

31. Laskin, A.; Smith, J. S.; Laskin, J., Molecular Characterization of Nitrogen-Containing Organic Compounds in Biomass Burning Aerosols Using High-Resolution Mass Spectrometry. *Environ. Sci. Technol.* **2009,** *43* (10), 3764-3771.

32. Iinuma, Y.; Bruggemann, E.; Gnauk, T.; Muller, K.; Andreae, M. O.; Helas, G.; Parmar, R.; Herrmann, H., Source characterization of biomass burning particles: The combustion of selected European conifers, African hardwood, savanna grass, and German and Indonesian peat. *J Geophys Res-Atmos* **2007,** *112* (D8).

33. Nielsen, C. J.; Herrmann, H.; Weller, C., Atmospheric chemistry and environmental impact of the use of amines in carbon capture and storage (CCS). *Chem Soc Rev* **2012,** *41* (19), 6684-6704.

34. Sexton, A. J.; Rochelle, G. T., Reaction Products from the Oxidative Degradation of Monoethanolamine. *Ind Eng Chem Res* **2011,** *50* (2), 667-673.

35. Zhu, L.; Schade, G. W.; Nielsen, C. J., Real-Time Monitoring of Emissions from Monoethanolamine-Based Industrial Scale Carbon Capture Facilities. *Environ. Sci. Technol.* **2013,** *47* (24), 14306-14314.

36. Hu, S. H.; Herner, J. D.; Robertson, W.; Kobayashi, R.; Chang, M. C. O.; Huang, S. M.; Zielinska, B.; Kado, N.; Collins, J. F.; Rieger, P.; Huai, T.; Ayala, A., Emissions of polycyclic aromatic hydrocarbons (PAHs) and nitro-PAHs from heavy-duty diesel vehicles with DPF and SCR. *J Air Waste Manage* **2013,** *63* (8), 984-996.

37. Nojima, K.; Kawaguchi, A.; Ohya, T.; Kanno, S.; Hirobe, M., Studies on Photochemical-Reaction of Air-Pollutants .10. Identification of Nitrophenols in Suspended Particulates. *Chem Pharm Bull* **1983,** *31* (3), 1047-1051.

38. Goff, E. U.; Coombs, J. R.; Fine, D. H.; Baines, T. M., Determination of N-Nitrosamines from Diesel-Engine Crankcase Emissions. *Anal Chem* **1980,** *52* (12), 1833-1836.

39. Rogge, W. F.; Hildemann, L. M.; Mazurek, M. A.; Cass, G. R.; Simonelt, B. R. T., Sources of Fine Organic Aerosol .1. Charbroilers and Meat Cooking Operations. *Environ. Sci. Technol.* **1991,** *25* (6), 1112-1125.

40. Wu, P. F.; Chiang, T. A.; Wang, L. F.; Chang, C. S.; Ko, Y. C., Nitro-polycyclic aromatic hydrocarbon contents of fumes from heated cooking oils and prevention of mutagenicity by catechin. *Mutat Res-Fund Mol M* **1998,** *403* (1-2), 29-34.

41. Abdullahi, K. L.; Delgado-Saborit, J. M.; Harrison, R. M., Emissions and indoor concentrations of particulate matter and its specific chemical components from cooking: A review. *Atmos. Environ.* **2013,** *71*, 260-294.

42. Timperley, M. H.; Vigorbrown, R. J.; Kawashima, M.; Ishigami, M., Organic Nitrogen-Compounds in Atmospheric Precipitation - Their Chemistry and Availability to Phytoplankton. *Can J Fish Aquat Sci* **1985,** *42* (6), 1171-1177.

43. Muller, C.; Iinuma, Y.; Karstensen, J.; van Pinxteren, D.; Lehmann, S.; Gnauk, T.; Herrmann, H., Seasonal variation of aliphatic amines in marine sub-micrometer particles at the Cape Verde islands. *Atmos Chem Phys* **2009,** *9* (24), 9587-9597.

44. Kuznetsova, M.; Lee, C.; Aller, J., Characterization of the proteinaceous matter in marine aerosols. *Mar Chem* **2005,** *96* (3-4), 359-377.

45. Matsumoto, K.; Uematsu, M., Free amino acids in marine aerosols over the western North Pacific Ocean. *Atmos. Environ.* **2005,** *39* (11), 2163-2170.

46. Schmeltz, I.; Hoffmann, D., Nitrogen-Containing Compounds in Tobacco and Tobacco-Smoke. *Chem Rev* **1977,** *77* (3), 295-311.

47. Hecht, S. S.; Hoffmann, D., Tobacco-Specific Nitrosamines, an Important Group of Carcinogens in Tobacco and Tobacco-Smoke. *Carcinogenesis* **1988,** *9* (6), 875-884.

48. Schade, G. W.; Crutzen, P. J., Emission of Aliphatic-Amines from Animal Husbandry and Their Reactions - Potential Source of N2o and Hcn. *J Atmos Chem* **1995,** *22* (3), 319-346.

49. Finlayson-Pitts, B. J.; Pitts, J. N., *Atmospheric chemistry : fundamentals and experimental techniques*. Wiley: New York, 1986; p 1-1098.

50. Nielsen, C. J.; D'Anna, B.; Karl, M.; Aursnes, M.; Boreave, A.; Bossi, R.; Bunkan, A.; Glasius, M.; Hallquist, M.; Hansen, A.; Kristensen, K.; Mikoviny, T.; Maguta, M.; Müller, M.; Nguyen, Q.; Westerlund, J.; Salo, K.; Skov, H.; Stenstrøm, Y.; Wisthaler, A. *Atmospheric Degradation of Amines (ADA) Summary Report: Photo-Oxidation of Methylamine, Dimethylamine and Trimethylamine*; CLIMIT project no. 201604; Norwegian Institute for Air Research: Kjeller, Norway, 28-01-2011, pp 1-140.

51. Pankow, J. F., An Absorption-Model of Gas-Particle Partitioning of Organic-Compounds in the Atmosphere. *Atmos. Environ.* **1994,** *28* (2), 185-188.

52. Odum, J. R.; Hoffmann, T.; Bowman, F.; Collins, D.; Flagan, R. C.; Seinfeld, J. H., Gas/particle partitioning and secondary organic aerosol yields. *Environ. Sci. Technol.* **1996,** *30* (8), 2580-2585.

53. Pui, D. Y. H.; Chen, S. C.; Zuo, Z. L., PM2.5 in China: Measurements, sources, visibility and health effects, and mitigation. *Particuology* **2014,** *13*, 1-26.

54. Phalen, R. F.; Cuddihy, R. G.; Fisher, G. L.; Moss, O. R.; Schlesinger, R. B.; Swift, D. L.; Yeh, H. C., Main Features of the Proposed Ncrp Respiratory-Tract Model. *Radiat Prot Dosim* **1991,** *38* (1-3), 179-184.

55. Murphy, S. M.; Sorooshian, A.; Kroll, J. H.; Ng, N. L.; Chhabra, P.; Tong, C.; Surratt, J. D.; Knipping, E.; Flagan, R. C.; Seinfeld, J. H., Secondary aerosol formation from atmospheric reactions of aliphatic amines. *Atmos Chem Phys* **2007,** *7* (9), 2313-2337.

56. Karl, M. *Atmospheric Degradation of Amines (ADA) Amines in aerosol – A review*; OR 60/2010; Norwegian Institute for Air Research: Kjeller, Norway, 17th September, 2009; pp 1-25.

57. Zhang, Q.; Anastasio, C.; Jimemez-Cruz, M., Water-soluble organic nitrogen in atmospheric fine particles (PM2.5) from northern California. *J Geophys Res-Atmos* **2002,** *107* (D11).

58. *IARC Monographs on the Evaluation of Carcinogenic Risks to Humans Volume 89 Smokeless Tobacco and Some Tobacco-specific N-Nitrosamines*; International Agency for Research on Cancer: Lyon, France, 2007; pp 1-626.

59. IARC Agents Classified by the IARC Monographs. http://monographs.iarc.fr/ENG/Classification/ClassificationsAlphaOrder.pdf (accessed 15/03/2015).

60. Kocak, D.; Özel, M. Z.; Gogus, F.; Hamilton, J. F.; Lewis, A. C., Determination of volatile nitrosamines in grilled lamb and vegetables using comprehensive gas chromatography - Nitrogen chemiluminescence detection. *Food Chem.* **2012,** *135* (4), 2215-2220.

61. Schothorst, R. C.; Somers, H. H. J., Determination of N-nitrosodiethanolamine in cosmetic products by LC-MS-MS. *Anal. Bioanal. Chem.* **2005,** *381* (3), 681-685.

62. Ramírez, N.; Özel, M. Z.; Lewis, A. C.; Marcé, R. M.; Borrull, F.; Hamilton, J. F., Determination of nicotine and N-nitrosamines in house dust by pressurized liquid extraction and comprehensive gas chromatography-Nitrogen chemiluminiscence detection. *J. Chromatogr. A* **2012,** *1219*, 180-187.

63. Grebel, J. E.; Suffet, I. H. M., Nitrogen-phosphorus detection and nitrogen chemiluminescence detection of volatile nitrosamines in water matrices: Optimization and performance comparison. *J. Chromatogr. A* **2007,** *1175* (1), 141-144.

64. Akyüz, M.; Ata, A., Seasonal variations of particle-associated nitrosamines by gas chromatography-mass spectrometry in the atmospheric environment of Zonguldak, Turkey. *Environ. Sci. Pollut. Res.* **2013,** *20* (10), 7398-7412.

65. Aragón, M.; Marcé, R. M.; Borrull, F., Determination of N-nitrosamines and nicotine in air particulate matter samples by pressurised liquid extraction and gas chromatography-ion trap tandem mass spectrometry. *Talanta* **2013,** *115*, 896-901.

66. Herrmann, S. S.; Granby, K.; Duedahl-Olesen, L., Formation and mitigation of N-nitrosamines in nitrite preserved cooked sausages. *Food Chem.* **2015,** *174*, 516-526.

67. Krasner, S. W.; Mitch, W. A.; McCurry, D. L.; Hanigan, D.; Westerhoff, P., Formation, precursors, control, and occurrence of nitrosamines in drinking water: A review. *Water Res* **2013,** *47* (13), 4433-4450.

68. Office of Environmental Health Hazard Assessment - California Public Health goal for N-nitrosodiemethylamine in drinking water. https://oehha.ca.gov/water/chemicals/n-nitrosodimethylamine (accessed 03-06-2017).

69. Rounbehler, D. P.; Krull, I. S.; Goff, E. U.; Mills, K. M.; Morrison, J.; Edwards, G. S.; Fine, D. H.; Fajen, J. M.; Carson, G. A.; Rheinhold, V., Exposure to N-Nitrosodimethylamine in a Leather Tannery. *Food Cosmet Toxicol* **1979,** *17* (5), 487-491.

70. Fajen, J. M.; Carson, G. A.; Rounbehler, D. P.; Fan, T. Y.; Vita, R.; Goff, U. E.; Wolf, M. H.; Edwards, G. S.; Fine, D. H.; Reinhold, V.; Biemann, K., N-Nitrosamines in the Rubber and Tire Industry. *Science* **1979,** *205* (4412), 1262-1264.

71. Sen, N. P.; Seaman, S.; Miles, W. F., Dimethylnitrosamine and Nitrosopyrrolidine in Fumes Produced during Frying of Bacon. *Food Cosmet Toxicol* **1976,** *14* (3), 167-170.

72. Pitts, J. N.; Grosjean, D.; Vancauwenberghe, K.; Schmid, J. P.; Fitz, D. R., Photo-Oxidation of Aliphatic-Amines under Simulated Atmospheric Conditions - Formation of

Nitrosamines, Nitramines, Amides, and Photo-Chemical Oxidant. *Environ. Sci. Technol.* **1978,** *12* (8), 946-953.

73. Ramírez, N.; Özel, M. Z.; Lewis, A. C.; Marcé, R. M.; Borrull, F.; Hamilton, J. F., Exposure to nitrosamines in thirdhand tobacco smoke increases cancer risk in non-smokers. *Environ. Int.* **2014,** *71*, 139-147.

74. *Health effects of amines and derivatives associated with CO_2 capture*; Division of Environmental Medicine, The Norwegian Institute of Public Health: Oslo, Norway, 2011.

75. Ridd, J. H., Nitrosation, Diazotisation, and Deamination. *Q Rev Chem Soc* **1961,** *15* (4), 418-441.

76. Hutchings, J. W.; Ervens, B.; Straub, D.; Herckes, P., N-Nitrosodimethylamine Occurrence, Formation and Cycling in Clouds and Fogs. *Environ. Sci. Technol.* **2010,** *44* (21), 8128-8133.

77. Özel, M. Z.; Hamilton, J. F.; Lewis, A. C., New Sensitive and Quantitative Analysis Method for Organic Nitrogen Compounds in Urban Aerosol Samples. *Environ. Sci. Technol.* **2011,** *45* (4), 1497-1505.

78. Hecht, S. S.; Hoffmann, D., N-Nitroso Compounds and Tobacco-Induced Cancers in Man. *IARC Sci. Publ.* **1991,** *105*, 54-61.

79. Sleiman, M.; Gundel, L. A.; Pankow, J. F.; Jacob, P.; Singer, B. C.; Destaillats, H., Formation of carcinogens indoors by surface-mediated reactions of nicotine with nitrous acid, leading to potential thirdhand smoke hazards. *PNAS* **2010,** *107* (15), 6576-6581.

80. Winickoff, J. P.; Friebely, J.; Tanski, S. E.; Sherrod, C.; Matt, G. E.; Hovell, M. F.; McMillen, R. C., Beliefs About the Health Effects of "Thirdhand" Smoke and Home Smoking Bans. *Pediatrics* **2009,** *123* (1), E74-E79.

81. *Child-specific exposure factors handbook*; EPA/600/R-06/096F; US EPA, National Center for Environmental Assessment: Office of Research and Development, Washington, DC 20460, September, 2008; pp 1-1 - 17-5.

82. EDGAR - Emissions Database for Global Atmospheric Research. CO2 time series 1990-2015 per region/country. . http://edgar.jrc.ec.europa.eu/overview.php?v=CO2ts1990-2015 (accessed 01-06-2017).

83. Global CCS Institute - Large-scale CCS facilities. http://www.globalccsinstitute.com/projects/large-scale-ccs-projects-definitions (accessed 20-06-2017).

84. Global CCS Institute - Boundary Dam Carbon Capture and Storage. http://www.globalccsinstitute.com/projects/boundary-dam-carbon-capture-and-storage-project (accessed 20-06-2017).

85. Air Liquide - CO2 cold capture system, Cryocap. https://www.airliquide.com/media/world-premiere-air-liquide-inaugurates-its-co2-cold-capture-system-cryocap (accessed 20-06-2017).
86. TCM Technologies for post-combustion CO2 capture. http://www.tcmda.com/en/Technology/ (accessed 20-06-2017).
87. Clean Air Task Force - Post-Combustion Capture. http://www.fossiltransition.org/pages/post_combustion_capture_/128.php (accessed 19-06-2017).
88. TCM Amine technology for post-combustion carbon capture http://www.tcmda.com/en/Technology/Amine-technology/ (accessed 01-06-2017).
89. Shao, R.; Stangeland, A. *Amines used in CO2 capture - health and environmental impacts*; The Bellona Foundation: Oslo, Norway, September, 2009; pp 1-49.
90. Cornell, S. E.; Jickells, T. D.; Cape, J. N.; Rowland, A. P.; Duce, R. A., Organic nitrogen deposition on land and coastal environments: a review of methods and data. *Atmos. Environ.* **2003,** *37* (16), 2173-2191.
91. Jickells, T.; Baker, A. R.; Cape, J. N.; Cornell, S. E.; Nemitz, E., The cycling of organic nitrogen through the atmosphere. *Philos T R Soc B* **2013,** *368* (1621).
92. Mace, K. A.; Duce, R. A., On the use of UV photo-oxidation for the determination of total nitrogen in rainwater and water-extracted atmospheric aerosol. *Atmos. Environ.* **2002,** *36* (39-40), 5937-5946.
93. Bronk, D. A.; Lomas, M. W.; Glibert, P. M.; Schukert, K. J.; Sanderson, M. P., Total dissolved nitrogen analysis: comparisons between the persulfate, UV and high temperature oxidation methods. *Mar Chem* **2000,** *69* (1-2), 163-178.
94. Sharp, J. H.; Rinker, K. R.; Savidge, K. B.; Abell, J.; Benaim, J. Y.; Bronk, D.; Burdige, D. J.; Cauwet, G.; Chen, W. H.; Doval, M. D.; Hansell, D.; Hopkinson, C.; Kattner, G.; Kaumeyer, N.; McGlathery, K. J.; Merriam, J.; Morley, N.; Nagel, K.; Ogawa, H.; Pollard, C.; Pujo-Pay, M.; Raimbault, P.; Sambrotto, R.; Seitzinger, S.; Spyres, G.; Tirendi, F.; Walsh, T. W.; Wong, C. S., A preliminary methods comparison for measurement of dissolved organic nitrogen in seawater. *Mar Chem* **2002,** *78* (4), 171-184.
95. Miyazaki, Y.; Fu, P. Q.; Ono, K.; Tachibana, E.; Kawamura, K., Seasonal cycles of water-soluble organic nitrogen aerosols in a deciduous broadleaf forest in northern Japan. *J Geophys Res-Atmos* **2014,** *119* (3), 1440-1454.
96. Montero-Martinez, G.; Rinaldi, M.; Gilardoni, S.; Giulianelli, L.; Paglione, M.; Decesari, S.; Fuzzi, S.; Facchini, M. C., On the water-soluble organic nitrogen concentration and mass size distribution during the fog season in the Po Valley, Italy. *Sci Total Environ* **2014,** *485*, 103-109.

97. Duan, F. K.; Liu, X. D.; He, K. B.; Dong, S. P., Measurements and Characteristics of Nitrogen-Containing Compounds in Atmospheric Particulate Matter in Beijing, China. *B Environ Contam Tox* **2009,** *82* (3), 332-337.

98. Russell, K. M.; Keene, W. C.; Maben, J. R.; Galloway, J. N.; Moody, J. L., Phase partitioning and dry deposition of atmospheric nitrogen at the mid-Atlantic US coast. *J Geophys Res-Atmos* **2003,** *108* (D21).

99. Miyazaki, Y.; Kawamura, K.; Sawano, M., Size distributions of organic nitrogen and carbon in remote marine aerosols: Evidence of marine biological origin based on their isotopic ratios. *Geophys Res Lett* **2010,** *37*.

100. Ochiai, N.; Ieda, T.; Sasamoto, K.; Fushimi, A.; Hasegawa, S.; Tanabe, K.; Kobayashi, S., Comprehensive two-dimensional gas chromatography coupled to high-resolution time-of-flight mass spectrometry and simultaneous nitrogen phosphorous and mass spectrometric detection for characterization of nanoparticles in roadside atmosphere. *J. Chromatogr. A* **2007,** *1150* (1-2), 13-20.

101. Özel, M. Z.; Ward, M. W.; Hamilton, J. F.; Lewis, A. C.; Raventós-Duran, T.; Harrison, R. M., Analysis of Organic Nitrogen Compounds in Urban Aerosol Samples Using GCxGC-TOF/MS. *Aerosol Sci. Tech.* **2010,** *44* (2), 109-116.

102. Richter, B. E.; Jones, B. A.; Ezzell, J. L.; Porter, N. L.; Avdalovic, N.; Pohl, C., Accelerated solvent extraction: A technique for sample preparation. *Anal Chem* **1996,** *68* (6), 1033-1039.

103. Camel, V., Recent extraction techniques for solid matrices-supercritical fluid extraction, pressurized fluid extraction and microwave-assisted extraction: their potential and pitfalls. *Analyst* **2001,** *126* (7), 1182-1193.

104. Mustafa, A.; Turner, C., Pressurized liquid extraction as a green approach in food and herbal plants extraction: A review. *Anal Chim Acta* **2011,** *703* (1), 8-18.

105. *Method 3545A Pressurized Fluid Extraction (PFE)*; 3545A - 1; U. S. Environmental Protection Agency Washingto, D.C., United States, January 1998, pp 1-10.

106. Dąbrowski, L.; Giergielewicz-Możajska, H.; Biziuk, M.; Gaca, J.; Nameiśnik, J., Some aspects of the analysis of environmental pollutants in sediments using pressurized liquid extraction and gas chromatography-mass spectrometry. *J. Chromatogr. A* **2002,** *957* (1), 59-67.

107. Ong, R.; Lundstedt, S.; Haglund, P.; Marriott, P., Pressurised liquid extraction-comprehensive two-dimensional gas chromatography for fast-screening of polycyclic aromatic hydrocarbons in soil. *J. Chromatogr. A* **2003,** *1019* (1-2), 221-232.

108. Ternes, T. A.; Bonerz, M.; Herrmann, N.; Loffler, D.; Keller, E.; Lacida, B. B.; Alder, A. C., Determination of pharmaceuticals, iodinated contrast media and musk

fragrances in sludge by LC/tandem MS and GC/MS. *J. Chromatogr. A* **2005,** *1067* (1-2), 213-223.

109. Frenich, A. G.; Ocana, R. M.; Vidal, J. L. M., Determination of Polycyclic Aromatic Hydrocarbons in Airborne Particulate Matter by Gas Chromatography-Triple Quadrupole Tandem Mass Spectrometry. *J. Aoac. Int.* **2010,** *93* (1), 284-294.

110. Aragón, M.; Marcé, R. M.; Borrull, F., Determination of phthalates and organophosphate esters in particulated material from harbour air samples by pressurised liquid extraction and gas chromatography-mass spectrometry. *Talanta* **2012,** *101*, 473-478.

111. Liu, Z. Y.; Phillips, J. B., Comprehensive 2-Dimensional Gas-Chromatography Using an on-Column Thermal Modulator Interface. *J Chromatogr Sci* **1991,** *29* (6), 227-231.

112. Phillips, J. B.; Xu, J. Z., Comprehensive Multidimensional Gas-Chromatography. *J. Chromatogr. A* **1995,** *703* (1-2), 327-334.

113. Lewis, A. C.; Carslaw, N.; Marriott, P. J.; Kinghorn, R. M.; Morrison, P.; Lee, A. L.; Bartle, K. D.; Pilling, M. J., A larger pool of ozone-forming carbon compounds in urban atmospheres. *Nature* **2000,** *405* (6788), 778-781.

114. Hamilton, J. F., Using Comprehensive Two-Dimensional Gas Chromatography to Study the Atmosphere. *J Chromatogr Sci* **2010,** *48* (4), 274-+.

115. Bruckner, C. A.; Prazen, B. J.; Synovec, R. E., Comprehensive two dimensional high-speed gas chromatography with chemometric analysis. *Anal Chem* **1998,** *70* (14), 2796-2804.

116. Seeley, J. V.; Kramp, F.; Hicks, C. J., Comprehensive two-dimensional gas chromatography via differential flow modulation. *Anal Chem* **2000,** *72* (18), 4346-4352.

117. Seeley, J. V.; Micyus, N. J.; McCurry, J. D.; Seeley, S. K., Comprehensive two-dimensional gas chromatography with a simple fluidic modulator. *Am Lab* **2006,** *38* (9), 24-26.

118. Mohler, R. E.; Prazen, B. J.; Synovec, R. E., Total-transfer, valve-based comprehensive two-dimensional gas chromatography. *Anal Chim Acta* **2006,** *555* (1), 68-74.

119. Wang, F. C. Y., New valve switching modulator for comprehensive two-dimensional gas chromatography. *J. Chromatogr. A* **2008,** *1188* (2), 274-280.

120. Marriott, P. J.; Kinghorn, R. M., Longitudinally modulated cryogenic system. A generally applicable approach to solute trapping and mobilization in gas chromatography. *Anal Chem* **1997,** *69* (13), 2582-2588.

121. Kinghorn, R. M.; Marriott, P. J., High speed cryogenic modulation - A technology enabling comprehensive multidimensional gas chromatography. *Hrc-J High Res Chrom* **1999,** *22* (4), 235-238.

122. Kinghorn, R. M.; Marriott, P. J.; Dawes, P. A., Design and implementation of comprehensive gas chromatography with cryogenic modulation. *Hrc-J High Res Chrom* **2000,** *23* (3), 245-252.

123. Marriott, P.; Kinghorn, R., Cryogenic solute manipulation in gas chromatography - the longitudinal modulation approach. *Trac-Trend Anal Chem* **1999,** *18* (2), 114-125.

124. Marriott, P. J.; Kinghorn, R. M., New operational modes for multidimensional and comprehensive gas chromatography by using cryogenic modulation. *J. Chromatogr. A* **2000,** *866* (2), 203-212.

125. Beens, J.; Adahchour, M.; Vreuls, R. J. J.; van Altena, K.; Brinkman, U. A. T., Simple, non-moving modulation interface for comprehensive two-dimensional gas chromatography. *J. Chromatogr. A* **2001,** *919* (1), 127-132.

126. Ledford, E. B.; Billesbach, C., Jet-cooled thermal modulator for comprehensive multidimensional gas chromatography. *Hrc-J High Res Chrom* **2000,** *23* (3), 202-204.

127. Focant, J. F.; Sjodin, A.; Patterson, D. G., Qualitative evaluation of thermal desorption-programmable temperature vaporization-comprehensive two-dimensional gas chromatography-time-of-flight mass spectrometry for the analysis of selected halogenated contaminants. *J. Chromatogr. A* **2003,** *1019* (1-2), 143-156.

128. Pursch, M.; Eckerle, P.; Biel, J.; Streck, R.; Cortes, H.; Sun, K.; Winniford, B., Comprehensive two-dimensional gas chromatography using liquid nitrogen modulation: set-up and applications. *J. Chromatogr. A* **2003,** *1019* (1-2), 43-51.

129. Semard, G.; Adahchour, M.; Focant, J. F., Comprehensive Two Dimensional Gas Chromatography. In *Comprehensive Analytical Chemistry*, 1st ed.; Ramos, L., Ed. Elsevier: Oxford, UK, 2009; Vol. 55, pp 15-48.

130. Lee, A. L.; Bartle, K. D.; Lewis, A. C., A model of peak amplitude enhancement in orthogonal two-dimensional gas chromatography. *Anal Chem* **2001,** *73* (6), 1330-1335.

131. Adahchour, M.; Beens, J.; Vreuls, R. J. J.; Brinkman, U. A. T., Recent developments in comprehensive two-dimensional gas chromatography (GC X GC) I. Introduction and instrumental set-up. *Trac-Trend Anal Chem* **2006,** *25* (5), 438-454.

132. Holm, T., Aspects of the mechanism of the flame ionization detector. *J. Chromatogr. A* **1999,** *842* (1-2), 221-227.

133. Tranchida, P. Q.; Franchina, F. A.; Dugo, P.; Mondello, L., Comprehensive Two-Dimensional Gas Chromatography-Mass Spectrometry: Recent Evolution and Current Trends. *Mass Spectrom Rev* **2016,** *35* (4), 524-534.

134. Fitch, W. L.; Szardenings, A. K.; Fujinari, E. M., Chemiluminescent nitrogen detection for HPLC: An important new tool in organic analytical chemistry. *Tetrahedron Lett* **1997,** *38* (10), 1689-1692.

135. Burgett, C. A.; Smith, D. H.; Bente, H. B., The nitrogen-phosphorus detector and its applications in gas chromatography. *J Chromatogr* **1977,** *134*, 57-64.

136. SRI The SRI Nitrogen-Phosphorus Detector http://srigc.com/cn/downloads/43/NPD.pdf (accessed 22-05-2017).

137. *Agilent 355 Sulfur and 255 Nitrogen Chemiluminescence Detectors*; G6600-90006; Agilent Technologies Inc.: Wilmington, DE, USA, 2012; pp 1-118.

138. Agilent - Nitrogen Chemiluminescence Detector - More Information. http://agilent.com/en-us/products/gas-chromatography/selective-detectors/nitrogen-chemiluminescence-detector/nitrogen-chem-detector (accessed 20-06-2017).

139. *Nitrosamine analysis by gas chromatography and Agilent 255 nitrogen chemiluminescence detector (NCD)*; 5989-6773EN; Agilent Technologies Inc.: USA, 2007; pp 1-2.

140. Yan, X. W., Sulfur and nitrogen chemiluminescence detection in gas chromatographic analysis. *J. Chromatogr. A* **2002,** *976* (1-2), 3-10.

141. Tomkins, B. A.; Griest, W. H.; Higgins, C. E., Determination of N-Nitrosodimethylamine at Part-Per-Trillion Levels in Drinking Waters and Contaminated Groundwaters. *Anal Chem* **1995,** *67* (23), 4387-4395.

142. Wang, C. X.; Firor, R. *Analysis of trace 2-ethylhexyl nitrate in diesel using chemiluminescence detector (NCD) - application brief*; 5990-6449EN; Agilent Technologies Inc.: USA, September 16, 2010; pp 1-4.

143. Jurado-Sanchez, B.; Ballesteros, E.; Gallego, M., Screening of N-nitrosamines in tap and swimming pool waters using fast gas chromatography. *J. Sep. Sci.* **2010,** *33* (4-5), 610-616.

144. Ramirez, N.; Vallecillos, L.; Lewis, A. C.; Borrull, F.; Marce, R. M.; Hamilton, J. F., Comparative study of comprehensive gas chromatography-nitrogen chemiluminescence detection and gas chromatography-ion trap-tandem mass spectrometry for determining nicotine and carcinogen organic nitrogen compounds in thirdhand tobacco smoke. *J. Chromatogr. A* **2015,** *1426*, 191-200.

145. Clean Air for London: A NERC funded scientific project.

146. Bohnenstengel, S. I.; Belcher, S. E.; Aiken, A.; Allan, J.; Allen, G.; Bacak, A.; Bannan, T. J.; Barlow, J. F.; Beddows, D.; Bloss, W. J.; Booth, A. M.; Chemel, C.; Coceal, O.; Di Marco, C. F.; Dubey, M. K.; Faloon, K. H.; Fleming, Z. L.; Furger, M.; Gietl, J. K.; Graves, R. R.; Green, D. C.; Grimmond, C. S. B.; Halios, C. H.; Hamilton, J. F.; Harrison, R. M.; Heal, M. R.; Heard, D. E.; Helfter, C.; Herndon, S. C.; Holmes, R. E.; Hopkins, J. R.; Jones, A. M.; Kelly, F. J.; Kotthaus, S.; Langford, B.; Lee, J. D.; Leigh, R. J.; Lewis, A. C.; Lidster, R. T.; Lopez-Hilfiker, E. D.; McQuaid, J. B.; Mohr, C.; Monks, P. S.; Nemitz, E.; Ng, N. L.; Percival, C. J.; Prevot, A. S. H.; Ricketts, H. M. A.; Sokhi, R.; Stone, D.;

Thornton, J. A.; Tremper, A. H.; Valach, A. C.; Visser, S.; Whalley, L. K.; Williams, L. R.; Xu, L.; Young, D. E.; Zotter, P., Meteorology, air quality, and health in London: The ClearfLo project. *B. Am. Meteorol. Soc.* **2014**.

147. Bigi, A.; Harrison, R. M., Analysis of the air pollution climate at a central urban background site. *Atmos. Environ.* **2010,** *44* (16), 2004-2012.

148. Kleffmann, J.; Heland, J.; Kurtenbach, R.; Lorzer, J.; Wiesen, P., A new instrument (LOPAP) for the detection of nitrous acid (HONO). *Environ. Sci. Pollut. Res.* **2002,** *Sp. Iss. 4*, 48-54.

149. Kleffmann, J.; Lorzer, J. C.; Wiesen, P.; Kern, C.; Trick, S.; Volkamer, R.; Rodenas, M.; Wirtz, K., Intercomparison of the DOAS and LOPAP techniques for the detection of nitrous acid (HONO). *Atmos. Environ.* **2006,** *40* (20), 3640-3652.

150. Cavalli, F.; Viana, M.; Yttri, K. E.; Genberg, J.; Putaud, J. P., Toward a standardised thermal-optical protocol for measuring atmospheric organic and elemental carbon: the EUSAAR protocol. *Atmos. Meas. Tech.* **2010,** *3* (1), 79-89.

151. Department of Environment Food & Rural Affairs, UK-AIR Data Archive. http://uk-air.defra.gov.uk/data/data_selector (accessed 15/03/15).

152. *Risk Assessment Guidance for Superfund Volume 1: Human Health Evaluation Manual (Part F, Supplemental Guidance for Inhalation Risk Assessment)*; Office of Superfund Remediation and Technology Innovation, U.S. Environmental Protection Agency: Washington DC, 2009.

153. OEHHA (California Office of Environmental Health Hazard Assessment) toxicity criteria database. http://oehha.ca.gov/risk/ChemicalDB/index.asp (accessed 01/03/2015).

154. *Implementation of the Cancer Guidelines and Accompanying Supplemental Guidance - Science Policy Council Cancer Guidelines Implementation Workgroup Communication 1: Application of the mode of action framework in mutagenicity determinations for carcinogenicity*; U.S. Environmental Protection Agency: Washington, DC, 2005.

155. *Assigning values to non-detected/non-quantified pesticide residues in human health food exposure assessments*; U.S. Environmental Protection Agency: Washington, DC, 2000.

156. WHO, *Air Quality Guidelines for Europe*. WHO Regional Publications: Copenhagen, Denmark, 2000.

157. *Risk Assessment Guidance for Superfund Volume 1 Human Health Evaluation Manual (Part A)*; Office of Emergency and Remedial Response: Washington, DC, 1989.

158. *Methods for Derivation of Inhalation Reference Concentrations and Application of Inhalation Dosimetry*; Office of Research and Development: Research Triangle Park, NC, 1994.

159. Hard, G. C., Effect of Age at Treatment on Incidence and Type of Renal Neoplasm Induced in the Rat by a Single Dose of Dimethylnitrosamine. *Cancer Res* **1979,** *39* (12), 4965-4970.

160. Peto, R.; Gray, R.; Brantom, P.; Grasso, P., Nitrosamine Carcinogenesis in 5120 Rodents - Chronic Administration of 16 Different Concentrations of Ndea, Ndma, Npyr and Npip in the Water of 4440 Inbred Rats, with Parallel Studies on Ndea Alone of the Effect of Age of Starting (3, 6 or 20 Weeks) and of Species (Rats, Mice or Hamsters). *IARC scientific publications* **1984,** (57), 627-665.

161. *US EPA Supplemental Guidance for Assessing Susceptibility from Early-Life Exposure to Carcinogens*; EPA/630/R-03/003F; U.S. Environmental Protection Agency: Washington, DC 20460, March 2005, pp 1-368.

162. Environmental Protection Agency, U. S., Exposure Factors Handbook: 2011 Edition. National Center for Environmental Assessment: Washington, DC, 2011. http://www.epa.gov/ncea/efh/pdfs/efh-complete.pdf (accessed 10/03/2015).

163. *Review of evidence on health aspects of air pollution - REVIHAAP Project*; World Health Organization (WHO): WHO Regional Office for Europe, Copenhagen, Denmark, 2013.

164. Air quality standards. http://ec.europa.eu/environment/air/quality/standards.htm (accessed 14th June).

165. Polycyclic Aromatic Hydrocarbons. http://webarchive.nationalarchives.gov.uk/20060715141954/http:/www.defra.gov.uk/environment/airquality/aqs/poly/index.htm (accessed 14th June).

166. Mahanama, K. R. R.; Daisey, J. M., Volatile N-nitrosamines in environmental tobacco smoke: Sampling, analysis, emission factors, and indoor air exposures. *Environ. Sci. Technol.* **1996,** *30* (5), 1477-1484.

167. U.S. Department of State - Mission China, Beijing Historical Data. http://www.stateair.net/web/historical/1/1.html (accessed 12-06-2017).

168. Michalski, R., Applications of Ion Chromatography for the Determination of Inorganic Cations. *Crit Rev Anal Chem* **2009,** *39* (4), 230-250.

169. Fostas, B. I.; Gangstad, A.; Nenseter, B.; Pedersen, S.; Sjovoll, M.; Sorensen, A. L., Effects of NOx in the Flue Gas Degradation of MEA. *Enrgy Proced* **2011,** *4*, 1566-1573.

170. Becker, K. *EUPHORE: Final report to the European commission*; EV5V-CT92-0059; Bergische Universität Wuppertal: Wuppertal, Germany, 1996.

171. EUPHORE home page. http://www.ceam.es/WWWEUPHORE/home.htm (accessed 17-01-17).

172. OSHA Method ORG-38 Volatile Nitrosamine Mixture II. https://www.osha.gov/dts/sltc/methods/organic/org038/org038.html (accessed 23-02-2017).

173. Thomas, D. H.; Rey, M.; Jackson, P. E., Determination of inorganic cations and ammonium in environmental waters by ion chromatography with a high-capacity cation-exchange column. *J. Chromatogr. A* **2002,** *956* (1-2), 181-186.

174. Mainey, A.; Winberry, W. T. *Compendium of Methods for the Determination of Inorganic Compounds in Ambient Air: Selection, Preparation and Extraction of Filter Material*; EPA/625/R-96/010a; Center for Environmental Research Information, U.S. Environmental Protection Agency: Cincinnati, OH 45268, June 1999, pp 3.1-1 - 3.1-26.

175. Perrino, C.; Canepari, S.; Catrambone, M., Comparing the Performance of Teflon and Quartz Membrane Filters Collecting Atmospheric PM: Influence of Atmospheric Water. *Aerosol Air Qual Res* **2013,** *13* (1), 137-147.

176. Farren, N. J.; Ramirez, N.; Lee, J. D.; Finessi, E.; Lewis, A. C.; Hamilton, J. F., Estimated Exposure Risks from Carcinogenic Nitrosamines in Urban Airborne Particulate Matter. *Environ. Sci. Technol.* **2015,** *49* (16), 9648-9656.

177. Clayden, J.; Greeves, N.; Warren, S.; Wothers, P., *Organic Chemistry*. Oxford University Press: 2001.

178. Ripp, J. *Analytical Detection Limit Guidance & Laboratory Guide for Determining Method Detection Limits*; PUBL-TS-056-96; Winsconsin Department of Natural Resources: Madison, WI, U.S., April 1996, pp 1-24.

179. *Product Manual for the Anion Self-Regenerating Suppressor 300 and the Cation Self-Regenerating Suppressor 300*; 031956; Dionex Corporation: Sunnyvale, CA, U.S., August 2007, pp 1-50.

180. Rocklin, R. D.; Pohl, C. A.; Schibler, J. A., Gradient Elution in Ion Chromatography. *J Chromatogr* **1987,** *411*, 107-119.

181. Nielsen, C. J.; D'Anna, B.; Dye, C.; Graus, M.; Karl, M.; King, S.; Maguto, M. M.; Muller, M.; Schmidbauer, N.; Stenstrom, Y.; Wisthaler, A.; Pedersen, S., Atmospheric chemistry of 2-aminoethanol (MEA). *Enrgy Proced* **2011,** *4*, 2245-2252.

182. Nielsen, C. J., D'Anna, B., Bossi, R., Bunkan, A. J. C., Dithmer, L., Glasius, M., Hallquist, M., Hansen, A. M. K., Lutz, A., Salo, K., Maguta, M. M., Nguyen, Q., Mikoviny, T., Müller, M., Skov, H., Sarrasin, E., Stenstrøm, Y., Tang, Y., Westerlund, J., Wisthaler, A. *Atmospheric Degradation of Amines (ADA): Summary report from atmospheric chemistry studies of amines, nitrosamines, nitramines and amides*. ; University of Oslo: Oslo, Norway, 2012; pp 1-169.

183. Nielsen, C. J.; D'Anna, B.; Dye, C.; George, C.; Graus, M.; Hansel, A.; Karl, M.; King, S.; Musabila, M.; Müller, M.; Schmidbauer, N.; Stenstrøm, Y.; Wisthaler, A. *Atmospheric Degradation of Amines (ADA) Summary Report: Gas phase photo-oxidation of 2-aminoethanol (MEA).* OR 8/2010; Norwegian Institute for Air Research (NILU): Norway, 2010; pp 1-63.

184. Borrás, E., Ródenas, M., Vera, T., Muñoz, A., Use of high-volume outdoor smog chamber photo-reactors for studying physical and chemical atmospheric aerosol formation and composition. *IOP Conf. Series: Earth and Environmental Science* **2015,** *28*, 012004.

185. Volkamer, R., Platt, U., Wirtz, K., Primary and secondary glyoxal formation from aromatics: Experimental evidence for the bicycloalkyl-radical pathway from benzene, toluene, and p-xylene. . *J. Phys. Chem. A* **2001,** *105*, 7865-74.

186. Jordan, A.; Haidacher, S.; Hanel, G.; Hartungen, E.; Mark, L.; Seehauser, H.; Schottkowsky, R.; Sulzer, P.; Mark, T. D., A high resolution and high sensitivity proton-transfer-reaction time-of-flight mass spectrometer (PTR-TOF-MS). *Int J Mass Spectrom* **2009,** *286* (2-3), 122-128.

187. Mikoviny, T.; Kaser, L.; Wisthaler, A., Development and characterization of a High-Temperature Proton-Transfer-Reaction Mass Spectrometer (HT-PTR-MS). *Atmos. Meas. Tech.* **2010,** *3* (3), 537-544.

188. Drewnick, F.; Hings, S. S.; DeCarlo, P.; Jayne, J. T.; Gonin, M.; Fuhrer, K.; Weimer, S.; Jimenez, J. L.; Demerjian, K. L.; Borrmann, S.; Worsnop, D. R., A new time-of-flight aerosol mass spectrometer (TOF-AMS) - Instrument description and first field deployment. *Aerosol Sci. Tech.* **2005,** *39* (7), 637-658.

189. Eichler, P.; Muller, M.; D'Anna, B.; Wisthaler, A., A novel inlet system for online chemical analysis of semi-volatile submicron particulate matter. *Atmos. Meas. Tech.* **2015,** *8* (3), 1353-1360.

190. Seakins, P. W., A brief review of the use of environmental chambers for gas phase studies of kinetics, chemical mechanisms and characterisation of field instruments. *Epj Web Conf* **2010,** *9*, 143-163.

191. Trebs, I.; Bohn, B.; Ammann, C.; Rummel, U.; Blumthaler, M.; Konigstedt, R.; Meixner, F. X.; Fan, S.; Andreae, M. O., Relationship between the NO2 photolysis frequency and the solar global irradiance. *Atmos. Meas. Tech.* **2009,** *2* (2), 725-739.

192. Nielsen, C. J.; Hoffman, D.; Herrmann, H. *Evaluation of worst case assumptions - atmospheric chemistry*; 20110302; Norwegian Institute for Air Research: TCM Mongstad, Norway, 2011; pp 1-30.

193. Sakamaki, F.; Hatakeyama, S.; Akimoto, H., Formation of Nitrous-Acid and Nitric-Oxide in the Heterogeneous Dark Reaction of Nitrogen-Dioxide and Water-Vapor in a Smog Chamber. *Int J Chem Kinet* **1983,** *15* (10), 1013-1029.

194. Raff, J. D.; Fnlayson-Pitts, B. J., Hydroxyl Radical Quantum Yields from Isopropyl Nitrite Photolysis in Air. *Environ. Sci. Technol.* **2010,** *44* (21), 8150-8155.

195. Rounbehler, D. P.; Reisch, J. W.; Coombs, J. R.; Fine, D. H., Nitrosamine Air Sampling Sorbents Compared for Quantitative Collection and Artifact Formation. *Anal Chem* **1980,** *52* (2), 273-276.

196. Foley, G. D. *Nitrosamines: method 2522*; National Institute for Occupational Safety and Health (NIOSH): U.S. Department of Health & Human Services, Washington, D.C., 15-08-1994, pp 2522-2525.

197. Padhye, L.; Wang, P.; Karanfil, T.; Huang, C. H., Unexpected Role of Activated Carbon in Promoting Transformation of Secondary Amines to N-Nitrosamines. *Environ. Sci. Technol.* **2010,** *44* (11), 4161-4168.

198. Mitch, W. A. *Literature Review of Nitrosamine and Nitramine Formation Chemistry Relevant to Carbon Capture*; Tasks 1 and 3 report; Gassnova SF: NO-3920 Porsgrunn, pp 1-37.

199. Nielsen, C. J., D'Anna, B., Galan, G. B., Wisthaler, A. *Atmospheric Chemistry - Dark Chemistry. EUPHORE, UCLM and UiO experiments.* ; 2211030-DC05; Tel-Tek: 2011.

200. Nielsen, C. J. *Atmospheric Chemistry - Dark Chemistry*; 2211030-DC06 v2; Tel-Tek: 2011.

201. Antonsen, S., Bunkan, A. J. C., D'Anna, B., Eichler, P., Farren, N., Hallquist, M., Hamilton, J. F., Kvarnliden, H., Mikoviny, T., Müller, M., Nielsen, C. J., Stenstrøm, Y., Tan, W., Wisthaler, A., Zhu, L., Atmospheric chemistry of *tert*-butylamine and AMP. *Energy Procedia* **2017**.

202. Kroll, J. H.; Ng, N. L.; Murphy, S. M.; Flagan, R. C.; Seinfeld, J. H., Secondary organic aerosol formation from isoprene photooxidation under high-NOx conditions. *Geophys Res Lett* **2005,** *32* (18).

203. Hatakeyama, S.; Izumi, K.; Fukuyama, T.; Akimoto, H.; Washida, N., Reactions of Oh with Alpha-Pinene and Beta-Pinene in Air - Estimate of Global Co Production from the Atmospheric Oxidation of Terpenes. *J Geophys Res-Atmos* **1991,** *96* (D1), 947-958.

204. Ng, N. L.; Chhabra, P. S.; Chan, A. W. H.; Surratt, J. D.; Kroll, J. H.; Kwan, A. J.; McCabe, D. C.; Wennberg, P. O.; Sorooshian, A.; Murphy, S. M.; Dalleska, N. F.; Flagan, R. C.; Seinfeld, J. H., Effect of NOx level on secondary organic aerosol (SOA) formation from the photooxidation of terpenes. *Atmos Chem Phys* **2007,** *7* (19), 5159-5174.

205. Perrin, D. D., *Dissociation Constants of Organic Bases in Aqueous Solution. IUPAC Chemical Data Series: Supplement 1972.* Buttersworth: London, 1972.

206. Riddick, J. A.; Bunger, W. B.; Sakano, T.; Weissberger, A., *Organic solvents : physical properties and methods of purification*. 4th ed.; Wiley: New York, 1986; p xv, 1325 p.

207. Yaws, C. L., *Handbook of vapor pressure*. Gulf Pub. Co.: Houston, 1994.

208. Kirk, R. E.; Othmer, D. F.; Grayson, M.; Eckroth, D., *Encyclopedia of chemical technology*. 3d ed.; Wiley: New York, 1978.

209. Onel, L.; Dryden, M.; Blitz, M. A.; Seakins, P. W., Atmospheric Oxidation of Piperazine by OH has a Low Potential To Form Carcinogenic Compounds. *Environ Sci Tech Let* **2014,** *1* (9), 367-371.

210. Hanst, P. L.; Spence, J. W.; Miller, M., Atmospheric Chemistry of N-Nitroso Dimethylamine. *Environ. Sci. Technol.* **1977,** *11* (4), 403-405.

211. Zahardis, J.; Geddes, S.; Petrucci, G. A., The ozonolysis of primary aliphatic amines in fine particles. *Atmos Chem Phys* **2008,** *8* (5), 1181-1194.

212. Vardoulakis, S., Human exposure: Indoor and outdoor. *Issues in Environmental Science and Technology* **2009,** *28*, 85-107.

213. Hildemann, L. M.; Markowski, G. R.; Cass, G. R., Chemical-Composition of Emissions from Urban Sources of Fine Organic Aerosol. *Environ. Sci. Technol.* **1991,** *25* (4), 744-759.

214. Chen, Y.; Ho, K. F.; Ho, S. S. H.; Ho, W. K.; Lee, S. C.; Yu, J. Z.; Sit, E. H. L., Gaseous and particulate polycyclic aromatic hydrocarbons (PAHs) emissions from commercial restaurants in Hong Kong. *J Environ Monitor* **2007,** *9* (12), 1402-1409.

215. Mugica, V.; Vega, E.; Chow, J.; Reyes, E.; Sanchez, G.; Arriaga, J.; Egami, R.; Watson, J., Speciated non-methane organic compounds emissions from food cooking in Mexico. *Atmos. Environ.* **2001,** *35* (10), 1729-1734.

216. Ho, S. S. H.; Yu, J. Z.; Chu, K. W.; Yeung, L. L., Carbonyl emissions from commercial cooking sources in Hong Kong. *J Air Waste Manage* **2006,** *56* (8), 1091-1098.

217. Ko, Y. C.; Cheng, L. S. C.; Lee, C. H.; Huang, J. J.; Huang, M. S.; Kao, E. L.; Wang, H. Z.; Lin, H. J., Chinese food cooking and lung cancer in women nonsmokers. *Am J Epidemiol* **2000,** *151* (2), 140-147.

218. Huang, Y.; Ho, S. S. H.; Ho, K. F.; Lee, S. C.; Yu, J. Z.; Louie, P. K. K., Characteristics and health impacts of VOCs and carbonyls associated with residential cooking activities in Hong Kong. *J Hazard Mater* **2011,** *186* (1), 344-351.

219. McDonald, J. D.; Zielinska, B.; Fujita, E. M.; Sagebiel, J. C.; Chow, J. C.; Watson, J. G., Emissions from charbroiling and grilling of chicken and beef. *J Air Waste Manage* **2003,** *53* (2), 185-194.

220. Zhu, L. Z.; Wang, J., Sources and patterns of polycyclic aromatic hydrocarbons pollution in kitchen air, China. *Chemosphere* **2003,** *50* (5), 611-618.

221. Schauer, J. J.; Kleeman, M. J.; Cass, G. R.; Simoneit, B. R. T., Measurement of emissions from air pollution sources. 1. C-1 through C-29 organic compounds from meat charbroiling. *Environ. Sci. Technol.* **1999,** *33* (10), 1566-1577.

222. Schauer, J. J.; Kleeman, M. J.; Cass, G. R.; Simoneit, B. R. T., Measurement of emissions from air pollution sources. 4. C-1-C-27 organic compounds from cooking with seed oils. *Environ. Sci. Technol.* **2002,** *36* (4), 567-575.

223. Lee, S. C.; Li, W. M.; Chan, L. Y., Indoor air quality at restaurants with different styles of cooking in metropolitan Hong Kong. *Sci Total Environ* **2001,** *279* (1-3), 181-193.

224. Alves, C. A.; Evtyugina, M.; Cerqueira, M.; Nunes, T.; Duarte, M.; Vicente, E., Volatile organic compounds emitted by the stacks of restaurants. *Air Qual Atmos Hlth* **2015,** *8* (4), 401-412.

225. Villanueva, F.; Tapia, A.; Amo-Salas, M.; Notario, A.; Cabanas, B.; Martinez, E., Levels and sources of volatile organic compounds including carbonyls in indoor air of homes of Puertollano, the most industrialized city in central Iberian Peninsula. Estimation of health risk. *Int J Hyg Envir Heal* **2015,** *218* (6), 522-534.

226. Bari, M. A.; Kindzierski, W. B.; Wheeler, A. J.; Heroux, M. E.; Wallace, L. A., Source apportionment of indoor and outdoor volatile organic compounds at homes in Edmonton, Canada. *Build Environ* **2015,** *90*, 114-124.

227. Waring, M. S.; Wells, J. R., Volatile organic compound conversion by ozone, hydroxyl radicals, and nitrate radicals in residential indoor air: Magnitudes and impacts of oxidant sources. *Atmos. Environ.* **2015,** *106*, 382-391.

228. Klein, F.; Platt, S. M.; Farren, N. J.; Detournay, A.; Bruns, E. A.; Bozzetti, C.; Daellenbach, K. R.; Kilic, D.; Kumar, N. K.; Pieber, S. M.; Slowik, J. G.; Temime-Roussel, B.; Marchand, N.; Hamilton, J. F.; Baltensperger, U.; Prevot, A. S. H.; El Haddad, I., Characterization of Gas-Phase Organics Using Proton Transfer Reaction Time-of-Flight Mass Spectrometry: Cooking Emissions. *Environ. Sci. Technol.* **2016,** *50* (3), 1243-1250.

229. Bruns, E. A.; El Haddad, I.; Slowik, J. G.; Kilic, D.; Klein, F.; Baltensperger, U.; Prevot, A. S. H., Identification of significant precursor gases of secondary organic aerosols from residential wood combustion. *Sci Rep-Uk* **2016,** *6*.

230. Klein, F.; Farren, N. J.; Bozzetti, C.; Daellenbach, K. R.; Kilic, D.; Kumar, N. K.; Pieber, S. M.; Slowik, J. G.; Tuthill, R. N.; Hamilton, J. F.; Baltensperger, U.; Prevot, A. S. H.; El Haddad, I., Indoor terpene emissions from cooking with herbs and pepper and their secondary organic aerosol production potential. *Sci Rep-Uk* **2016,** *6*.

231. de Gouw, J.; Warneke, C., Measurements of volatile organic compounds in the earths atmosphere using proton-transfer-reaction mass spectrometry. *Mass Spectrom Rev* **2007,** *26* (2), 223-257.

232. DeCarlo, P. F.; Kimmel, J. R.; Trimborn, A.; Northway, M. J.; Jayne, J. T.; Aiken, A. C.; Gonin, M.; Fuhrer, K.; Horvath, T.; Docherty, K. S.; Worsnop, D. R.; Jimenez, J. L., Field-deployable, high-resolution, time-of-flight aerosol mass spectrometer. *Anal Chem* **2006,** *78* (24), 8281-8289.

233. Williams, L. R.; Gonzalez, L. A.; Peck, J.; Trimborn, D.; McInnis, J.; Farrar, M. R.; Moore, K. D.; Jayne, J. T.; Robinson, W. A.; Lewis, D. K.; Onasch, T. B.; Canagaratna, M. R.; Trimborn, A.; Timko, M. T.; Magoon, G.; Deng, R.; Tang, D.; Blanco, E. D. L. R.;

Prevot, A. S. H.; Smith, K. A.; Worsnop, D. R., Characterization of an aerodynamic lens for transmitting particles greater than 1 micrometer in diameter into the Aerodyne aerosol mass spectrometer. *Atmos. Meas. Tech.* **2013,** *6* (11), 3271-3280.

234. Fullana, A.; Carbonell-Barrachina, A. A.; Sidhu, S., Volatile aldehyde emissions from heated cooking oils. *J Sci Food Agr* **2004,** *84* (15), 2015-2021.

235. Katragadda, H. R.; Fullana, A.; Sidhu, S.; Carbonell-Barrachina, A. A., Emissions of volatile aldehydes from heated cooking oils. *Food Chem.* **2010,** *120* (1), 59-65.

236. Umano, K.; Shibamoto, T., Analysis of Acrolein from Heated Cooking Oils and Beef Fat. *J Agr Food Chem* **1987,** *35* (6), 909-912.

237. Gardner, H. W., Oxygen Radical Chemistry of Poly-Unsaturated Fatty-Acids. *Free Radical Bio Med* **1989,** *7* (1), 65-86.

238. Scrimgeour, C., Chemistry of Fatty Acids. In *Bailey's Industrial Oil and Fat Products*, 6th ed.; John Wiley & Sons, Inc.: 2005; Vol. 1, pp 1-43.

239. Przybylski, R. Canola Oil: Physical and Chemical Properties. http://www.canolacouncil.org/media/515239/canola_oil_physical_chemical_properties_1.pdf (accessed 20-04-2017).

240. Frankel, E. N., Chemistry of autoxidation: mechanism, products and flavor significance. In *Flavor chemistry of fats and oils*, The American Oil Chemists' Society: 1985; pp 1-34.

241. Choe, E.; Min, D. B., Mechanisms and factors for edible oil oxidation. *Compr Rev Food Sci F* **2006,** *5* (4), 169-186.

242. Belitz, H. D.; Grosch, W.; Schieberle, P., *Food Chemistry*. 4th ed.; Springer Science & Business Media: 2009.

243. Wood, J. D.; Richardson, R. I.; Nute, G. R.; Fisher, A. V.; Campo, M. M.; Kasapidou, E.; Sheard, P. R.; Enser, M., Effects of fatty acids on meat quality: a review. *Meat Sci* **2004,** *66* (1), 21-32.

244. Cassee, F. R.; Arts, J. H. E.; Groten, J. P.; Feron, V. J., Sensory irritation to mixtures of formaldehyde, acrolein, and acetaldehyde in rats. *Arch Toxicol* **1996,** *70* (6), 329-337.

245. US EPA Acute Exposure Guideline Levels - Acrolein. https://www.epa.gov/aegl/acrolein-results-aegl-program (accessed 21-04-2017).

246. Wang, C. K.; Chang, L. W.; Chang, H.; Yang, C. H.; Tsai, M. H.; Tsai, H. T.; Lin, P., Pulmonary changes induced by trans,trans-2,4-decadienal, a component of cooking oil fumes. *Eur Respir J* **2010,** *35* (3), 667-675.

247. Loza-Tavera, H., Monoterpenes in essential oils - Biosynthesis and properties. *Chemicals Via Higher Plant Bioengineering* **1999,** *464*, 49-62.

248. Salido, S.; Altarejos, J.; Nogueras, M.; Sanchez, A.; Luque, P., Chemical composition and seasonal variations of rosemary oil from southern Spain. *J Essent Oil Res* **2003,** *15* (1), 10-14.

249. Novak, J.; Bahoo, L.; Mitteregger, U.; Franz, C., Composition of individual essential oil glands of savory (Satureja hortensis L., Lamiaceae) from Syria. *Flavour Frag J* **2006,** *21* (4), 731-734.

250. Bolechowski, A.; Moral, R.; Bustamante, M. A.; Paredes, C.; Agullo, E.; Bartual, J.; Carbonell-Barrachina, A. A., Composition of Oregano Essential Oil (Origanum vulgare) as Affected by the Use of Winery-Distillery Composts. *J Essent Oil Res* **2011,** *23* (3), 32-38.

251. Kashkooli, A. B.; Saharkhiz, M. J., Essential Oil Compositions and Natural Herbicide Activity of Four Denaei Thyme (Thymus daenensis Celak.) Ecotypes. *J Essent Oil Bear Pl* **2014,** *17* (5), 859-874.

252. Wang, Z. F.; Chen, P.; Yu, L. L.; Harrington, P. D., Authentication of Organically and Conventionally Grown Basils by Gas Chromatography/Mass Spectrometry Chemical Profiles. *Anal Chem* **2013,** *85* (5), 2945-2953.

253. Kumar, N.; Lohani, H.; Lehari, A.; Dwivedi, K. N., Composition of oil from rosemary (Rosmarinus officinalis L.) grown in Kumaon hills of Uttaranchal. *Indian Perfumer* **2004,** *48* (4), 411-414.

254. Menon, A. N.; Padmakumari, K. P.; Jayalekshmy, A.; Gopalakrishnan, M.; Narayanan, C. S., Essential oil composition of four popular Indian cultivars of black pepper (Piper nigrum L.). *J Essent Oil Res* **2000,** *12* (4), 431-434.

255. Rouatbi, M.; Duquenoy, A.; Giampaoli, P., Extraction of the essential oil of thyme and black pepper by superheated steam. *J Food Eng* **2007,** *78* (2), 708-714.

256. Jelen, H. H.; Gracka, A., Analysis of black pepper volatiles by solid phase microextraction-gas chromatography: A comparison of terpenes profiles with hydrodistillation. *J. Chromatogr. A* **2015,** *1418*, 200-209.

257. Raman, G.; Gaikar, V. G., Microwave-assisted extraction of piperine from Piper nigrum. *Ind Eng Chem Res* **2002,** *41* (10), 2521-2528.

258. Parthasarathy, V. A.; Chempakam, B.; Zachariah, T. J., *Chemistry of spices*. CABI Pub.: Wallingford, UK ; Cambridge, MA, 2008; p 1-445.

259. Youssefi, S.; Waring, M. S., Transient Secondary Organic Aerosol Formation from Limonene Ozonolysis in Indoor Environments: Impacts of Air Exchange Rates and Initial Concentration Ratios. *Environ. Sci. Technol.* **2014,** *48* (14), 7899-7908.

260. Olive oil chemical characteristics. https://www.oliveoilsource.com/page/chemical-characteristics (accessed 06-05-2017).

261. Zhao, Y. L.; Hu, M.; Slanina, S.; Zhang, Y. H., Chemical compositions of fine particulate organic matter emitted from Chinese cooking. *Environ. Sci. Technol.* **2007,** *41* (1), 99-105.

262. Zhao, Y. L.; Hu, M.; Slanina, S.; Zhang, Y. H., The molecular distribution of fine particulate organic matter emitted from Western-style fast food cooking. *Atmos. Environ.* **2007,** *41* (37), 8163-8171.

263. Young, D. E.; Allan, J. D.; Williams, P. I.; Green, D. C.; Flynn, M. J.; Harrison, R. M.; Yin, J.; Gallagher, M. W.; Coe, H., Investigating the annual behaviour of submicron secondary inorganic and organic aerosols in London. *Atmos Chem Phys* **2015,** *15* (11), 6351-6366.

264. Robinson, A. L.; Subramanian, R.; Donahue, N. M.; Bernardo-Bricker, A.; Rogge, W. F., Source apportionment of molecular markers and organic aerosol. 3. Food cooking emissions. *Environ. Sci. Technol.* **2006,** *40* (24), 7820-7827.

265. Nolte, C. G.; Schauer, J. J.; Cass, G. R.; Simoneit, B. R. T., Highly polar organic compounds present in meat smoke. *Environ. Sci. Technol.* **1999,** *33* (19), 3313-3316.

266. Bender, D. A., *Nutritional biochemistry of the vitamins*. 2nd ed.; Cambridge University Press: Cambridge, UK ; New York, N.Y., 2003; p 1-488.

267. Abdulmumeen, H. A.; Risikat, A. N.; Sururah, A. R., Food: Its preservatives, additives and applications. *International Journal of Chemical and Biochemical Sciences* **2012,** *1*, 36-47.

268. Grajales-Lagunes, A.; Rivera-Bautista, C.; Ruiz-Cabrera, M.; Gonzalez-Garcia, R.; Ramirez-Telles, J.; Abud-Archila, M., Effect of lactic acid on the meat quality properties and the taste of pork Serratus ventralis muscle. *Agr Food Sci* **2012,** *21* (2), 171-181.

269. Arey, J.; Zielinska, B.; Harger, W. P.; Atkinson, R.; Winer, A. M., The Contribution of Nitrofluoranthenes and Nitropyrenes to the Mutagenic Activity of Ambient Particulate Organic-Matter Collected in Southern-California. *Mutat Res* **1988,** *207* (2), 45-51.

270. American meat institute - sodium nitrite. http://www.meatsafety.org/ht/d/sp/i/45243/pid/45243 (accessed 12-05-2017).

271. Gibis, M., Heterocyclic Aromatic Amines in Cooked Meat Products: Causes, Formation, Occurrence, and Risk Assessment. *Compr Rev Food Sci F* **2016,** *15* (2), 269-302.

272. Murkovic, M.; Weber, H. J.; Geiszler, S.; Frohlich, K.; Pfannhauser, W., Formation of the food associated carcinogen 2-amino-1-methyl-6-phenylimidazo[4,5-b]pyridine (PhIP) in model systems. *Food Chem.* **1999,** *65* (2), 233-237.

273. Cross, A. J.; Sinha, R., Meat-related mutagens/carcinogens in the etiology of colorectal cancer. *Environ Mol Mutagen* **2004,** *44* (1), 44-55.

274. Sugimura, T., Overview of carcinogenic heterocyclic amines. *Mutat Res-Fund Mol M* **1997,** *376* (1-2), 211-219.

275. Buettner, A., *Springer Handbook of Odor*. Springer: 2017; p 1100.

276. Resconi, V. C.; Escudero, A.; Campo, M. M., The Development of Aromas in Ruminant Meat. *Molecules* **2013,** *18* (6), 6748-6781.

277. Martins, S. I. F. S.; Jongen, W. M. F.; van Boekel, M. A. J. S., A review of Maillard reaction in food and implications to kinetic modelling. *Trends Food Sci Tech* **2000,** *11* (9-10), 364-373.

278. Fisher, C.; Scott, T. R., *Food Flavours: Biology and Chemistry*. Royal Society of Chemistry: Cambridge UK, 1997.

279. US agricultural research service - national nutrient databased for standard reference release 28. https://ndb.nal.usda.gov/ndb/search/list (accessed 12-05-2017).

280. Kataoka, H., Methods for the determination of mutagenic heterocyclic amines and their applications in environmental analysis. *J. Chromatogr. A* **1997,** *774* (1-2), 121-142.

281. Liu, S.; Taylor, L. T.; Borgerding, M. F.; Coleman, W. M.; Bombick, B. R., Trace Analysis of Mutagenic Heterocyclic Aromatic Amines in Cigarette Smoke Condensate and its Base Fractions via Silylation-GC-MS. *Contributions to Tobacco Research* **2013,** *25* (5), 550-562.

282. Byun, M. W.; Ahn, H. J.; Kim, J. H.; Lee, J. W.; Yook, H. S.; Han, S. B., Determination of volatile N-nitrosamines in irradiated fermented sausage by gas chromatography coupled to a thermal energy analyzer. *J. Chromatogr. A* **2004,** *1054* (1-2), 403-407.

283. Domanska-Blicharz, K.; Rachubik, J.; Kowalski, B., Occurrence of volatile N-nitrosamines in Polish tinned foods. *B Vet I Pulawy* **2005,** *49* (3), 319-322.

284. Ozel, M. Z.; Gogus, F.; Yagci, S.; Hamilton, J. F.; Lewis, A. C., Determination of volatile nitrosamines in various meat products using comprehensive gas chromatography-nitrogen chemiluminescence detection. *Food Chem Toxicol* **2010,** *48* (11), 3268-3273.

285. Research Station at Institute of Ocean and Earth Science, University of Malaya. http://www.ioes.um.edu.my/research_facilities.html (accessed 18-06-2017).

286. WMO Global Atmospheric Watch Station Information System (GAWSIS). https://gawsis.meteoswiss.ch/GAWSIS//index.html#/ (accessed 12-04-2017).

287. Neale, R.; Slingo, J., The maritime continent and its role in the global climate: A GCM study. *J Climate* **2003,** *16* (5), 834-848.

288. Carpenter, L. J.; Fleming, Z. L.; Read, K. A.; Lee, J. D.; Moller, S. J.; Hopkins, J. R.; Purvis, R. M.; Lewis, A. C.; Muller, K.; Heinold, B.; Herrmann, H.; Fomba, K. W.; van Pinxteren, D.; Muller, C.; Tegen, I.; Wiedensohler, A.; Muller, T.; Niedermeier, N.; Achterberg, E. P.; Patey, M. D.; Kozlova, E. A.; Heimann, M.; Heard, D. E.; Plane, J. M.

C.; Mahajan, A.; Oetjen, H.; Ingham, T.; Stone, D.; Whalley, L. K.; Evans, M. J.; Pilling, M. J.; Leigh, R. J.; Monks, P. S.; Karunaharan, A.; Vaughan, S.; Arnold, S. R.; Tschritter, J.; Pohler, D.; Friess, U.; Holla, R.; Mendes, L. M.; Lopez, H.; Faria, B.; Manning, A. J.; Wallace, D. W. R., Seasonal characteristics of tropical marine boundary layer air measured at the Cape Verde Atmospheric Observatory. *J Atmos Chem* **2010,** *67* (2-3), 87-140.

289. Lawrence, M. G.; Jockel, P.; von Kuhlmann, R., What does the global mean OH concentration tell us? *Atmos Chem Phys* **2001,** *1*, 37-49.

290. Bloss, W. J.; Evans, M. J.; Lee, J. D.; Sommariva, R.; Heard, D. E.; Pilling, M. J., The oxidative capacity of the troposphere: Coupling of field measurements of OH and a global chemistry transport model. *Faraday Discuss* **2005,** *130*, 425-436.

291. Behrenfeld, M. J.; O'Malley, R. T.; Siegel, D. A.; McClain, C. R.; Sarmiento, J. L.; Feldman, G. C.; Milligan, A. J.; Falkowski, P. G.; Letelier, R. M.; Boss, E. S., Climate-driven trends in contemporary ocean productivity. *Nature* **2006,** *444* (7120), 752-755.

292. Dunmore, R. E.; Hopkins, J. R.; Lidster, R. T.; Mead, M. I.; Bandy, B. J.; Forster, G.; Oram, D. E.; Sturges, W. T.; Phang, S. M.; Abu Samah, A.; Hamilton, J. F., Development of a Combined Heart-Cut and Comprehensive Two-Dimensional Gas Chromatography System to Extend the Carbon Range of Volatile Organic Compounds Analysis in a Single Instrument. *Separations* **2016,** *3* (3).

293. Dominick, D.; Latif, M. T.; Juneng, L.; Khan, M. F.; Amil, N.; Mead, M. I.; Nadzir, M. S. M.; Moi, P. S.; Abu Samah, A.; Ashfold, M. J.; Sturges, W. T.; Harris, N. R. P.; Robinson, A. D.; Pyle, J. A., Characterisation of particle mass and number concentration on the east coast of the Malaysian Peninsula during the northeast monsoon. *Atmos. Environ.* **2015,** *117*, 187-199.

294. Charlson, R. J.; Langner, J.; Rodhe, H.; Leovy, C. B.; Warren, S. G., Perturbation of the Northern-Hemisphere Radiative Balance by Backscattering from Anthropogenic Sulfate Aerosols. *Tellus A* **1991,** *43* (4), 152-163.

295. Coakley, J. A.; Cess, R. D.; Yurevich, F. B., The Effect of Tropospheric Aerosols on the Earths Radiation Budget - a Parameterization for Climate Models. *J Atmos Sci* **1983,** *40* (1), 116-138.

296. Tahir, N. M.; Suratman, S.; Fong, F. T.; Hamzah, M. S.; Latif, M. T., Temporal Distribution and Chemical Characterization of Atmospheric Particulate Matter in the Eastern Coast of Peninsular Malaysia. *Aerosol Air Qual Res* **2013,** *13* (2), 584-595.

297. Ismail, M.; Yuen, F. S.; Abdullah, S. S., Particulate Matter Status and its Relationship with Meteorological Factors in the East Coast of Peninsular Malaysia. *Journal of Engineering and Applied Sciences* **2016,** *11* (12), 2588-2593.

298. Draxler, R. R.; Rolph, G. D. HYSPLIT (HYbrid Single-Particle Lagrangian Integrated Trajectory) model. www.arl.noaa.gov/HYSPLIT.php (accessed 25-03-2017).

299. Carslaw, D. C.; Ropkins, K., openair - An R package for air quality data analysis. *Environ Modell Softw* **2012,** *27-28*, 52-61.

300. Carslaw, D. C. *The openair manual - open-source tools for analysing air pollution data. Manual for version 1.1-4.*; King's College London, 2015.

301. NOAA Integrated Surface Database. https://www.ncdc.noaa.gov/isd (accessed 25-03-2017).

302. *East Coast Economic Region Development Council 2012 Annual Report*; East Coast Economic Region Development Council: Kuala Lumpur, Malaysia, 2012; pp 1-167.

303. ECERDC East Coast Economic Region. http://www.ecerdc.com.my/en/ (accessed 18-06-2017).

304. WHO *WHO Air quality guidelines for particulate matter, ozone, nitrogen dioxide and sulfur dioxide. Global update 2005. Summary of risk assessment.*; WHO/SDE/PHE/OEH/06.02; WHO Press, World Health Organization: Geneva, Switzerland, 2006, 2006; pp 1-20.

305. Bowen, H. J. M., *Environmental chemistry of the elements*. Academic Press: London, 1979.

306. Boreddy, S. K. R.; Kawamura, K., A 12-year observation of water-soluble ions in TSP aerosols collected at a remote marine location in the western North Pacific: an outflow region of Asian dust. *Atmos Chem Phys* **2015,** *15* (11), 6437-6453.

307. Fisher, J. A.; Jacob, D. J.; Wang, Q. Q.; Bahreini, R.; Carouge, C. C.; Cubison, M. J.; Dibb, J. E.; Diehl, T.; Jimenez, J. L.; Leibensperger, E. M.; Lu, Z. F.; Meinders, M. B. J.; Pye, H. O. T.; Quinn, P. K.; Sharma, S.; Streets, D. G.; van Donkelaar, A.; Yantosca, R. M., Sources, distribution, and acidity of sulfate-ammonium aerosol in the Arctic in winter-spring. *Atmos. Environ.* **2011,** *45* (39), 7301-7318.

308. Legrand, M.; Pasteur, E. C., Methane sulfonic acid to non-sea-salt sulfate ratio in coastal Antarctic aerosol and surface snow. *J Geophys Res-Atmos* **1998,** *103* (D9), 10991-11006.

309. Savoie, D. L.; Prospero, J. M., Comparison of Oceanic and Continental Sources of Non-Sea-Salt Sulfate over the Pacific-Ocean. *Nature* **1989,** *339* (6227), 685-687.

310. Keywood, M. D.; Ayers, G. P.; Gras, J. L.; Boers, R.; Leong, C. P., Haze in the Klang Valley of Malaysia. *Atmos Chem Phys* **2003,** *3*, 591-605.

311. EDGAR - Emissions Database for Global Atmospheric Research. http://edgar.jrc.ec.europa.eu/overview.php?v=431 (accessed 09-04-2017).

312. Murphy, J. G.; Gregoire, P. K.; Tevlin, A. G.; Wentworth, G. R.; Ellis, R. A.; Markovic, M. Z.; Vandenboer, T. C., Observational constraints on particle acidity using measurements and modelling of particles and gases. *Faraday Discuss* **2017,** *xx*, 1-17.

313. Hennigan, C. J.; Izumi, J.; Sullivan, A. P.; Weber, R. J.; Nenes, A., A critical evaluation of proxy methods used to estimate the acidity of atmospheric particles. *Atmos Chem Phys* **2015,** *15* (5), 2775-2790.

314. Gwynn, R. C.; Burnett, R. T.; Thurston, G. D., A time-series analysis of acidic particulate matter and daily mortality and morbidity in the Buffalo, New York, region. *Environ Health Persp* **2000,** *108* (2), 125-133.

315. Schindler, D. W., Effects of Acid Rain on Freshwater Ecosystems. *Science* **1988,** *239* (4836), 149-157.

316. Charlson, R. J.; Lovelock, J. E.; Andreae, M. O.; Warren, S. G., Oceanic Phytoplankton, Atmospheric Sulfur, Cloud Albedo and Climate. *Nature* **1987,** *326* (6114), 655-661.

317. Graf, H. F.; Feichter, J.; Langmann, B., Volcanic sulfur emissions: Estimates of source strength and its contribution to the global sulfate distribution. *J Geophys Res-Atmos* **1997,** *102* (D9), 10727-10738.

318. Haywood, J. M.; Ramaswamy, V., Global sensitivity studies of the direct radiative forcing due to anthropogenic sulfate and black carbon aerosols. *J Geophys Res-Atmos* **1998,** *103* (D6), 6043-6058.

319. Haywood, J.; Boucher, O., Estimates of the direct and indirect radiative forcing due to tropospheric aerosols: A review. *Rev Geophys* **2000,** *38* (4), 513-543.

320. Sareen, N.; Carlton, A. G.; Surratt, J. D.; Gold, A.; Lee, B.; Lopez-Hilfiker, F. D.; Mohr, C.; Thornton, J. A.; Zhang, Z. F.; Lim, Y. B.; Turpin, B. J., Identifying precursors and aqueous organic aerosol formation pathways during the SOAS campaign. *Atmos Chem Phys* **2016,** *16* (22), 14409-14420.

321. Saxena, P.; Hildemann, L. M., Water-soluble organics in atmospheric particles: A critical review of the literature and application of thermodynamics to identify candidate compounds. *J Atmos Chem* **1996,** *24* (1), 57-109.

322. Novakov, T.; Penner, J. E., Large Contribution of Organic Aerosols to Cloud-Condensation-Nuclei Concentrations. *Nature* **1993,** *365* (6449), 823-826.

323. Facchini, M. C.; Mircea, M.; Fuzzi, S.; Charlson, R. J., Cloud albedo enhancement by surface-active organic solutes in growing droplets. *Nature* **1999,** *401* (6750), 257-259.

324. Kerminen, V. M., Relative roles of secondary sulfate and organics in atmospheric cloud condensation nuclei production. *J Geophys Res-Atmos* **2001,** *106* (D15), 17321-17333.

325. Freitas, A. D.; Martins, L. D.; Solci, M. C., Size-Segregated Particulate Matter and Carboxylic Acids over Urban and Rural Sites in Londrina City, Brazil. *J Brazil Chem Soc* **2012,** *23* (5), 921-930.

326. Jiang, Y.; Zhuang, G.; Wang, Q.; Liu, T.; Huang, K.; Fu, J. S.; Li, J.; Lin, Y.; Zhang, R.; Deng, C., Characteristics, sources and formation of aerosol oxalate in an Eastern Asia

megacity and its implication to haze pollution. *Atmos Chem Phys Discuss* **2011,** *11*, 22075-22112.

327. Sempere, R.; Kawamura, K., Comparative Distributions of Dicarboxylic-Acids and Related Polar Compounds in Snow Rain and Aerosols from Urban Atmosphere. *Atmos. Environ.* **1994,** *28* (3), 449-459.

328. Uchiyama, S., The Behaviour of Oxalic Acid in Atmospheric Aerosols. *J. Jpn. Soc. Atmos. Environ.* **1996,** *31* (4), 141-148.

329. Myriokefalitakis, S.; Tsigaridis, K.; Mihalopoulos, N.; Sciare, J.; Nenes, A.; Kawamura, K.; Segers, A.; Kanakidou, M., In-cloud oxalate formation in the global troposphere: a 3-D modeling study. *Atmos Chem Phys* **2011,** *11* (12), 5761-5782.

330. Carlton, A. G.; Turpin, B. J.; Lim, H. J.; Altieri, K. E.; Seitzinger, S., Link between isoprene and secondary organic aerosol (SOA): Pyruvic acid oxidation yields low volatility organic acids in clouds. *Geophys Res Lett* **2006,** *33* (6).

331. Tan, Y.; Lim, Y. B.; Altieri, K. E.; Seitzinger, S. P.; Turpin, B. J., Mechanisms leading to oligomers and SOA through aqueous photooxidation: insights from OH radical oxidation of acetic acid and methylglyoxal. *Atmos Chem Phys* **2012,** *12* (2), 801-813.

332. Huang, X. F.; Yu, J. Z.; He, L. Y.; Yuan, Z. B., Water-soluble organic carbon and oxalate in aerosols at a coastal urban site in China: Size distribution characteristics, sources, and formation mechanisms. *J Geophys Res-Atmos* **2006,** *111* (D22).

333. Yamasoe, M. A.; Artaxo, P.; Miguel, A. H.; Allen, A. G., Chemical composition of aerosol particles from direct emissions of vegetation fires in the Amazon Basin: water-soluble species and trace elements. *Atmos. Environ.* **2000,** *34* (10), 1641-1653.

334. Huang, X. F.; Yu, J. Z., Is vehicle exhaust a significant primary source of oxalic acid in ambient aerosols? *Geophys Res Lett* **2007,** *34* (2).

335. Boreddy, S. K. R.; Kawamura, K.; Jung, J. S., Hygroscopic properties of particles nebulized from water extracts of aerosols collected at Chichijima Island in the western North Pacific: An outflow region of Asian dust. *J Geophys Res-Atmos* **2014,** *119* (1), 167-178.

336. Ginoux, P.; Prospero, J. M.; Gill, T. E.; Hsu, N. C.; Zhao, M., Global-Scale Attribution of Anthropogenic and Natural Dust Sources and Their Emission Rates Based on Modis Deep Blue Aerosol Products. *Rev Geophys* **2012,** *50*.

337. UNEP *Global Assessment of Sand and Dust Storms*; United Nations Environment Programme: Nairobi, 2016; pp 1-123.